



**HAL**  
open science

# Enhancement of spectrum sensing in cognitive radio : providing reliable spectral opportunities

Azza Moawad

► **To cite this version:**

Azza Moawad. Enhancement of spectrum sensing in cognitive radio : providing reliable spectral opportunities. Networking and Internet Architecture [cs.NI]. Université de Bretagne occidentale - Brest, 2020. English. NNT : 2020BRES0074 . tel-03635895v2

**HAL Id: tel-03635895**

**<https://theses.hal.science/tel-03635895v2>**

Submitted on 8 Apr 2022

**HAL** is a multi-disciplinary open access archive for the deposit and dissemination of scientific research documents, whether they are published or not. The documents may come from teaching and research institutions in France or abroad, or from public or private research centers.

L'archive ouverte pluridisciplinaire **HAL**, est destinée au dépôt et à la diffusion de documents scientifiques de niveau recherche, publiés ou non, émanant des établissements d'enseignement et de recherche français ou étrangers, des laboratoires publics ou privés.

# THESE DE DOCTORAT DE

L'UNIVERSITE  
DE BRETAGNE OCCIDENTALE

ECOLE DOCTORALE N° 601  
*Mathématiques et Sciences et Technologies  
de l'Information et de la Communication*  
Spécialité : *Télécommunications*

Par

**Azza MOAWAD**

**Enhancement of Spectrum Sensing in Cognitive Radio :  
Providing Reliable Spectral Opportunities.**

**Thèse présentée et soutenue à Brest, le 10 décembre 2020**  
**Unité de recherche : Lab-STICC**

## **Rapporteurs avant soutenance :**

Denis HAMMAD Professeur des universités, Université du Littoral, Calais, France  
Cornel IOANA Maître de conférences, HDR, INP Grenoble, France

## **Composition du Jury :**

Président du Jury :	Christian JUTTEN	Professeur émérite des université, INP Grenoble, France
Examineurs :	Emanuel RADOI Marwa EL-BOUZ Denis HAMMAD Cornel IOANA	Professeur des universités, UBO Brest, France Enseignant-Chercheuse, HDR, ISEN Brest, France Professeur des universités, Université du Littoral, Calais, France Maître de conférences, HDR, INP Grenoble, France
Dir. de thèse :	Roland GAUTIER	Maître de conférences, Hors-Classe, HDR, UBO Brest, France
Co-dir. de thèse :	Koffi-Clément YAO	Maître de conférences, HDR, UBO, Brest, France
Invité(s) :	Ali MANSOUR Mohamed ABAZA	Professeur, ENSTA Bretagne, Brest, France Associate Professor, AASTMT, Cairo, Egypt

# ACKNOWLEDGEMENT

---

I am very grateful to ALLAH for all his blessings. I would also like to thank my parents, husband and daughters for what they have contributed towards my education. Their unconditional love, constant support, great advice and prayers over the past years are something that I cannot thank them for enough. Additionally, knowing that my success in completing my Ph.D would be a source of happiness for them, I was further motivated to work hard.

I am sincerely grateful for my thesis directors, Dr. Roland Gautier, for his support and encouragement and for giving me the opportunity to learn and develop, and Dr. Koffi-Clément Yao for the time he took to evaluate my contributions, the problems he noticed, and the discussions we had, which helped me to progress in my work and results. I am deeply indebted to my thesis supervisor, Prof. Ali Mansour, for his valuable comments, discussions, and encouragement. I thank him for always being available and helpful.

I want to thank Prof. Christian Jutten from the University of Grenoble for being the president of my Ph.D. committee. I also would like to thank the rapporteurs Prof. Denis Hamad from the University of Littoral Côte d'Opale and Dr. Ioana Cornel from the University of INP Grenoble for their valuable comments and corrections. I also thank Prof. Emanuel Radio from Université de Bretagne Occidentale and Dr. Marwa El-Bouz from ISEN Brest, for accepting to be the examiners of my dissertation.

Moreover, I would like to express my hearty thanks to Prof. Mohamed El Mahallawy, the head of the department of Electronics and Communications Engineering from Arab Academy for Science and Technology and Maritime Transport (AASTMT), Egypt, for his continuous support along my Ph.D work and his eagerness to give me the time to accomplish my research work. Also, I am deeply thankful for my friends especially Eng. Nihal Sameh and Eng. Mai AbdelMoniem. They always encouraged me in this challenge.

Finally, I would like to thank my colleagues with whom I had fruitful discussions during the preparation of my thesis: Dr. Mohamed Abaza from Arab Academy for Science and Technology and Maritime Transport (AASTMT), Egypt, Dr. Ahmed Ali

from Carlton University, Canada, Dr. El Nasser Salah El deen from McGill University, Canada, and last but not least, Dr. Karim Seddik from the American University in Cairo (AUC), Egypt.

# RÉSUMÉ

---

Le partage dynamique du spectre (Dynamic Spectrum Sharing DSS) vise à améliorer l'efficacité d'accès aux bandes de fréquences sous-utilisées. Dans le mode entrelacé d'accès au spectre, la Radio Cognitive permet à un utilisateur sans licence (utilisateur secondaire SU) d'accéder de manière opportuniste aux bandes de spectre sous licence lorsque l'utilisateur sous licence (utilisateur principal PU) est absent. Dès lors, la détection du signal émis par le PU constitue l'étape primordiale pour l'accès au spectre en Radio Cognitive. L'objectif principal de la thèse est de concevoir un système de détection fiable, capable de détecter un signal assimilable au bruit, dans un contexte non-coopératif. Nous exploitons la puissance de l'analyse cepstrale pour développer un système capable de détecter les signaux à spectre étalé. Nous avons proposé un détecteur PassBand-AutoCesptrum (PB-ACD), qui réalise la détection par rapport au pic dominant de l'auto-cepstre dans certains cas ou par rapport à la valeur moyenne des pics dans d'autres cas. Les techniques proposées ont montré une grande fiabilité pour la détection des signaux à spectre étalé et des signaux ultra large bande (UWB). En outre, nous avons proposé la technique PB-ACD améliorée pour lisser les fluctuations des estimateurs d'autocorrélation en utilisant l'algorithme TVD (Total Variation Denoising) pour la réduction du bruit. Nous avons étendu nos travaux au cas du spectre à très large bande composé de plusieurs sous-bandes de fréquences. La première phase de la procédure consiste en la détection des frontières entre les différentes sous-bandes de fréquences avant d'effectuer par la suite la détection du signal du PU. À cet effet, nous avons introduit l'algorithme DLSD (Differential Log Spectral Density) pour identifier les limites spectrales du spectre large bande cible. Ensuite, pour la détection du signal du PU, nous avons développé le détecteur BaseBand-AutoCepstrum (BB-ACD) qui extrait les informations du signal en bande de base avant d'appliquer la technique de détection basée sur l'auto-cepstre. La technique BB-ACD permet de prendre en compte l'incertitude sur les fréquences qui peut résulter de la mauvaise détection des limites spectrales. Enfin, la méthode du cepstre de puissance améliorée est introduite par le détecteur de covariance Cepstrale (CCD) pour détecter les signaux modulés numériquement.



# TABLE OF CONTENTS

---

<b>Acknowledgement</b>	<b>i</b>
<b>Résumé</b>	<b>iii</b>
<b>List of Figures</b>	<b>ix</b>
<b>List of Tables</b>	<b>xiv</b>
<b>Abbreviations</b>	<b>xiv</b>
<b>List of Symbols</b>	<b>xix</b>
<b>Mathematical Notations</b>	<b>xxvii</b>
<b>1 Introduction</b>	<b>1</b>
1.1 Background . . . . .	1
1.2 Thesis Contributions . . . . .	4
1.3 Thesis Organization . . . . .	8
<b>2 State-of-The-Art</b>	<b>11</b>
2.1 Introduction . . . . .	11
2.2 Overview On Cognitive Radios . . . . .	12
2.2.1 Cognitive Capability of Cognitive Radio Networks . . . . .	14
2.2.2 Tasks of Cognitive Radio Systems . . . . .	15
2.2.3 Cognitive Radio Paradigms . . . . .	17
2.2.4 Cognitive Radio Bands . . . . .	18
2.3 Literature Review on Spectrum Sensing Techniques . . . . .	19
2.3.1 NarrowBand Spectrum Sensing . . . . .	23
2.3.2 WideBand Spectrum Sensing . . . . .	37
2.4 Spectrum Sensing By Scattering Operators . . . . .	39
2.4.1 Overview on Scattering Transform . . . . .	39

## TABLE OF CONTENTS

---

2.4.2	Reprocessing of Received Signals by The Scattering Operators . .	42
2.4.3	Numerical Results and Insights . . . . .	43
2.5	Enhancement of Primary User Detection Through Channel Estimation .	46
2.5.1	Channel Impairments: Overview . . . . .	46
2.5.2	System Model . . . . .	48
2.5.3	Problem Formulation and Proposed Solution . . . . .	50
2.5.4	Numerical Results and Insights . . . . .	55
2.6	Summary . . . . .	58
<b>3</b>	<b>Cepstral Analysis Approaches for Spectrum Sensing in Cognitive Radio</b>	<b>59</b>
3.1	Introduction . . . . .	59
3.2	Related Work . . . . .	60
3.2.1	Overview on Cepstral Analysis . . . . .	61
3.2.2	Application of Cepstral Analysis in Communications . . . . .	65
3.3	System Description and Channel Model . . . . .	66
3.3.1	System Model . . . . .	66
3.3.2	Signal and Channel Model . . . . .	67
3.4	Spectrum Sensing Technique By The Autocepstrum Approach . . . . .	68
3.4.1	Detection of Direct Sequence-Spread Spectrum Signals By The PB-ACD Technique . . . . .	69
3.4.2	Application of The PB-ACD Technique to Detecting Frequency- Hopping and Chirp Spread Spectrum Signals . . . . .	96
3.5	Spectrum Sensing by The Smoothed PB-ACD Technique . . . . .	107
3.5.1	Fluctuations Smoothing by The Total Variation Denoising Based on The Majorization-Minimization Algorithm: . . . . .	110
3.5.2	Application of the Proposed Smoothing Process to the Case of Detecting a DS-SS Signal: . . . . .	112
3.6	Numerical Results and Discussions . . . . .	117
3.7	Summary . . . . .	125
<b>4</b>	<b>Wideband Spectrum Sensing Technique By Cepstral Analysis Approaches</b>	<b>127</b>
4.1	Introduction . . . . .	127
4.2	Related Work . . . . .	130
4.3	Problem Formulation of Wideband Spectrum Sensing . . . . .	133
4.3.1	Phase I: Identification of Spectral Boundaries . . . . .	134

4.3.2	Phase II: Primary User Detection . . . . .	137
4.4	The Proposed Wideband Spectrum Sensing Approach . . . . .	137
4.4.1	Identification of Spectral Boundaries By Cepstral Analysis . . . . .	138
4.5	PU Detection Under Frequency Uncertainty by The BB-ACD Technique:	149
4.6	Numerical Results and Discussions . . . . .	153
4.6.1	Performance Evaluation of The Proposed Edge Detection Ap- proach: . . . . .	154
4.6.2	Detection of Noise-Like Signals Under Carrier Frequency Uncer- tainty By The BB-ACD Technique: . . . . .	159
4.7	Summary . . . . .	164
<b>5</b>	<b>Spectrum Sensing By Cepstral Covariance Detection in Cognitive Radio</b>	<b>166</b>
5.1	Introduction . . . . .	166
5.2	Signal Model and System Description . . . . .	167
5.3	Detection By The Cepstral Covariance Technique . . . . .	167
5.4	Design Characteristics of The Cepstral Covariance Detector . . . . .	169
5.5	Numerical Results and Discussions . . . . .	171
5.5.1	Detection Performance of The CCD Algorithm . . . . .	171
5.5.2	Complexity Analysis . . . . .	174
5.6	Summary . . . . .	176
<b>6</b>	<b>Conclusion and Future Work</b>	<b>177</b>
	<b>Conclusion</b>	<b>177</b>
6.1	Conclusions . . . . .	177
6.2	Recommendations for Future Work . . . . .	179
	<b>Appendix A</b>	<b>182</b>
A.1	Derivation of The Generalized Expression of The $\log -\chi_v^2$ for $\nu$ Degrees of Freedom . . . . .	182
A.2	Expression for The False-alarm Probability . . . . .	184
	<b>Appendix B</b>	<b>186</b>
B.1	Maximum-to-Minimum Eigenvalue Detection Algorithm . . . . .	186
B.2	Energy with Minimum Eigenvalue Detection Algorithm . . . . .	186

TABLE OF CONTENTS

---

<b>Appendix C</b>	<b>187</b>
C.1 Validation of a Chosen Majorizer Equation . . . . .	187
<b>Appendix D</b>	<b>188</b>
D.1 The Statistical Distribution of A Random Variable follows Modulus Log Chi-Squared Distribution . . . . .	188
<b>Appendix E</b>	<b>189</b>
E.1 Review on General Expressions of The PSD of Basic Digitally Modulated Signals . . . . .	189
<b>List of Publications</b>	<b>192</b>
<b>Bibliography</b>	<b>195</b>

# LIST OF FIGURES

---

1.1	The interplay among the system complexity, the detection accuracy, and the processing time . . . . .	3
1.2	A summary of the research pillars and contributions . . . . .	6
2.1	The global estimation of the growth rate in subscriptions of mobile communications and electronic elements technologies (Source: Cisco) . . . .	12
2.2	A logical diagram that illustrates the differences among conventional radio, SDR, and CR . . . . .	14
2.3	An illustration of the opportunistic and the fixed spectrum sharing models in CRs . . . . .	15
2.4	Different tasks of a cognitive radio system . . . . .	16
2.5	The hierarchy of spectrum sensing techniques as classified based on the type of the accessed spectrum model . . . . .	23
2.6	A demonstration of a typical operation of an interweave CR system . . .	24
2.7	The block diagram of a conventional energy detector . . . . .	26
2.8	The interplay between the false-alarm probability and the detection threshold of a conventional ED for different sample sizes . . . . .	27
2.9	The detection probability of a conventional ED for detecting for detecting Independent and Identically Distributed (IID) signals . . . . .	28
2.10	The receiver operating characteristics of an energy detector in case of a Gaussian PU signal . . . . .	29
2.11	The block diagram of a matched filter detector; $\mathcal{T}_{MFD}$ denotes the test statistic of the detector and $\eta_{MFD}$ is the detection threshold . . . . .	30
2.12	The detection probability of a MFD based on a static threshold . . . . .	31
2.13	The block diagram of the EigenValue-based Detection (EVD); $\mathcal{T}_{EVD}$ denotes the test statistic of the detector and $\eta_{EVD}$ is the detection threshold . . . . .	31
2.14	A comparison of the detection probabilities of the ED and EVD for different false-alarm probabilities . . . . .	32

2.15	The block diagram of a cyclostationary feature detector; $\mathcal{T}_{CFD}$ denotes the test statistic of the detector and $\eta_{CFD}$ is the detection threshold . . . . .	35
2.16	The spectral correlation of a real BPSK signal . . . . .	35
2.17	The block diagram of a conventional wavelet-based edge detector; $S_y(f)$ denotes the power spectral density of the received signal and $WT_S(f)$ is the wavelet transform of the signal's PSD . . . . .	38
2.18	The block diagram of a multi-band joint detector . . . . .	38
2.19	A hierarchal representation of a typical scattering network . . . . .	41
2.20	A functional block diagram of signals detection by the proposed ST-based detector . . . . .	43
2.21	A comparison of the detection probabilities for detecting a DS-SS signal by using the ED and the STD techniques . . . . .	45
2.22	A comparison of the detection probabilities for detecting a chirp signal by using the ED and the STD techniques . . . . .	45
2.23	A demonstration of the different multipath propagation mechanisms . . . . .	47
2.24	A block diagram represents the proposed method; $y(n)$ is the received PU signal, $y_{eq}(n)$ stands for the equalized received signal, $\hat{h}$ represents the estimated channel impulse response, and $\psi_{MD}(n)$ denotes the Morlet-Derivative Wavelet (MDW) function . . . . .	49
2.25	An illustration of the frequency localization of the real Morlet and the MDW functions . . . . .	52
2.26	The distribution of noise and faded Primary User (PU) signals with a 10-taps Channel . . . . .	56
2.27	The misdetection probability of the Principal Component Analysis (PCA)-based Energy Detection (ED) with a 5-taps channel . . . . .	57
2.28	The misdetection probability for different false-alarm values for a 5-taps channel after employing the proposed channel estimation technique followed by the equalization process . . . . .	57
3.1	A general description a communication scenario between Secondary User (SU) and PU networks . . . . .	66
3.2	An illustration of various autocepstrum analysis of Direct Sequence-Spread Spectrum (DS-SS) signal and the Additive White Gaussian Noise (AWGN); $T_d = 10$ msec and $f_c = 10$ MHz . . . . .	71
3.3	Comparing the cepstrum and the autocepstrum of a DS-SS signal . . . . .	72

3.4	The simulated and theoretical Receiver Operating Characteristics (ROC) curves of the PassBand-AutoCespectrum Detection (PB-ACD) technique . . . . .	80
3.5	The ROC curves of the PB-ACD simulated for different Signal-to-Noise-Ratio (SNR) values for real-valued Gaussian signals . . . . .	81
3.6	Comparison of the ROC curves for the PB-ACD and ED techniques for different SNR values for real-valued Gaussian signals . . . . .	82
3.7	Comparison of the ROC curves for the PB-ACD and ED techniques simulated for different signal sizes at -5 dB for real-valued Gaussian signals . . . . .	83
3.8	The frame structure for periodic sensing . . . . .	90
3.9	The achievable SU's throughput for the ED technique . . . . .	93
3.10	SU's achievable throughput for the PB-ACD technique . . . . .	94
3.11	A comparison of the achievable SU's throughput between the ED and the PB-ACD techniques . . . . .	94
3.12	A comparison of the achievable SU's throughput between the ED and the PB-ACD techniques based on the CLT assumption . . . . .	95
3.13	An example of a SFH-SS/FSK signal . . . . .	99
3.14	The spectrum of the hopping subcarriers . . . . .	100
3.15	The power spectral density of the SFH-SS/FSK signal . . . . .	101
3.16	The autocepstral peaks of the SFH-SS/FSK signal . . . . .	102
3.17	An example of the chirp/FSK signal that sweeps within 1 msec . . . . .	106
3.18	A demonstration of the autocepstrum and the autocepstrogram of a chirp/FSK signal . . . . .	107
3.19	The proposed smoothing process; $\hat{R}_y(\tau)$ is the autocorrelation estimate of the received signal; $\hat{\rho}_o(\tau)$ is the ACE fluctuations; $\tilde{\rho}_o(\tau)$ is the smoothed ACE fluctuations; $\tilde{R}_y(\tau)$ represents the smoothed autocorrelation estimate	108
3.20	The effect of applying the smoothing process on the estimated Power Spectral Density (PSD) . . . . .	115
3.21	The estimated PSD after applying the Total Variation Denoising-Mazjorization-Minimization (TVD-MM) algorithm to the fluctuations of the AutoCorrelation Estimators (ACEs) of the received signal; the signal is sampled at Nyquist's rate . . . . .	116
3.22	Performance evaluation of the PB-ACD as compared to ED for fixed $P_{FA}$	117
3.23	Detection probability of the PB-ACD as compared to ED for 64-QAM PU signal . . . . .	119

3.24 Detection probability of the PB-ACD as compared to ED for an OFDM PU signal in AWGN channel . . . . . 120

3.25 The detection probability of the PB-ACD as compared to the smoothed PB-ACD and different state-of-the-art techniques for detection a DS-SS signal; PB-ACD<sub>s</sub> denotes the smoothed PB-ACD technique . . . . . 121

3.26 The detection probability of the PB-ACD as compared to the smoothed PB-ACD and different state-of-the-art techniques for detection an Impulse Radio-Ultra WideBand (IR-UWB) signal; PB-ACD<sub>s</sub> denotes the smoothed PB-ACD technique . . . . . 122

3.27 The detection probability of the Averaged Passband-AutoCesptrum Detection (APB-ACD) as compared to ED and EVD techniques to detect Slow Frequency Hopping-Spread Spectrum (SFH-SS) PU signal . . . . . 123

3.28 The detection probability of the APB-ACD as compared to ED and EVD techniques to detect a chirp/FSK PU signal . . . . . 124

4.1 A general description of the wideband spectrum sensing problem . . . . . 135

4.2 The sequence of operations of the proposed WBSS approach . . . . . 138

4.3 Illustration of the effect of applying the DLSD to the AWGN spectrum . . 140

4.4 An example of a wideband spectrum that consists of consecutive subbands 141

4.5 The spectral edges when applying the proposed DLSD algorithm for the high SNR case (the average SNR is 5.9 dB for  $\sigma_w^2 = 14.7$  dB) . . . . . 142

4.6 The spectral edges when applying the proposed DLSD algorithm for the medium SNR case (the average SNR is 0.6 dB for  $\sigma_w^2 = 20$  dB) . . . . . 143

4.7 The spectral edges when applying the proposed DLSD algorithm for the low SNR case (the average SNR is -3.4 dB for  $\sigma_w^2 = 24$  dB) . . . . . 144

4.8 The spectral edges when applying the proposed DLSD algorithm with denoising for the low SNR case (the average SNR is -3.4 dB for  $\sigma_w^2 = 24$  dB) . . . . . 145

4.9 The spectral edges when applying the proposed DLSD algorithm if impulsive noise is imposed at average SNR of 5.7 dB . . . . . 146

4.10 The spectral edges when applying the proposed DLSD algorithm with denoising if impulsive noise is imposed at average SNR of 5.7 dB . . . . . 147

4.11 The system architecture of the proposed baseband autocepstrum technique; CLT denotes the circular topological filter . . . . . 150

4.12	The autocepstrum of the passband DS-SS signal; a large peak is located at a quefrequency value that is equivalent to the reciprocal of the signal's operating frequency of 1 GHz . . . . .	151
4.13	The frequency domain version of the autocepstrum of the baseband DS-SS signal which reveals periodicity at multiples of 1 MHz . . . . .	152
4.14	An example of a noisy spectral model . . . . .	156
4.15	A comparison of the probability of false detection of an original edge by the DLSD technique evaluated as opposed to wavelet-based techniques . . . . .	157
4.16	A comparison of the probability of misdetecting an original spectral boundary by the DLSD technique evaluated as opposed to wavelet-based techniques . . . . .	158
4.17	A comparison of the average detection error probability of the DLSD technique evaluated as opposed to wavelet-based techniques . . . . .	159
4.18	The detection probability of the BB-ACD technique for different modulation schemes . . . . .	160
4.19	The detection probability of the BB-ACD as compared to the PB-ACD under carrier frequency uncertainty for detecting a DS-SS signal; PB-ACD <sub>FE</sub> refers to the applying the PB-ACD in case of frequency errors . . . . .	161
4.20	The detection performance of the BB-ACD technique as compared to the PB-ACD technique in Rayleigh fading channel; PB-ACD <sub>Ray</sub> refers to employing the PB-ACD technique in Rayleigh fading channel . . . . .	161
4.21	The detection performance of the BB-ACD technique as compared to the PB-ACD technique in a frequency selective fading channel . . . . .	163
5.1	A functional block diagram of the proposed System; $\mathcal{T}[\mathcal{K}_{cc}]$ denotes the test statistic of the proposed detector . . . . .	168
5.2	The detection probability of the CCD technique for different modulation schemes . . . . .	171
5.3	The detection probability of the CCD technique in case of a wireless microphone signal . . . . .	172
5.4	The detection probability of the Cepstral Covariance Detection (CCD) technique for detecting IID Gaussian signals . . . . .	174
5.5	The time complexity analysis of the proposed CCD algorithm as compared to ED, EVD, CAVD, and logDet-CAVD algorithms . . . . .	175

# LIST OF TABLES

---

2.1	Comparison between the cognitive radio paradigms . . . . .	17
2.2	Comparison of the different spectrum sensing techniques . . . . .	36
2.3	Simulation parameters for the scattering-based energy detection . . . . .	44
2.4	Simulation Setup . . . . .	56
3.1	Variants of the cepstral analysis terms . . . . .	65
4.1	The SNR specifications per subband of an example of a wideband spectrum . . . . .	141
4.2	Simulation parameters of the edge-detection phase . . . . .	155
4.3	Spectral Specifications of one randomly generated spectral model; the noise variance $\sigma_w^2 = 20$ dB . . . . .	155
4.4	Comparing wavelet analysis to cepstral analysis for edge detection in wideband spectrum sensing . . . . .	162
4.5	Summary of the computational complexity of the DLSD algorithm as compared to the WTMP algorithm . . . . .	164

# ABBREVIATIONS

---

- ACEs** AutoCorrelation Estimators. xi, 6, 61, 107–109, 111, 112, 114–116, 125, 126, 131
- APB-ACD** Averaged Passband-AutoCespectrum Detection. xii, 6, 8, 96, 98, 105, 121–123
- AWGN** Additive White Gaussian Noise. x, 6, 7, 43, 67, 70–72, 99, 114, 118, 121, 122, 125, 126, 136, 138, 140, 143, 144, 150, 152, 154
- BB-ACD** BaseBand AutoCespectrum Detection. 7–9, 131, 149, 151, 153, 154, 163, 165
- C-SS** Chirp-Spread Spectrum. 6, 8, 96, 101, 104, 125
- CA** Cepstral Analysis. 5, 9, 61, 62, 65, 96, 130, 132, 133, 137, 138, 181
- CAVD** Covariance Absolute Value Detection. 172–174, 176
- CCD** Cepstral Covariance Detection. xiii, 7–9, 167, 170, 171, 173–176
- CFD** Cyclostationary Feature Detection. 19, 20, 33, 34
- CLT** Central Limit Theorem. 26, 48, 77, 79, 93, 100, 118, 149, 171
- CR** Cognitive Radio. 1, 2, 4, 5, 8, 12–15, 17–19, 21, 23, 29, 46, 48, 50, 55, 56, 58, 65, 66, 69, 90, 91, 97, 108, 109, 118, 126, 132, 134, 136, 137, 146, 170, 176, 181
- CSS** Compressive Spectrum Sensing. 21, 22, 38, 39
- DLSD** Differential Log Spectral Density. 7, 8, 131, 138–140, 142–146, 148, 153–158, 164, 165
- DS-SS** Direct Sequence-Spread Spectrum. x, 42–44, 58, 60, 67–73, 96, 98, 112, 114, 117, 118, 120, 131, 149
- ED** Energy Detection. x–xii, 19, 20, 27, 28, 32, 35, 42–44, 49, 55, 57, 58, 79, 82, 83, 92, 93, 118, 119, 122, 123, 163, 173, 175, 176
- EME** Energy with Minimum Eigenvalue. 32, 119, 123
- EVD** EigenValue-based Detection. ix, xii, 20, 31, 32, 118, 119, 122, 123, 171, 173, 176
- FFT** Fast Fourier Transform. 20, 25, 29, 34, 118, 124, 163, 175

- FH-SS** Frequency Hopping-Spread Spectrum. 6, 8, 96–98, 105, 121, 123, 125
- IID** Independent and Identically Distributed. 27, 28, 32, 77, 79, 82, 170, 173, 174
- IR-UWB** Impulse Radio-Ultra WideBand. xii, 8, 17, 118, 120–122
- MBSA** Multi-Band Spectrum Access. 5, 7, 8, 165
- MDW** Morlet-Derivative Wavelet. x, 49, 52, 54
- ME** Maximum Eigenvalue. 32, 33, 119, 122, 123, 171
- MFD** Matched Filter Detection. 19, 20, 29–31, 118, 120
- MLBS** Machine Learning Based Sensing. 19, 21, 36
- MM** Majorization-Minimization. 111, 125, 142
- MME** Maximum-to-Minimum Eigenvalue. 32, 119, 122, 123
- NBSS** NarrowBand Spectrum Sensing. 19, 23, 37
- NPL** Neyman-Pearson Lemma. 6, 24, 73, 167, 173
- OFDM** Orthogonal Frequency Division Multiplexing. 65, 118, 130, 161, 172
- PB-ACD** PassBand-AutoCespectrum Detection. xi, 5–8, 72, 73, 80–83, 90, 92, 93, 95, 96, 107, 114, 118–121, 125, 131, 149, 153, 165
- PC** Power Cepstrum. 7, 9, 64, 168–170, 173
- PCA** Principal Component Analysis. x, 55, 57, 58, 173, 176
- PDF** Probability Density Function. 75, 152, 153
- PN** Pseudo Noise. 102, 104, 105, 117
- PSD** Power Spectral Density. xi, 64, 69, 70, 73, 76, 82, 96–98, 102–105, 107, 114–116, 135–140, 145, 150, 151, 154, 164, 170, 173, 175
- PU** Primary User. x, 2, 4–7, 9, 16–18, 20, 21, 23, 24, 27, 28, 30, 32, 37, 42, 44, 48, 50, 54–56, 58, 65–69, 71, 72, 90, 91, 98, 116–120, 131, 134, 136, 138, 170, 173, 174
- ROC** Receiver Operating Characteristics. xi, 25, 27, 30, 79–83
- SBSA** Single-Band Spectrum Access. 5, 8, 118, 125, 165
- SDR** Software Defined Radios. 12, 13, 19

- SFH-SS** Slow Frequency Hopping-Spread Spectrum. xii, 98, 121–123
- SNR** Signal-to-Noise-Ratio. xi, 7, 9, 20, 27, 28, 39, 44, 55, 58, 61, 79, 81, 82, 91, 93, 114, 118–123, 125, 133, 138–140, 142, 144, 154, 160, 165, 173, 176
- SS** Spread Spectrum. 4, 6, 61, 66, 96, 109
- ST** Scattering Transform. 8, 12, 39, 40, 42, 44, 49, 53, 54, 58
- STD** Scattering Transform-based Detection. 42–44, 58
- SU** Secondary User. x, 2, 16–18, 20, 28, 42, 66, 67, 90, 91, 133, 134, 136
- TVD** Total Variation Denoising. 110, 111, 116, 125
- TVD-MM** Total Variation Denoising-Majorization-Minimization. xi, 6, 9, 114–116, 125, 126, 142, 156–158
- WBSS** WideBand Spectrum Sensing. 7, 19, 22, 37, 131–134, 137, 138
- WTMM** Wavelet Transform Modulus Maxima. 132, 142, 143, 154, 156–158
- WTMP** Wavelet Transform Multiscale Product. 132, 163
- WTMS** Wavelet Transform Multiscale Sum. 132, 154, 156–158



# LIST OF SYMBOLS

---

$H_0$	Null hypothesis
$H_1$	Alternative hypothesis
$y(t)$	The received signal at the CR receiver
$w(t)$	The imposed noise on the received PU signal
$\sigma_w^2$	The noise variance
$s(t)$	The transmitted PU signal
$h_s(t; \tau)$	The impulse response of a time-varying fading channel
$\tau$	A time lag
$L(y)$	The likelihood ratio
$p(y; H_0)$	The probability density function of the received signal under the null hypothesis
$p(y; H_1)$	The probability density function of the received signal under the alternative hypothesis
$P_D$	The probability of detection
$p(H_1 H_1)$	The conditional probability of deciding an occupied spectral hole while it is actually busy
$P_{FA}$	The false-alarm probability
$p(H_1 H_0)$	The conditional probability of deciding on the presence of a PU while it is actually idle
$P_{MD}$	The probability of miss-detection
$P_{CN}$	The probability of correct no-detection
$\mathcal{Y}(k)$	The FFT of the received signal
$\mathcal{T}_{ED}[\mathcal{Y}]$	The test statistic of the conventional energy detector
$y(n)$	The discrete time-domain signal
$\eta_{ED}$	The detection threshold of the conventional energy detector
$N$	The sequence length

$\gamma$	Signal-to-noise ratio
$\mathcal{T}_{MFD}[\mathcal{Y}]$	The test statistic of the matched filter detector
$\eta_{MFD}$	The detection threshold of the conventional MFD
$x_{MF}^*(n)$	The complex conjugate of the allocated pilot samples
$E_s$	The energy of the PU signal
$\eta_{EVD}$	The approximated detection threshold of the eigenvalue-based detector
$F_{app}^{-1}(\cdot)$	The approximated distribution function of the eigenvalue ratio
$R_y(t, \tau)$	The cyclic correlation function
$\alpha_c$	The cyclic frequency parameter
$S_y(\alpha_c, f)$	The spectral correlation function
$\mathcal{T}_{CFD}[\mathcal{Y}]$	The detection test statistic of the CFD
$Y(f)$	The spectrum of the received signal
$D_h$	A diagonal $N \times N$ channel gain matrix
$X_{n_s}(f)$	The spectrum of the $n_s^{th}$ signal
$W(f)$	The spectrum of the additive noise
$\mathcal{S}$	The set of subbands in a wideband spectrum
$r_f$	The $M \times 1$ measurement vector
$M$	An arbitrary integer describing a number of measurements or segments
$\Phi$	The $M \times N$ sensing matrix
$y_f$	The projection of the received signal in the frequency domain
$x_0(t)$	An arbitrary time-domain signal
$\phi(t)$	A low-pass filter of a time support $T$
$\psi(t)_{\lambda_s \in \Lambda_s}$	The wavelet function describing a band-pass filter
$\lambda_s$	The center frequency of the wavelet filter
$\psi_{\lambda_s}(t)$	A mother wavelet function
$\hat{\psi}_{\lambda_s}(\omega)$	The Fourier Transform of a mother wavelet function
$Wx_0$	The wavelet transform of a given signal $x_0(t)$
$S_{m_s c} x_0(t)$	The average of the signal $x_0(t)$ obtained by the low-pass filter $\phi(t)$
$Ux$	The scattering operator
$m_{sc}$	The decomposition order of the scattering network
$\mathcal{T}_{STD}(\mathcal{Y})$	The test statistic fo the STD technique

---

$y_{ST}(i_s)$	The $i_s^{th}$ scattering coefficient
$I_s$	Represents the number of the scattering coefficients
$\sigma_r^2$	The variance of the Rayleigh random process
$\sigma_{ST}^2$	The variance of the scattered signal under $H_0$
$a_T(t)$	The attenuation function describing the total channel impairments
$a_P(t)$	The attenuation function due to the path-loss
$a_S(t)$	The attenuation function due to shadowing
$a_F(t)$	The attenuation function due to multipath fading
$\bar{H}(f, t)$	The complex channel attenuation function due to fading
$i_p$	The multipath index
$l_{i_p}$	A signal fading transmission path
$\tau_{i_p}$	The arrival time of a copy of the transmitted signal along the path $i_p$
$c$	The speed of light
$a_{i_p}$	The attenuation factor of the path $i_p$
$\theta$	A Boolean parameter indicating the absence or the presence of PU
$n$	The discrete time index
$n_c$	The discrete time-shift
$x(n)$	An arbitrary discrete-time domain signal
$x_c(n)$	The analyzed complex discrete time-domain signal
$k$	The discrete frequency variable
$y_{eq}(n)$	The equalized received signal
$\hat{h}$	The estimated channel impulse response
$\psi_{MD}(n)$	The Morlet-Derivative function
$h(n; n_c)$	The discrete channel impulse response
$A_b(n)$	The baseband signal with phase of $\phi_s(n)$
$s(n)$	The discrete time-domain signal
$s_a(n)$	The analytic version of the discrete time-domain signal $s(n)$
$s_{a_r}$	The real part of the analytic signal $s_a(n)$
$s_{a_I}$	The imaginary parts of the analytic signal $s_a(n)$
$a_{n_c}$	The discrete time-domain representation of the path attenuation
$\tau_{n_c}$	The discrete time-domain representation of the path delay of the propagation channel

$N_l$	The number of propagation paths in the transmission medium
$\psi_M(t)$	The complex analytic Morlet function
$f_0$	An arbitrary sinusoidal frequency parameter
$\sigma_G$	Time spread of a Gaussian pulse
$\Psi_M(f)$	The spectrum of the Morlet wavelet function
$\psi_{MD}(t)$	Time-domain representation of the Morlet-Derivative wavelet function
$\psi_{MD}(f)$	Frequency-domain representation of the Morlet-Derivative wavelet function
$\Delta_f$	Frequency resolution of the Morlet function
$\tilde{A}(n)$	Complex envelope of the analytical signal $s_a(n)$
$a$	An arbitrary constant
$b$	An arbitrary constant
$k$	The discrete frequency-domain parameter
$Y(k)$	The spectrum of the noisy received in the discrete frequency-domain
$k_c$	The discrete frequency parameter of the carrier signal
$\omega_{sh}$	The angular frequency shift of the Morlet-Derivative wavelet function
$k_{ch}$	The frequency location of the discrete channel impulse response
$m_{ch}$	An integer multiple of $k_{ch}$
$k_\psi$	The maximum wavelet frequency
$D_W(k)$	The discrete spectrum of the filtered faded PU signal with the wavelet function $\mathcal{W}(k)$
$N_0$	Power spectral density of an AWGN signal
$G_E(f)$	Transfer function of the equalization filter
$H(k)$	The channel transfer function
$H^*(k)$	The conjugate of the channel transfer function
$\hat{n}$	The discrete quefrequency variable
$R_x(n_c)$	The discrete autocorrelation function of the signal $x(n)$
$X'(k)$	The first derivative of $X(k)$
$c_c(\hat{n})$	The complex cepstrum
$\log$	The natural logarithm
$X_c(\omega)$	The DTFT of the signal $x_c(n)$
$Z_c$	A complex quantity
$N_c$	The number of samples used to evaluate the complex cepstrum

---

$c_r(\hat{n})$	The real cepstrum
$N_r$	The number of employed samples to evaluate the real cepstrum
$c_p(\hat{n})$	The phase cepstrum
$c_{pc}(\hat{n})$	The power cepstrum
$c_a(\hat{n})$	The autocepstrum
$c_d(\hat{n})$	The differential cepstrum
$s(t)$	The transmitted PU signal
$A_s$	The carrier amplitude
$f_c$	The carrier frequency
$\theta$	The carrier signal phase at $t = 0$
$T_d$	Duration of a rectangular pulse
$d(t)$	The data modulating signal; a non-overlapping sequence of rectangular pulses of duration $T_d$
$p(t)$	The spreading waveform
$p_i$	one spreading pulse or <i>chip</i>
$T_c$	The chip duration
$R_s(\tau)$	The autocorrelation function of $s(t)$
$R_d(\tau)$	The autocorrelations of the data
$R_p(\tau)$	The autocorrelations of the spreading waveforms
$N_s$	The length of the m-sequence pseudo random spreading code
$m_s$	The degree of a chosen primitive polynomial
$T_{carr}$	The reciprocal of the carrier frequency
$x_P(t)$	The faded PU signal
$N_{carr}$	The number of samples corresponding to $T_{carr}$
$\mathcal{T}_1[c_a]$	The detection test statistic of the autocepstrum detector
$\eta_1$	The detection threshold of the autocepstrum detector
$\mathcal{K}(m)$	The cumulant generating function
$M_X(t)$	The moment generating function
$\Gamma(\cdot)$	The upper incomplete <i>gamma</i> function
$\mathfrak{K}_m$	The cumulant of order $m$
$\psi_d(\cdot)$	The <i>digamma</i> function

$\psi_p^{(1)}(x)$	The <i>polygamma</i> function
$\log -\chi_\nu^2$	The log-Chi squared distribution with $\nu$ degrees of freedom
$\sigma_z^2$	The variance of a random variable $Z$
$Z(\hat{k})$	The natural logarithm of the PSD of a PU signal
$f_{C_a}(c_a; H_1)$	The probability density function of the random variable $C_a$
$S_y(f)$	The PSD of the received signal
$F_R(r)$	The Cumulative Distribution Function (CDF) of the random variable $R$
$\alpha_E$	The scale parameter of the Exponential distribution
$\tau_s$	The sensing duration
$T_f$	The frame durations
$C_0$	The channel capacity of the SU signal under $H_0$
$C_1$	The channel capacity of the SU signal under $H_1$
$B_s$	The bandwidth of the SU signal
$SNR_s$	The SNR of the secondary link assuming point-to-point transmission in the secondary network
$P_s$	The received power of the SU signal
$P_w$	The noise power
$P_p$	The interference power measured at the CR receiver
$R_{avg}(\tau_s, \eta_1)$	The average throughput for the secondary network
$N_{sub}$	The number of subbands in a wideband spectrum
$h_{hop}(t)$	The hopping signal
$\phi_{h_i}$	The phase of a local oscillator
$s_{FH}$	The frequency-hopped transmit signal
$S_d(f)$	The PSD of the data signal before hopping
$H_{hop}(f)$	The PSD of the hopping waveform
$S_{FH}(f)$	The PSD of the transmitted FH-SS signal
$\mathcal{T}_2[c_a]$	The detection test statistic of the averaged autocepstral detector
$N_p$	The number of autocepstral peaks
$\eta_2$	The detection threshold of the averaged autocepstral detector based on the maximum ratio combing

---

$s_{c-ss}(t)$	A chirp waveform
$a_E(t)$	The envelope of the chirp signal
$\phi_{c-ss}(t)$	The chirp angle
$\Pi(t)$	A rectangular pulse shape
$T_p$	The duration of a rectangular pulse
$h_g(t)$	A complex Gaussian signal
$s_{PN-C}(t)$	A pseudo noise chirp signal
$c(t)$	The waveform of the PN-sequence
$\hat{\rho}_{R_y}(\tau)$	The fluctuations of the autocorrelation estimators
$F(\cdot)$	A representation of a functional
$\alpha_r$	The regularization parameter of the TVD-MM algorithm
$f_{s_N}$	The Nyquist's rate
$\mathcal{B}$	The bandwidth of a wideband spectrum
$r(t)$	The received wideband signal by the CR receiver
$s_{n_s}(t)$	The $n_s^{th}$ signal occupying the $n_s^{th}$ subband, $\mathcal{B}_{n_s}$
$S_r(f)$	The PSD of the observed signal $r(t)$ at the CR front-end
$a_{n_s}^2$	The PSD level in the $n_s^{th}$ subband
$\gamma_0(f)$	The relative PSD variations of the transmitted wideband signal to the noise
$f_{n_s}$	The location of $n_s^{th}$ spectral boundary
$D(f)$	The differential log spectral density function
$\mathcal{T}[\mathcal{A}]$	The test statistic of the DLSD peak detector
$\mathcal{A}[i]$	The $i^{th}$ peak value within the set of peaks of length $L_p$ points defined in the quefreny domain
$\eta_p$	The detection threshold of the edge detector
$B(t)$	A baseband signal
$O(t)$	The output of the CTF after applying Hilbert filtering
$\mathcal{K}_{cc}(\tau_e)$	The test statistic of the cepstral covariance detector
$\tau_e$	The time between two consecutive peaks in the power cespectrum of a digital signal
$\mathcal{T}[\mathcal{K}_{cc}]$	The test statistic of the cepstral covariance detector
$N_{cc}$	The number of cepstral covariance peaks
$\eta_{cc}$	The detection threshold of the CCD technique

*List of Symbols*

---

- $\mathbb{F}(\hat{f})$  The enhanced power cepstrum  
 $\hat{h}(f)$  A sinusoid shaping function

# MATHEMATICAL NOTATIONS

---

$(\cdot)^{-1}$	The inverse of a matrix
$\forall$	For all
$\in$	An element of
$*$	Convolution operator
$\mathbb{E}[\cdot]$	The ensemble average
$\text{erf}(\cdot)$	Error function
$\text{erfc}(\cdot)$	Complementary error function
$ \cdot $	The absolute value
$\mathcal{F}\{\cdot\}$	Fourier transform operator
$\mathcal{F}^{-1}\{\cdot\}$	Inverse Fourier transform operator
$\text{arg}[\cdot]$	The argument operator
$\mathbb{R}$	The set of real numbers
$\langle \cdot \rangle$	The averaging operator
$(\cdot)^H$	The Hilbert transform
$Q(\cdot)$	Gaussian-Q function
$Q_M(\cdot)$	Marcum-Q function
$\ \cdot\ _1$	$\ell_1$ norm of a vector
$\ \cdot\ _2$	$\ell_2$ norm of a vector
$\text{erfc}(jz)$	Complex complementary error function of the quantity $z$
$\text{erfi}(\cdot)$	The Faddeeva function
$\text{erfi}(\cdot)$	Imaginary error function
$Q(\cdot, \cdot)$	The regularized <i>gamma</i> function



# INTRODUCTION

---

## 1.1 Background

The spectral bandwidth is a valuable resource that needs to be sufficiently available in order to meet the growing demands for wireless services. The increased popularity of Internet-based data applications and the growth of the mobile data traffic have led to the problem of spectrum congestion. Indeed, a paradoxical situation has been introduced due to setting licensed frequency bands to specific cellular networks, where on one side, there is a spectrum scarcity due to the demand density, on the other side, there is an inefficient spectrum utilization. The evolution of the wireless technologies aims to fulfill the needs for higher data rates and the increased number of users. As a result, a major rethinking in the resource allocation policies led to a massive research activity in the concept of Cognitive Radio (CR). The CR technology, which is endowed with spectrum awareness, thrusts itself as a suitable candidate to solve the problem of the scarce radio resources. Such technology can be integrated with the next cellular wireless standards.

In 1999, Mitola *et al.* have proposed the concept of CR as a path breaking transformation in the radio technology [1]. They have provided the conceptual possibilities for improving the utilization of the heavily congested radio spectrum. Moreover, Haykin in [2] has defined a CR system as an intelligent wireless communication system that is aware of the surroundings, able to learn from them, and accordingly adapts its parameters to meet the users' needs. Also, he has discussed the emergent behavior of cognitive radios as well as the interference temperature as a new metric for interference quantification and management. Recently, the research is directed towards providing cellular wireless systems integrated with CRs. For instance, one of the primary goals of the Fifth Generation (5G) technology is to bring and interconnect wireless and wired systems with a large variety of services, which requires the cognitive capability of communication networks. While a little has been achieved so far for having a fully

CR system, and the practical deployment of a 5G-CR based system poses challenges in the network infrastructure which limits the integration between both technologies, the 5G New Radio (NR) standard allows for some basic spectrum sharing technologies [3], [4].

Despite the fact that the commercial 5G networks are currently hardly operational in some countries, this has not stopped engineers to think towards the Sixth Generation (6G) technology that is concerned with adaptivity, cognition, and resiliency of communication. This makes the CR approaches and concepts are good candidates to be realized in the next mobile communication standards. For this purpose, the first global summit on the 6G wireless standards was held in the beginning of 2019 to discuss some academic speculations about the possible potentials of 6G technology [5]. Further, the USA Federal Communication Commission has announced the opening of the terahertz wave spectrum, ranging from 95 GHz to 3 Tera-Hertz (THz), for experiments on next standards, as well as a full of a 21.5 GHz spectrum for testing of unlicensed devices [6]. Nevertheless, a possible 6G-CR based system could provide self-regulating mobile radios and also facilitate a seamless mobile convergence across different networks.

The CR networks encompass the opportunistic use of spectrum and the rights of users to transmit over such spectrum. Based on the ownership (license) of spectrum users, the users with the CRs desirous of opportunistic use of the spectrum are usually referred to as the SUs. On the other hand, the incumbent (licensed) users occupying the spectrum are referred to as the PUs. For example, this hierarchy is obvious in the operation of the SUs in the TV band while the PU is the television broadcasting companies in the licensed TV frequency bands. A secondary user could sense the spectrum and use a white band of frequencies in the television channel if it is idle. Another class of the users hierarchy may occur due to differences in the technology capability of the radio devices. Capable users are those who may have access to side information regarding the transmission of non-capable users. They exploit the side information to avoid interfering with the less capable users.

A key technology applying the CR concept is the Dynamic Spectrum Access (DSA) technology [7]. This technology uses the understanding-by-building methodology to learn from the environment, and hence corresponds to statistical variations by adapting its internal states in real-time to access the spectral resources dynamically. To apply DSA to a radio spectrum, a CR system must perform three main functions: spec-

trum sensing, spectrum analysis (e.g., channel estimation), and spectrum management. Through spectrum sensing, a CR system detects spectrum holes to decide on the presence of licensed users. This process must be done with high accuracy and in a short sensing time. The interplay among the system complexity, the detection accuracy, and the processing time which characterize a signal detector is demonstrated in Figure 1.1. Trade-offs among these factors have been addressed in many researches [8]. Due to its crucial role in providing a suitable spectrum for an unlicensed user transmission, several spectrum sensing algorithms have been formulated in the literature [9]. In general, spectrum sensing techniques can be categorized into spectrum sensing for spectrum opportunities and spectrum sensing for interference detection. The first category is concerned with allocating spectrum holes in a target spectrum in either non-cooperative or cooperative behaviors, whereas the sensing techniques of the second category are based on measuring a tolerable level of interference by the licensed users [10].

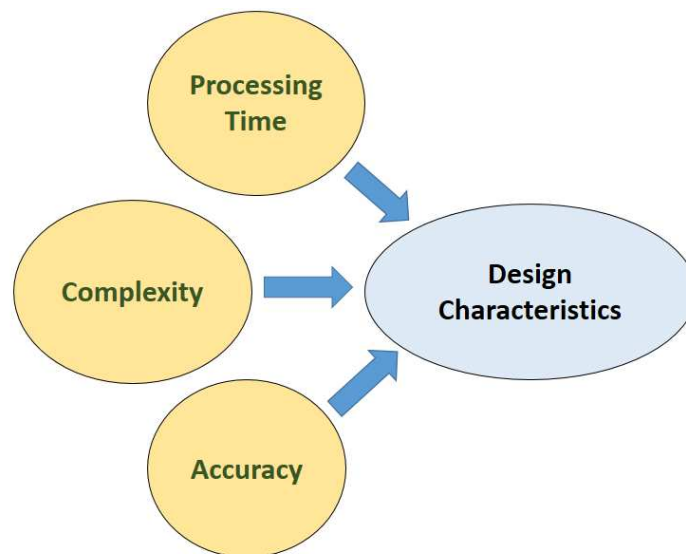


Figure 1.1 – The interplay among the system complexity, the detection accuracy, and the processing time

Since a complete reception process must involve both signal detection and channel estimation, the channel estimation process must be performed to learn the channel behavior and adapt the parameters of a CR system. For example, a pilot-assisted modulation has been proposed in [11] to detect the signal in fast fading channels with known pilot symbols. An illustration of channel estimation under the Bayesian ap-

proach in CRs is shown [12]. In the literature, challenges associated with spectrum sensing are addressed with suggested solutions on how sensing errors may affect the channel estimation decisions and vice versa. Basically, the research studies in [13] and [14] have considered the joint problem of the spectrum sensing and the channel estimation processes and illustrated the interrelation between them. They have also made some investigations on the dependence of different channel estimation schemes on the obtained sensing decisions. Essentially, this dependence reflects the importance of developing efficient spectrum sensing algorithms.

In fact, there are different factors that impose challenges on the spectrum sensing performance. These factors include the hardware complexity, the hidden PU problem, and the sensing duration and frequency [10]. For instance, in wireless applications, terminals are required to perform spectrum sensing with a high sampling rate, high resolution analog-to-digital converters with a large dynamic range, and high speed signal processors. This entails the increased hardware complexity and the longer time for processing. Also, the hidden PU problem occurs when a weak signal occupies a desired frequency band but it is undetectable by the CR receiver. This is either due to an obstacle, the transmission channel effects, such as multipath fading, or due to the noise-like nature of PU signals such as Spread Spectrum (SS) signals. This problem can be partially avoided if the hopping pattern is known and a perfect synchronization to the signal can be achieved. Nevertheless, licensed users can claim their frequency bands anytime while a CR is operating on their bands. So, in order to prevent any interference to/from licensed owners, a CR should be able to identify their activity as quickly as possible and should vacate the band immediately. This requirement poses a limit on the performance of sensing algorithms and creates a challenge for the design of a CR system.

## 1.2 Thesis Contributions

The main objective of the thesis is to develop means of enhancing the process of spectrum sensing in CR so as to provide more spectral opportunities, and hence increase the throughput of a secondary network. Among the previously mentioned challenges, we choose to tackle the detection problem of a hidden Primary User (PU). Our choice is motivated by the following reasons:

- Due to the noisy variations at the CR receiver, the detection errors may occur

due to falsely detecting the presence of a possible PU signal. False-alarms lead to the loss of potential spectral resources.

- A licensed user's signal may appear hidden at the CR receiver's side, if it naturally behaves like noise. For example, a SS signal with the Low-Probability-of-Intercept (LPI) property may cause the misdetection of the PU signal. This results in mistakenly declaring a vacant channel. In this case, the transmission of the CR user's signal will cause interference to the licensed user which will affect its Quality of Service (QoS).
- The detection of a hidden PU is a difficult task when detection is performed by a non-cooperative system. On the other hand, prior knowledge of the PU signal's features must be provided to facilitate the detection process, which is performed by a cooperative system.

Based on the aforementioned reasons, our target is to devise a robust spectrum sensing algorithm while operating in a non-cooperative detection scenario. Therefore, the important characteristic of the detection algorithm is to be able to exploit the distinguished features in a signal. The identification of hidden features of a target signal helps to differentiate between the signal of a significant user signal and the noise, which helps in mitigating the misdetection and false-alarm problems.

Remarkably, the concept of Cepstral Analysis (CA) has a strong impact on several applications comprising audio and speech processing, as well as mechanical systems [15], [16], [17]. In the literature, it has been employed in the fields of signal classification or features detection [18], [19]. Thus, the CA approach is used to identify certain features hidden in a signal that can be revealed in the cepstral domain. According to the variants of the CA approach, a certain CA variant is chosen in order to fit a specific application. That is why a researcher must be aware of the problem under analysis, and whether employing the CA approach will unleash significant details about the signal in the logarithmic domain. In our proposed work, we employed the CA approach to tackle the misdetection and false-alarm problems in the context of CR in the Single-Band Spectrum Access (SBSA) and the Multi-Band Spectrum Access (MBSA) approaches.

A summary of the research pillars by which we constructed our presented study is shown in Figure 1.2. Specifically, our main contributions are listed as follows:

1. Spectrum sensing algorithm for SBSA:
  - (a) A PB-ACD technique for detecting spread spectrum signals and its: we em-

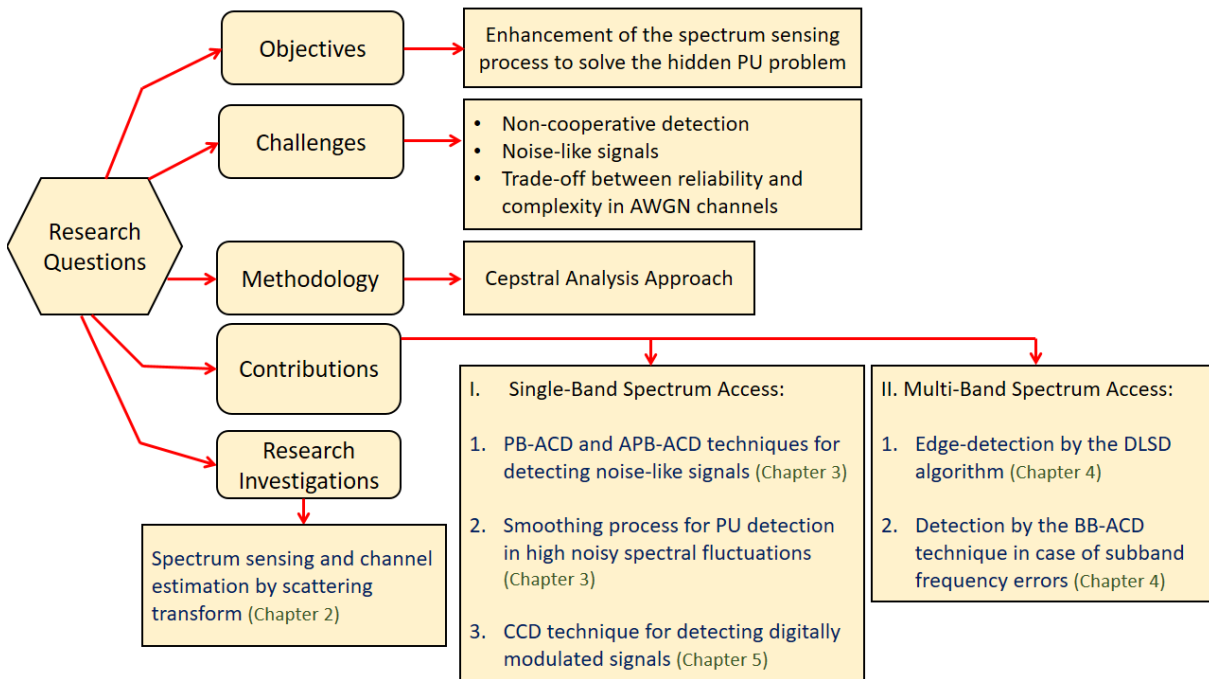


Figure 1.2 – A summary of the research pillars and contributions

ploy the proposed approach to detect a spread spectrum PU signal in the AWGN and the Rayleigh fading channels. The misdetection problem of a possible SS signal occupies a desired frequency band leads to erroneous sensing results. The blind theme of the proposed approach implies that no knowledge of the spreading code employed in a SS signal is provided to the CR receiver. The corresponding detection threshold is analytically computed. A theoretical analysis of the sensing-threshold-throughput trade-off of the PB-ACD technique is also introduced. Further, the distributions of the detection test statistic are derived under the null and the alternative hypotheses based on Neyman-Pearson Lemma (NPL). Also, the APB-ACD technique is introduced for detecting Frequency Hopping-Spread Spectrum (FH-SS) and Chirp-Spread Spectrum (C-SS) signals.

- (b) An improved PB-ACD by means of fluctuations smoothing: an improved PB-ACD technique is presented for detecting noise-like signals in AWGN. This is provided through a signal smoothing process in which the TVD-MM algorithm is employed to smooth to the fluctuations of the ACEs of the received signal to reduce the unwanted spectral fluctuations.

- (c) A generalized spectrum sensing approach for detecting digitally modulated signals by the CCD technique: the proposed CCD exploits the periodicity inherited in the Power Cepstrum (PC) of digitally modulated signals to detect their presence in a specific frequency band. By correlating the signals' PC to a sinusoidal signal having the fundamental frequency equal to the PC's periodic frequency, the signal component will be enhanced and the detector will simultaneously reject the noisy spectral variations that lead to possible false-alarms.

## 2. Spectrum sensing algorithm for MBSA:

- (a) Edge-detection technique by the Differential Log Spectral Density (DLSD) algorithm for WideBand Spectrum Sensing (WBSS): we propose the DLSD algorithm for the edge detection phase in order to detect the spectral boundaries within the wideband of interest. Also, we present a mathematical framework of the proposed algorithm under AWGN channels. An expression for the detection threshold of the proposed detector is derived according to its statistical properties. The simulation results have shown a superior performance of the proposed edge detection algorithm to different wavelet-based techniques at relatively low-to-medium noise power levels (i.e., at an average SNR over the range [0,6] dB). Used in conjunction with denoising, the proposed edge detector shows good detection results at high noise power levels (i.e., below an average SNR of 0 dB). The performance of the proposed algorithm is tested when impulsive noise is imposed.
- (b) Detection of a PU signal under the uncertainty of the subbands' center frequencies by the BaseBand AutoCepstrum Detection (BB-ACD) technique: the BB-ACD technique is formulated for detecting noise-like signals when there may be possible errors in the identified center frequencies of the intended subbands. The proposed BB-ACD consists of a circular topological filter followed by the autocepstrum detection. The circular topological filter utilizes the circular topology of a typical sinusoidal signal to separate the baseband signal or its squared version. The detection of a noise-like PU signal, or a conventional digitally modulated signal, by the PB-ACD technique depends on the presence of a strong peak appearing at a quefrequency<sup>1</sup> value

---

1. Quefrequency: It defines the inverse of the distance between successive log-spectral lines in a signal's cepstrum [20].

equivalent to the reciprocal of the center frequency of a certain subband. Due to the possible frequency estimation errors from the edge detection phase, the PB-ACD gives a poor performance. A mathematical analysis of the detection threshold is presented according to the statistical distribution of the devised detection test statistic. Through simulations, we provided comparisons of the BB-ACD technique with the PB-ACD technique to show the efficacy of the proposed technique when the problem of center frequency errors is encountered in frequency selective fading channels.

### 1.3 Thesis Organization

This thesis includes the presented research work in six chapters. First, the state-of-the-art techniques and a literature review are covered in chapter 2. Chapters 3 and 4 introduce the proposed detection techniques for the SBSA and the MBSA cases, respectively. The CCD techniques is discussed in chapter 5 and the conclusions with the future work are drawn in chapter 6. In particular, this thesis is organized as follows:

Chapter 2 reviews the state-of-the-art of the spectrum sensing techniques in CR systems. It covers the advantages and the disadvantages of these techniques and also it discusses the challenges facing the spectrum sensing process. Further, this chapter introduces the suggested spectrum sensing and channel estimation techniques through Scattering Transform (ST), and gives some insights about the obtained results, as well as highlighting the strengths and limitations of the proposed techniques.

Chapter 3 presents the proposed PB-ACD algorithm for detecting noise-like signals such as spread spectrum and IR-UWB signals. The proposed technique is considered for the SBSA scenario in which a specific CR receiver tests the availability of a narrow frequency band. A mathematical analysis of the proposed detector is formulated and its performance is compared with different state-of-the-art techniques. Moreover, The APB-ACD technique is presented for detecting FH-SS and C-SS signals and the mathematical demonstration of the proposed detection technique is introduced.

Chapter 4 discusses the two phases of wideband spectrum sensing, namely: the edge detection and the PU detection. In this chapter, we introduce the DLSD algorithm for

detecting the spectral boundaries of the intended subbands. The devised algorithm is compared to different wavelet-based edge detection techniques showing high detection performance at medium-to-high SNR values. Used in conjunction with denoising by TVD-MM algorithm, the edge detection is improved at a low SNR level. Moreover, we tackled the problem of detecting PU signal occupying a specific narrow frequency band when uncertainty of the subband's center frequency is encountered. For this purpose, we formulated the BB-ACD technique in which the periodicity inherited in the signal's PC in baseband.

Chapter 5 proposes the CCD technique to detect digitally modulated signals by evaluating the PC of the received signal and correlating it to a shaping function, which has a fundamental frequency equals to the PC's periodic frequency. The aim of employing a shaping function is to enhance the peaks that occur in the PC while simultaneously rejecting the noisy spectral variations.

Chapter 6 provides the conclusions of the presented research work and gives some prospects for further investigations related to the scope of the thesis, in which a dual spectrum sensing and channel estimation technique is suggested based on CA approaches, and also the role of employing Artificial Intelligence (AI) algorithms in cooperative sensing is discussed.



# STATE-OF-THE-ART

---

## 2.1 Introduction

In the last two decades, the world has witnessed a great growth in the global mobile traffic. This growth is expected to increase more in data volume by 2021 as compared to 2005 [21]. The trend of this exponential growth, as shown in Figure 2.1, is expected to even continue to 2030, as predicted by the International Telecommunication (ITU) [22]. Therefore, without making use of the unoccupied spectrum bands, the radio frequency becomes under-utilized. Indeed, as many academic research studies about the 6G technology is gradually taking momentum, scientific speculations claim that after 30 years of effort, 6G will eventually see the full potential of a Cognitive Radio (CR) system [23], [24].

In fact, the design of any wireless system must consider the transmission data rates, the geographical coverage area, the suitable transmission power, and the mobility of users. Generally, various communication systems can be classified into:

- High-power wide area systems (cellular systems), which support mobile users roaming over wide coverage areas.
- Low-power local area systems, such as cordless telephone systems.
- Low-power wide area systems, which are designed to support low data rate services such as paging systems.
- High-speed local area systems, which are designed to allow for high data rate services, such as wireless Local Area Networks (LANs).

Obviously, the first two classes are designed for voice applications, whereas the last two classes are designed for data applications. In the design and implementation of these systems, some challenges occur. Such challenges include radio resource allocation, management of the Medium Access Control (MAC) layer, the mobility management, Quality of Service (QoS), and security. A very important challenge is the radio resource allocation as well as the need for spectrum management in order to handle

the increase in the number of users. In this case, CR-based systems can provide the appropriate solution.

This chapter provides an overview on the CR concepts and tasks. It also reviews and compares the practical results of different spectrum sensing techniques employed for the radio-scene analysis process. Section 2.2 demonstrates the main tasks of CR systems and introduces the CR transmission paradigms. A literature review on different types of spectrum sensing techniques is presented in section 2.3 in addition to highlighting the challenges that limit their performance. Moreover, our research investigations and results on the applicability of the ST to be used in spectrum sensing and channel estimation are introduced in section 2.4 and 2.5, respectively. Finally, conclusions and important insights are summarized in section 2.6.

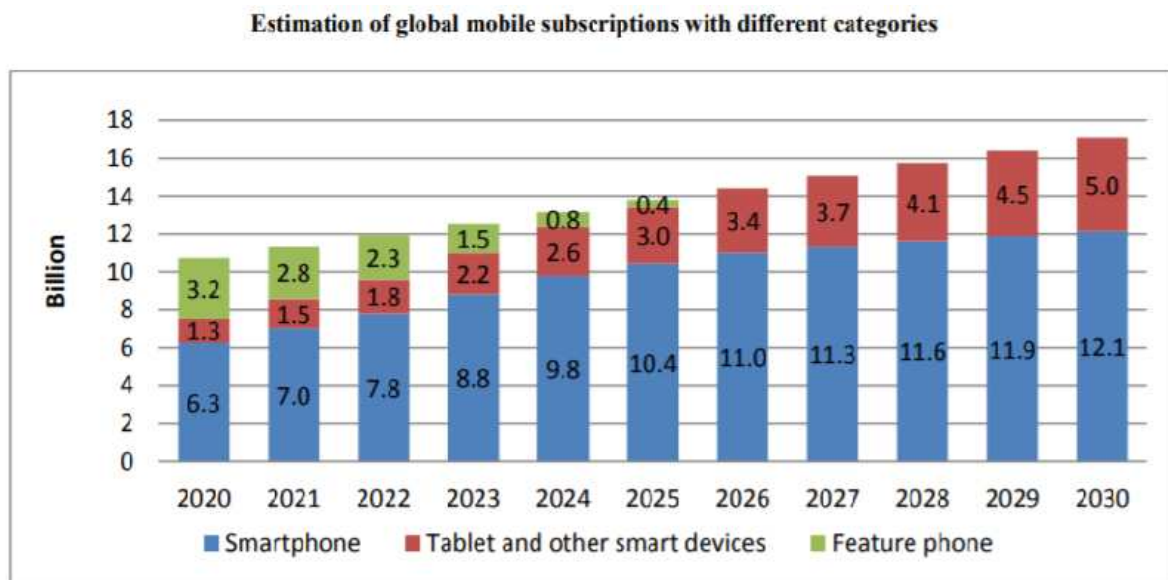


Figure 2.1 – The global estimation of the growth rate in subscriptions of mobile communications and electronic elements technologies (Source: Cisco) [24]

## 2.2 Overview On Cognitive Radios

At the beginning of 1990s, Joseph Mitola, a vice president and a distinguished professor at Stevens Institute of Technology, introduced the concept of Software Defined Radios (SDR). The motivation behind this concept was started over the past 20 years in order to design communication systems that involve a combination of software and

hardware systems away from pure hardware-based systems. SDR have a radio frequency with a software-controlled tuner. Signals are being processed using a reconfigurable device such as a Field-Programmable Gate Array (FPGA) or a digital signal processor. Therefore, their ability to reconfigure the modulation scheme makes them SDR. In his dissertation [25], Mitola introduced CRs as SDR with Artificial Intelligence (AI). These radios are capable of sensing and reacting according to changes in the surroundings. Simon Haykin also suggested another definition for a CR system in 2005. He defined it as "an intelligent wireless communications system that is aware of its surrounding environment and uses the methodology of understanding-by-building to learn from the environment and adapt its internal states to statistical variations in the incoming RF stimuli by making corresponding changes in certain operating parameters in real-time".

Figure 2.2 shows the internal structure of the conventional radios, the SDR, and the CRs. The spectrum licensing scheme set by the USA Federal Communications Commission (FCC) leads to an inefficient usage of the radio spectrum. When the radio spectrum allocated to licensed users is not used, it cannot be occupied by unlicensed users. Therefore, legacy systems have to operate only on a dedicated spectrum band and cannot adapt the transmission band according to the change in the environment. Due to the static spectrum allocation policy, spectrum holes arise; This is shown in Figure 2.3. Spectrum holes are frequency bands that are allocated to licensed users and are not utilized in all times and locations, therefore, they could be occupied by unlicensed users.

There are some limitations in the spectrum access due to the fixed spectrum licensing policy which can be mentioned as follows [26]:

- Fixed-type spectrum usage is designated.
- Spectrum access is prohibited for unlicensed users.
- There is a large chunk of licensed spectra for dedicated for a large communication region.

Consequently, the main objective of CR systems is to enhance the utilization of the radio frequency spectrum by sensing the target spectrum. Then, the information gained by the spectrum sensing device is exploited by the spectrum management function. Finally, the spectrum mobility unit will control the operation of spectrum changes and search for available spectral opportunities.

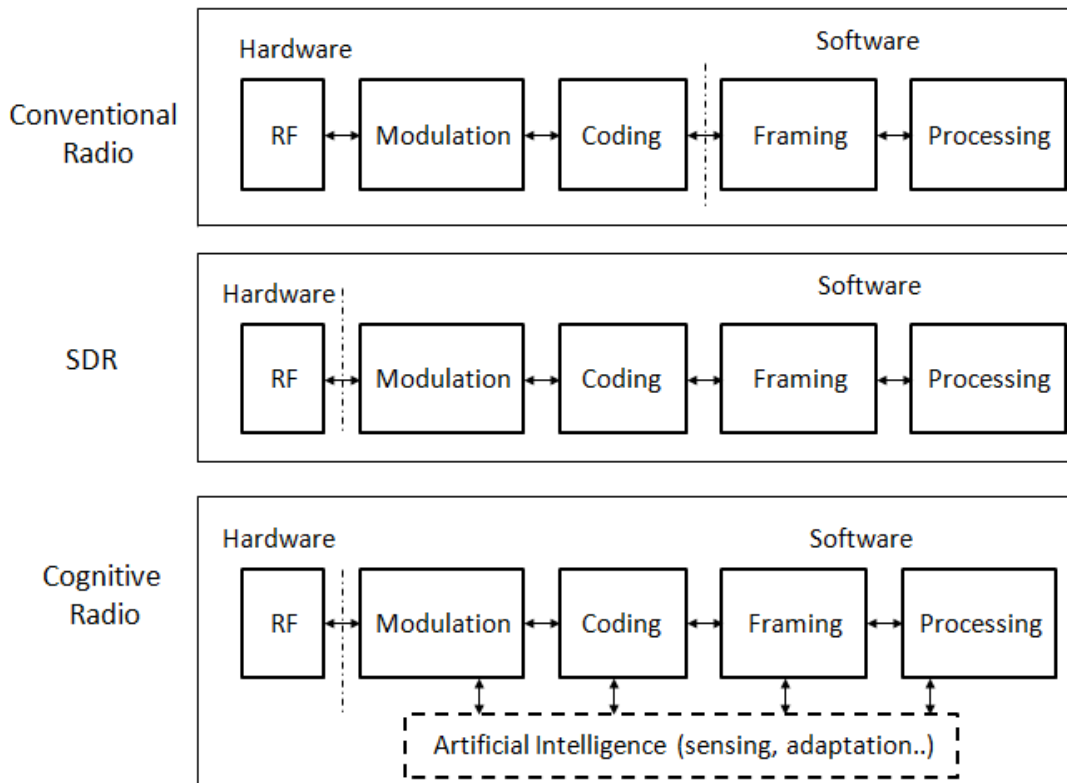


Figure 2.2 – A logical diagram that illustrates the differences among conventional radio, SDR, and CR [26]

### 2.2.1 Cognitive Capability of Cognitive Radio Networks

Multiple domains such as knowledge, model-based reasoning and negotiation can remark the cognitive capability of a CR system. Conceptually, any radio etiquette with different aspects, including RF bands and air interfaces, can be equipped with knowledge and reasoning tools. Remarkably, CRs are characterized by their agility that differentiates them from conventional radios. This agility is described by [27]:

- Frequency agility: it refers to the followed strategies to find the available spectrum which requires the design of good algorithms and protocols for appropriately selecting the transmission frequencies.
- Technology agility: it refers to operating a single radio device over various access technologies. It includes seamless interoperability which can be enabled by multiplatform radios that are realized as system-on-a-chip platforms and can operate as Bluetooth, WiFi, and GPS transceivers.

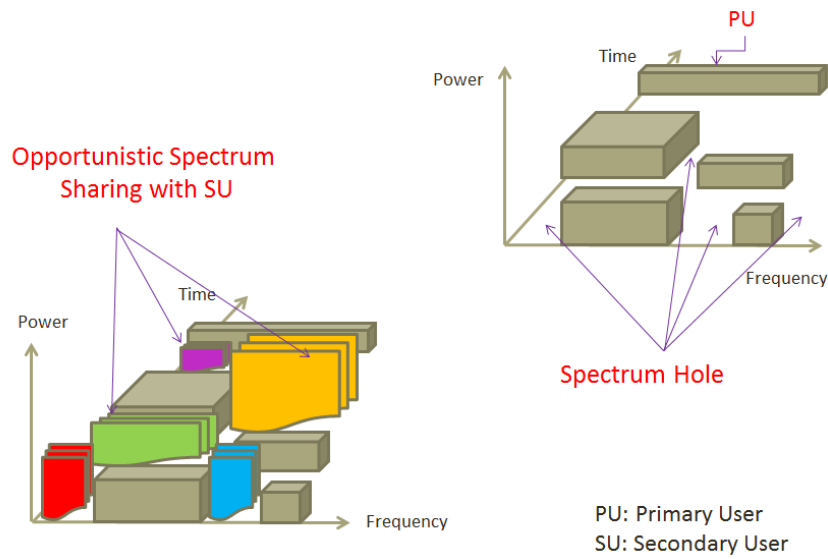


Figure 2.3 – An illustration of the opportunistic and the fixed spectrum sharing models in CRs

- Protocol agility: depending on the devices they connect with, CR devices contain a reconfigurable protocol stack so that they can proactively and reactively adapt their protocol.

Such cognitive behavior could extend to networks of radios so that they mimic human behavior in a civilized society. Eventually, this implies a framework that senses the surrounding conditions to identify opportunistic spectra.

## 2.2.2 Tasks of Cognitive Radio Systems

A typical cognitive radio system performs different tasks through a cognitive cycle by which it obtains the required information to reuse a specific frequency band. The distribution of these tasks and their interconnection to each other, illustrated in Figure 2.4, are summarized as follows:

- Spectrum sensing: the main objective of the spectrum sensing process is to measure the status of a target spectrum and the activity of a Primary User (PU). This is accomplished by a CR transceiver that detects a spectrum hole and the appropriate method of accessing it (i.e. duration, transmission power) without interfering with the PU signal.
- Spectrum analysis: information gained from the spectrum sensing process is then analyzed to get knowledge about spectrum holes (e.g. interference estima-

tion, availability duration, probability of collision with a PU according to sensing error). After that, a decision to access the spectrum is made by maximizing the throughput of the Secondary User (SU) while maintaining the interference caused to the PU below a required threshold.

- Spectrum access: this is performed on the MAC protocol layer to avoid collisions with a PU or with other SUs. The receiver must be synchronized with the transmitter in order to receive the signal successfully.
- Spectrum mobility: it is related to the changing on the frequency band. When a PU starts to access a frequency band that is occupied by an SU, the SU should switch to another frequency band that is idle. This change is called hand-off. Consequently, the protocol parameters at different layers in the protocol stack must be modified to match the new frequency band. Further, this hand-off mechanism must ensure that the data transmission by the SU can continue in the new band.

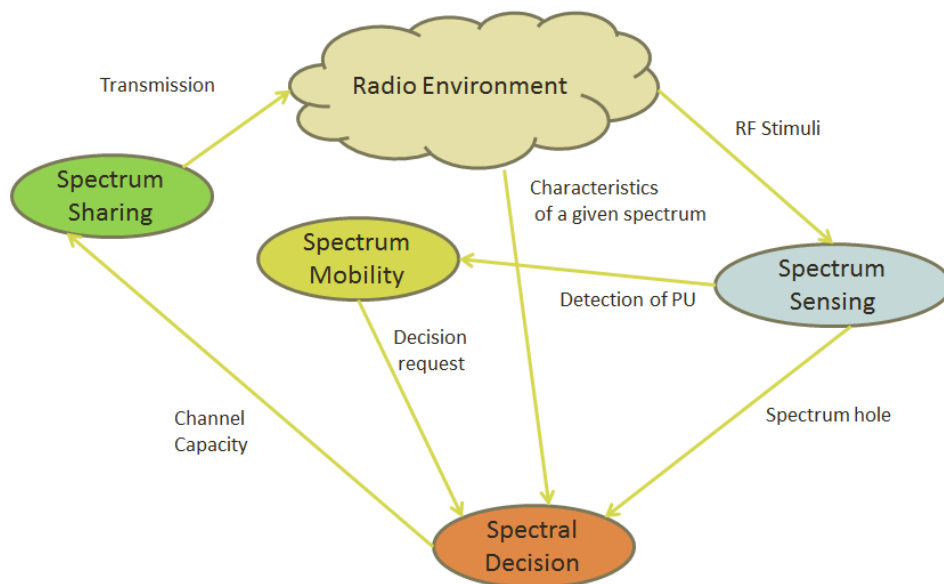


Figure 2.4 – Different tasks of a cognitive radio system

### 2.2.3 Cognitive Radio Paradigms

The definition of cognitive radio systems has evolved over the years to include different paradigms (i.e., spectrum sharing models). These paradigms, compared in Table 2.1, are classified into the following paradigms [27]:

Table 2.1 – Comparison between the cognitive radio paradigms

Terms	Interweave	Underlay	Overlay
<b>Description</b>	Transmits for idle status	Simultaneous transmission with PU is allowed	Simultaneous transmission with PU is allowed
<b>Side Information</b>	PU activity	Channel strengths affecting PU	Cooperative system, knowledge of PU message and channel is required
<b>Power Level</b>	Transmits at any level for idle status	Limited by interference constraint	Limited by interference constraint
<b>Restrictions</b>	False-alarm; transmission ceased if PU presents	Limited to short-range applications	Network complexity

- 1- **Interweave Paradigm:** the idea of an opportunistic communication model was the original purpose for formulating the concept of a CR system which is so called later as an interweave CR system. In this model, the CR system has to monitor periodically the radio spectrum and detect the activity of possible PUs in different parts of the spectrum; Then, it allows communication over spectrum holes (i.e., temporary space-time-frequency voids) and ceases transmission once a PU activity is declared.
- 2- **Underlay Paradigm:** in this model, it is mandatory that the concurrent cognitive/non-cognitive transmission may be established if only the generated interference by the SUs at the PUs receivers does not exceed a pre-defined threshold. This can be satisfied by using multiple antennas to guide the SUs signals away from the PUs signals. Further, the interference constraint could be met by spreading the SU signal over a wide bandwidth below the noise floor and then despread it at the CR receiver. Examples of the signal spreading include Spread Spectrum (SS) and IR-UWB communications.

2- **Overlay Paradigm:** in overlay-enabled systems, knowledge of the PUs' codebooks and their messages must be provided at the CR receiver. For example, if the non-cognitive users follow a uniform communication standards based on a publicized codebook, this information could be easily obtained and hence could be utilized in different ways. On the one hand, this information can be exploited to cancel the interference caused by the PUs at the SUs receivers. On the other hand, the CR users can assign part of their transmission power for their communication and the remainder is to assist (i.e., relay) the PUs transmission.

## 2.2.4 Cognitive Radio Bands

The propagation environment of CR networks must be well understood in order to design these networks efficiently. The knowledge of the propagation characteristics will help in the design, implementation, and analysis of different transmission strategies. The amount of interference that may be imposed on the PU signal must be kept in mind as an important feature affecting the CR system design. The interference level depends on the transmission power of the CR as well as the characteristics of the wireless propagation channel. Cognitive radios may operate over a wide range of the frequency spectrum. The bands below about 3.5 GHz have a lower propagation loss and are sought after by all services. Therefore, these bands are ideal candidates for the deployment of cognitive radio networks but not necessarily exclusive. They have different primary systems, each with its service type, architecture, bandwidth, and tolerance to interference. Some candidate frequency bands for CR systems are mentioned below [28]:

- *UHF bands:* these bands are currently used by the broadcast television. Terrestrial broadcasting transmitters tend to have high antennas (hundreds of meters) and large powers (kilowatt range). In this service, the transmission is one-way, the transmitting antenna may be outside the area containing the cognitive radios and the TV customers are generally fixed. In 2010, the US FCC adopted rules to allow unlicensed radio transmitters to operate in the broadcast television spectrum at locations where the spectrum is not being used by the licensed services. We find that the IEEE 802.11af, IEEE 802.22 and IEEE 802.19.1 are operating over TV white spaces (54 to 60 MHz, TV channel 2; 76 to 88 MHz, TV channels 5 and 6; 174 to 216 MHz, TV channels 7 to 13; 470 to 608 MHz, TV channels 14 to 36;

and 614 to 698 MHz, TV channels 38 to 51). The unused TV spectrum can be used as white spaces.

- *Cellular bands*: typical cellular bands are centered near 800/900 MHz, 1.8/1.9 GHz, 2.1 GHz, 2.3 GHz, and 2.5 GHz. Cellular networks have wide coverage, with cell site antennas mounted at rooftops of buildings. This is a two-way service, with the cell sites generally in the same region as the cognitive radios, and the cellular customers can be mobile.
- *Fixed wireless access bands*: these bands provide two-way broadband service. They are centered near 2.5 and 3.5 GHz. Fixed wireless systems are similar to cellular networks in layout, with the customers located at fixed locations, such as companies and homes.

## 2.3 Literature Review on Spectrum Sensing Techniques

The broad definition of a vacant opportunity comes in terms of an idle frequency band, a time slot, a geographical area, a code dimension, or the angle-of-arrival of a signal. Many investigations on spectrum sensing techniques have focused in exploring vacant frequency bands.

Different spectrum sensing techniques have been introduced over the last decade. Based on the scanned bandwidth of the target frequency range, these techniques can be classified into NarrowBand Spectrum Sensing (NBSS) and WBSS techniques. In the NBSS approaches, a CR system scans only one frequency band, whereas in the WBSS approaches a number of sub-channels are scanned, either simultaneously or sequentially. In the literature, several NBSS algorithms and techniques have been formulated. These techniques include ED, Matched Filter Detection (MFD), covariance-based detection, Cyclostationary Feature Detection (CFD), and Machine Learning Based Sensing (MLBS) [9].

Due to its calculation and implementation simplicity, ED has been used extensively in the literature. In the design of an energy detector, there must be an accurate modeling of the detection test statistic, and also a prior knowledge of the noise power is required at the CR receiver. Regarding the estimation of the noise power, an experimental study is covered in [29] in which a practical realization of energy detectors by SDR is introduced. In the proposed study, it has been shown that an inaccurate modeling of the detectors test statistic leads to a deterioration in the detection performance.

For this purpose, the authors of [30] have proposed a histogram-based method to determine the detection threshold when a large sample size is sufficiently collected. From the observed samples, two histograms are obtained to indicate the presence or absence of a possible PU signal. This detection threshold is chosen to fit certain false-alarm and misdetection probabilities. However, in noisy and fading environments, the detection of PUs becomes a difficult task [31]. This gives the existence of the SNR wall phenomenon, which is the SNR value below which all the detectors will fail to detect the presence of a signal even for large channel observations [32]. This phenomenon has been mathematically validated through mathematical modeling in [33]. In order to provide an accurate prediction of the SNR wall constraints, the authors in [34] have introduced a prediction method to estimate the noisy variations as well as the Rayleigh fading coefficients. Moreover, theoretical analysis of energy detection that is based on a dynamic selection of the detection threshold is given in [35].

A suitable alternative approach to the energy detector is the matched filter detector which is described to be the optimum detector that maximizes the SNR in Additive White Gaussian Noise (AWGN) channel [36]. Since the MFD technique requires prior knowledge of the PU's signal parameters, which is not feasible practically, a blind estimation technique is proposed in [37] to extract the signals parameters. However, the pre-processing offered by the blind parameter estimator increases the detector complexity and the sensing time as well. Another approach is presented in [38] to increase the sensing efficiency of the MFD by introducing a dynamic selection of the detection threshold. On the other hand, the covariance-based detection techniques offer a blind approach for the PU detection that is based on calculating the covariance matrix of the received signal. By exploiting the correlation of the signals samples, the detector uses this characteristic to distinguish between the noise and the signal. Different techniques have been developed based on the covariance-based detection such as the EVD [39].

A superior sensing technique than ED, MFD, and the covariance-based detection is offered by the CFD approach, in which the inherited cyclostationary features in a PU signal is revealed and utilized for the signal detection. In [40], the authors have evaluated the performance of the cyclostationary detector for different modulation schemes. Also, the authors in [41] have shown the employment of the cyclostationary Fast Fourier Transform (FFT) Accumulation Method (FAM) to tackle the problem of hidden SUs signals and in order to improve more users recognition. To improve the detection performance of the CFD, the authors in [42] have shown the effect of employ-

ing various windowing functions such as rectangular and Kaiser window functions on the detection probability.

As the nowadays trend is guided to employing the MLBS approaches in the signal detection, many research studies have found applications in the context of CR by developing MLBS techniques [43]. Formulated as a classification problem, a MLBS detector decides on the states of a specific frequency band using either a supervised or unsupervised learning techniques. This kind of detection uses different features such as the energy statistic or the probability vector to determine the availability of a channel. Accordingly, several investigations have been carried out on how to apply the MLBS techniques in the spectrum sensing process. For instance, the authors of [44] propose the use of the K-means algorithm and the Support Vector Machine (SVM) method to formulate a spectrum sensing model. Precisely, the model applied the K-means algorithm at the beginning of the sensing process find the transmission patterns of the PUs, then the SVM method is used to decide on the presence or absence of the PU signal. Also, ML has been proposed by the authors of [45] for Compressive Spectrum Sensing (CSS). The proposed algorithm is formulated to estimate the sparsity level and this allows the selection of a suitable number of measurements for an accurate signal recovery. Nevertheless, the MLBS techniques have been involved in optimizing the detection decision in cooperative sensing in CR networks [46].

For WBSS, the wide spectrum of interest is usually divided into a number of subbands, then the sensing process is performed, either sequentially or simultaneously, by employing a suitable NBSS algorithm. Sequential sensing approaches require a longer processing time and also a high energy due to using high-rate ADCs. For timely communication, such approaches are inefficient and also costly. On the other hand, parallel or simultaneous sensing is faster but requires a large number of sensors and synchronization which impose a high implementation complexity. CSS is considered as a way forward to decrease the acquired number of samples [47]. For this purpose, a number of studies have shown that most of the subbands comprising a wide spectrum are rarely utilized or not at all. In this case, the wideband spectrum signals can be considered sparse. This characteristic has encouraged a wide area of research to investigate more about CS or the sub-Nyquist techniques to speed up the WBSS process [48], [49]. In CSS, the original sparse signal is recovered only from a number of few measurements. To apply CSS, three main operations must be included: the sparse signal representation, the coding with the measurement matrix, and the sparse recovery.

Essentially, the sparsity level, the measurement matrix and the choice of the decoding technique affect the optimal number of samples. In [50], the authors have investigated on the estimation of the sparsity level and modify the number of measurements accordingly. Nevertheless, other authors have introduced the blind CSS approach in which no prior knowledge of the sparsity level is required. More discussions on the WBSS approaches are presented in chapter 4.

Many problems may face an unlicensed transmitter. For example, it may not always be able to detect the signal of a licensed transmitter due to channel impairments and its geographic location. In other words, the licensed user may be out of range. This causes interference with the receiver of the licensed user. This problem is called the hidden node problem. Cooperative sensing techniques may solve this problem. In cooperative sensing, the spectrum sensing information from multiple secondary users is exchanged to reach the optimum decision of detecting the presence of primary users. This is accomplished by two different networks, namely, a sensor network and an operational network. First, a sensor network collects some information about the presence of PUs. Second, a spectrum usage map is created distributed to the operational network of secondary users for optimizing the spectrum access. Using this technique, the detection probability can be improved in multipath scenarios. On the other hand, computation overhead is a disadvantage as compared with non-cooperative sensing.

Cooperative sensing has been suggested to solve the hidden terminal problem. The studies in [51] has discussed cooperative sensing as an optimization problem, such that optimizing the decision fusion under the Neyman-Pearson and the Bayesian criteria, as well as deciding on the optimum number of cooperative user or performance improvement. In [52], the performance of cooperative sensing in fading channel has been compared to a single node detection. Also, analytical expressions for the average detection probability under different detection scenarios such as the single node detection, the diversity reception, and the cooperative spectrum sensing in fading channels have been derived in [52]. In these studies, the selection of the detection threshold is considered as fixed. In [53], dynamic selection of detection threshold according to the noise level variation has the high probability of detection. As a summary, Figure 2.5 illustrates the classification of the different spectrum sensing techniques.

In the light of the recent research studies, this section provides an overall survey of the popular spectrum sensing techniques, and also introduces the recent advances in this field. We also highlight the efficiency and limitations of these techniques as

reviewed in the literature. Further, we present a demonstration of the detection performance of some of the aforementioned techniques through simulations.

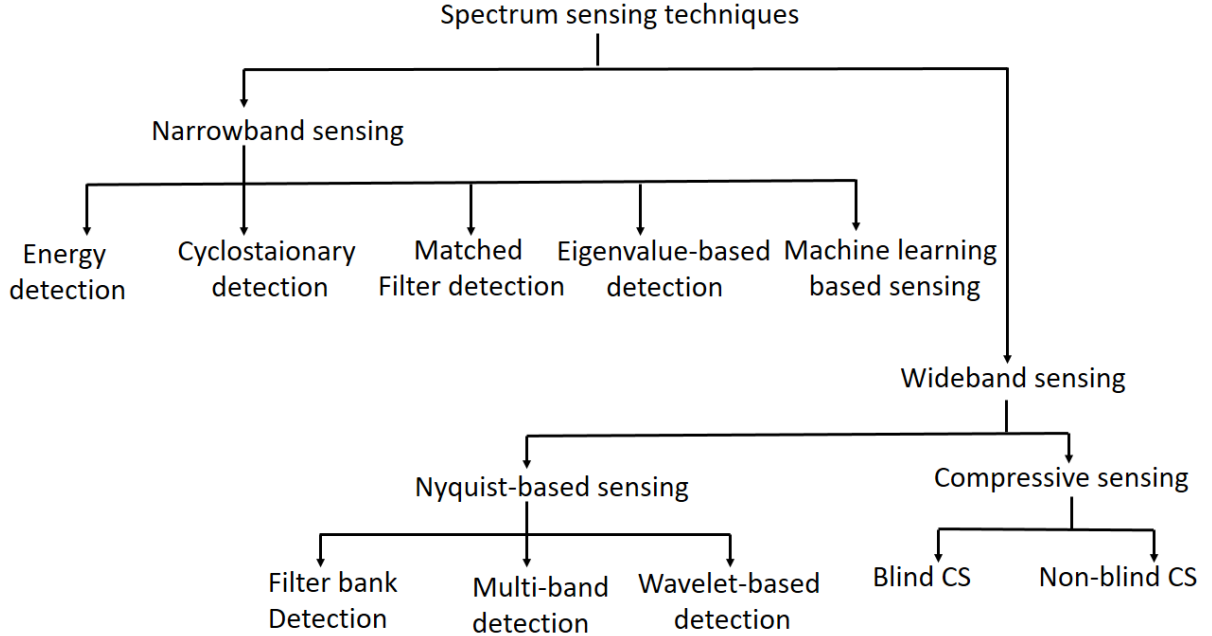


Figure 2.5 – The hierarchy of spectrum sensing techniques as classified based on the type of the accessed spectrum model

### 2.3.1 NarrowBand Spectrum Sensing

Hereinafter, we discuss the different classes of NBSS techniques in CR. We introduce a description of the mathematical model, the advantages and the disadvantages of these techniques. In our work, we apply the interweave CR paradigm in which a CR user is allowed to access a licensed frequency band when its idle. A demonstration of how an interweave CR works is shown in Figure 2.6. In general, the detection problem of a PU signal can be presented as a binary hypothesis testing. In such formulation, the null hypothesis, denoted by  $H_0$ , refers to the absence state of the PU signal, where the alternative hypothesis, denoted by  $H_1$ , refers to the presence of a PU signal in the licensed spectrum. The received signal at the CR receiver can be defined as [54]:

$$y(t) = \begin{cases} w(t) & : \text{Under } H_0 \\ x(t) + w(t) & : \text{Under } H_1 \end{cases} \quad (2.1)$$

where  $w(t)$  is the thermal noise imposed on the received PU signal that can be modeled as a Gaussian distributed process with a variance  $\sigma_w^2$ . The faded PU signal is given by:

$$x(t) = s(t) * h_s(t; \tau) \quad (2.2)$$

where  $s(t)$  is the PU transmitted signal,  $*$  denotes the convolution operator, and  $h_s(t; \tau)$  is the sensing channel that is generally described as a time-varying fading channel with a time lag, denoted by  $\tau$ .

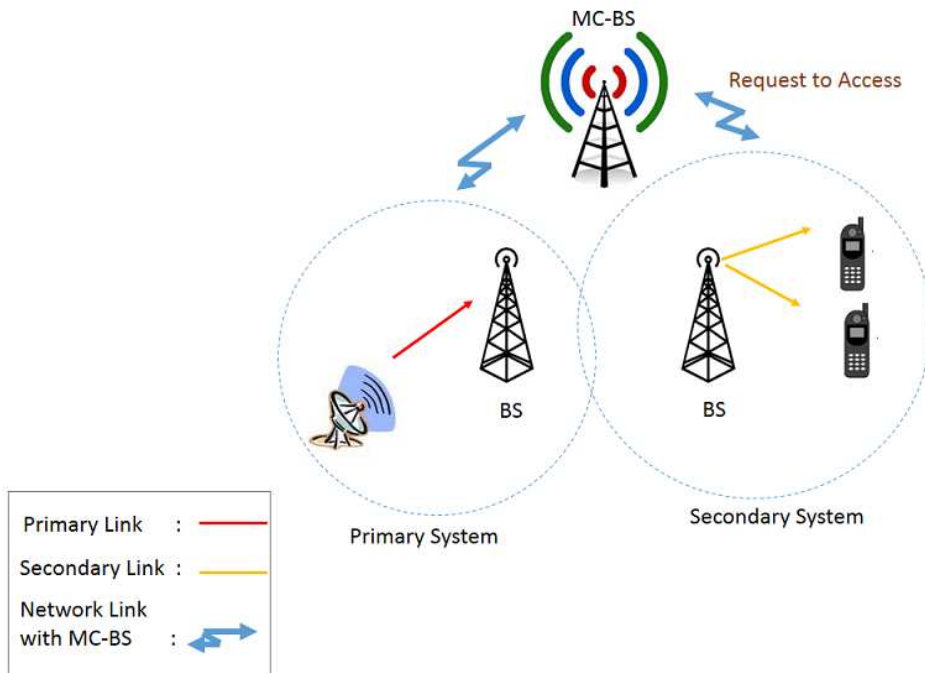


Figure 2.6 – A demonstration of a typical operation of an interweave CR system

In a spectrum sensing process, the sensing threshold is an important design parameter of any signal detector. Indeed, a detector with a non properly adjusted threshold leads to a degraded sensing performance. Based on an appropriate selection of a detection threshold, the sensing decision is made. It means that the choice of the detection threshold reflects the offered accuracy of any spectrum sensing algorithm. Based on the NPL, a detector decides  $H_1$  if the likelihood ratio  $L(y)$  is greater than a threshold  $\eta$ . The likelihood ratio is given by [54]:

$$L(y) = \frac{p(y; H_1)}{p(y; H_0)} \quad (2.3)$$

where  $p(y;H_1)$  and  $p(y;H_0)$  denote the probability density function of the received signal under the alternative and the null hypotheses, respectively. To evaluate the detection performance of the spectrum sensing techniques, an important metric is considered which is the ROC curve. It evaluates the detector performance in terms of the following metrics:

- The probability of detection,  $P_D$ : it describes the probability of the SU to declare the presence of a PU signal. It is given in terms the conditional probability  $P_D = p(H_1|H_1)$  of deciding an occupied spectral hole while it is actually busy.
- The false-alarm probability,  $P_{FA}$ : it describes the probability of deciding on the presence of a PU in a spectral hole while it is actually idle. It is given in terms of the conditional probability  $P_{FA} = p(H_1|H_0)$ .
- The probability of miss-detection,  $P_{MD}$ : it describes the probability of a miss-detected target while the detector declares a spectral hole. It is given in terms of the detection probability as  $P_{MD} = 1 - P_D$ .
- The probability of correct no-detection,  $P_{CN}$ : it describes the correct probability of having a spectral hole, which is given by  $P_{CN} = 1 - P_{FA}$ .

### Energy Detection

The detector computes the energy of the received signal by the CR user and compares it to a threshold. If the computed energy exceeds the decision threshold, the PU is considered present; otherwise, the channel is considered idle. Figure 2.7 shows the block diagram of the conventional energy detector that calculates the energy as the squared magnitude of the FFT averaged over the number of samples of the received signal. The test statistic of the ED is given by:

$$\mathcal{T}_{ED}[\mathcal{Y}] = \frac{1}{N} \sum_{k=1}^N [\mathcal{Y}(k)]^2 \underset{H_0}{\overset{H_1}{\gtrless}} \eta_{ED} \quad (2.4)$$

where  $\mathcal{Y}(k)$  denotes the FFT of the received signal represented in the discrete time domain as  $y(n)$ , and  $\eta_{ED}$  denotes the detection threshold of the Energy Detection (ED) technique. The value of the detection threshold depends on the noise variance. Thus, the detection performance is affected by the appropriate selection of  $\eta_{ED}$ .

Despite its simplicity, the ED technique cannot distinguish between the noise and the PU signal. That is why the detection decision is subjected to a high uncertainty

and results in a low detection performance in low SNR values, as shown in [31]. The two performance metrics ( $P_D, P_{FA}$ ) can be evaluated using the Central Limit Theorem (CLT)<sup>1</sup> when the sample size  $N$  of the observed signal is large enough to approximate the test statistics as Gaussian random variables [55]. For the conventional ED, these two probabilities are given by [54]:

$$P_D = Q\left(\frac{\eta_{ED} - N(1 + \gamma)}{\sqrt{2N(1 + \gamma)^2}}\right) \quad (2.5)$$

$$P_{FA} = Q\left(\frac{\eta_{ED} - N\sigma_w^2}{\sqrt{2N\sigma_w^4}}\right) \quad (2.6)$$

where  $\gamma$  is the SNR, and  $Q(\cdot)$  is the Gaussian Q-function that describes the tail probability of the normal distribution with zero mean and unit variance which is given by [54]:

$$Q(x) = \frac{1}{\sqrt{2\pi}} \int_x^\infty \exp\left(-\frac{t^2}{2}\right) dt. \quad (2.7)$$

consequently, the detection threshold is expressed in terms of a target  $P_{FA}$  as follows:

$$\eta_{ED} = \sigma_w^2 \left( Q^{-1}(P_{FA} \sqrt{2N} + N) \right) \quad (2.8)$$

Based on equation (2.8), the sensing threshold of the energy detector depends on the noise power, thus it is sensitive to the noise uncertainty. Figure 2.8 demonstrates the relation between the false-alarm probability and the detection threshold as a function of the number of samples of the observed signal as indicated in equation (2.6). At a specific detection threshold, as the number of samples increases, the probability of

---

1. CLT states that when a large number of independent random variables are added, their normalized sum tends toward a normal distribution even if the original variables themselves are not normally distributed.

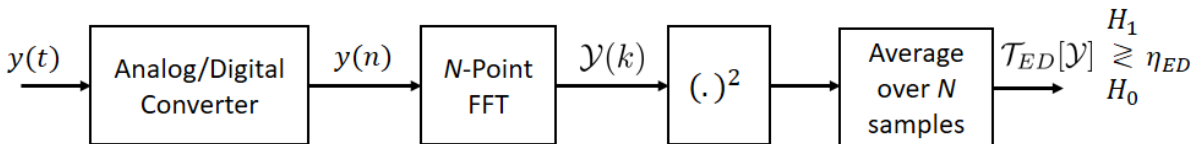


Figure 2.7 – The block diagram of a conventional energy detector

falsely declaring a PU increases assuming the PU signal is a complex Gaussian signal. Further, another example is illustrated in Figure 2.9 showing the detection probability of a conventional ED for detecting Independent and Identically Distributed (IID) signals [8]. At certain SNR levels, the detection probability increases as  $P_{FA}$  increases. As mentioned previously, a simple figure of merit to describe the performance of an energy detector is given in terms the ROC curve – a plot of the  $P_D$  against  $P_{FA}$  as the threshold varies from 0 to  $\infty$ . An example of the ROC curve of an ED is shown in Figure 2.10 for different SNR values. The analysis is carried out based on the work of Y. Liang *et al.* in [8] for detecting Gaussian-like PU signals. To improve the detection performance of ED, several approaches have been proposed using dynamic thresholds. For example, the authors of [56] addressed the selection of the threshold by using a constant false-alarm rate method.

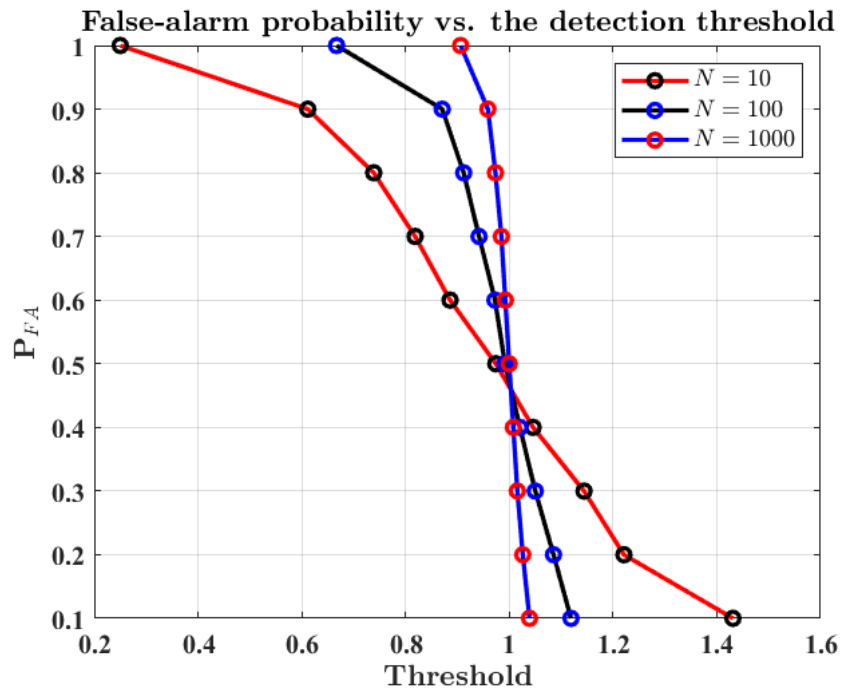


Figure 2.8 – The interplay between the false-alarm probability and the detection threshold of a conventional ED for different sample sizes [8]

This method consists of bounding the probability of false-alarm and then iteratively updating the value of the threshold to maximize the probability of detection. Also, a Discrete Fourier transform (DFT) filter bank method to dynamically select the threshold that minimizes the spectrum-sensing error in the presence of noise is proposed in

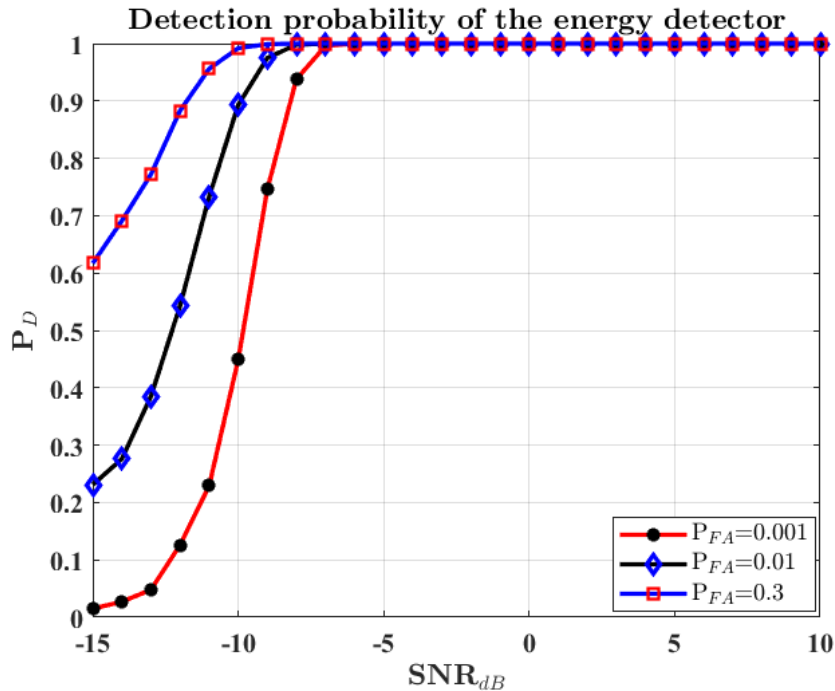


Figure 2.9 – The detection probability of a conventional ED for detecting IID signals [8]

[57]. The double-threshold technique is introduced in [58] to deal with the noise uncertainty. Although this double-threshold algorithm decreases the collision between the PU and the SU signals, its detection performance is not guaranteed for low SNR values, and its sensitivity to noise uncertainty is very high.

### Matched Filter Detection

Matched filtering is known as the optimal method for the detection of PUs when the transmitted signal is known. It is a linear filter designed to maximize the output SNR for a given input signal. It is obtained by correlating a known signal, with an unknown signal to detect the presence of the known signal in the unknown one. This is equivalent to convolving the unknown signal with a time-reversed version of the signal. Convolution is at the heart of matched filters. Convolution does essentially with two functions that it places one function over another function and outputs a single value suggesting a level of similarity, and then it moves the first function an infinitesimally small distance and finds another value. The end result comes in the form of

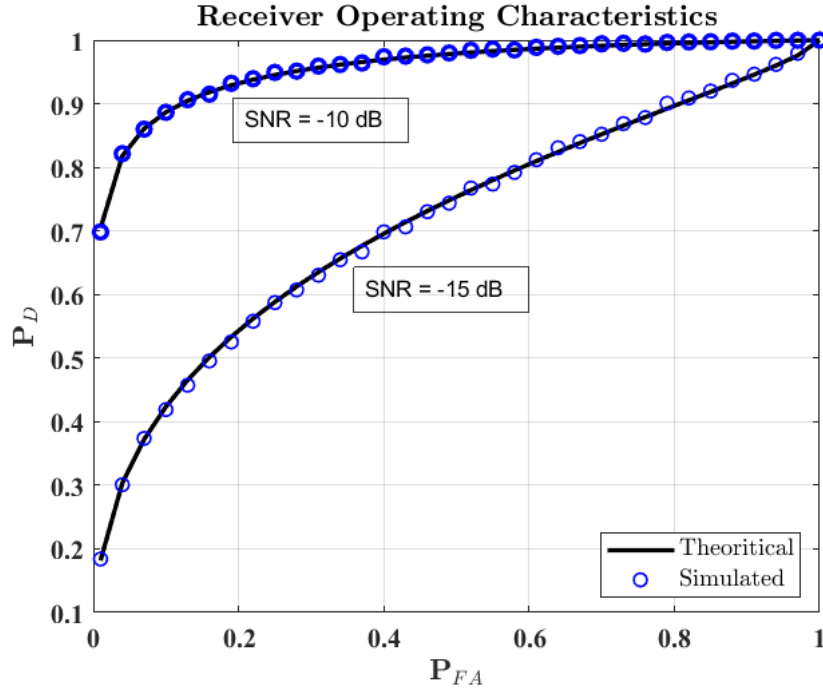


Figure 2.10 – The receiver operating characteristics of an energy detector in case of a Gaussian PU signal [8]

a graph which peaks at the point where the two images are most similar. To employ matched filters in CR systems, a perfect knowledge of the primary users signaling features such as, the bandwidth, the operating frequency, the modulation type, the pulse shaping and the frame format must be provided. One approach to implement the MFD technique is by taking the FFT of two signals, then multiplying their coefficients and after that taking the Inverse Fast Fourier Transform (IFFT) of the result, the output can be found out [38]. The major advantage of a matched filter is that it needs less time to achieve high processing gain and probability of false alarm and missed detection due to coherent detection. The disadvantages of using the MFD technique are as follows:

- It would require a dedicated sensing receiver for all primary user signal types.
- It requires the prior information of primary user signal which is very difficult to be available at the CRs.
- Its large power consumption is a drawback as various receiver algorithms need to be executed for the signal detection.

The block diagram of a conventional MFD is shown in Figure 2.11.

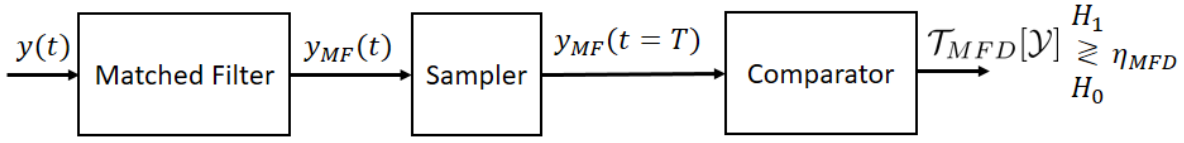


Figure 2.11 – The block diagram of a matched filter detector;  $\mathcal{T}_{MFD}$  denotes the test statistic of the detector and  $\eta_{MFD}$  is the detection threshold

The test statistic characterizing the MFD is given by [38]:

$$\mathcal{T}_{MFD}[\mathcal{Y}] = \frac{1}{N} \sum_{n=1}^N y(n)x_{MF}^*(n) \underset{H_0}{\overset{H_1}{\gtrless}} \eta_{MFD} \quad (2.9)$$

where  $\mathcal{T}_{MFD}$  denotes the test statistic of the MFD,  $\eta_{MFD}$  is the detection threshold and  $x_{MF}^*(n)$  denotes the complex conjugate of the allocated pilot samples defining the matched filter. The ROC criterion of the MFD is described by  $P_D$  and  $P_{FA}$ . They are expressed by [38]:

$$P_D = Q\left(\frac{\eta_{MFD} - E_s}{\sqrt{E_s\sigma_w^2}}\right) \quad (2.10)$$

$$P_{FA} = Q\left(\frac{\eta_{MFD}}{\sqrt{E_s\sigma_w^2}}\right) \quad (2.11)$$

where  $E_s$  is the energy of the PU signal. Accordingly, the detection threshold is obtained by:

$$\eta_{MFD} = Q^{-1}(P_{FA})\sqrt{E\sigma_w^2} \quad (2.12)$$

Based on equation (2.12), the detection threshold is given as function of the signal energy as well as the noise variance. Since a complete knowledge of the PU signal is unreasonable and impractical, some communication systems employ a pilot stream or synchronization codes to obtain the required information. The MFD that is based on a static threshold leads to less accurate detection results due to the noise uncertainty. Motivated by this problem, authors in [38] suggested the use of the dynamic threshold selection to enhance the detection performance. Illustration of the detection performance of the MFD, based on an averaging filter [59], for a static threshold is shown in Figure 2.12.

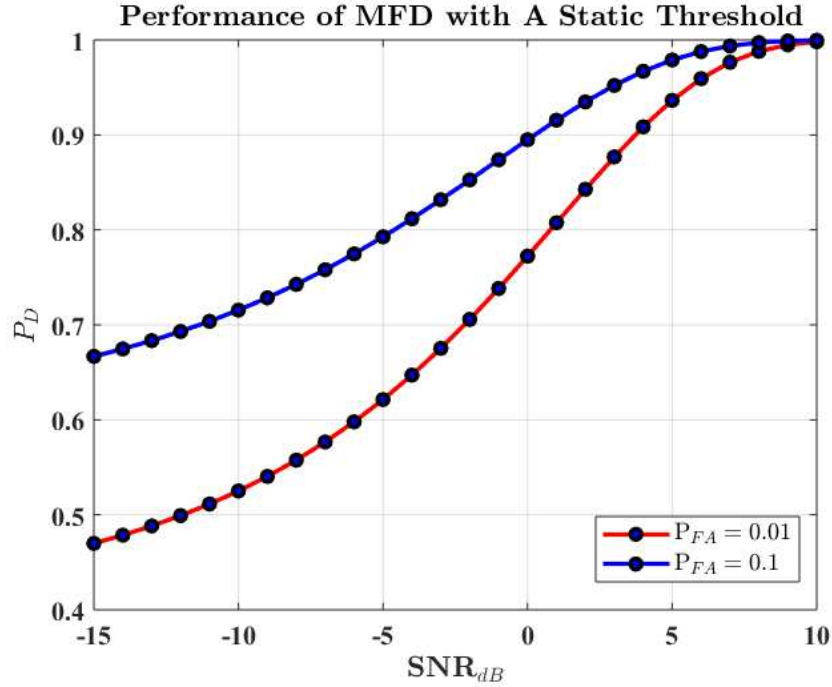


Figure 2.12 – The detection probability of a MFD based on a static threshold [59]

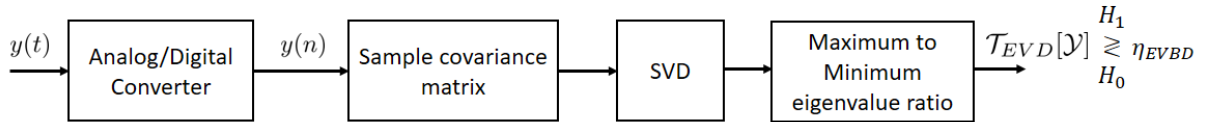


Figure 2.13 – The block diagram of the EVD;  $\mathcal{T}_{EVD}$  denotes the test statistic of the detector and  $\eta_{EVD}$  is the detection threshold

### Covariance-Based Detection

Different detection techniques are used based on the evaluation of the covariance matrix of the received signal. The EVD technique is considered as one of the covariance-based detection techniques that uses the sample covariance of the received signal and the singular value decomposition to detect the presence of a possible PU signal [39]. The inherited correlation between signal samples can be reflected on the eigenvalues of the covariance matrix which can be used to formulate the detection test statistic. The EVD techniques can be categorized into noise-power based and non-noise-power based techniques. There are several EVD techniques that do not require the estimation

of the noise power. These algorithms include the Maximum-to-Minimum Eigenvalue (MME) [39] in which deciding on the presence or absence of the PU signal depends on the ratio of the maximum to the minimum eigenvalues, and also the Energy with Minimum Eigenvalue (EME) algorithm.

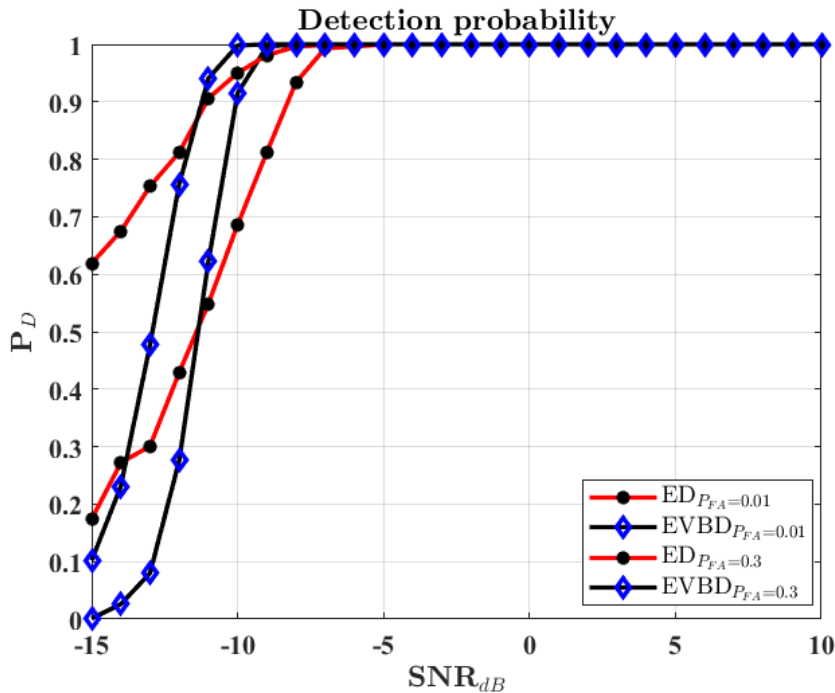


Figure 2.14 – A comparison of the detection probabilities of the ED and EVD for different false-alarm probabilities

Despite the fact that the MME detector does not require any knowledge on the transmitted signal characteristics neither on the noise variance, its high computational complexity due to the high data processing is the main drawback. EME [60], and Maximum-Eigenvalues-Trace (MET) [61]. On the other hand, the noise-power based algorithms include the Maximum Eigenvalue (ME) which has a better performance than the non-noise power based techniques [62]. The sequence of operation to evaluate the test statistic of the EVD is shown in Figure 2.13. A comparison between the MME and the ED is shown in Figure 2.14 based on the results obtained in [39] for detecting IID signals. For the MME algorithm, the desired expression of the detection threshold based on the probability of false alarm can be found in [39]. Also, the approximated

detection threshold of the ME,  $\eta_{EVD}$ , is given by [63]:

$$\eta_{EVD} = F_{app}^{-1}(1 - P_{FA}) \quad (2.13)$$

where  $F_{app}^{-1}(\cdot)$  is the approximated distribution function of the eigenvalue ratio<sup>2</sup>.

### Cyclostationary Feature Detection

The cyclostationary is a generalization of the stationarity property that can be interpreted as a periodicity of the statistical properties of a process [64]. Physical phenomena that involve periodicities give rise to random data for which appropriate probabilistic models exhibit periodically time-variant parameters. For example, in communications, periodicity arises from sampling, scanning, modulating, multiplexing, and coding operations. For these and many other examples, the periodicity can be an important characteristic that should be reflected in an appropriate probabilistic model. Therefore, stationary processes, with their time-invariant probabilistic parameters, are in general inadequate for the study of such phenomena. There are many other sources for the generation of cyclostationarity, such as the amplitude modulation, the pulse-amplitude,-width, and -position modulation, the phase or frequency modulation, etc.

The CFD is a method for detecting the PU transmissions by exploiting the cyclostationary features of the received signals. A signal is said to be cyclostationary, if its autocorrelation is a periodic function of time with some period. Signals used in practical applications have periodic statistical properties such as the mean and the autocorrelation. On the other hand, stationary signals are random signals with physical parameters that do not change with time. In fact, synchronized ensembles of a random process result in a cyclostationary process, whereas asynchronous ensembles of a process results in a stationary process. A cyclostationary detector utilizes the fact that the communication signals often have a repeating structure over some length of time. Therefore, cyclostationary signals are said to exhibit a cyclic correlation that is

2.  $F_{app}^{-1}(\cdot)$  is obtained from the  $f_{app}(t_R)$  which is the probability density function of the eigen ratio. It is given by  $f_{app}(t_R) = [\int_0^\infty l f_{l_1}(t_R l) f_{l_k}(l) dl] \cdot I_{\{t_R > 1\}}$ ;  $f_{l_1}(t_R l)$  is the distribution of the largest eigenvalue and  $f_{l_k}(l)$  is that of the smallest one. The symbol  $I_{\{\cdot\}}$  is an indicator function [63]

expressed by [64]:

$$\begin{aligned} R_y(t, \tau) &= R_y(t + T_0, \tau) \\ &= \mathbb{E} [y(t + \tau)y^*(t - \tau) \exp(j2\pi\alpha_c t)] \end{aligned} \quad (2.14)$$

where  $\mathbb{E}[\cdot]$  denotes the expectation operator,  $\tau$  is the time lag, and  $\alpha_c$  denotes the cyclic frequency. The Fourier transform of the cyclic autocorrelation gives the cyclic spectra. Equivalently, it is given in terms of the time-averaged autocorrelation by [64]:

$$R_y(t, \tau) = \lim_{T_0 \rightarrow \infty} \frac{1}{T} \int_{-\frac{T_0}{2}}^{\frac{T_0}{2}} y(t + \frac{\tau}{2})y(t - \frac{\tau}{2}) \exp(-j2\pi\alpha_c t) dt \quad (2.15)$$

The corresponding spectral correlation function is given by:

$$S_y(\alpha_c, f) = \int_{-\infty}^{\infty} R_y(\alpha_c, \tau) \exp(-j2\pi f \tau) d\tau \quad (2.16)$$

For cyclostationary signals,  $S_y(\alpha_c, f)$  is non zero for specific values of  $\alpha_c$  and  $f$ , while for a stationary noise  $S_y(\alpha_c, f)$  will be zero for  $\alpha_c = 0$ . An example of the spectral correlation of a BPSK signal is shown in Figure 2.15. This distinguishing feature is used for detecting the presence of a PU signal in a spectral hole. Different algorithms have been formulated to evaluate the spectral correlation function such as the FFT accumulation method and the spectral strip correlation method [65]. The former method applies the Fourier transform of the correlation product between the spectral components smoothed over time while the method is the Fourier transform of the correlation products between the spectral and temporal components over time. In some applications, such as the wireless microphone detection, the detection test statistic is given by [66]:

$$\mathcal{T}_{CFD}[\mathcal{Y}] = \max_{f, \alpha_c} \frac{S_y(\alpha_c, f)}{S_y(0, f)} \underset{H_0}{\overset{H_1}{\gtrless}} \eta_{CFD} \quad (2.17)$$

Experimentally, the detection threshold is evaluated by evaluating the spectral correlation and the cyclic spectra when the signal is present. The values of the cyclic spectra indicate the correlation of two frequency-shifted versions of the cyclostationary signals. These values occur at cycle frequencies. To measure the degree of correlation between two frequency-shifted versions of a cyclostationary signal, the term spectral coherence is used. Figure 2.16 shows the block diagram for the CFD. Cyclostationary techniques

provide a better detection performance than ED techniques [66].

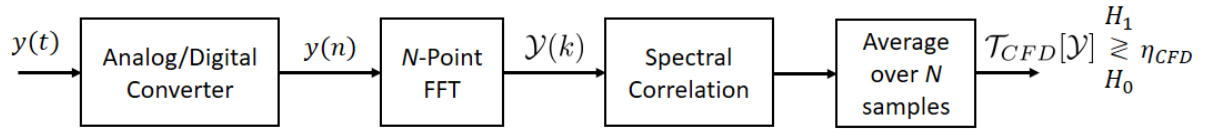


Figure 2.15 – The block diagram of a cyclostationary feature detector;  $T_{CFD}$  denotes the test statistic of the detector and  $\eta_{CFD}$  is the detection threshold

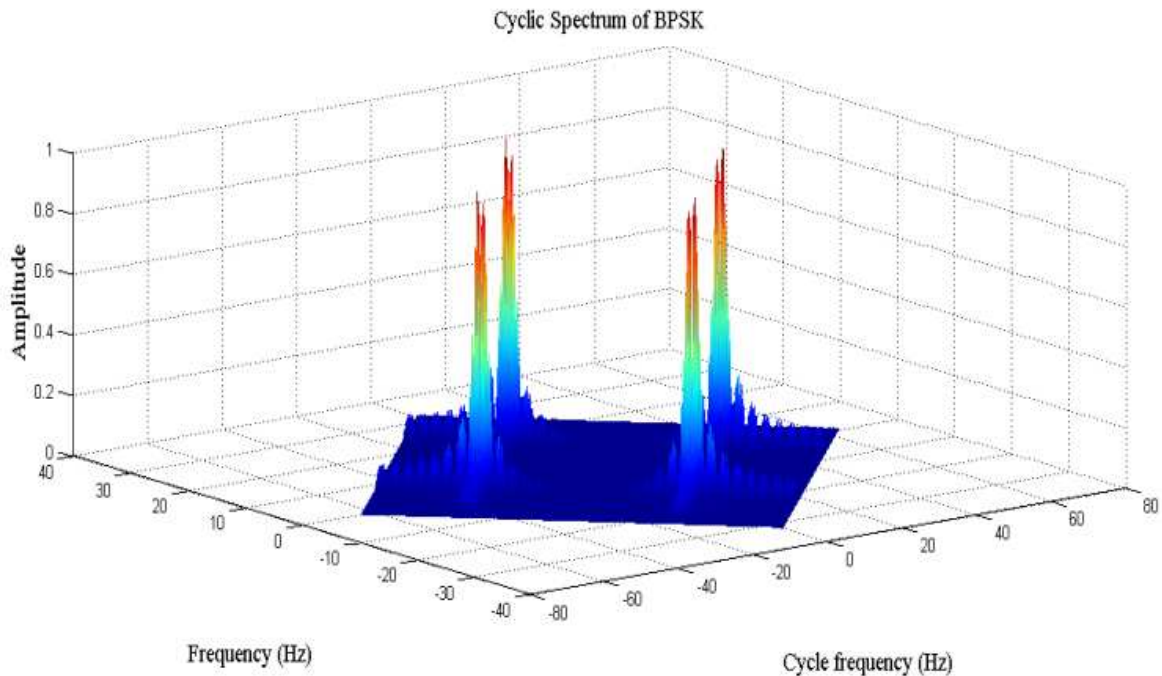


Figure 2.16 – The spectral correlation of a real BPSK signal [64]

Further, their ability to differentiate between signals and noise allows these techniques to be less susceptible to noise uncertainty and hence have a lesser probability of false-alarm compared to energy detection-based techniques. The performance of the cyclostationary detection can be further enhanced by increasing the number of samples. However, this can result in an increase in the sensing time and the complexity as the length of the received signal increases. A balance between the sensing time and the performance detection must be found to reduce this complexity while achieving an

acceptable detection performance.

Table 2.2 – Comparison of the different spectrum sensing techniques

<b>Sensing Technique</b>	<b>Advantages</b>	<b>Disadvantages</b>
<b>Energy Detection</b>	- Easy to implement -No prior knowledge of PU's parameters is required	- High false-alarm rate - Unreliable at low SNR - Sensitive to noise
<b>Matched Filter Detection</b>	- Optimal detection in AWGN channel	-Prior knowledge of the PU signal is required
<b>Covariance-Based Detection</b>	- No prior knowledge of PU's parameters is required -Exploits signal correlation	- Large computational complexity
<b>Cyclostationary Feature Detection</b>	- Robust against noise - Able to distinguish between noise and signal -Low false-alarms at low SNR	- Large sensing time - Large computational complexity
<b>Machine Learning Based Sensing</b>	- Reliable detection if sufficient training is accomplished	- Complex computation - Fast learning adaptation is required - Large database has to be built

### Machine Learning Based Sensing

Recently, MLBS techniques have found applications in many fields of signal detection and classification, by which complex mathematical calculations can be applied to analyze signals and also provide interpretation of data patterns [67], [68]. For this purpose, ML techniques employ learning, reasoning and decision making approaches. Several research investigations have been introduced to exploit ML approaches in the context of CR [69], [70]. The sensing algorithms based on ML deal with the signal detection process as a classification problem in which a classifier, supervised or unsupervised, decides on the channel occupancy status. The ML algorithms employed for spectrum sensing in CR include Gaussian mixture model, K-nearest-neighbor, or support vector regression. To evaluate the performance of the MLBS techniques several metrics encompass detection and false-alarm probabilities, the average training time of the learning algorithm, as well as the classification time delay. A brief comparison

between the different NBSS techniques is given in Table 2.2. Nevertheless, there are other NBSS techniques, which involve waveform detection [71], detection based on principal component analysis [72], and cumulative power spectral density detection [73]. Also, the spectrum sensing for full-duplex cognitive radio systems is discussed in [74], and the recurrence quantification analysis approach is employed for spectrum sensing in [75].

### 2.3.2 WideBand Spectrum Sensing

High data rates characterize the design objectives of the next generation of communication systems, thus a larger bandwidth is required to accommodate the evolution of the communication standards. Accordingly, the CR systems need to scan a wide spectrum to find the best available subbands. Thus, several approaches of multiband and WBSS techniques have been investigated in the literature [76]. In the following, we review the most relevant WBSS techniques and also discuss their advantages and disadvantages.

#### Nyquist Wideband Spectrum Sensing

Standards analog-to-digital converter are employed in the conventional WBSS techniques to sample a wideband signal at the Nyquist's rate. These techniques include the wavelet-based detection, the multi-band detection, and the filter bank detection.

##### 1- Wavelet-Based Detection

Different wavelet-based detection approaches have been considered for spectrum sensing in CR by performing edge detection of the spectral boundaries of a wide spectrum. This is inspired by the capabilities of the wavelet transform to characterize irregular shapes in a signal. The general structure of the wavelet-based detector is shown in Figure 2.17.

##### 2- Multi-Band Joint Detection

This detection approach senses the presence or absence of a PU signal over multiple frequency bands at once using a one of the narrowband spectrum sensing techniques. The objective of this approach is to find an optimum threshold vector to increase the detection probability for all bands jointly by solving an optimization problem. Figure 2.18 shows the structure of the multi-band joint detector.

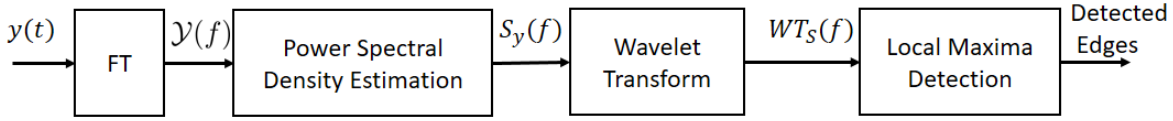


Figure 2.17 – The block diagram of a conventional wavelet-based edge detector;  $S_y(f)$  denotes the power spectral density of the received signal and  $WT_S(f)$  is the wavelet transform of the signal's PSD



Figure 2.18 – The block diagram of a multi-band joint detector

### Sub-Nyquist Wideband Sensing

All the aforementioned Nyquist-based sensing techniques have limitations regarding the high sampling rate and the high power consumption. These limitations are not suitable for the next generation of the communication systems. To tackle these problems, several CSS techniques have been proposed [77], [78]. Consider a wide spectrum that consists of  $N_{sub}$  subbands. Assuming that most of these subbands are idle, we can express the spectrum of the received signal as [9]:

$$Y(f) = \sum_{n \in \mathcal{S}} D_h x_n(f) + W(f) \tag{2.18}$$

where  $D_h$  is a diagonal  $N \times N$  channel gain matrix,  $X_n(f)$  and  $W(f)$  are the spectrum of the  $n_s^{th}$  signal and the additive noise, and  $\mathcal{S}$  is the set of subbands in a wide spectrum. In order to acquire the compressed signal, the received signal is sensed using a measurement matrix, which is given by:

$$r_f = \Phi y_f \tag{2.19}$$

where  $r_f$  is the  $M \times 1$  measurement vector,  $M$  is the number of measurements which depends on the sparsity level,  $\Phi$  denotes the  $M \times N$  sensing matrix, and  $y_f$  is the projection of the received signal in the frequency domain. The sensing decision is obtained after reconstructing the signal using a sparse recovery technique. By allocating the zero and non-zero components of the signal, these location are employed to obtain the detection status. The basic concept of compressive wideband spectrum sensing was first introduced by Tian *et al.* in [79]. In their proposed work, the received signal is transformed into a digital signal by an analog-to-information converter. Their approach have some drawbacks such as the complexity of the computational burden as well as the design imperfections of the converter could affect the sensing results. There are two types of CSS: the blind and non-blind CSS techniques. Several researches concerning both types can be found in [80].

## 2.4 Spectrum Sensing By Scattering Operators

The reduction of the false-alarm probability for a target detection probability is one of the main objectives when designing a reliable spectrum sensing. Among different spectrum sensing techniques, the Energy Detection (ED) technique is widely used due to its implementation simplicity. However, since it cannot differentiate between useful signals and noise, it gives a poor performance in a low SNR environment [31]. In the following proposed work, we employ the ST, which provides a method for a hierarchal signal representation based on deep Convolutional Networks (ConvNets), as a pre-processing step before applying the ED technique. The multi-stage architecture of a scattering network analyses the signal of interest into its significant features through every stage. Our main objective is to take advantage of the sparsity provided through the wavelet filtering, the nonlinearity and the pooling processes to detect the presence of a signal. Due to the cascaded theme of the ConvNets, the noise effect can be revealed and reduced at every stage.

### 2.4.1 Overview on Scattering Transform

Scattering transform is originally developed based on wavelet filtering to provide an informative and a stable presentation for the classification of signals. The idea was initially motivated by developing deep ConvNets which can describe the internal struc-

ture of signals due to their hierarchal nature [81]. Following the developed work on ConvNets by LeCun, J. Bruna and S. Mallat have suggested the use of ST via ConvNets to find a time-invariant signal representation the is suitable for signals classification [82]. Moreover, S. Mallat *et al.* have found applications of scattering networks in audio and image processing as a solution for the averaging offered by the Mel-frequency spectrogram [83].

To describe the operation of ST, which is based on the wavelet analysis, we begin with describing the wavelet transform of a signal  $x_0(t)$ , which is a convolution with a low-pass filter  $\phi(t)$  of a time support  $T$ , followed by another convolution of  $x_0(t)$  with the wavelet function  $\psi(t)_{\lambda_s \in \Lambda_s}$  which denotes a band-pass filter. With  $\lambda_s$  being the center frequency of the filter, a dilated mother wavelet can be defined by:

$$\psi_{\lambda_s}(t) = \lambda_s \psi_{\lambda_s}(\lambda_s t), \hat{\psi}_{\lambda_s}(\omega) = \hat{\psi}_{\lambda_s}\left(\frac{\omega}{\lambda_s}\right) \quad (2.20)$$

where  $\hat{\psi}_{\lambda_s}(\omega)$  is the Fourier transform of  $\psi_{\lambda_s}(t)$ . The wavelet transform of  $x_0(t)$ , defined by  $Wx_0$ , can be described by:

$$Wx_0 = (x_0 * \phi(t), x_0 * \psi_{\lambda_s}(t))_{t \in \mathbb{R}, \lambda_s \in \Lambda_s} \quad (2.21)$$

The hierarchal description of a scattering network can be described as follows [83]:

- At the root of the network, we obtain an average signal description according to:

$$S_0 x_0(t) = x_0 * \phi(t) \quad (2.22)$$

- To gain the high frequency information, we apply the scattering operator  $Ux$  (i.e., wavelet transform modulus operator), which is given by:

$$U_1 x_0(t, \lambda_{s_1}) = |x_0 * \psi_{\lambda_{s_1}}(t)| \quad (2.23)$$

- To regain stabilization, the operator is averaged out by:

$$S_1 x_0(t, \lambda_{s_1}) = U_1 x_0(t, \lambda_{s_1}) * \phi(t) \quad (2.24)$$

$S_1 x_0(t, \lambda_{s_1})$  is defined as the first order scattering coefficients. These are computed with wavelets  $\psi_{\lambda_{s_1}}(t)$ .

- Next, the output of the first order scattering operator is convolved with second

wavelet function  $\psi_{\lambda_{s_2}}(t)$ , and then we obtain the second order coefficients after averaging:

$$S_2x_0(t, \lambda_{s_1}, \lambda_{s_2}) = |U_1x_0(t, \lambda_{s_1}) * \psi_{\lambda_{s_2}}(t)| * \phi(t) \quad (2.25)$$

These operations are repeated iteratively until the residual of the signal energy reaches a minimum value (i.e., theoretically zero) as demonstrated in Figure 2.19. To generalize, for any order  $m_{sc} \geq 1$ , the iterated wavelet modulus operator is given by:

$$U_{m_{sc}}x_0(t, \lambda_{s_1}, \lambda_{s_2}, \dots, \lambda_{s_{m_{sc}}}) = |||x_0 * \psi_{\lambda_{s_1}}(t)| * \psi_{\lambda_{s_2}}(t)| * \dots * \psi_{\lambda_{s_{m_{sc}}}}(t)| \quad (2.26)$$

and the scattering coefficients at order  $m$  is given as:

$$S_{m_{sc}}x(t, \lambda_{s_1}, \lambda_{s_2}, \dots, \lambda_{s_{m_{sc}}}) = U_{m_{sc}}x_0(t, \lambda_{s_1}, \lambda_{s_2}, \dots, \lambda_{s_{m_{sc}}}) * \phi(t) \quad (2.27)$$

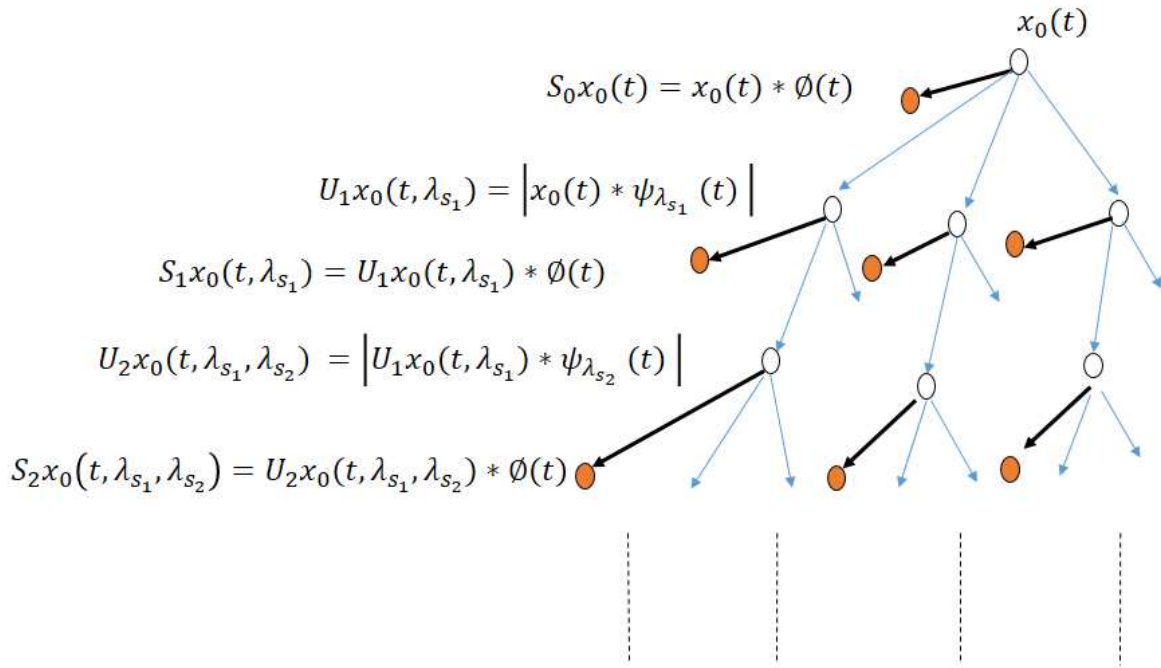


Figure 2.19 – A hierarchal representation of a typical scattering network

## 2.4.2 Reprocessing of Received Signals by The Scattering Operators

A binary hypothesis test can simply describe the received signal  $y(t)$  by [54]:

$$y(t) = s(t) + w(t), \text{ under } H_1 \quad (2.28)$$

where  $H_1$  indicates the occupancy of a channel. On the other hand, when noise only presents,  $y(t)$  becomes:

$$y(t) = w(t), \text{ under } H_0 \quad (2.29)$$

where  $H_0$  indicates an idle status,  $w(t)$  is the noise imposed at the receiver input, and  $s(t)$  the PU received signal by the SU receiver. In [82], it has been shown that the first order scattering coefficients measures the time variation of signal amplitude within frequency bands covered by wavelet filter banks. For further analysis, co-occurrence coefficients reflecting the noise and the interference can be provided through deeper decomposition. In wavelet theory, filtering with wavelets is a measure of projection of a signal into the wavelet basis. So, by a proper choice of the wavelet function, significant signal measurements can be obtained while reducing the noise effect. A block diagram to demonstrate the idea of processing the received signal in the scattering domain is shown in Figure 2.20.

Our work proposed in [84] has investigated the effects of using the ST before applying ED on detecting a DS-SS PU signal. When compared with the conventional ED, although the results have shown that both techniques yield the same detection performance, the simplicity of implementation and low computational burden remark energy detectors. As an alternative approach, we exploited the average first order scattering coefficients to form the detection test statistic of the Scattering Transform-based Detection (STD). The steps of this processing before applying spectrum sensing are summarized as follows:

- The received signal is processed for the signal decomposition. The resultant first order scattering coefficients are used for the signal detection process.
- The first order scattering coefficients are used to form a test statistic  $\mathcal{T}_{STD}$  which is compared to a detection threshold  $\eta_{STD}$ . The test statistic is given by:

$$\mathcal{T}_{STD}(\mathcal{Y}) = \frac{1}{I_s} \sum_{i_s=1}^{I_s} y_{ST}(i_s) \quad (2.30)$$

where  $y_{ST}(i_s)$  denotes the  $i_s^{th}$  scattering coefficient and  $I_s$  represents the number of scattering coefficients.

- The noise variance is assumed to be known. This information can be provided off-line through experimental measurements. If the noise is assumed to be a zero mean AWGN with a unit variance  $\sigma_w^2$ , the processed noise through the complex modulus wavelet decomposition and averaging result in a Rayleigh distributed process. Since the variance of a Rayleigh process  $\sigma_r^2$  is defined by [84]:

$$\sigma_r^2 = \sigma_w^2 \cdot (2 - \pi/2) \quad (2.31)$$

In this case, variance of the scattered signal under  $H_0$  is given by:

$$\sigma_{ST}^2 = \sigma_w^2 \cdot (2 - \pi/2) \|\psi_\lambda\|^2 \quad (2.32)$$

For sufficiently large number of scattering coefficients, the distribution of the test statistic follows a Gaussian distribution with a variance denoted by  $\sigma_{ST}^2$ . Based on the NP's Lemma, the detection threshold is found according to equation (2.3).

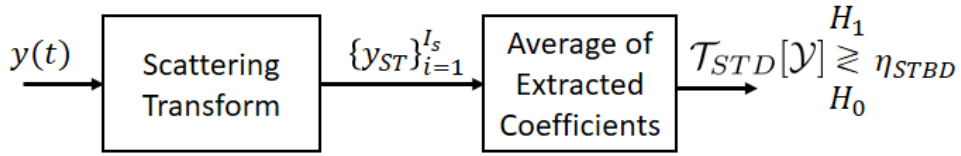


Figure 2.20 – A functional block diagram of signals detection by the proposed ST-based detector

### 2.4.3 Numerical Results and Insights

In the following, we aim to evaluate the detection performance of the STD as compared to the conventional ED by using the first order scattering coefficients. This evaluation is performed in AWGN channel. The performance evaluation is formulated in terms of calculating the detection probability,  $P_D$ , at a pre-defined false-alarm probability. The simulation parameters are summarized in Table 2.3. The simulations are conducted for DS-SS and chirp signals. We choose to detect a DS-SS signal without

having knowledge of the pseudo random spreading code. As shown in Figure 2.21, the ED outperforms the STD at SNR of -15 dB. The average of the first order scattering coefficients starts to have a significance effect for detection at SNR of -6 dB and both detectors yield the same performance of SNR over -4 dB. Although the STD is able to detect the DS-SS signal, the first order scattering coefficients at low SNR values are not sufficient to reveal the DS-SS signal's features.

While the application of the ST in audio signals and images has proven its capability to reveal noisy or interfere structures, a deeper signal decomposition is required with the analysis of time series. In this case, the complexity of the scattering network and the data processing time may increase. For this reason, we stick our analysis in decomposing the received signal up to the first order scattering coefficients. Further, we applied the STD to detect a chirp PU signal, as shown in Figure 2.22, to analyze the efficiency of the STD in detecting the frequency variations encountered in the chirp signal. Although the ED outperformed the STD for the SNR over the range [-15, -8] dB, the STD gives better detection results than ED over -9 dB. We notice that the frequency variations in the chirp signal have a good effect in the first order scattering coefficients which helped in detecting the presence of the PU signal. From the previous analysis, we find that a further processing to the first order scattering coefficient is needed to reveal only the DS-SS signal features such as the code rate. These features can be used to detect the PU signal.

Table 2.3 – Simulation parameters for the scattering-based energy detection

Parameters	Description / Value
PU Signal Type	Chirp Spread Spectrum BPSK/DS-SS
Channel	AWGN
Sampling Frequency	20 GHz
Frequency range of chirp signal	1 kHz -3 GHz
Average time of $\phi(t)$	2 msec
Sequence Length	Chirp Signal: 5000 BPSK/DS-SS: 4410
Monte Carlo Iterations	$10^3$
False-alarm probability	$P_{FA_1} = 0.02$ $P_{FA_2} = 0.2$
SNR Range	[-15, 10] dB

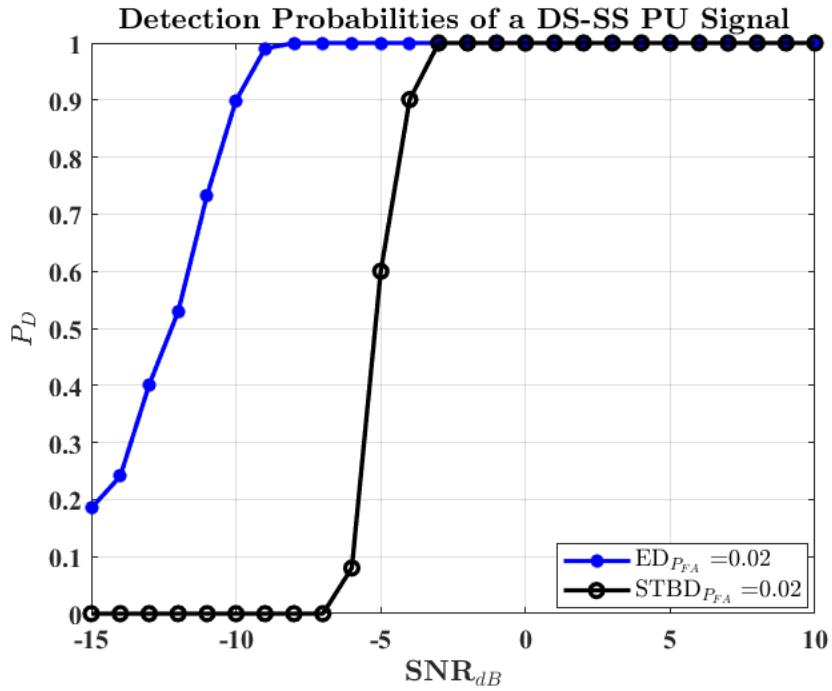


Figure 2.21 – A comparison of the detection probabilities for detecting a DS-SS signal by using the ED and the STD techniques

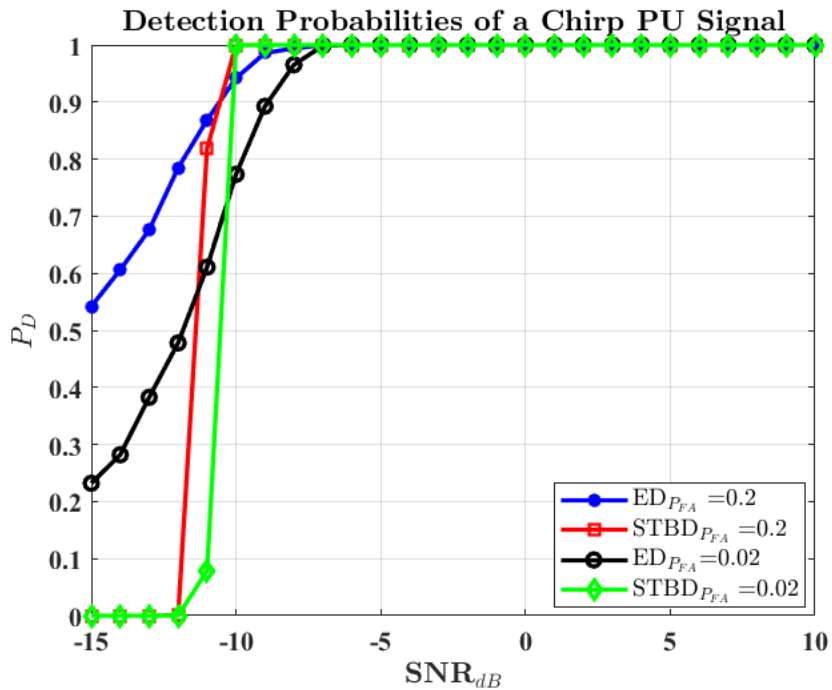


Figure 2.22 – A comparison of the detection probabilities for detecting a chirp signal by using the ED and the STD techniques

## 2.5 Enhancement of Primary User Detection Through Channel Estimation

There are many challenges affecting the signal detection for the spectrum sensing process in CR. One of these challenges is the detection of a received signal transmitted through a multipath environment. The detection process becomes difficult and makes it hard for an occupied band to be correctly detected. In such cases, the incumbent users may be miss-detected, which consequently increases the sensing errors. In this section, we present our proposed solution to mitigate this problem. We introduce the use of a blind channel estimation technique based on the ST to acquire the required channel state information and henceforth, apply channel equalization to remove its effect. Before illustrating the proposed technique, we give a quick overview over possible channel impairments that affect signals detection.

### 2.5.1 Channel Impairments: Overview

The performance of a communication system is determined by the behavior of the transmission medium. In wireless channels, the characterization of the channel state variation over a short time span is a difficult task. However, this information must be obtained to provide a reliable communication. There are different types of wireless channels, such as: urban, suburban, indoor, and underwater. Accordingly, the transmission path between the transmitter and the receiver can be altered from simple line-of-sight to a drastically obstructed one. Hence, different propagating environments mechanisms are used in modeling the wireless channel.

Broadly speaking, these mechanisms can be generally attributed to reflection, diffraction, and scattering. Reflections appear when the plane waves are incident upon a surface with dimensions that are very large compared to the wavelength. Diffraction occurs if an obstruction blocks the transmitted signal, so secondary waves are generated behind it. As for scattering, it arises when the incident wavelength is in the order of or larger than the dimension of the irregular-shaped blocking object. Figure 2.23 indicates the different multipath propagation mechanisms [85], [86]. Due to these mechanisms, the effect of the propagation medium on the transmitted signal can be described roughly by three independent phenomena:

- Path-loss

- Shadowing
- Multipath Fading

While path-loss is a deterministic effect that depends on the distance between the transmitter and the receiver, shadowing and multipath fading have a stochastic nature.

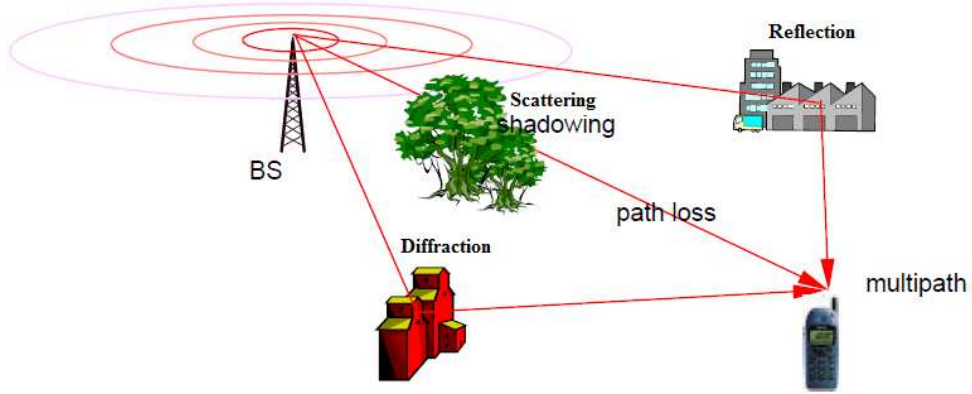


Figure 2.23 – A demonstration of the different multipath propagation mechanisms [86]

Multipath fading leads to significant attenuation changes within small-time scales. For generality, the attenuation due to the aforementioned channel impairments is given by [86]:

$$a_T(t) = a_P(t) a_S(t) a_F(t) \quad (2.33)$$

where  $a_P(t)$ ,  $a_S(t)$ ,  $a_F(t)$  are the attenuation due to the path-loss, shadowing, and multipath fading, respectively. The fading problem caused by multipath propagation in wireless communication is modeled by the Rayleigh distribution. The Rayleigh fading process is characterized by its power spectral density and its autocorrelation function. The autocorrelation function depends on the Doppler frequency which corresponds to the relative motion of the receiver and the transmitter. The fading channel might have a time-varying or a frequency varying attenuating impact on the transmitted signal. Due to the time and frequency variations, we denote the complex attenuation due to fading by  $|\tilde{H}(f, t)|$ , so the magnitude is given by

$$a_F(t) = |\tilde{H}(f, t)| \quad (2.34)$$

In multipath fading, many copies of the transmitted signal each have followed a different path  $i_p$  which has a different length  $l_{i_p}$  depending on the propagation channel. Because of this difference, each signal copy traveling along a path arrives with a differ-

ent delay  $\tau_{i_p}$  that is given by:

$$\tau_{i_p} = \frac{l_{i_p}}{c} \quad (2.35)$$

where  $c$  is the speed of light. Each signal copy is attenuated differently. The attenuation factor of the path  $i_p$  is denoted by  $a_{i_p}$ . At the receiver, these copies are either interfere constructively or destructively. If each element in the propagation environment is static, the received signal will suffer from the delay spread only and the channel is said to be time-invariant. On the other hand, if any movement is encountered, the channel is said to be time-variant.

## 2.5.2 System Model

To reduce the misdetection probability, the PU detection is first performed by applying an energy detection to make sure if the CR receiver has a missed detection probability greater than or equal to 50%. The system architecture is illustrated in Figure 2.18. Assume that the received signal at the CR is given by:

$$y(n) = \theta x(n) + w(n) \quad (2.36)$$

where  $\theta$  is a Boolean parameter indicating the absence or the presence of PU,  $x(n)$  is the faded PU signal, and  $w(n)$  is the noise signal. The parameter  $\theta = 0$  means that we have  $H_0$  hypothesis (i.e., PU is absent), otherwise  $\theta = 1$ , and  $H_1$  is declared (i.e., PU exists). The energy of the received signal is measured and compared with a detection threshold. If the test statistic is composed of a number of observed features that is large enough to invoke the CLT, the test statistic follows a Gaussian distribution [55]. If the energy detector declares  $H_1$ , the misdetection probability, denoted by  $P_{MD}$ , is given by [54]:

$$P_{MD} = Pr\{T[y] < \eta | H_1\} \quad (2.37)$$

where  $\eta$  denotes the detection threshold. If the  $P_{MD}$  exceeds 50%, then the detector declares a misdetection case. It means that there is some useful information in the received signal but it is very weak to be detected, so that the channel estimation and equalization processes must be employed to improve the identification of an occupied frequency band.

Since no pilot symbols or preambles are used to get the channel information, the proposed channel estimation technique is considered as a semi blind-based approach.

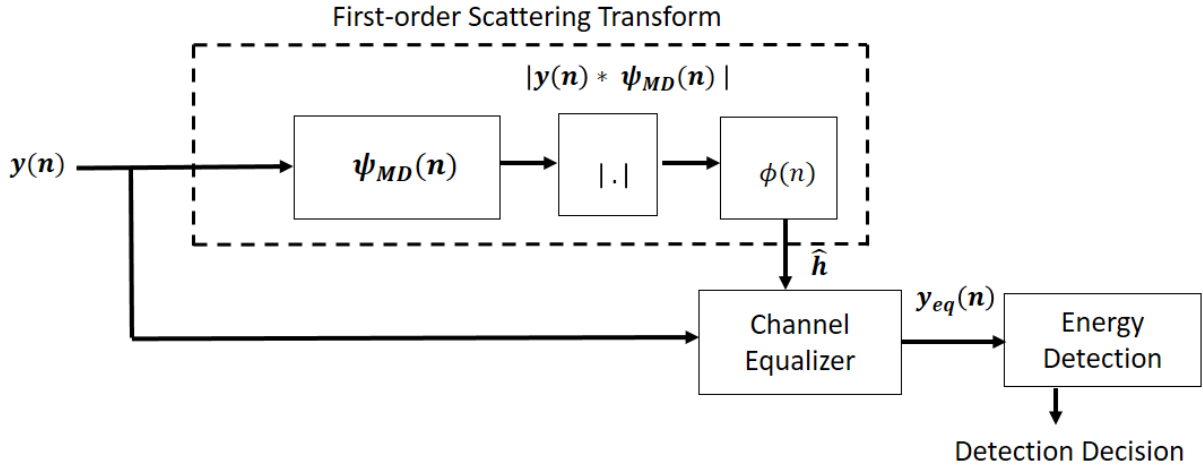


Figure 2.24 – A block diagram represents the proposed method;  $y(n)$  is the received PU signal,  $y_{eq}(n)$  stands for the equalized received signal,  $\hat{h}$  represents the estimated channel impulse response, and  $\psi_{MD}(n)$  denotes the MDW function

However, we apply the ST using MDW to analyze signal variations due to the channel impairments. It is shown in [83] that scattering operators can be used to characterize a structure of the pitch filter of voiced and unvoiced sound waves. This characterization assumes a very narrow filter structure. In this work, we introduce the use of a first order scattering transform to estimate the fading channel coefficients through the modification of the Morlet function by using its first derivative in the wavelet analysis. This modification shows a better frequency localization which is essential to capture the spectral channel variations.

As mentioned in the previous section, when a signal is analyzed through a scattering network, the noise effect is reduced through the network layers. This is due to the fact that the projection of the noise on the wavelet bases becomes insignificant. So, the choice of the mother wavelet function is essential to acquire the signal variation. Since sinusoidal signals are used so often in passband communication, the Morlet function and its derivative become suitable choices [86]. Eventually, by getting the required channel information, a channel equalization based on minimum-mean-squared error method to remove the channel effect, and thus the equalized received signal is processed again by ED to identify the presence of a user. Figure 2.24 gives an illustration of the proposed system structure.

### 2.5.3 Problem Formulation and Proposed Solution

We consider that both the PU signal and the wavelet function to be analytic signals. Also, we assume that the multipath propagation channel is discrete, time-invariant, and frequency selective Rayleigh fading channel. An example of such channel can be given by the two-ray Rayleigh channel model or the three-ray Rician channel model if a strong line-of-sight component exists. Accordingly, we can represent the general model of the received signal in discrete-time domain as [86]:

$$y(n) = \sum_{k_c} h(n; n_c) s(n - n_c) + w(n) \quad (2.38)$$

where  $h(n; n_c)$  is the discrete channel impulse response given as a function of the discrete time index  $n = 0, 1, \dots, N - 1$ , with  $N$  being the sequence length, and the time-shift  $n_c$ . The signal  $s(n)$  is the digital modulated transmitted PU signal and  $w(n)$  is the noise samples at the CR receiver. For time-invariant, linear, and frequency-selective channel,  $h(n; n_c)$  is reduced to  $h(0; n_c) = h(n_c)$ . It means that, although the channel behavior does not vary with respect to time, each propagation path had different channel attenuation and path delay. So,  $h(n_c)$  is defined as the time-invariant impulse response of the transmission channel to a unit impulse transmitted at time 0. To define  $s(n)$  and  $h(n_c)$ , consider the passband representation of the transmitted PU signal  $s(n)$  such that the real valued signal is expressed by:

$$s(n) = A_b(n) \cos(2\pi f_c n + \phi_s(n)) \quad (2.39)$$

where  $A_b(n)$  is the baseband version of the PU signal with phase of  $\phi_s(n)$  and  $f_c$  is the carrier frequency. Since the analytic representation of signals is more appropriate in practical signal processing, we define  $s_a(n)$  as the analytic version of the signal  $s(n)$  that is given by:

$$s_a(n) = s_{a_r}(n) + j s_{a_I}(n) \quad (2.40)$$

where  $s_{a_r}$  and  $s_{a_I}$  are its the real and imaginary parts, respectively. The real part  $s_{a_r}$  is the original real-valued signal  $s(n)$ , whereas the imaginary part  $s_{a_I}$  is the Hilbert transform of  $s(n)$ . Accordingly, we can rewrite  $s_a(n)$  as:

$$s_a(n) = A_b(n) [\cos(2\pi f_c n + \phi_s(n)) + j \sin(2\pi f_c n + \phi(n))] \quad (2.41)$$

equivalently, we obtain:

$$s_a(n) = A_b(n) \exp(j\phi_s(n)) \exp(j2\pi f_c n) \quad (2.42)$$

Then, we define the complex envelope of the analytic signal  $s_a(n)$  by:

$$\tilde{A}(n) = A_b(n) \exp(j\phi_s(n)) \quad (2.43)$$

and the time-invariant channel can be define by:

$$h(n_c) = \sum_{n_c=1}^{N_l} a_{n_c} \delta(n_c - \tau_{n_c}) \quad (2.44)$$

where  $a_{n_c}$  and  $\tau_{n_c}$  are the  $n_c^{\text{th}}$  path attenuation and the path delay of the propagation channel, respectively, and  $N_l$  denotes the number of propagation paths in the transmission medium. Therefore, the received signal can be expressed by:

$$y(n) = \sum_{n_c} h(n_c) \tilde{A}(n - n_c) \exp(j2\pi f_c (n - n_c)) + w(n) \quad (2.45)$$

eventually, the received signal,  $y(n)$ , is processed to extract the necessary channel information.

### Channel Estimation

Let us consider the complex analytic Morlet function  $\psi_M(t)$  which is defined in time domain by [87], [88]:

$$\psi_M(t) = [\exp(-j2\pi f_0 t) - \exp(-2\pi^2 f_0^2 \sigma_G^2)] \exp\left(\frac{-t^2}{2\sigma_G^2}\right) \quad (2.46)$$

where  $f_0$  is the sinusoidal frequency, and  $\sigma_G$  represents the spread of the Gaussian function. The Fourier transform of  $\psi_M(t)$  is given by [88]:

$$\begin{aligned} \Psi_M(f) = & \sqrt{2\pi}\sigma_G [\exp(-2\pi^2\sigma_G^2(f - f_0)^2) \\ & - \exp(-2\pi^2\sigma_G^2 f^2) \exp(-2\pi^2\sigma_G^2 f_0^2)] \end{aligned} \quad (2.47)$$

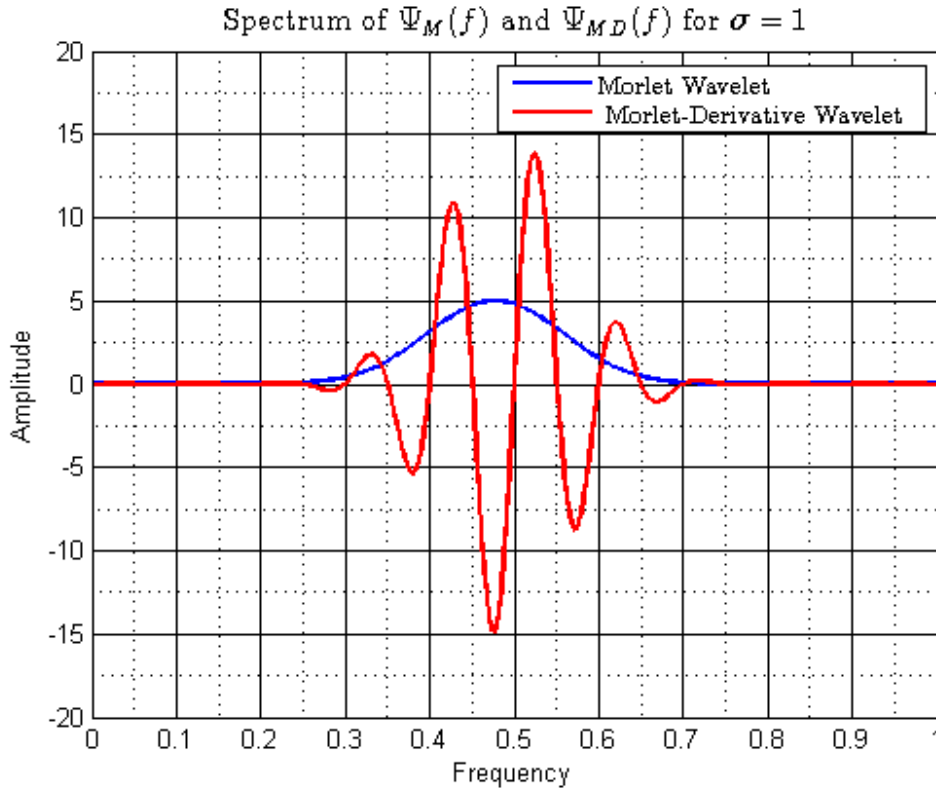


Figure 2.25 – An illustration of the frequency localization of the real Morlet and the MDW functions

and the MDW function is defined by:

$$\psi_{MD}(t) = \frac{d}{dt}\psi_M(t) \quad (2.48)$$

So, based on the Fourier transform properties, equation (2.48) can be represented in the frequency domain by:

$$\Psi_{MD}(f) = j2\pi f\Psi_M(f) \quad (2.49)$$

The Morlet wavelet function has a good time resolution that is controlled by the time-spread of the Gaussian window but a poor frequency resolution [87]. In Figure 2.25, a comparison between the real Morlet and the real MDW functions is given regarding frequency resolutions and support. From the figure, it is shown that the real Morlet-derivative is admissible, compactly supported with better frequency resolution than the real Morlet wavelet function. In order to calculate the frequency resolution of the developed function, we start by the general definition of the frequency resolution,  $\Delta_f$ ,

that is given by [89]:

$$\Delta_f^2 = \frac{\int_{-\infty}^{\infty} f^2 |\psi(f)|^2 df}{\int_{-\infty}^{\infty} |\psi(f)|^2 df} \quad (2.50)$$

to simplify the numerator, we use of the following formula from the famous Gaussian integrals that is given by [90]:

$$\int_{-\infty}^{\infty} x_0^{-m_l} \exp(-ax_0^2 + bx) dx = \sqrt{\frac{\pi}{a}} \exp\left(\frac{b^2}{4a}\right) \sum_{m_k=0}^{m_l/2} \frac{m_l!}{k!(m_l - 2m_k)!} \frac{(2b)^{m_l - 2m_k}}{(4a)^{m_l - m_k}} \quad (2.51)$$

where  $a = 4\pi^2\sigma_G^2$  and  $b$  are constants, and  $m_l$  and  $m_k$  are integers. By using equations (2.38) and (2.40), we obtain the expression for the frequency resolution of the MDW which is given by:

$$\Delta_f = \frac{f_0^2 + \frac{\sqrt{3}}{2a} - 0.5}{f_0 + \frac{1}{4af_0}} \quad (2.52)$$

where  $f_0$  is the frequency of the MW.

To illustrate how the proposed channel estimation is performed by the ST, let us define the noisy received signal in the discrete frequency domain which is given as:

$$Y(k) = H(k)S(k) + W(k) \quad (2.53)$$

where  $k$  is the discrete frequency. For the case of three-path propagation model,  $Y(k)$  can be given by:

$$Y(k) = \left[ c_0 + c_1 \exp\left(-j\frac{2\pi n_{c_1} k}{N}\right) + c_2 \exp\left(-j\frac{2\pi n_{c_2} k}{N}\right) \right] S_a(k) + W(k) \quad (2.54)$$

where  $Y(k)$  is the received signal represented in frequency domain,  $c_0$ ,  $c_1$  and  $c_2$  are path attenuations, the terms  $\frac{2\pi n_{c_1}}{N}$  and  $\frac{2\pi n_{c_2}}{N}$  are the relative frequencies indicating the phase shifts caused by the path delays, and  $N$  denotes the sequence length of the received signal. The frequency domain of  $s_a(n)$  is given by:

$$S_a(K) = N\tilde{A}(k - k_c) \quad (2.55)$$

where  $k_c$  is the discrete frequency parameter of the carrier signal. To apply the ST in the frequency domain, the analytic signal must be processed by a constant-Q filter bank (i.e., complex Morlet wavelet filter) formed by dilating MDWs. It means that the wavelet function  $\psi_{MD}(t)$  must be shifted in frequency such that the maximum wavelet frequency coincides with the relative shifted frequency of the multipath components. To demonstrate how this is achieved, we shift first the MDW function with an angular shift frequency,  $\omega_{sh}$ , and then calculate the wavelet transform of the received signal by:

$$WT\{y(n)\} = y(n) * (\psi_{MD}(n) \exp(j\omega_{sh})) + w(n) * \psi_{MD}(n) \exp(j\omega_{sh}) \quad (2.56)$$

where  $\omega_{sh}$  is given by:

$$\omega_{sh} = \frac{2\pi}{N} (m_{ch}k_{ch} - k_{\psi}) \quad (2.57)$$

where  $k_{ch}$  is the frequency location of the discrete channel impulse response,  $m_{ch}$  denotes an integer multiple of  $k_{ch}$ , and  $k_{\psi}$  is the maximum wavelet frequency. For simplicity, we define the path delay in terms of the number of samples per a symbol. By getting the Fourier transform of equation (2.45), defined by Fourier transform, we have:

$$\mathcal{F}(WT\{y(n)\}) = D_W(k) + \mathcal{W}(k) \quad (2.58)$$

where  $\mathcal{F}(\cdot)$  denotes the Fourier transform operator. We define  $D_W(k)$  and  $\mathcal{W}(k)$  as the filtered faded PU signal with the wavelet function and the filtered noise spectrum, respectively:

$$D_W(k) = S_a(k)H(k)\Psi(k - k_{sh}) \quad (2.59)$$

$$\mathcal{W}(k) = W(k)\Psi_{MD}(k - k_{sh}) \quad (2.60)$$

The filtered noise term in equation (2.47) can be reduced to  $\sqrt{\frac{N_0}{2}}\Psi_{MD}(k)$  if the noise is a bandpass white Gaussian noise with a power spectral density,  $N_0$ . Eventually, we obtain a scaled noisy version of the channel coefficients that is given by:

$$\mathcal{F}(WT\{y(n)\}) = c_{ch} \hat{H}(k) \quad (2.61)$$

where  $\hat{H}(k)$  is the estimated channel coefficient and  $c_{ch}$  is a scaling factor that results from the wavelet peak and the amplitude of  $S_a(k)$ .

## Channel Equalization

To reverse the effect of distortion of the transmitted signals due to channel impairments, a perfect equalization process must be employed. Different types of channel equalizers were developed in literature among which zero-forcing and the Minimum Mean Squared Error (MMSE)-based equalizers are popular. The former is the simplest but has the disadvantage of boosting up the noise level at the equalizer output. On the other hand, the latter is robust against noise. In this work, we applied the MMSE-based equalizer. In this equalization process, we need to find the transfer function  $G_E(f)$  such that the Mean Squared Error (MSE) is minimized. The error is given by [91]:

$$MSE = E|G_E(k)Y(k) - S_a(k)|^2 \quad (2.62)$$

accordingly, the required function is expressed by [91]:

$$G_E(k) = \frac{H^*(k)}{|H(k)|^2 + \frac{1}{\gamma}} \quad (2.63)$$

where  $H^*(k)$  is the conjugate of the original channel transfer function  $H(k)$  and  $\gamma$  is the SNR.

### 2.5.4 Numerical Results and Insights

In order to evaluate the misdetection performance after applying the proposed channel estimation method, simulations are conducted and the misdetection results are compared with ED based on the PCA. The PCA technique has been applied as a multi-antenna CR system, such that it yields a filtered copy of the PU signal and results in an improved SNR [72]. Table 2.4 shows the employed simulation parameters.

First, to apply the ED technique, we need to estimate the distribution of the test statistic through a histogram and then deduce the noise variance. In case of 5-taps and 10-taps channels, the test statistic follows the Gaussian distribution. This is shown in Figure 2.26. To evaluate the ED-PCA as proposed in [92], the misdetection probability is calculated in the case of 5-taps channel; This is shown in Figure 2.27.

In Figure 2.28, we find a reduction of the misdetection probability when the proposed channel estimation technique is employed as compared to the ED-PCA technique. Precisely, the misdetection probability is reduced by around 44% and 30% for

Table 2.4 – Simulation Setup

Parameters	Description / Value
PU Signal Type	BPSK
Channel	Frequency selective, time invariant Rayleigh Channel
Sampling Frequency	1 kHz
Carrier Frequency	20 kHz
Sequence Length	$10^6$
Noise	Circularly Symmetric Complex Gaussian (CSCG)
No. of MonteCarlo Iterations	$10^6$
False Alarm Probability	$P_{FA_1} = 0.02$ $P_{FA_2} = 0.6$
SNR Range	-20 dB to 20 dB

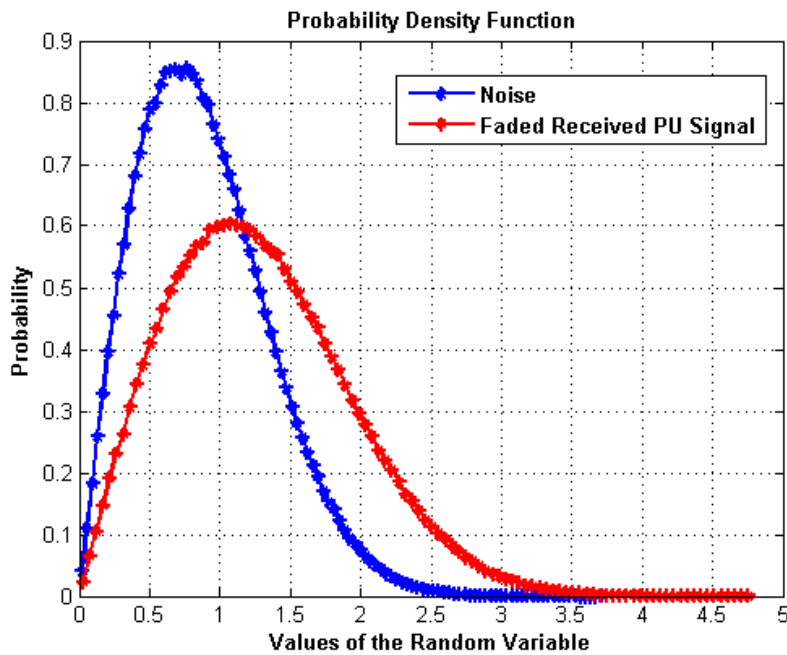


Figure 2.26 – The distribution of noise and faded PU signals with a 10-taps Channel

$P_{FA}$  of 0.01 and 0.2, respectively, after applying the proposed channel estimation approach.

However, it is worth mentioning that as the number of channel taps increases, then the number of wavelet filter increases as well as the complexity of the CR system. Also, the improved performance obtained through the proposed technique depends on our

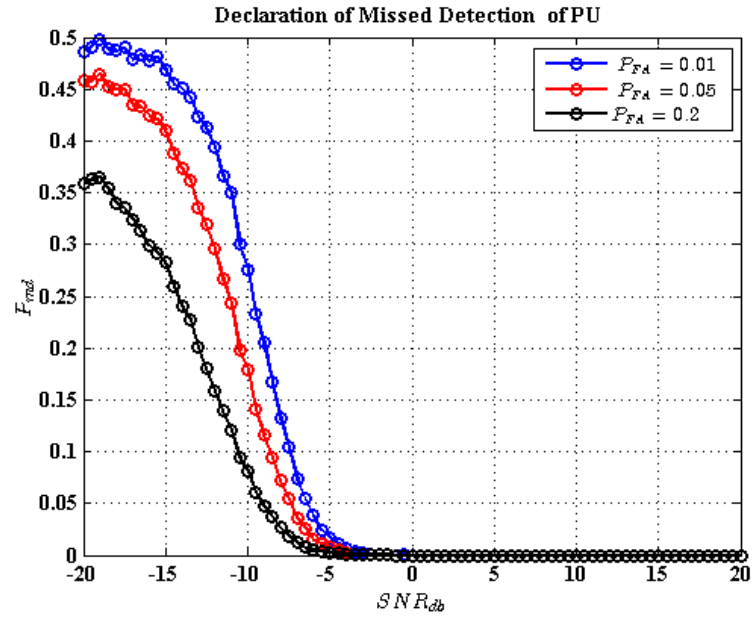


Figure 2.27 – The misdetection probability of the PCA-based ED with a 5-taps channel

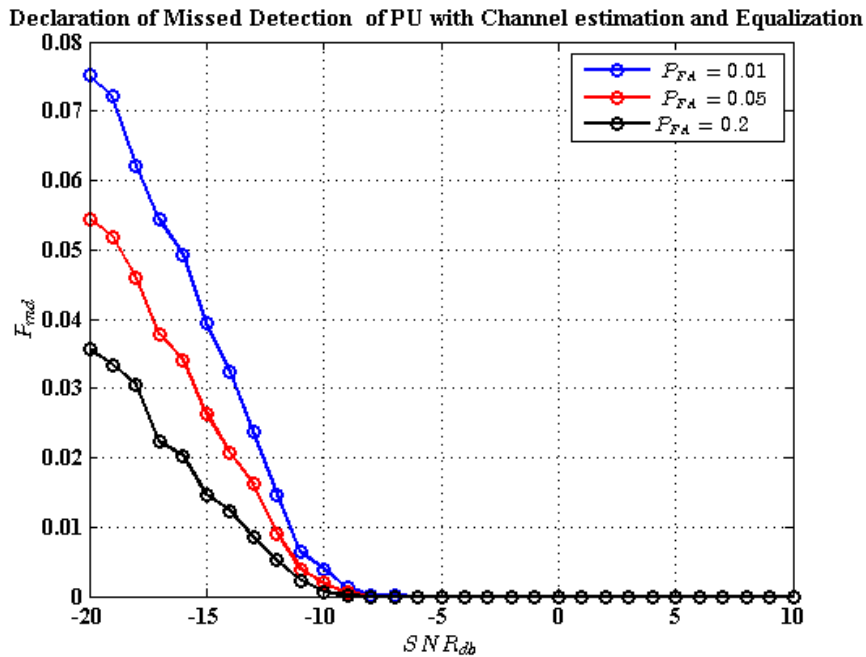


Figure 2.28 – The misdetection probability for different false-alarm values for a 5-taps channel after employing the proposed channel estimation technique followed by the equalization process

strong assumption on having a very narrowband filter which could face challenges in the practical implementation. We deduce that the efficacy of employing the scattering transform approach to detect time series lies in devising a method to extract the hidden details of a target signal.

## 2.6 Summary

In this chapter, an overview on the basic concepts of CRs has been introduced. We have discussed the different types of spectrum sensing techniques for the cases of narrowband and wideband spectrum access. The scope of our research thesis focuses on the non-cooperative spectrum sensing techniques. Further, our investigations on applying the scattering operators for spectrum sensing have been presented for detecting the DS-SS and chirp PU signals. The carried out analysis has shown the capability of the STD to detect the presence of PU signals at medium-to-high SNRs, but its detection performance deteriorates at low SNR values. This infers that more processing to the scattering coefficients is recommended to reveal some distinguishing patterns for detection. On the other hand, the STD performs better in detecting the chirp PU signal which means that the detector is able to utilize the frequency variations in the chirp signal to improve the detection process.

Moreover, we have introduced the application of the ST before ED in the frequency domain for estimating the fading coefficients for the Rayleigh channel to reduce the probability of misdetection. The effect of applying the proposed technique in reducing the  $P_{MD}$  is tested as compared to applying only the ED-PCA based technique. Despite the increased complexity of the proposed channel estimation technique due to the number of filters, it reduces the chances of miss-detecting a PU signal. In accordance with our investigations on the ST in CR, our aim is to provide a reliable non-cooperative PU detector in a low SNR environment. Obviously, such detector must be low in the computational and the implementation complexities in order to add a practical advantage in CR systems. It also needs to be able to reveal specific features that can differentiate between different signals. These motives have established our concern towards exploiting the different variants of cepstral analysis in CR for spectrum sensing, which is discussed in chapter 3.

# CEPSTRAL ANALYSIS APPROACHES FOR SPECTRUM SENSING IN COGNITIVE RADIO

---

## 3.1 Introduction

The problem of detecting Spread Spectrum (SS) Primary User (PU) signals becomes harder than the PU detection of classic signals. This is due to the fact that their power is distributed over a wide frequency band, which can reduce the SNR at the Cognitive Radio (CR) receiver. Consequently, the misdetection of a possible SS signal may cause harmful interference to the licensed receivers. In this chapter, we propose a solution for the misdetection problem of SS PU signals by employing Cepstral Analysis (CA) approaches. The incitement of our choice of the CA techniques is highly motivated by its ability to reveal some characteristics hidden in a signal in the cepstral domain. These characteristics include induced periodicities due to delays, echoes, harmonics, or multipath channel effects [93].

We introduce semi-blind spectrum sensing techniques based on CA approaches for interweave CR systems. The main scope of this chapter is to mitigate the problem of weak signal detection to allow for an interference-free spectrum sharing model. The misdetection problem of a legitimate user occupies a desired frequency band leads to erroneous sensing results. Based on the periodicity revealing property of some cepstral variants, we formulate a spectrum sensing technique based on the PassBand-AutoCepstrum Detection (PB-ACD) approach. In section 3.2, we review the related work to the detection of SS signals and we provide an overview on basic cepstral variants and their applications in signal detection. The system and signal models of the carried out analysis are described in section 3.3. In section 3.4, we introduce the PB-ACD technique to detect Direct Sequence-Spread Spectrum (DS-SS) signals in Additive

White Gaussian Noise (AWGN) channels. We extend our analysis to the detection of Frequency Hopping-Spread Spectrum (FH-SS), and Chirp-Spread Spectrum (C-SS) PU signals. The blind theme of the proposed approach implies that no knowledge of the spreading code employed in the SS signal is provided at the CR receiver. For the case of the DS-SS PU signal, a mathematical formulation of the detection problem is formulated. Further, the statistical distribution of the detection test statistic is derived under the null and the alternative hypotheses based on the Neyman-Pearson Lemma (NPL) for the case of a real-valued Gaussian noise. Also, the Receiver Operating Characteristics (ROC) metrics are derived in terms of the false-alarm and detection probabilities for the case of a Circularly Symmetric Complex Gaussian (CSCG) noise. The corresponding detection threshold is analytically computed. To provide a broader analysis of the PB-ACD technique for detecting SS signals, a mathematical formulation of the Averaged PassBand-AutoCepstrum Detection (APB-ACD) technique is carried out for the cases of the FH-SS and C-SS signals. Also, a theoretical analysis of the sensing-threshold-throughput trade-off of the PB-ACD technique is presented to highlight the impact of choosing a suitable detection threshold on the achievable throughput of the CR system.

Since in the PB-ACD techniques the PU detection depends on monitoring the presence of a large cepstral peak at the reciprocal of the carrier frequency, this peak may suffer from high noisy fluctuations. These spectral fluctuations may affect the detection performance. In order to enhance the detection results, we introduce the smoothed PB-ACD technique in section 3.5. The proposed smoothing process is performed before employing the PB-ACD technique to reduce the fluctuations experienced in the Auto-Correlation Estimators (ACEs) before evaluating the Power Spectral Density (PSD) of the received signal. The smoothing process includes applying the Total Variation Denoising (TVD) technique based on the Majorization-Minimization (MM) algorithm to reduce the unwanted spectral fluctuations. The performance of the proposed spectrum sensing algorithms is compared with different state-of-the-art techniques in terms of the detection probability in section 3.6. The chapter summary is given in section 3.7.

## 3.2 Related Work

In the literature, there are some employed methods to detect DS-SS signals. For example, the author of [94] has proposed a method for detecting DS-SS signals by

evaluating the fluctuations of the autocorrelation estimators. The proposed method utilizes the fact that the fluctuations of the ACEs of a significant signal and the background noise are distinguishable. Also, the authors of [95] have proposed an autocorrelation estimation based detection methods to detect SS signals. In particular, the detector searches for the autocorrelation peaks that may occur at integer times of the chip duration of a pseudo-random sequence. Then, the detection decision is made by the cumulative peak-to-average criteria. Although the proposed method in [95] has shown a good detection performance at low SNR values, it requires the prior knowledge of the chip duration.

Moreover, a robust spectrum sensing scheme based on the generalized order statistics has been proposed in [96] than can be employed for detecting SS signals. The proposed detector provides a protection against the background noise and analyzes the false-alarm and detection probabilities under noise uncertainty. However, the detection accuracy of the order statistics detector depends on increasing the size of the analyzed samples, which may increase the processing time.

Cepstral Analysis (CA) is a logarithmic based approach for detecting signal features. Analyzing a given signal in the cepstral domain has gained much interest in different fields such as speech and image processing [16]. Also, we can find applications of the CA techniques in mechanical and communication applications [97]. The cepstral signal processing concept was applied for echoes detection in seismic waves [18]. Based on the homomorphic capabilities of cepstral analysis, it is also used to estimate the frequency response of multipath fading channels. Hereinafter, we review the basic definitions of different cepstral variants to remark their significant applications in the filed of signal detection.

### 3.2.1 Overview on Cepstral Analysis

The concept of cepstrum was firstly introduced by Bogert, Healy, and Tukey to analyze time series in the logarithmic frequency domain [20]. Their investigations revealed that the logarithmic spectrum of a signal containing echoes has an additive component reflecting the size and the delay of the echo. Moreover, they introduced new terminologies such as: the *cepstrum* and the *quefrequency*. In the literature, the cepstrum is generally defined as the inverse Fourier transform of the logarithmic magnitude spectrum of a signal. Cepstral analysis has been widely used in audio and image processing for its

ability to reveal hidden features about signals. According to the variants of the CA approach, a certain CA variant is chosen to fit a specific application. That is why a researcher must be aware of the problem under analysis, and whether employing the CA approach will unleash significant details about the signal in the logarithmic domain. For example, the cepstrum of a pure sinusoidal signal does not show significant peaks, however, an echoed version added to it could show such significance. Before describing the different cepstral variants, let us define the following variables:

- $n$ : The discrete-time domain
- $x(n)$ : An arbitrary discrete-time domain signal
- $x_c(n)$ : The analyzed complex discrete time domain signal.
- $k$ : The discrete frequency variable
- $X(k)$ : The Fourier Transform of  $x(n)$ .
- $\mathcal{F}\{.\}$ , and  $\mathcal{F}^{-1}\{.\}$ : The Fourier and inverse Fourier transform operators, respectively
- $\hat{n}$ : The discrete quefrequency variable, which is a measure of alternative time in the cepstral domain
- $R_x(n_c)$ : The discrete autocorrelation function of the signal  $x(n)$  at a time lag of  $n_c$
- $X'(k)$ : The first derivative of  $X(k)$

Generally, there exist different variants of CA terms such as:

- 1- **Complex cepstrum**: it describes the logarithmic operation applied on the complex spectrum of a signal. Given a complex discrete-time signal  $x_c(n)$ , the exact definition of the complex cepstrum is given by [98]:

$$c_c(\hat{n}) = \frac{1}{2\pi} \int_{-\pi}^{\pi} \log [X_c(\omega)] \exp(j\omega n) d\omega \quad (3.1)$$

where  $\log$  stands for the natural logarithm and  $X_c(\omega)$  is the Discrete-Time Fourier Transform (DTFT) of  $x_c(n)$ , which is given by:

$$X_c(\omega) = \sum_{n=-\infty}^{\infty} x_c(n) \exp(-j\omega n) \quad (3.2)$$

where  $\omega$  denotes the angular frequency ( $-\pi < \omega \leq \pi$ ). Generally, the complex

logarithm  $\log [Z_c]$  of a complex quantity  $Z_c$  is defined as:

$$\log [Z_c] = \log |Z_c| + j \arg [Z_c] \quad (3.3)$$

where  $\arg[\cdot]$  denotes the argument operator. In practice, the complex cepstrum is computed using the Discrete Fourier Transform (DFT), which is a sampled version of the DTFT. The signal DFT  $X(k)$  defined by [98]:

$$X_c(k) = \sum_{n=0}^{N_c} x_c(n) \exp\left(-j\frac{2\pi kn}{N_c}\right) \quad (3.4)$$

where  $N_c$  is the number of data points used in evaluating the complex cepstrum. Thus, the complex cepstrum is given by:

$$c_c(\hat{n}) = \frac{1}{\sqrt{N_c}} \sum_{k=0}^{N_c-1} (\log |X_c(k)| + j \arg [X_c(k)]) \exp\left(j\frac{2\pi kn}{N_c}\right) \quad (3.5)$$

The main challenge in computing the complex cepstrum is the implementation of the complex logarithm and computation of the angle  $\arg [X_c(k)]$  due to the problem of unwrapping the phase function. The accurate implementation of the unwrapping is a practical challenge [99]. However, the invertible advantage of the complex cepstrum makes it applicable in signals processing that involves homomorphic filtering such as speech, image, or seismic data processing.

- 2- **Real cepstrum:** due to the implementation difficulties of the complex cepstrum, the real cepstrum is usually used in practice [98]. It defines the logarithmic operation on the real spectrum of a signal. The real cepstrum is given by [98]:

$$c_r(\hat{n}) = \frac{1}{\sqrt{N_r}} \sum_{k=0}^{N_r-1} \log |X_c(k)| \exp\left(j\frac{2\pi kn}{N_r}\right) \quad (3.6)$$

where  $N_r$  is the number of employed samples to evaluate the real cepstrum. Since the phase is discarded in the real signals, the real cepstrum is symmetric across the zero-point. In fact, the real cepstrum sequence is equivalent to

the even part of the complex cepstrum [98]:

$$c_r(\hat{n}) = \frac{c_c(\hat{n}) + c_c(-\hat{n})}{2} \quad (3.7)$$

An added advantage of the real cepstrum over the real cepstrum is that only the first half of the the cesprum sequence is taken into account in calculations. For simplicity, the real cepstrum is referred as the *cepstrum* and  $c_r(\hat{n})$  is equivalent to  $c(\hat{n})$  for convenience.

3- **Phase cepstrum:** the inverse DFT of the phase of the complex logarithm defines the phase cepstrum. It is given by:

$$c_p(\hat{n}) = \frac{1}{\sqrt{N_r}} \sum_{k=0}^{N_r-1} \arg [X_c(k)] \exp \left( j \frac{2\pi k n}{N_r} \right) \quad (3.8)$$

Due to the difficulties in implementation and computation, the usage of the phase cepstrum is minimal in practical applications.

4- **Power cepstrum:** the basic foundation of cepstral analysis is based on the evaluation of the Power Cepstrum (PC) as described by Bogert *et al.* [20]. The PC is defined as the squared magnitude of the inverse Fourier transform of the logarithmic square magnitude of the signal spectrum or simply the logarithmic power spectrum of a signal [20], [100]. The expression of the power cepstrum is given by:

$$c_{pc}(\hat{n}) = \left| \frac{1}{N_r} \sum_{k=0}^{N_r-1} \log |X(k)|^2 \exp \left( j \frac{2\pi k n}{N_r} \right) \right|^2$$

The PC finds applications in mechanical systems such as analyzing the periodic effects caused by a vibrating machine for fault detection in a turbine blade or a gearbox [101].

In the literature, there are other cepstral variants that include the differential cepstrum, which is the inverse Fourier transform of the first derivative of the signal's log-spectrum, and the autocepstrum that is defined by the inverse Fourier transform of the signal's log-PSD. A summary of the different cepstral variants is given in Table 3.1.

Table 3.1 – Variants of the cepstral analysis terms

Definition	Mathematical Description
Complex Cepstrum	$c_c(\hat{n}) = \mathcal{F}^{-1}\{\log X(k)\}$
Real Cepstrum	$c_r(\hat{n}) = \mathcal{F}^{-1}\{\log  X(k) \}$
Phase Cepstrum	$c_p(\hat{n}) = \mathcal{F}^{-1}\{\log (\arg [X_c(k)])\}$
Power Cepstrum	$c_{pc}(\hat{n}) = 4 c_R(\hat{n}) ^2$
Differential Cepstrum	$c_d(\hat{n}) = \mathcal{F}^{-1}\left\{\frac{X'(k)}{X(k)}\right\}$
Autocepstrum	$c_a(\hat{n}) = \mathcal{F}^{-1}\{\log \mathcal{F}\{R_x(n_c)\}\}$

### 3.2.2 Application of Cepstral Analysis in Communications

In communications applications, the homomorphic abilities of CA approaches have been utilized in different ways. For example, the authors in [102] introduced an algorithm based on a CA method to estimate the channel response of a frequency selective multipath channel. Moreover, the authors in [103] presented a pre-filtering method for a time delay estimation in reverberant environments for two or more microphones based on the homomorphic deconvolution.

In the literature, the employment of CA concepts in CR systems, radio frequency signal detection or signals classification was rarely used. For example, a method for the automatic recognition of different Orthogonal Frequency Division Multiplexing (OFDM) waveforms based in cepstral features is presented in [19]. Moreover, the authors of [104] have introduced a WideBand Temporal Sensing (WBTS) approach based on a cepstral envelope detector. Precisely, the involvement of the cepstrum-based spectrum envelope detector is to adapt to dynamic changes that may occur in the configuration of a PU channel. The rationale of this approach is to use a cepstral feature vector to detect the changes in the spectrum envelope of a PU signal within a given frequency band. To the best of our knowledge, there are no further CR applications that exploiting CA methods, which makes the scope of our research is relatively novel.

### 3.3 System Description and Channel Model

Generally, a Cognitive Radio (CR) system can be designed based on a specific spectrum sharing model. As discussed in chapter 2, there are mainly three CR paradigms among which a CR sharing model can be chosen. The following analysis is carried out for the interweave CR system through which a secondary access to a licensed spectrum is viable only if the interference at the PU receiver is avoided.

#### 3.3.1 System Model

We depict the general detection problem of a spread spectrum signal as a binary hypothesis testing problem. In such formulation, the null hypothesis is denoted by the  $H_0$  where the alternate hypothesis is denoted by  $H_1$ . This is based on the absence or the presence of a PU in a scanned frequency band. The proposed CR system model is described in Figure 3.1. In this model, the SU at node *A* senses the PU transmission activity through the sensing channel. If the sensing operation declares a vacant channel, the SU node *A* initiates its transmission through the access channel. Needless to say, the information about the access channel can be provided through pilot-based channel estimation techniques [11]. As shown in Fig. 3.1, the interference from a possible PU can be guaranteed based on errors in the sensing results. This leads to the misdetection problem which may occur if the PU signal is a SS signal. The connecting channels can be defined as follows:

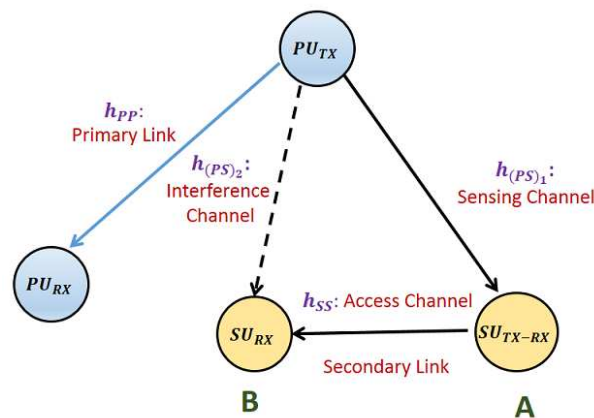


Figure 3.1 – A general description a communication scenario between SU and PU networks

- The *downlink* between the PU transmitter and the detector installed at the SU transmitter at node A, denoted by the channel  $h_{(PS)_1}$ . The received signal  $y_A(t)$ , at node A, can be defined as:

$$y_A(t) = \begin{cases} w_{ST}(t) & : \text{Under } H_0 \\ s_{PU}(t) * h_{(PS)_1}(t; \tau) + w_{ST}(t) & : \text{Under } H_1 \end{cases} \quad (3.9)$$

where  $s_{PU}(t)$  is the PU transmitted signal,  $*$  denotes the convolution product,  $h_{(PS)_1}(t; \tau)$  is the sensing channel generally described as time varying fading channel with a delay defined by  $\tau$ , and  $w_{ST}(t)$  is the thermal noise presented, modeled as AWGN, at the detector of A.

- The *uplink* between SU transmitter and receiver denoted by the channel  $h_{SS}$ .
- The *downlink* between the PU transmitter and the SU receiver is  $h_{(PS)_2}$ .
- The *uplink* between PU transmitter and receiver is  $h_{(PP)}$ . In the following, we will refer to  $s_{PU}(t)$  as  $s(t)$  since we are considering only the PU signal in our analysis.

The misdetection of PU at SU receiver is evaluated as  $1 - P_D$ , where  $P_D$  denotes the detection probability. Also, the Correct-No-Detection probability,  $P_{CN}$ , is evaluated by  $1 - P_{FA}$  where  $P_{FA}$  denotes the false-alarm probability. Accordingly, The received signal  $y_B(t)$ , at node B, can be defined as:

$$y_B(t) = \begin{cases} s_{PU}(t) * h_{(PS)_2}(t; \tau) \\ + s_{SU}(t) * h_{(SS)}(t; \tau) + w_{SR}(t) & : 1 - P_D \\ s_{SU}(t) * h_{(SS)}(t; \tau) + w_{SR}(t) & : 1 - P_{FA} \end{cases} \quad (3.10)$$

where  $s_{SU}(t)$  stands for the SU transmitted signal,  $h_{(PS)_2}(t; \tau)$  is the interference channel generally described as time-varying fading channel with delay defined by  $\tau$ , and  $w_{SR}(t)$  is the thermal noise presented, modeled as AWGN, at the SU receiver of B.

### 3.3.2 Signal and Channel Model

As mentioned earlier, our focus is on detecting low-probability of intercept signals. Specifically, we propose an algorithm to detect a DS-SS signal that is denoted by  $s_{PU}(t)$  defined in equation (3.9). Since we are concerned with detecting the PU signal, we will refer to  $s_{PU}(t)$  as  $s(t)$  for simplicity in the following analysis. In designing the

algorithm, we assume all channels information is provided at the CR system so that we are concerned with the spectrum sensing only. Accordingly, we consider the sum of faded PU signal, which is given by:

$$x_p(t) = s(t) * h_{(PS)_1}(t; \tau) \quad (3.11)$$

In order to build up the algorithm based on the autocepstrum of the received PU signal. Let us define the signal  $s(t)$  by [105]:

$$s(t) = A_s d(t) p(t) \cos(2\pi f_c t + \theta_c) \quad (3.12)$$

where  $s(t)$  is the passband representation of DS-SS,  $A_s$  is the carrier amplitude,  $d(t)$  is the data signal,  $p(t)$  is the spreading waveform,  $f_c$  is the carrier frequency, and  $\theta_c$  is the carrier signal phase at  $t = 0$ . The data modulating signal  $d(t)$  is a non-overlapping sequence of rectangular pulses of duration  $T_d$ , each of which has an amplitude of +1 or -1 if the data bit is '1' or '0', respectively. Moreover, the spreading waveform  $p(t)$  is given by [105]:

$$p(t) = \sum_{i=-\infty}^{\infty} p_i \mathcal{P}(t - iT_c) \quad (3.13)$$

where each  $p_i$  represents one spreading pulse or *chip* which equals +1 or -1, and  $T_c$  is the chip duration. The chip waveform  $\mathcal{P}(t)$  is designed ideally to avoid inter-chip interference [105]. In the following analysis, we employ the maximal-length-shift-register sequence (i.e., m-sequence) to generate the DS-SS signal [105].

### 3.4 Spectrum Sensing Technique By The Autocepstrum Approach

The autocepstrum of a time-domain signal can be defined by the inverse Fourier transform of the natural logarithm of the signal's PSD. The steps to calculate the autocepstrum can be summarized as follows:

- 1- Estimate the autocorrelation of the received signal.
- 2- Evaluate the Fourier transform and its magnitude.
- 3- Compute the natural logarithm.

4- Finally, evaluate its inverse Fourier transform.

Hereinafter, we employ the autocepstrum approach to analyze the received DS-SS signal at the CR receiver.

### 3.4.1 Detection of Direct Sequence-Spread Spectrum Signals By The PB-ACD Technique

According to equation (3.12), the autocorrelation function of  $s(t)$  is given by [105]:

$$R_s(\tau) = \frac{A_s^2}{2} R_d(\tau) R_p(\tau) \cos(2\pi f_c \tau) \quad (3.14)$$

where  $R_d(\tau)$  and  $R_p(\tau)$  are the autocorrelations of the data and the spreading waveforms, respectively [105]:

$$\begin{aligned} R_d(\tau) &= \Lambda\left(\frac{\tau}{T_d}\right) \\ R_p(\tau) &= -\frac{1}{N_s} + \frac{N_s + 1}{N_s} \sum_{i=-\infty}^{\infty} \Lambda\left(\frac{\tau - iN_s T_c}{T_c}\right) \end{aligned} \quad (3.15)$$

where  $\Lambda(\cdot)$  is the triangular function<sup>1</sup> and  $N_s$  is the length of the m-sequence pseudo random spreading code defined by  $N_s = 2^{m_s} - 1$ , for  $m_s$  is the degree of a chosen primitive polynomial.

It is important to mention that the autocorrelation of a periodic function is periodic as well. Our target is to investigate this periodicity in the cepstrum domain since the CR system has no information about the PU signal. In order to complete the evaluation of the autocepstrum of  $s(t)$ , taking the Fourier transform of equation (3.14) results in the passband PSD, which is given by [105]:

$$S_s(f) = \frac{A_s^2}{4} [S_{sl}(f - f_c) + S_{sl}(f + f_c)] \quad (3.16)$$

where  $S_{sl}(f)$  is the lowpass equivalent density defined by:

$$S_{sl}(f) = T_c^2 \text{sinc}^2(fT_c) \quad (3.17)$$

---

1. The computation of the autocorrelation function in equation (3.15) is a consequence of a rectangular shape that we used in the signal. If the rectangular shape is replaced by a raised-cosine pulse or any other shape, then the computation of  $R_s(\tau)$  will be modified.

To investigate the periodicity of (3.17) in the cepstrum domain, we define:

$$\begin{aligned} Z_{sl}(f) &= \log[S_{sl}(f)] \\ &= 2 \log[T_c] + 2 \log[\sin(\pi T_c f)] - 2 \log[\pi T_c f] \end{aligned} \quad (3.18)$$

It is shown in equation (3.18) that the natural logarithm of the lowpass PSD of a DS-SS signal is periodic because of the term  $\log[\sin(\pi T_c f)]$  with an inclination and shift along the y-axis due to the other terms. Moreover, referring to equation (3.16), the natural logarithm of the passband PSD is a shift at the carrier frequency  $f_c$ . By getting the inverse Fourier transform of equation (3.17), the periodic behavior of the signal gives spectral lines, and their peaks are employed to formulate our detection techniques.

To design a detector based on periodic features appearing in the cepstral domain, we need to investigate different types of periodicities that may occur based on  $R_s(\tau)$ . According to equation (3.15), we have three sources of possible periodicities that arise from the data waveform, the pseudo-random spreading code, and the carrier signal. In Figure 3.2, we illustrate the evaluation of the autocepstrum of the AWGN, the spreading waveform, and the baseband and passband versions of the DS-SS signal. In fact, Figure 3.2 shows the autocepstrum analysis of each autocorrelation term appearing in equation (3.15). Also, Figure 3.3 shows a comparison of evaluating the cepstrum and the autocepstrum of a DS-SS signal. Consequently, we observe the following properties:

- The autocepstrum of the pseudo-random spreading code has few peaks repeating at multiple of  $N_s T_c$ . This resembles the autocepstrum peaks of the AWGN, that has a peak at zero quefrequency at almost zero elsewhere.
- The autocepstrum of the baseband  $s(t)$  gives spectral lines at integer multiples of  $T_d$  with one major peak and  $T_d$  and other negative peaks.
- The passband version of  $s(t)$  gives spectral lines in the autocepstrum occurring at integer multiple of the carrier period  $T_{carr} = \frac{1}{f_c}$  with one major peak at  $T_{carr}$  and the rest are negatives.
- The cepstrum of the DS-SS shown in Figure 3.3 shows no significant peaks along the quefrequency values.

The result in Figure 3.3 is due to the fact that a peak occurring in the cepstral domain reflects harmonics that are multiple of periodicities in the spectrum. In other words, the cepstrum of a pure sinusoidal signal does not show significant peaks, however, an echoed version added to it could show such significance.

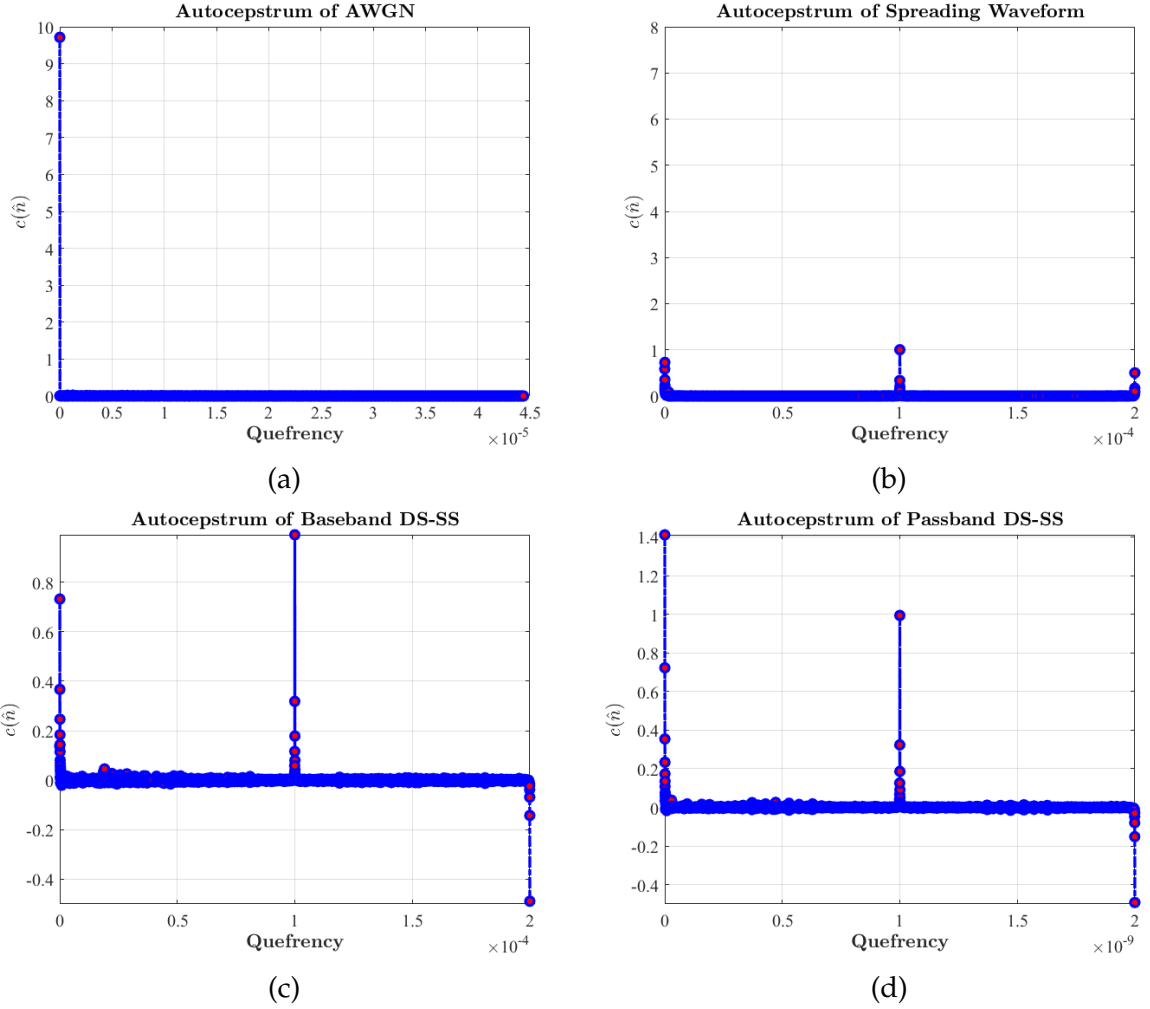


Figure 3.2 – An illustration of various autocepstrum analysis of DS-SS signal and the AWGN;  $T_d = 10$  msec and  $f_c = 10$  MHz

On the other hand, the autocepstrum of the DS-SS shows a major peak value reflecting these harmonics and correlation. This conclusion is mainly our motivation to choose the autocepstrum approach in our analysis. Based on these insights, we formulate a detection schemes that is based on a single cepstral peak occurring at  $T_{carr}$ . As mentioned earlier, we consider the faded PU signal, denoted by  $x_P(t)$ , we can redefine the detection problem of a possible spread spectrum PU at node A by:

$$y(t) = \begin{cases} w(t) & : \text{Under } H_0 \\ x_P(t) + w(t) & : \text{Under } H_1 \end{cases} \quad (3.19)$$

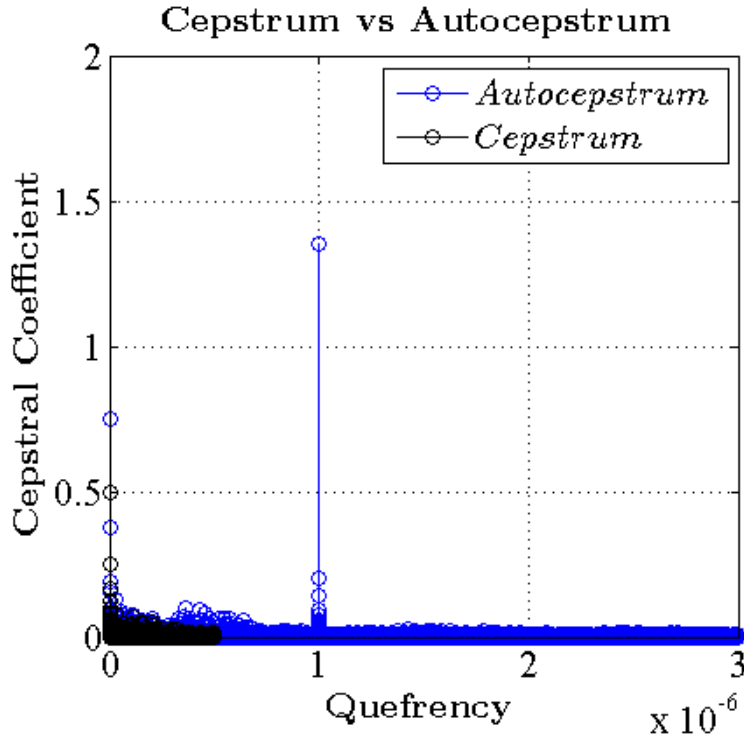


Figure 3.3 – Comparing the cepstrum and the autocepstrum of a DS-SS signal

The proposed detection approach is based on the distinguished features illustrated in Figure 3.3. In other words, by applying the autocepstrum approach under the null hypothesis, we obtain approximately only one peak at the zero quefrequency. Thus, the significance of this approach to mitigate the misdetection problem due to the undefined nature of a PU signal is measurable in terms of the occurrence of spectral line peaks at non-zero quefrequencies.

### Proposed Detectors Based on The Autocepstrum Approach

The proposed PB-ACD scheme is formulated based on the detection of a single cepstral peak occurring at  $T_{carr}$ . According to the fact that the autocepstrum of the AWGN is zero for all nonzero quefrequencies values, the detection problem can be formulated as:

$$\begin{cases} H_0 & : |c_a(\hat{n})|_{\hat{n}=N_{carr}} = 0 \\ H_1 & : |c_a(\hat{n})|_{\hat{n}=N_{carr}} \neq 0 \end{cases} \quad (3.20)$$

where  $N_{carr}$  is the number of samples corresponding to  $T_{carr}$ . To apply the proposed spectrum sensing algorithm, we have to estimate the autocorrelation of the received signal, evaluate the PSD, and get the inverse Fourier transform of its natural logarithm. To evaluate the detection results, we employ the detection test statistic given by:

$$\mathcal{T}_1[c_a] = |c_a(\hat{n})|_{\hat{n}=N_{carr}} \underset{H_0}{\overset{H_1}{\geq}} \eta_1 \quad (3.21)$$

where the detection threshold  $\eta_1$  can be evaluated based on the choice of a specific communication scenario, taking into consideration the transmission paths.

Another way to formulate the autocepstrum detector is to picture the detection problem as detecting a random peak value [54]. A reasonable approach might be to average the autocepstrum of the received samples and use this averaged value as a test statistic,  $\mathcal{T}'[c_a]$ , and compare it to a detection threshold,  $\eta'$ . In this case, the test statistic of the autocepstrum detector becomes:

$$\mathcal{T}'[c_a] = \frac{1}{N_p} \sum_{i=1}^{N_p} |c_a(i)| \underset{H_0}{\overset{H_1}{\geq}} \eta' \quad (3.22)$$

where  $N_p$  denotes the number of the autocepstral peaks. In order not to confuse the reader, in our study we refer by the autocepstrum detector to all the types of detectors that are based on calculating the autocepstrum of the received signal. These detectors include the PB-ACD technique and also the Averaged PassBand-AutoCepstrum Detection (APB-ACD) technique which will be discussed in subsection 3.4.2. It is important to mention that in the case of the DS-SS signal  $\mathcal{T}_1$  and  $\mathcal{T}'$  are the same, since we are considering only one autocepstral peak. Throughout our analysis, we find it more convenient to employ  $\mathcal{T}'$  for detecting Frequency Hopping and Chirp spread spectrum techniques, which will be discussed in subsection 3.4.2.

### Distribution of Log-Chi-Squared Random Variable

In order to derive the statistics of the proposed detector based on the NPL, we first discuss the statistics of the log-Chi-squared distribution. Let  $A$  be a random variable with the Gaussian distribution of zero mean and unit variance denoted by  $\mathcal{N}(0,1)$ . If  $X = A^2$ , then  $X$  is said to follow the Chi-squared distribution denoted by  $\chi_v^2$ . If  $Z = \log X$ , and by employing one-to-one transformation, we obtain an expression for the

Log-Chi-squared distribution with one degree of freedom,  $\log -\chi_1^2$ , as follows:

$$f_Z(z) = \frac{1}{\sqrt{2\pi}} \sqrt{\exp(z)} \exp\left(-\frac{\exp(z)}{2}\right), z > 0 \quad (3.23)$$

we can make use of the cumulant generating function to find the first and second moments [64]. The cumulant generating function is given by:

$$\mathcal{K}(m) = \log(E[\exp(z)^m]) = \log(\mathbb{E}[X^m]) \quad (3.24)$$

where  $m$  is an integer,  $\mathbb{E}[X^m]$  is the  $m^{\text{th}}$  moment of  $X$  and the moment generating function of the random variable  $X$  is defined by  $M_X(t) = \mathbb{E}[\exp(tX)]$  [106]. Thus, the moment generating function of  $\chi_1^2$  distribution is given by [107]:

$$\mu_m = \frac{2^m \Gamma(\frac{1}{2} + m)}{\Gamma(\frac{1}{2})} \quad (3.25)$$

where  $\Gamma(\cdot)$  is the upper incomplete *gamma* function<sup>2</sup>. By applying equation (3.24) into equation (3.23), we get:

$$\mathcal{K}(m) = m \log(2) + \log\left[\Gamma\left(\frac{1}{2} + m\right)\right] - \log\left[\Gamma\left(\frac{1}{2}\right)\right] \quad (3.26)$$

Thus, we can compute the required moments by applying the following formula relating cumulants and moments [107]:

$$\mu_m = \mathfrak{K}_m + \sum_{i=1}^{m-1} \binom{m-1}{i-1} \mathfrak{K}_i \mu_{i-m} \quad (3.27)$$

where  $\mathfrak{K}_m$  is the cumulant of order  $m$  obtained through the derivative of the CGF evaluated at the required moment order. Hence, we obtain the first and second cumulants by:

$$\mathfrak{K}_1 = \log 2 + \psi_d\left(\frac{1}{2}\right), \mathfrak{K}_2 = \psi_p^{(1)}\left(\frac{1}{2}\right) \quad (3.28)$$

---

2. For complex numbers with a positive real part, the *gamma* function is defined by the integral:  $\Gamma(z_0) = \int_0^\infty x_0^{z_0-1} \exp(-x_0) dx_0$ ,  $\Re > 0$ . For any positive integer  $m$ , the *gamma* function is represented by  $\Gamma(m) = (m-1)!$ .

where  $\psi_d(\cdot)$  is the *digamma* function<sup>3</sup>, which can be defined using Stirling's approximation for  $x > 0$  by [108]:

$$\psi_d(x) = \frac{\Gamma'(x)}{\Gamma(x)} \approx \log(x) + \frac{1}{2x} \quad (3.29)$$

and the first derivative of  $\psi_d(\cdot)$  is called the *polygamma* function which is denoted by  $\psi_p^{(1)}(x)$  [108]. Definition of the *polygamma* function can be given as:

$$\psi_p^{(1)}(x) \approx \frac{1}{x} - \frac{1}{2x^2} \quad (3.30)$$

We deduce from equations (3.22) and (3.25) that the mean of the  $\log -\chi_1^2$  is the first cumulant such that:

$$\mathbb{E}[Z] = \mu_Z = k_1 \quad (3.31)$$

Similarly, by employing equation (3.25), we can evaluate the second moment  $\mathbb{E}[Z^2(\hat{k})]$  as well as the variance  $\sigma_Z^2$ , where  $\hat{k}$  denotes the corresponding discrete frequency parameter in the cepstral domain.

For the  $\log -\chi_\nu^2$  with  $\nu$  degrees of freedom, the derived Probability Density Function (PDF) derived in equation (3.23), can be expressed by:

$$f_Z(z) = \frac{1}{2^{\frac{\nu}{2}} \Gamma(\frac{\nu}{2})} [\exp(z)]^{\nu/2} \exp\left(-\frac{\exp(z)}{2}\right), z > 0 \quad (3.32)$$

where  $\Gamma(\cdot)$  denotes the *upper incomplete gamma* function<sup>4</sup>. To find the first moment,  $\mu_Z$ , we compute the ensemble average of the  $\log -\chi_\nu^2$  PDF by:

$$\mathbb{E}[Z] = \int_0^{x_0} \frac{z}{2^{\frac{\nu}{2}} \Gamma(\frac{\nu}{2})} [\exp(z)]^{\nu/2} \exp\left(-\frac{\exp(z)}{2}\right) dz, 0 < x_0 < \infty \quad (3.33)$$

If we substitute  $R = \exp(z)$  and employ the integration by parts method, we obtain:

$$\mathbb{E}[Z] = \log(\exp(x_0)) \frac{\Gamma_L(\frac{\nu}{2}, 1)}{\Gamma(\frac{\nu}{2})} \left[ \frac{1}{2^{\frac{\nu}{2}}} - \frac{1}{2} \right] \quad (3.34)$$

3. The *digamma* function is a special function which is given by the logarithmic derivative of the *gamma* function.

4. For a positive integer  $s$ , the *upper incomplete gamma* function is generally expressed by:  $\Gamma(s, x_0) = \int_{x_0}^{\infty} t^{s-1} \exp(-t) dt$ .

where  $\Gamma_L(\cdot, \cdot)$  denotes the *lower incomplete gamma* function<sup>5</sup>.

Similarly, we obtain the second moment of  $Z$  by:

$$\mathbb{E}[Z^2] = \left[ \frac{\Gamma_L\left(\frac{\nu}{2}, \exp(x_0)\right)}{2^{\frac{\nu}{2}} \Gamma\left(\frac{\nu}{2}\right)} \right] \left[ (\log[\exp(x_0)])^2 - 2 \log(\exp(x_0)) \right] \quad (3.35)$$

To simplify the expressions obtained in equations (3.34) and (3.35), we express the rational function  $\frac{\Gamma_L(\cdot, \cdot)}{\Gamma(\cdot)}$  by the  $\mathbb{P}(\cdot, \cdot)$  which represents the *regularized gamma* function<sup>6</sup>. Thus, the first moment can be simplified to:

$$\mathbb{E}[Z] = \log(\exp(x_0)) \mathbb{P}\left(\frac{\nu}{2}, 1\right) \left[ \frac{1}{2^{\frac{\nu}{2}}} - \frac{1}{2} \right] \quad (3.36)$$

also, the second moment of  $Z$  can be reduced to:

$$\mathbb{E}[Z^2] = \mathbb{P}\left(\frac{\nu}{2}, 1\right) \left[ (\log[\exp(x_0)])^2 - 2 \log(\exp(x_0)) \right] \quad (3.37)$$

Consequently, to evaluate  $\sigma_Z^2 = \mathbb{E}[Z^2] - (\mathbb{E}[Z])^2$ , we can use the obtained results in equations (3.36) and (3.37). Further, the detailed derivation of the  $\log - \chi_\nu^2$  distribution and the corresponding false-alarm probability of an autocepstrum detector are given in Appendix A.

### Derivation of The Receiver Operating Characteristic for The Case of Central $\log - \chi_\nu^2$ Real-Valued Signals

Generally, we can define the autocepstrum of a signal in the discrete quefreny domain by:

$$c_a(\hat{n}) = \frac{1}{\sqrt{N}} \sum_{\hat{k}=0}^{N-1} Z(\hat{k}) \exp\left(\frac{j2\pi\hat{k}\hat{n}}{N}\right) \quad (3.38)$$

where  $N$  is the sequence length and  $Z(\hat{k})$  is the natural logarithm of the signal's PSD. Since the distribution of the noise at the CR receiver is assumed to be Gaussian, the PSD of the noise follows a Chi-squared distribution with one degree of freedom. Hence, the distribution of the natural logarithm of the noise PSD follows  $\log - \chi_\nu^2$  distribu-

5. The *lower incomplete gamma function* is given by:  $\Gamma_L(s, x_0) = \int_0^{x_0} t^{s-1} \exp(-t) dt$ .

6.  $\mathbb{P}(s, x_0)$  represents the *regularized gamma* function which is the cumulative distribution function for the Gamma random variables with the shape parameter  $s$ .

tion. Being a unitary transform, the inverse Fourier transform defined in equation (3.38) maintains the same distribution for the autocepstrum coefficient  $c_a(\hat{n})$ . Moreover, since the set of coefficients of  $\{c_a(\hat{n})\}$  is a sum of rotated IID  $\log -\chi_V^2$  random variable  $Z(\hat{k}) \exp\left(\frac{j2\pi\hat{k}\hat{n}}{N}\right)$ , the distribution of this sum can be analyzed according to two assumptions:

1. **If  $N$  is sufficiently large:** in this case, we can invoke the CLT. Hence, the test statistic is assumed to follow Gaussian distribution [54]. Based on the test statistic defined in equation (3.22), we find that  $\mathcal{T}'[c_a]$  follows normal distribution,  $\mathcal{N}(\mu_{c_0}, \sigma_{c_0}^2)$ , where  $\sigma_{c_0}^2$  denotes the variance of the autocepstrum coefficients under  $H_0$ . In this case, we must obtain the right-tail probability of the proposed test statistic under  $H_0$  for a fixed value of  $P_{FA}$ . This is generally can be expressed by [54]:

$$P_{FA} = \int_{\{C_a: \mathcal{T}' > \eta'\}} f_{C_a}(c_a; H_0) dr = \alpha_{FA} \quad (3.39)$$

where  $\eta'$  is the detection threshold,  $\alpha_{FA}$  is the  $P_{FA}$  value, and  $f_{C_a}(c_a; H_0)$  is the probability density function of a random process  $C_a$  under  $H_0$ . In particular, the false-alarm probability, for  $\mu_{c_0} = 0$ , is given by:

$$P_{FA} = Q\left(\frac{\eta'}{\sqrt{\frac{\sigma_{c_0}^2}{N}}}\right) \quad (3.40)$$

where  $Q(\cdot)$  denotes the Gaussian Q-function<sup>7</sup>. Similarly,  $\mathcal{T}'[c_a]$  under  $H_1$  follows normal distribution,  $\mathcal{N}(\mu_{c_1}, \sigma_{c_1}^2)$ , where  $\sigma_{c_1}^2$  denotes the variance of the autocepstrum coefficients under  $H_1$ . Thus, the detection probability can be expressed by [54]:

$$P_D = Q\left(\frac{\eta' - \mu_{c_1}}{\sqrt{\frac{\sigma_{c_1}^2}{N}}}\right) \quad (3.41)$$

Thus, the detection threshold can be expressed by:

$$\eta' = \sqrt{\frac{\sigma_{c_0}^2}{N}} Q^{-1}(P_{FA}) \quad (3.42)$$

---

7. The Q-function represents the tail distribution function of the normal distribution and  $\mu_{c_0}$  is the mean of the test statistic under  $H_0$ . It is given by:  $Q(x) = \frac{1}{\sqrt{2\pi}} \int_x^\infty \exp\left(-\frac{u^2}{2}\right) du$ .

To obtain an expression for the proposed detection threshold,  $\eta_1$ , we have to evaluate  $\mu$  and  $\sigma$ . The mean of  $c_a(\hat{n})$  is found from equation (3.31) by:

$$\mathbb{E}[c_a(\hat{n})] = \frac{1}{\sqrt{N}} \sum_{\hat{k}=0}^{N-1} \mathbb{E}[Z(\hat{k})] \exp\left(\frac{j2\pi\hat{k}\hat{n}}{N}\right) \quad (3.43)$$

where  $\mathbb{E}[Z(\hat{k})]$  is denoted by  $\mu_Z$ . The term  $\sum_{\hat{k}=0}^{N-1} \exp\left(\frac{j2\pi\hat{k}\hat{n}}{N_r}\right)$  yields the following:

$$\sum_{\hat{k}=0}^{N-1} \exp\left(\frac{j2\pi\hat{k}\hat{n}}{N_r}\right) = \begin{cases} N & : \text{if } \hat{n} = 0 \\ \frac{1-(-1)^{\hat{n}}}{1-\exp(j\pi\hat{n}N_r)} & : \text{elsewhere} \end{cases} \quad (3.44)$$

However, for large value of  $N_r$ , this sum yields approximately zero for  $\hat{n} \neq 0$ . Hence, this leads to:

$$\mathbb{E}[c_a(\hat{n})|_{\hat{n}=0}] = \mu_{c_a} = \mu_Z \sqrt{N} \quad (3.45)$$

Then, the variance is found by:

$$\text{Var}[c(\hat{n})] = \mathbb{E}[c_a^2(\hat{n})] - \mu_{c_a}^2 \quad (3.46)$$

thus, we need to find the second moment of  $c_a(\hat{n})$  to get the variance. The second moment is given by:

$$\begin{aligned} \mathbb{E}[c_a^2(\hat{n})] &= \frac{1}{N} \mathbb{E} \left[ \left( \sum_{\hat{k}=0}^{N-1} Z(\hat{k}) \exp\left(\frac{j2\pi\hat{k}\hat{n}}{N}\right) \right)^2 \right] \\ &= \frac{1}{N} \sum_{\hat{k}, \hat{k}'} \mathbb{E} [Z(\hat{k})Z(\hat{k}')] \exp\left(\frac{j2\pi(\hat{k} + \hat{k}')\hat{n}}{N}\right) \end{aligned} \quad (3.47)$$

for different values of  $\hat{k}$  and  $\hat{k}'$ , and assuming  $Z(\hat{k})$  and  $Z(\hat{k}')$  are uncorrelated, we get:

$$\mathbb{E}[c_a^2(\hat{n})] = \begin{cases} \frac{1}{N} \sigma_z^2 & : \hat{k}, \hat{k}' = 0 \\ \frac{1}{N} \mathbb{E}[Z^2(\hat{k})] \sum_{\hat{k}=0}^{N-1} \exp\left(\frac{j4\pi\hat{k}\hat{n}}{N}\right) & : \hat{k} = \hat{k}' \neq 0 \\ 0 & : \hat{k} \neq \hat{k}' \end{cases} \quad (3.48)$$

where  $\sigma_z^2 = \text{Var}[Z(\hat{k})]$ . Since the proposed detection scheme is based on the choice

of the autocepstral coefficients for  $\hat{n} \neq 0$ , and from equation (3.48), the exponential sum yields zero at  $\hat{n} \neq 0$  as well, then we finally get:

$$\text{Var}[c_a(\hat{n})] \approx \frac{1}{N} \sigma_Z^2 \quad (3.49)$$

Basically, each pair of  $(P_D, P_{FA})$  identifies the ROC curve which represents the reliability of a specific detector by describing. This pair is associated with a particular threshold to make the sensing decision at a specific Signal-to-Noise (SNR) value. As the threshold value increases, the  $P_{FA}$  and  $P_D$  decrease. A reliable detection decision can be remarked if the ROC curve is above the  $45^\circ$  line [54]. A  $45^\circ$  ROC curve can be attained if the detector decision ignores all the processed data and bases its decision on flipping a coin. Based on the CLT assumption mentioned, we employed the obtained results in equations (3.40) and (3.41) to plot the ROC curves of the proposed autocepstrum detector and compare them with the conventional energy detector. Figure 3.4 shows the simulated and theoretical ROC curve for the case of detecting real valued IID Gaussian signals at -5 dB. We started by employing a few number of samples (i.e.,  $N = 10$ ) to show the effect of increasing the sequence length on the detection performance. The simulation were carried on 10000 Monte Carlo iterations. We also compared the ROC metrics of the autocepstrum detector with the ED technique for  $N = 100$  at SNR of 0 dB and -5 dB as shown in Figure 3.5. We notice that with a few samples at SNR of -5 dB the proposed technique outperforms the ED technique as shown in Figure 3.6. In particular, for 100 samples, the proposed technique is superior to the ED technique at -5 dB.

Although the detection performance of an energy detector increases as the signal size increases, the noise suppression effect through the calculation of the autocepstrum of the received signal makes the performance of the proposed detector better than the ED technique as illustrated in Figure 3.7. We also note that as the number of samples increases ( $N=1000$ ), both techniques behaves similarly.

2. **If  $N$  represents a few number of samples:** this is a situation where the number of communication paths is limited. Thus, the autocepstral coefficients  $c_a(\hat{n})$  follows  $\log -\chi_1^2$ . Hence, the right-tail probability of  $\log -\chi_1^2$  distribution is obtained by:

$$P_{FA} = \int_{\eta_1}^{\infty} \frac{1}{\sqrt{2\pi}} \sqrt{\exp(z)} \exp\left(-\frac{\exp(z)}{2}\right) dz \quad (3.50)$$

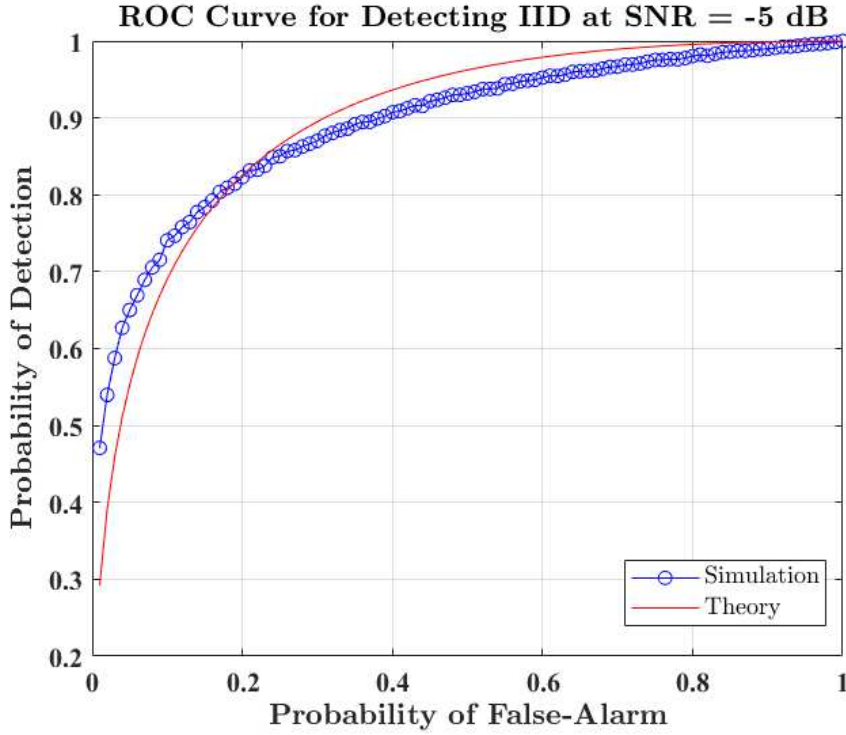


Figure 3.4 – The simulated and theoretical ROC curves of the PB-ACD technique

The integral in equation (3.50) can be simplified by methods of substitution.

If we define  $x_0 = \exp(z)$  and the noise variance is given by  $\sigma_w^2$ , it yields:

$$P_{FA} = \int_{\exp(\eta_1)}^{\infty} \frac{\sigma_w}{\sqrt{2\pi}x_0} \exp\left(-\frac{x_0\sigma_w}{2}\right) dx_0 \quad (3.51)$$

then, if we let  $u = \sqrt{\frac{x_0\sigma_w^2}{2}}$ , we obtain:

$$P_{FA} = \frac{2}{\sqrt{\pi}} \int_{\frac{\sigma_w}{\sqrt{2}}\sqrt{\exp(\eta_1)}}^{\infty} \exp(-u^2) du \quad (3.52)$$

hence, the integral in equation (3.52) can be expressed by:

$$P_{FA} = 2 Q\left(\frac{\sigma_w}{\sqrt{2}}\sqrt{\exp(\eta_1)}\right) \quad (3.53)$$

The detection threshold for a fixed value of  $P_{FA}$  and unit noise variance is found

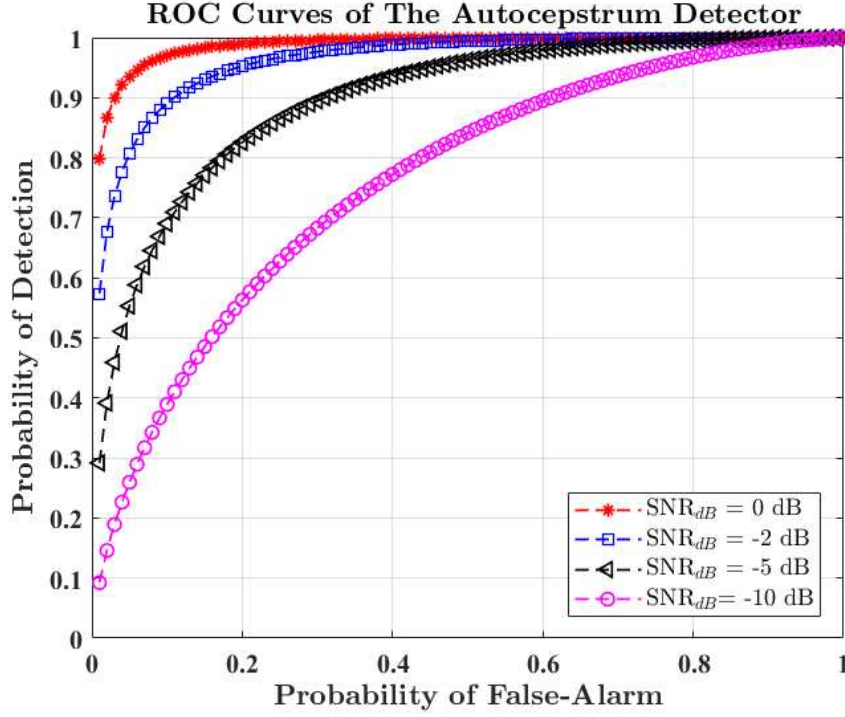


Figure 3.5 – The ROC curves of the PB-ACD simulated for different SNR values for real-valued Gaussian signals

by:

$$\eta_1 = 2 \log \left[ \sqrt{2} Q^{-1} \left( 0.5 P_{FA} \right) \right] \quad (3.54)$$

therefore, we find that the false-alarm probability in equation (3.53) depends on the appropriate selection of the detection threshold.

Recall the general expression of the probability of detection  $P_D$ :

$$P_D = Pr [\mathcal{T}_1 > \eta_1 | H_1] = \int_{\eta_1}^{\infty} f_{C_a}(c_a; H_1) dy \quad (3.55)$$

where  $f_{C_a}(c_a; H_1)$  denotes the probability density function of  $C_a$ .

To find the detection probability that characterizes the proposed detector, we need to derive an expression for  $f_{C_a}(c_a; H_1)$  first. Under  $H_1$ , the received signal at the CR receiver is given by:

$$y(t) = x_p(t) + w(t) \quad (3.56)$$

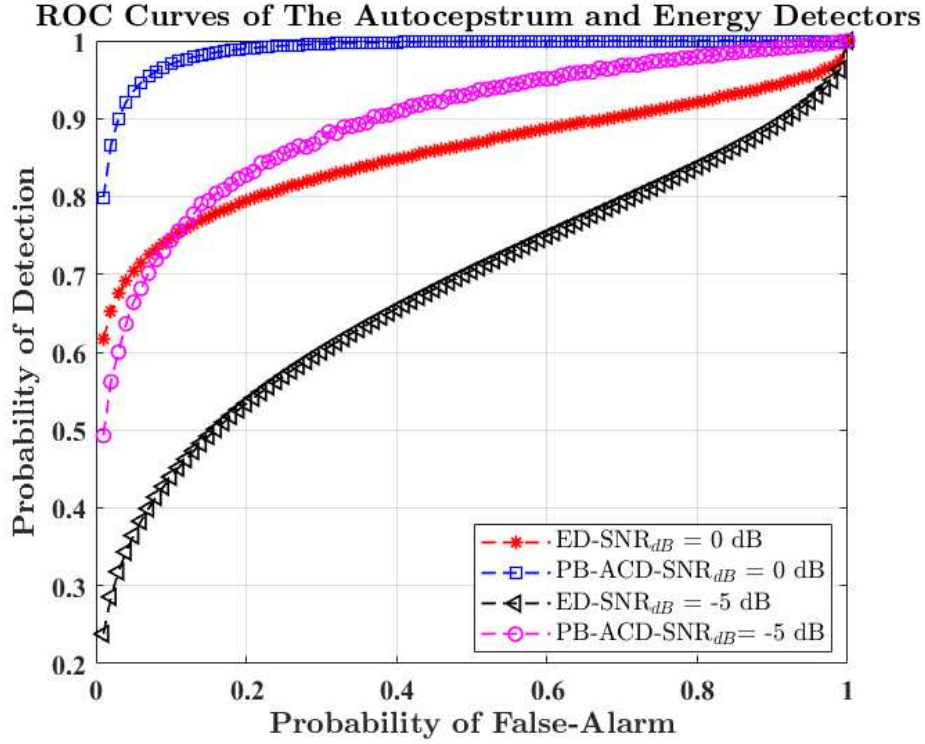


Figure 3.6 – Comparison of the ROC curves for the PB-ACD and ED techniques for different SNR values for real-valued Gaussian signals

The PU signal is assumed to be an IID random process with zero mean and variance  $\sigma_{x_p}^2$ . First, we will consider the case of having a real-valued Gaussian PU signal that is independent of the noise at the SU receiver. Thus, the PSD of the received signal becomes:

$$S_y(f) = S_{x_p}(f) + S_w(f) \quad (3.57)$$

under the aforementioned assumptions,  $S_y(f)$  follows a central  $\chi_2^2$  with two degrees of freedom. For simplicity in notation, we will refer to  $S_y(f)$  as the random process  $R$ . The general expression for the central  $\chi_v^2$  is described by [106]:

$$f_R(r) = \frac{r^{\frac{v}{2}-1} \exp(-\frac{r}{2})}{2^{\frac{v}{2}} \Gamma(\frac{v}{2})}, \quad r > 0 \quad (3.58)$$

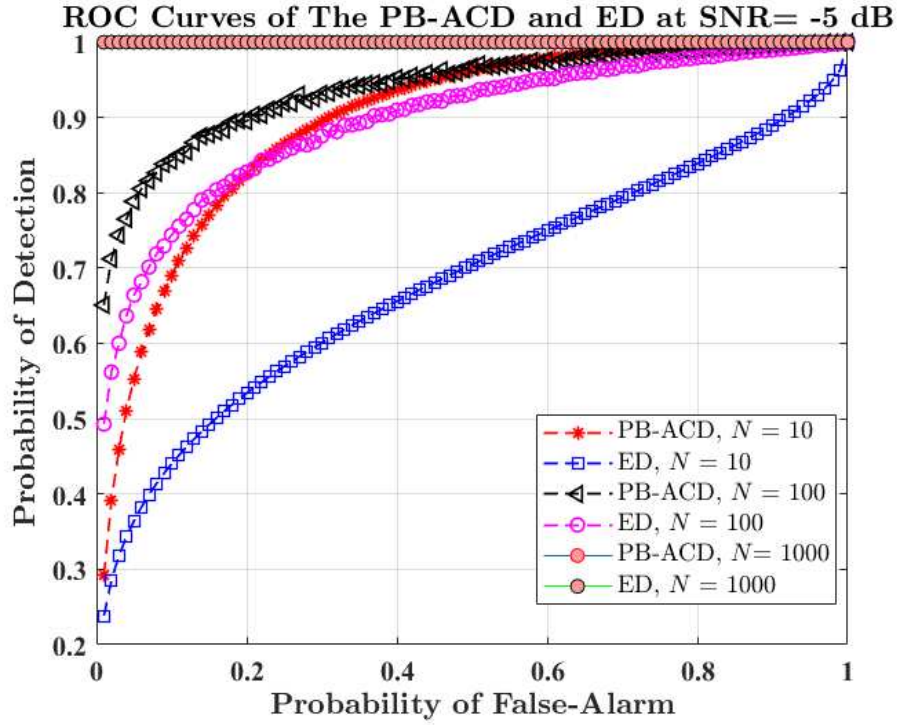


Figure 3.7 – Comparison of the ROC curves for the PB-ACD and ED techniques simulated for different signal sizes at -5 dB for real-valued Gaussian signals

where  $\nu$  denotes the number of degrees of freedom, and  $\Gamma(\cdot)$  is the *upper incomplete gamma* function, which is expressed by:

$$\Gamma(m) = (m - 1)! \quad (3.59)$$

defined for any positive integer  $m$ . For  $\nu = 2$ , equation (3.58) becomes:

$$f_R(r) = \frac{\exp(-\frac{r}{2})}{2}, \quad r > 0 \quad (3.60)$$

which reduces to an Exponential distribution with the decay rate of 2. If  $Z = \log[R]$ , then the test statistic under  $H_1$  follows *log-exponential* distribution. The cumulative distribution function of  $R$  is described by:

$$F_R(r) = \int_0^r f_R(r) dr = 1 - \exp\left(-\frac{r}{2}\right) \quad (3.61)$$

then the cumulative distribution function of  $Z$  is given by:

$$\begin{aligned}
 F_Z(z) &= Pr [Z \leq z] \\
 &= Pr [\log r \leq z] = Pr [r \leq \exp(z)] \\
 &= 1 - \exp\left(-\frac{\exp(z)}{2}\right)
 \end{aligned} \tag{3.62}$$

then, by differentiating equation (3.62) we obtain:

$$f_Z(z) = \frac{d}{dz} F_Z(z) = \frac{1}{2} \exp\left(-\frac{\exp(z)}{2}\right) \exp(z), \quad z > 1 \tag{3.63}$$

To find the detection probability, we solve the given integral:

$$P_D = \frac{1}{2} \int_{\eta_1}^{\infty} \exp\left(-\frac{\exp(z)}{2}\right) \exp(z) dz \tag{3.64}$$

by using the method of substitution, and by letting  $x_0 = \exp(z)$ ,  $P_D$  is obtained as:

$$P_D = \exp\left(-\frac{\sigma_x^2}{2} \exp(\eta_1)\right) \tag{3.65}$$

where  $\sigma_x^2$  denotes the variance of the signal  $x_p(t)$ . By substituting  $\eta_1$  from equation (3.65) into  $P_{FA}$  found in equation (3.53) and for  $\sigma_s^2 = 1$ , the mathematical relation joining  $P_{FA}$  and  $P_D$  is given by:

$$P_{FA} = Q\left(j\sqrt{2\log P_D}\right) \tag{3.66}$$

Since the Gaussian Q-function is usually defined for real non-negative arguments, expressions involving the Q-function are usually applicable only for a limited range of values of the physical parameters involved [109]. Therefore, the extension of the Q-function to the complex plane results in more powerful representations that are independent on the physical parameters. The equivalent to the complex Q-function is the complex complementary error function which is used more often in detection problems that involves complex arguments [109], [110]. Given in terms of the Faddeeva

function<sup>8</sup>[109], the complex complementary error function is given by:

$$erfc(jz) = \mathfrak{w}(z) \exp(z^2) \quad (3.67)$$

where  $\mathfrak{w}(z)$  is the Faddeeva function which is given in terms of the Fresnel integral [109]. Since  $Q(z) = 0.5 \operatorname{erfc}\left(\frac{z}{\sqrt{2}}\right)$  where  $\operatorname{erfc}(\cdot)$  is the complementary error function<sup>9</sup>. The false-alarm probability, defined in equation (3.66), can be expressed by:

$$P_{FA} = 0.5 \operatorname{erfc}\left(j\sqrt{2\log P_D}\right) \quad (3.68)$$

### Derivation of The Receiver Operating Characteristic for The Case of Non-Central $\log -\chi_v^2$ Real-Valued Signals

Under  $H_0$ , the distribution of  $S_y(f)$ , denoted by  $R$  for simplicity, for real Gaussian noise with mean  $\mu_w$  is the non-central  $\chi_1^2$ . The non-centrality parameter is given by:

$$\lambda = \sum_i^k \mu_i^2 \quad (3.69)$$

thus, the non-central  $\chi_1^2$  of one degree of freedom is given by [106]:

$$f_R(r) = \chi^2(1, \lambda) = \frac{r^{-1/2} \exp\left(-\frac{r+\lambda}{2}\right)}{\sqrt{2} \Gamma\left(\frac{1}{2}\right)} \left[ \frac{\exp(-\sqrt{r\lambda}) + \exp(\sqrt{r\lambda})}{2} \right] \quad (3.70)$$

Similarly, the distribution of the test static in this case for  $Z = \log[R]$  is described by:

$$f_Z(z) = \frac{1}{\sqrt{2\pi}} \exp\left(\frac{z}{2}\right) \exp\left(-\frac{\exp(z) + \lambda}{2}\right) \left[ \frac{\exp(-\sqrt{\exp(z)\lambda}) + \exp(\sqrt{\exp(z)\lambda})}{2} \right] \quad (3.71)$$

8. The Faddeeva function, or Kramp function, is a scaled complex complementary error function which is related to the Fresnel integral, to Dawson's integral, and to the Voigt function. It arises in various physical problems in describing electromagnetic response in complicated media. It is given by the integral:  $\mathfrak{w}(z) = \exp(-z^2) \left(1 + j \frac{2}{\sqrt{\pi}} \int_0^z \exp(t^2) dt\right)$ .

9. The complementary error function is given by  $\operatorname{erfc}(x) = \frac{2}{\sqrt{\pi}} \int_x^\infty \exp(-t^2) dt$

hence, the false-alarm probability is obtained by:

$$\begin{aligned}
 P_{FA} &= \int_{\eta}^{\infty} f_Z(z) dz \\
 &= C \left[ \int_{\exp(\eta)}^{\infty} x_0^{-1/2} \exp(-x_0(\frac{1}{2} + \lambda)) dx_0 + \int_{\exp(\eta)}^{\infty} x_0^{-1/2} \exp(x_0(\frac{-1}{2} + \lambda)) dx_0 \right]
 \end{aligned} \tag{3.72}$$

where  $C = \frac{\exp(-\lambda/2)}{\sqrt{2\pi}}$  and  $x_0 = \exp(z)$ . The two integrals given by equation (3.72) can be solved using integration by methods of substitution. Let  $I_I$  and  $I_{II}$  denote the two integrals representing  $P_{FA}$  such that:

$$\begin{aligned}
 I_I &= \int_{\exp(\eta)}^{\infty} x_0^{-1/2} \exp(-a x_0) dx_0 \\
 I_{II} &= \int_{\exp(\eta)}^{\infty} x_0^{-1/2} \exp(b x_0) dx_0
 \end{aligned} \tag{3.73}$$

where  $a = \lambda + \frac{1}{2}$  and  $b = \lambda - \frac{1}{2}$ . To solve for  $I_I$ , let  $u = \sqrt{a x_0}$ , hence:

$$\begin{aligned}
 I_I &= 2\sqrt{a} \int_{\sqrt{a \exp(\eta_1)}}^{\infty} \exp(-u^2) du = \sqrt{a\pi} \operatorname{erfc}(\sqrt{a \exp(\eta_1)}) \\
 &= \sqrt{\left(\lambda + \frac{1}{2}\right) \pi} \operatorname{erfc}\left(\sqrt{\left(\lambda + \frac{1}{2}\right) \exp(\eta_1)}\right)
 \end{aligned} \tag{3.74}$$

Likewise, by employing the imaginary error function that is given by [110]:

$$\operatorname{erfi}(z) = \frac{2}{\sqrt{\pi}} \int_0^z \exp(t^2) dt \tag{3.75}$$

the second integral,  $I_{II}$ , is obtained as:

$$\begin{aligned}
 I_{II} &= \sqrt{b\pi} \left( 1 - \operatorname{erfi}(\sqrt{a \exp(\eta_1)}) \right) \\
 &= \sqrt{\left(\lambda - \frac{1}{2}\right) \pi} \left( 1 - \operatorname{erfi}\left(\sqrt{\left(\lambda - \frac{1}{2}\right) \exp(\eta_1)}\right) \right)
 \end{aligned} \tag{3.76}$$

thus, by combining the two integrals we get:

$$P_{FA} = \frac{\exp(-\lambda/2)}{\sqrt{2}} \left[ \sqrt{\left(\lambda + \frac{1}{2}\right)} \pi \operatorname{erfc} \left( \sqrt{\left(\lambda + \frac{1}{2}\right) \exp(\eta_1)} \right) + \sqrt{\left(\lambda - \frac{1}{2}\right)} \pi \left( 1 - \operatorname{erfi} \left( \sqrt{\left(\lambda - \frac{1}{2}\right) \exp(\eta_1)} \right) \right) \right] \quad (3.77)$$

Based on equation (3.77), the false-alarm probability is a function of the non-centrality parameter and the detection threshold.

Under  $H_1$ , the distribution of  $S_r(f)$  follows a non-central  $\chi_2^2$  of two degrees of freedom with  $\lambda = \sum_{i=1}^2 \mu_i^2$ , which is given by:

$$f_R(r) = \frac{1}{2} \exp\left(-\frac{r+\lambda}{2}\right) I_0(\sqrt{\lambda r}) \quad (3.78)$$

where  $I_0$  denotes the modified Bessel function of the first kind. Consequently, the distribution of  $Z$  is given by the Rice density function:

$$f_Z(z) = \frac{1}{2} \exp\left(-\frac{\exp(z) + \lambda}{2}\right) I_0(\sqrt{\lambda \exp(z)}) \exp(z) \quad (3.79)$$

In order to find  $P_D$ , let us define  $x_0 = \sqrt{\exp(z)}$  and  $d^2 = \lambda$ , hence we need to solve the following integral such that:

$$P_D = \int_{\sqrt{\exp(\eta_1)}}^{\infty} x_0 I_0(dx_0) \exp\left(-\frac{x_0^2 + d^2}{2}\right) dx_0 \quad (3.80)$$

Recall the expression of the Marcum Q-function  $Q_M(\cdot)$ , which is given by [111]:

$$Q_M(a, b) = \int_b^{\infty} x_0 \left[\frac{x_0}{a}\right]^{M-1} \exp\left[-\frac{x_0^2 + d^2}{2}\right] I_{M-1}(bx_0) dx_0 \quad (3.81)$$

where  $M$  denotes the order of the  $Q_M$ . By comparing the integral in equation (3.79) to equation (3.80),  $P_D$  can be expressed by:

$$P_D = Q_1(\sqrt{\lambda}, \sqrt{\exp(\eta_1)}) \quad (3.82)$$

The Marcum Q-function is a monotonic and log-concave function which is a general-

ized form of the Gaussian Q-function. One possible approximation of equation (3.81) is given for a large value of  $\eta_1$  using the asymptotic form of the zero-order modified Bessel function of the first kind [111]. This approximation comes in the form of:

$$Q_1(a, b) = \sqrt{\frac{b}{a}} Q(b - a) \quad (3.83)$$

by applying equation (3.83) to equation (3.82), we obtain:

$$Q \left[ \exp \left( \frac{\eta_1}{2} \right) - \lambda^{1/2} \right] = P_D \frac{\lambda^{1/4}}{\exp(\eta_1/4)} \quad (3.84)$$

The Chernoff bound of the Gaussian Q-function is given by [112]:

$$Q(x) \leq \exp\left(-\frac{x^2}{2}\right), \quad x > 0 \quad (3.85)$$

by employing Equation (3.85) in equation (3.84) we obtain:

$$\left[ \frac{\eta_1}{2} - \exp \left( \frac{\eta_1}{2} \right) \right] = 2 \log \left[ P_D \lambda^{1/4} \right] - \sqrt{\lambda} \quad (3.86)$$

By referring to the left-hand side of equation (3.86) as the  $\eta_{\log}$ , equation (3.86) can be rewritten as:

$$\eta_{\log} = 2 \log \left[ P_D \lambda^{1/4} \right] - \sqrt{\lambda} \quad (3.87)$$

which is a function of the detection threshold as well as the non-centrality parameter  $\lambda$ .

### Derivation of The Receiver Operating Characteristic for The Case of Circularly Symmetric Complex Gaussian Signals

Generally, if a random variable is said to be a Circularly Symmetric Complex Gaussian (CSCG), its real and imaginary parts are independent and have equal variance. Basically, if  $y(t) = w(t)$  under  $H_0$ , and the noise is said to be CSCG signal, thus  $|W(f)|$  follows Rayleigh distribution. Therefore, the distribution of  $S_y(f) = S_w(f)$  is given by the Exponential distribution [107]:

$$f_R(r) = \frac{1}{\alpha_E} \exp\left(\frac{-r}{\alpha_E}\right), \quad \alpha_E > 0, \quad r > 0 \quad (3.88)$$

where  $\alpha_E$  is the scale parameter of the distribution. Then, the distribution of the log PSD of the received noise is given in terms of the log-Exponential distribution by:

$$f_Z(z) = \frac{1}{\alpha_E} \exp\left(-\frac{\exp(z)}{\alpha_E} + z\right), \quad \alpha_E > 0, z > 1 \quad (3.89)$$

the false-alarm probability is given by:

$$P_{FA} = \int_{\eta_1}^{\infty} f_Z(z) dz = \exp\left(-\frac{\eta}{\alpha_E}\right) \quad (3.90)$$

Under  $H_1$ , the received signal's PSD  $S_y(f) = S_{xp}(f) + S_w(f)$  indicates a sum of squares of two Rayleigh distributed signals that are independent to each other. Equivalently, we have  $S_{xp}(f)$  and  $S_w(f)$  follows Exponential distribution. Their joint CDF is given by:

$$F_R(r) = 1 - \exp\left(-\frac{r}{\alpha_E}\right) - \frac{r}{\alpha_E} \exp\left(-\frac{r}{\alpha_E}\right) \quad (3.91)$$

By differentiating the CDF, we obtain:

$$f_R(r) = \frac{r}{\alpha_E^2} \exp\left(-\frac{r}{\alpha_E}\right) \quad (3.92)$$

where  $f_R(r)$  is the log-Erlang( $m_E, \alpha_E$ ) distribution<sup>10</sup> which is a special case of the Gamma distribution [107] and  $m_E$  is the number of random variables. The difference between the Erlang and the Gamma distribution is that in the Gamma distribution  $m_E$  can be non-integer [107]. Consequently, the statistical distribution that describes the characteristics of the test statistic under  $H_1$  is given by:

$$f_Z(z) = \frac{r}{\alpha_E^2} \exp(2z) \exp\left(-\frac{\exp(z)}{\alpha_E}\right) \quad (3.93)$$

which represents the log-Erlang( $m_E, \alpha_E$ ) distribution for  $m = 2$ . Thus the detection probability is described by:

$$P_D = \exp\left(-\frac{\exp(\eta_1)}{\alpha_E}\right) \left[ \frac{\exp(\eta_1)}{\alpha_E} + \frac{1}{\alpha_E^2} \right] \quad (3.94)$$

10. The Erlang distribution with the shape parameter,  $m_E \in \mathbb{N}$ , and the scale parameter,  $\alpha_E > 0$ , corresponds to a sum of  $m_E$  independent exponential distributions with the exponential rate  $\alpha_E$ .

### Threshold-Sensing-Throughput Trade-off

In the following, we study the problem of designing the sensing duration to maximize the achievable throughput for the secondary network while the PU is sufficiently protected. We introduce the problem of designing the suitable detection threshold that maximizes the SU's throughput. Also, we formulate the mathematical presentation of threshold-sensing-throughput trade-off and we employ the proposed PB-ACD technique to show that the formulated problem has an optimal sensing and threshold that yields the highest throughput for the CR network.

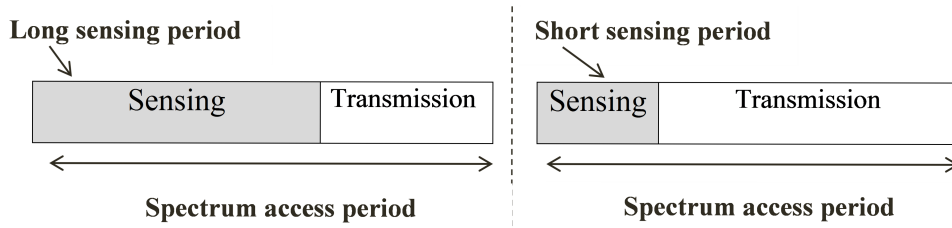


Figure 3.8 – The frame structure for periodic sensing

For a CR network designed with periodic spectrum sensing, each frame consists of one sensing slot and one data transmission slot [8]. The sensing and frame durations are denoted by  $\tau_s$  and  $T_f$ , respectively. The frame structure and the sensing-throughput trade-off is demonstrated in Figure 3.8. First, we start by describing the throughput of the CR network in two different scenarios by which it can operate at the PU frequency band. These scenarios are defined as follows:

1. When the PU signal is not present and there is no false-alarms generated by the SU signal, the achievable throughput of the SU link is described by [8]:

$$R_0 = \frac{T_f - \tau_s}{T_f} C_0 [(1 - P_{FA}) P(H_0)] \quad (3.95)$$

where  $C_0$  denotes the capacity of the SU signal under  $H_0$ ,  $P(H_0)$  is the absence probability of the PU, and  $(1 - P_{FA})$  describes the correct-no-detection probability,  $P_{CN}$ . Generally, if the PU and SU signals are assumed as Gaussian distributed and independent to each other,  $C_0$  describes the capacity of the secondary network when it operates in the absence of the PU signals. Thus, we can define it by:

$$C_0 = B_s \log_2 [1 + SNR_s] \quad (3.96)$$

where  $B_s$  is the bandwidth of the SU signal,  $SNR_s = \frac{P_s}{P_w}$  denotes the SNR of the secondary link assuming point-to-point transmission in the secondary network,  $P_s$  is the received power of the SU signal and  $P_w$  is the noise power.

2. When the PU is active but miss-detected by the CR receiver, then the achievable SU throughput is given by:

$$R_1 = \frac{T_f - \tau_s}{T_f} C_1 [(1 - P_D) P(H_1)] \quad (3.97)$$

where  $C_1$  is the capacity of the SU signal under  $H_1$ ,  $P(H_1)$  is the active probability of the PU, and  $(1 - P_D)$  refers to the misdetection probability  $P_{MD}$ . The capacity of the SU under  $H_1$  is given by:

$$C_1 = B_s \log_2 \left[ 1 + \frac{SNR_s}{SNR_p + 1} \right] \quad (3.98)$$

where  $SNR_s = \frac{P_s}{P_w}$  denotes the SNR of the primary link and  $P_p$  is the interference power measured at the CR receiver.

Thus, the average throughput for the secondary network is given by:

$$R_{avg}(\tau_s, \eta_1) = R_0(\tau_s, \eta_1) + R_1(\tau_s, \eta_1) \quad (3.99)$$

Since  $C_0 > C_1$ , the equation (3.99) can be approximated by:

$$R_{avg}(\tau_s, \eta_1) \approx R_0(\tau_s, \eta_1) \quad (3.100)$$

From the literature, the sensing-throughput trade-off is formulated as an optimization problem which is stated as:

$$\begin{aligned} \max_{\tau_s} \quad & \tilde{R}_{avg}(\tau_s, \eta_1) = R_0(\tau_s, \eta_1) \\ \text{s.t} \quad & P_D \geq \bar{P}_D \end{aligned} \quad (3.101)$$

where  $\bar{P}_D$  denotes the target detection probability which is set to be close but not equal to 1 in order to allow the protection of the PU while the SU is allowed to access the frequency band when it is idle. For this reason, the activity probability of the PU is considered small such that it is economically advisable to explore the SU for the intended

frequency band. An example of the achievable SU's throughput for ED based on equation (3.99) is shown in Figure 3.8 where  $R_{avg}(\tau_s, \eta_1)$  denotes the average throughput. When the PB-ACD technique is applied while choosing  $P_D = \bar{P}_D$ , we employ the expressions of  $P_{FA}$  and  $P_D$  derived in equations (3.90) and (3.84) for the case of CSCG signal and noise in equation (3.100). By differentiating equation (3.100) with respect to  $\tau_s$ , it can be verified that:

$$\frac{\tilde{R}'_{avg}}{C_0 P(H_0)} = -\frac{1}{T_f} + \frac{1}{T_f} \exp\left(-\frac{\eta_1}{\alpha_E}\right) \quad (3.102)$$

where  $\tilde{R}'_{avg}$  denotes the first derivative of the approximated average throughput of the SU network. By using the fact that the function  $\exp\left(-\frac{\eta_1}{\alpha_E}\right)$  is upper bounded by 0 for large values of  $\eta_1$ , thus:

$$\lim_{\tau \rightarrow T_f} \tilde{R}'_{avg} < C_0 P(H_0) \left( -\frac{1}{T_f} + \frac{1}{T_f} \exp\left(-\frac{\eta_1}{\alpha_E}\right) \right) < 0 \quad (3.103)$$

also,

$$\lim_{\tau_s \rightarrow 0} \tilde{R}'_{avg} = +\infty \quad (3.104)$$

From equations (3.103) and (3.104), we note that there is a maximum point of  $\tilde{R}_{avg}$  within the frame interval  $T_f$ . Moreover, by differentiating equation (3.100) with respect to  $\eta_1$ , we find that:

$$\frac{\tilde{R}'_{avg}}{C_0 P(H_0)} = \alpha_E \exp\left(-\frac{\eta_1}{\alpha_E}\right) - \frac{\alpha_E \tau}{T_f} \exp\left(-\frac{\eta_1}{\alpha_E}\right) \quad (3.105)$$

thus, we obtain:

$$\lim_{\eta_1 \rightarrow +\infty} \tilde{R}'_{avg} < C_0 P(H_0) \left( 1 - \frac{1}{\tau_s} \right) \exp\left(-\frac{\eta_1}{\alpha_E}\right) < 0 \quad (3.106)$$

also,

$$\lim_{\eta_1 \rightarrow 0} \tilde{R}'_{avg} = \alpha_E C_0 P(H_0) \left( 1 - \frac{1}{\tau_s} \right) \quad (3.107)$$

We find that as  $\eta_1$  increases,  $P_{FA}$  decreases hence the throughput increases. Thus, there is a unique point of  $\eta_1$  at which the maximum throughput of the SU link is achieved at certain sensing interval  $\tau_s$ . For the case of the PB-ACD detector, the achievable SU's

throughput is shown in Figure 3.9 and an overall comparison of  $R_{avg}$  between ED and the PB-ACD is illustrated in Figure 3.11 which shows that the PB-ACD provides an increased SU's throughput.

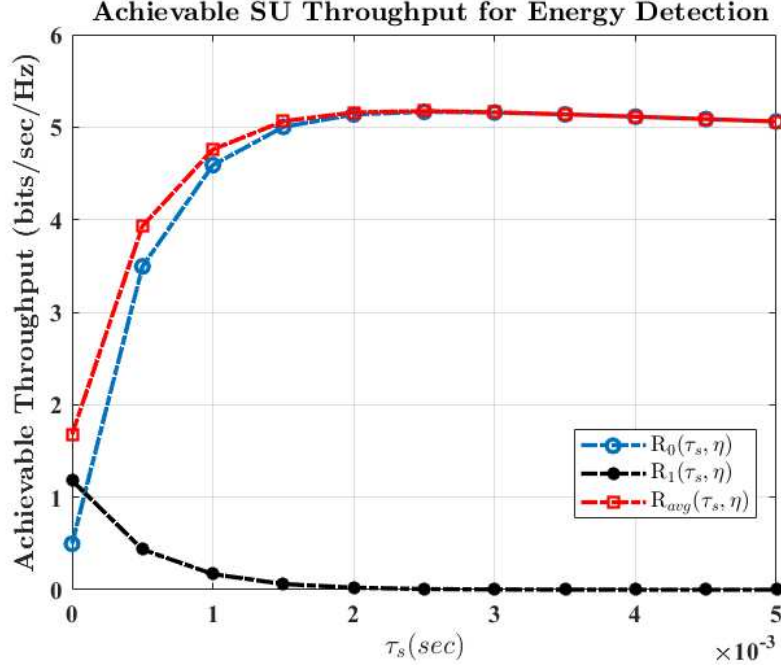


Figure 3.9 – The achievable SU's throughput for the ED technique [8]

Moreover, we study the average throughput of the proposed PB-ACD technique based on the CLT approximation of the proposed detector analyzed from equation (3.39) to equation (3.42). As discussed earlier, a high probability of detection is required to guarantee the protection of the quality-of-service of the primary network. Therefore, for a given target detection probability,  $\bar{P}_D$ , the probability of false-alarm is expressed by:

$$P_{FA} = Q\left(Q^{-1}(\bar{P}_D) \sqrt{SNR_p} + \sqrt{\tau_s f_s SNR_p}\right) \quad (3.108)$$

Since the sequence length is calculated based on the sensing duration  $\tau_s$ , such that  $N = f_s \tau_s$ , the value of  $P_{FA}$  is affected by the sensing time during a time frame  $T_f$ .

For the sake of comparison, we present the simulation results in Figure 3.12 for the proposed PB-ACD technique and compare it with energy detection. The frame duration is set to  $T_f = 100$  msec, the prior probability that a target frequency band is active is assumed  $P(H_1) = 0.2$ , the received SNR from the secondary user transmitter is  $SNR_s = 20$  dB, and  $SNR_p = -15$  dB, whereas as the sampling frequency is assumed

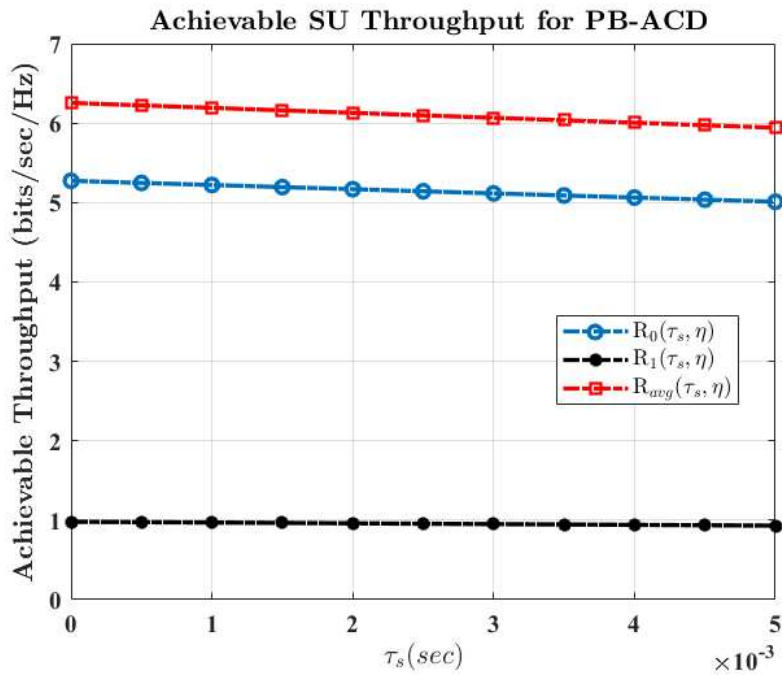


Figure 3.10 – SU’s achievable throughput for the PB-ACD technique

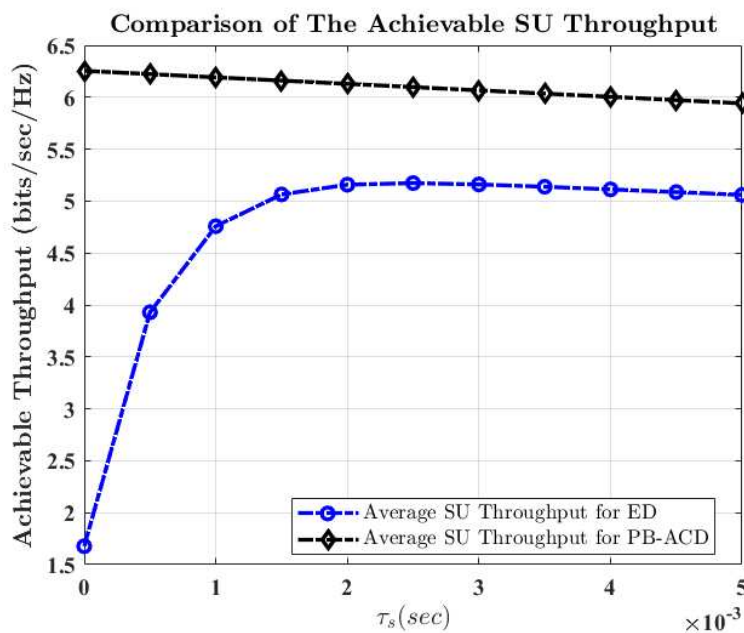


Figure 3.11 – A comparison of the achievable SU’s throughput between the ED and the PB-ACD techniques

to be 6 MHz. The target probability is set to 90%, whereas the sensing time is ranging from 0 to 5 msec. As shown in Figure 3.12, the achievable throughput of the proposed sensing technique is higher compared to the respective throughput to the conventional energy detector. Analytically, we see that the probability of false-alarm given in equation (3.108) is lower than that of the energy detection technique, such that [8]:

$$P_{FA_{ED}} = Q\left(Q^{-1}(\bar{P}_D)\sqrt{2 SNR_p + 1} + \sqrt{\tau_s f_s} SNR_p\right) \quad (3.109)$$

Thus, by referring to equation (3.95), the term  $1 - P_{FA}$ , which represents the probability of correct no detection, increases for the proposed PB-ACD technique that consequently increases the average throughput of the SU. One can clearly see that the average achievable throughput of the proposed PB-ACD technique is much higher than energy detection for short sensing durations. As the sensing time increases, both techniques achieve the same throughput at  $\tau_s = \frac{T_f}{2}$ . As the sensing time increases within the frame duration, the average throughput decreases.

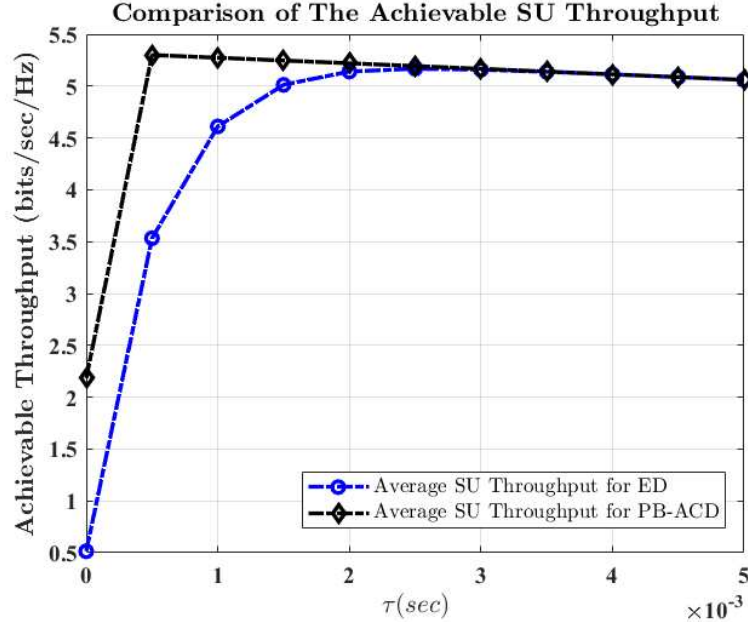


Figure 3.12 – A comparison of the achievable SU’s throughput between the ED and the PB-ACD techniques based on the CLT assumption

### 3.4.2 Application of The PB-ACD Technique to Detecting Frequency-Hopping and Chirp Spread Spectrum Signals

The increased dimensionality of the signals by SS techniques has the goal of making eavesdropping and/or jamming more difficult. In particular, if there are more dimensions in the signal to consider, its probability-of-intercept will be low. In the SS techniques, the main method of increasing the dimensionality of the signals is to increase their spectral occupancy. In section 3.4, we started to discuss the impact of applying the PB-ACD technique for detecting DS-SS signals. In the following, we broaden our investigations on the capability of the CA approaches to detect other SS techniques such as, FH-SS and C-SS. We introduce the APB-ACD technique which exploits the average of the autocepstral peaks inherited in the FH-SS and C-SS signals.

#### Detection of FH-SS Signals by The APB-ACD Technique

In FH-SS, the carrier frequency of the sinusoidal signal modulated by the data is changed periodically over a predetermined bandwidth. This is achieved by hopping the center frequency of the carrier signal among  $N_{sub}$  contiguous but non-overlapping frequency bands in a pseudo random manner. In this case, the overall spectrum occupancy is increased by the factor  $N_{sub}$ . Mathematically, the hopping signal can be represented by [113]:

$$h_{hop}(t) = \sum_{i=-\infty}^{\infty} p(t - iT_c) \cos(2\pi f_i t + \phi_i) \quad (3.110)$$

where  $p(t)$  denotes the pulse shape used for the hopping waveform which is typically represented as a square pulse. Also,  $f_i \in \{f_1, f_2, \dots, f_{N_{sub}}\}$  are the  $N_{sub}$  hop frequencies, and  $\phi_{h_i}$  are the phases of each oscillator. The Frequency-Hopped (FH) transmitted signal is given by [113]:

$$s_{FH} = [s_d(t) h_{hop}(t)]_{BPF} \quad (3.111)$$

where  $s_d(t)$  is the bandpass data signal that depends on the employed modulation scheme, and the bandpass filter, applied to the quantity within  $[.]_{BPF}$ , is designed to transmit the sum frequencies part of the signal. The FH signal occupies a separate frequency band that is determined by the hopping sequence as the time advances. Thus, the PSD of the transmitted signal is seems to spread on the average over the

entire band. If each frequency band is utilized  $\frac{1}{N_{sub}}$  of the time, the overall spectrum will be similar to that seen in DS-SS systems when averaged over a sufficiently long time period [113].

Normally, the reception of a FH-SS signal can be accomplished through coherent detection in which the despread signal  $y(t)$  is obtained by multiplying the incoming signal and filtering out the images or by non-coherent detection. In the coherent detection, the knowledge of the hopping pattern is required. For the interweave CR system, the identification of the PU signal is not a main task for spectrum sensing, however, only detecting the signal presence is the target. Thus, without knowing the hopping pattern, detection of a possible PU FH-SS signal becomes a challenge. Our objective is to utilize the periodicity inherited in the FH-SS signal in the cepstral domain to detect its presence. The PSD of a FH-SS signal can be expressed by [113]:

$$S_{FH}(f) = S_d(f) * H_{hop}(f) \quad (3.112)$$

where  $S_d(f)$  is the PSD of the data signal before hopping and  $H_{hop}(f)$  denotes the PSD of the hopping waveform. As an example, let us consider the PSD when BPSK with coherent frequency hopping is used. From previous developments, the passband PSD of the BPSK is given by [36]:

$$S_d(f) = \frac{A_s T_b}{4} [\text{sinc}^2(T_b(f - f_c)) + \text{sinc}^2(T_b(f + f_c))] \quad (3.113)$$

Assuming that all the hop frequencies are equally likely and the frequency spacing between the hop frequencies to be an integer multiple of the hop rate, then  $H_{hop}(f)$  can be expressed by [113]:

$$\begin{aligned} H_{hop}(f) \approx & \frac{1}{N_{sub}^2} \sum_{i=1}^{N_{sub}} [\delta(f - f_i) + \delta(f + f_i)] \\ & + \frac{T_c}{N_{sub}} \left(1 - \frac{1}{N_{sub}}\right) \sum_{i=1}^{N_{sub}} [\text{sinc}^2(T_b(f - f_i)) + \text{sinc}^2(T_b(f + f_i))] \end{aligned} \quad (3.114)$$

By applying equation (3.111), the PSD of the transmitted FH-SS signal is given by [113]:

$$S_{FH}(f) = \frac{PT_b}{2N_{sub}} \sum_{i=1}^{N_{sub}} [\text{sinc}^2(T_b(f - f_i - f_c)) + \text{sinc}^2(T_b(f + f_i + f_c))] \quad (3.115)$$

where the constant  $P = \frac{A_s^2 T_c}{2}$ . Referring to Equation (3.105), the PSD of the FH-SS signal is the sum of  $N_{sub}$  replicas of the PSD of the information signal each located at certain hopping frequency. If  $i = 1$  and  $f_i + f_c = f_0$ , equation (3.115) can be rewritten as:

$$S_{FH_{i=1}}(f) = \frac{PT_b}{2N_{sub}} \left[ \text{sinc}^2(T_b(f - f_0)) + \text{sinc}^2(T_b(f + f_0)) \right] \quad (3.116)$$

We find that the result obtained in equation (3.116) is similar to the analysis carried on in equations (3.16) and (3.17). Consequently, we find that for  $k = 1$ , the natural logarithm of  $S_{FH}(f)$  experiences periodicities since the natural logarithm of  $\text{sinc}(\cdot)$  function gives negative periodicity. Since the spectrum of a FH-SS signal includes  $N_{sub}$  terms each located at different  $f_0$ , thus the inverse Fourier transform of  $S_{FH}(f)$  will include not only one major autocepstral peak like the case of the DS-SS signal. In this case, the detection of a FH-SS PU signal can be formulated based on averaging these autocepstral peaks.

In Figure 3.13, we give an example of a SFH-SS signal. The SFH-SS scheme is characterized by having one or multiple symbols transmitted per hop. It is used to reduce the effects of radio signal fading and to minimize the effects of interference from radio channels that are operating on the same radio frequency. In the given example in Figure 3.13, we employ 4-ary Frequency Shift Keying (4-FSK) modulation where the FSK frequency tones are  $f_1 = 2$  MHz, and  $f_2 = 8$  MHz. The length of the data sequence is 10000 samples and the pseudo-number sequence generator consists of 4 flip-flops. The length of the PN segment per hop is 3 such that every segment corresponds to a specific hopping carrier frequency among 8 possible values. Since we assume that a carrier hops to a new frequency after transmitting two FSK symbols or equivalently, 4 information bits. The considered data rate is 1 Mbps and the range of the scanned bandwidth is over about [10,34] MHz. The spectrum of the 8 subcarriers is shown in Figure 3.14 and the PSD of the frequency-hopped signal is shown in Figure 3.15. By computing the autocepstrum of given SFH-SS/FSK signal, the autocepstral coefficients are manifested as significant peaks as shown in Figure 3.16. These peaks reflect the presence of the subcarrier signals in the analyzed signal.

By averaging the autocepstral peaks we can identify the presence of FH-SS signal in a target frequency band. In particular, the proposed technique for detecting FH-SS signals is designed to combine the autocepstral peaks to formulate the APB-ACD technique. By combing these peaks which occur at integer multiple of  $\frac{1}{f_i + f_c}$ , the detection

test statistic can be expressed as:

$$\mathcal{T}_2[c_a] = \frac{1}{N_p} \sum_{i=1}^{N_p} [|c_a(i)|] \underset{H_0}{\overset{H_1}{\gtrless}} \eta_2 \quad (3.117)$$

where  $N_p$  denotes the number of autocepstral peaks and  $\eta_2$  denotes the detection threshold. To find an expression for the detection threshold, we need to find the suitable statistical distribution of  $\mathcal{T}_2[c_a]$ . Obviously, the statistical distribution of the detector test statistic is influenced by  $N_p$  and the distribution of  $c_a(i)$ . Under  $H_0$  and in the case of real-valued AWGN signal,  $S_y(f)$  follows a Chi-squared distribution.

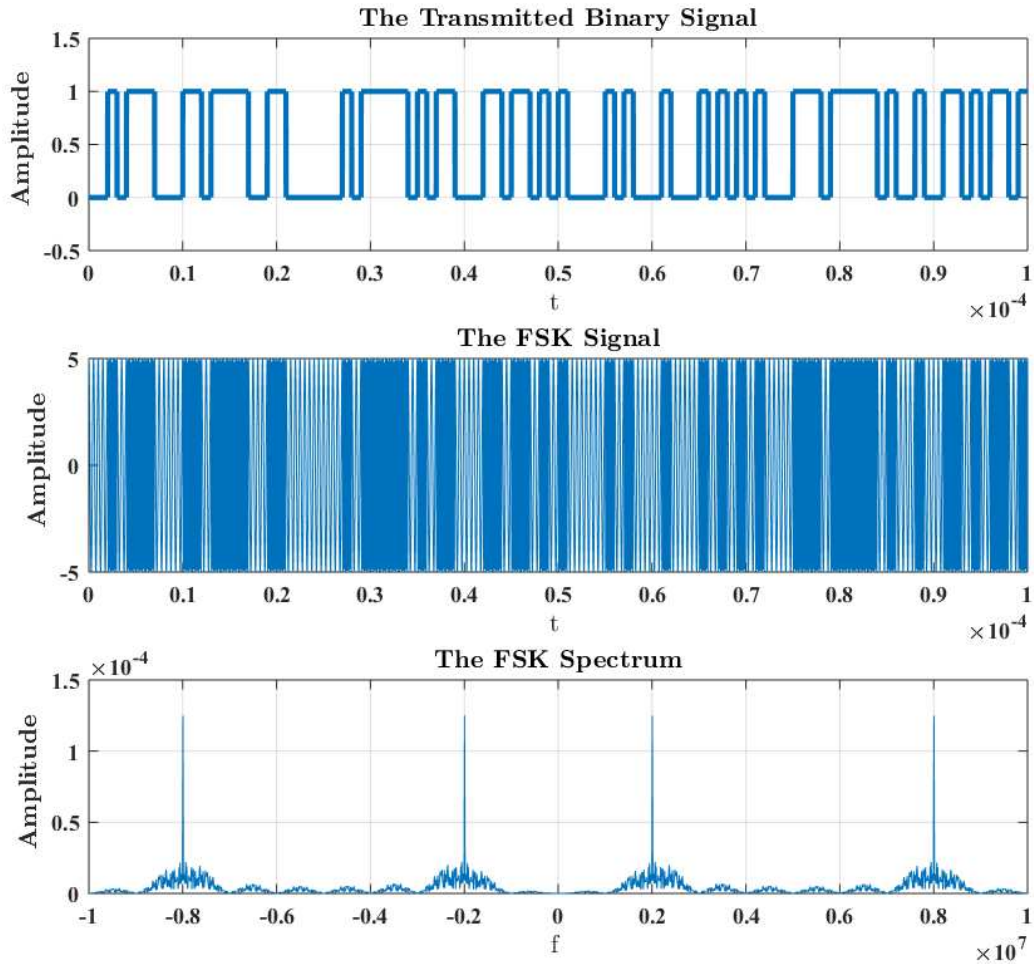


Figure 3.13 – An example of a SFH-SS/FSK signal

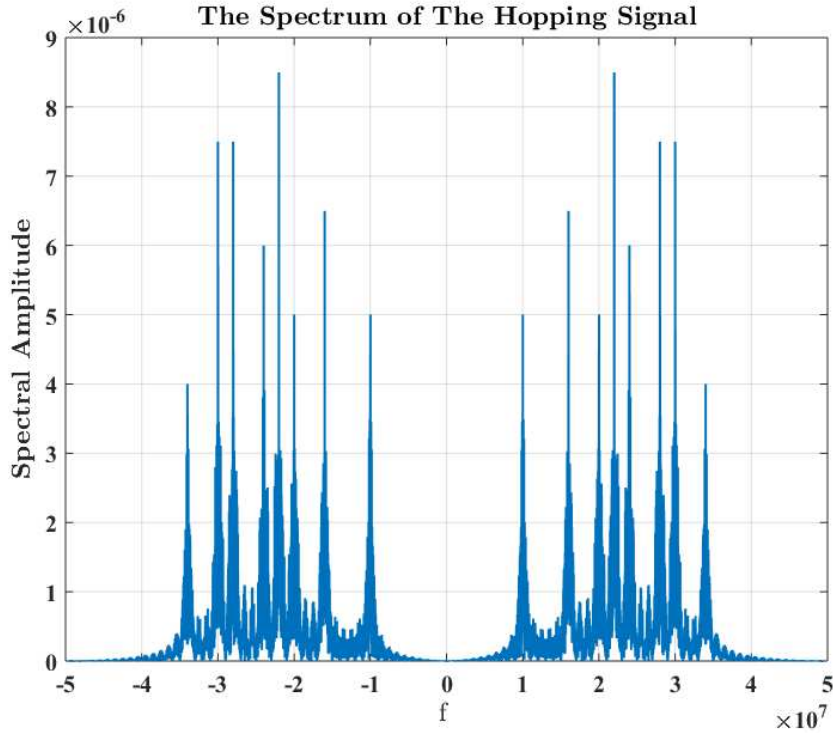


Figure 3.14 – The spectrum of the hopping subcarriers

If we denote  $S_w(f)$  by the random process  $R$ , it is required to find the distribution of  $U_R = |\log R|$ . The false-alarm probability and the corresponding threshold can be found based on the generalized expression of the  $\log -\chi_v^2$  distribution carried on in Appendix A. Also, by referring to  $\mathcal{T}_2[c_a]$  in equation (3.117), if  $N_p$  is sufficiently large and the set of the autocepstral peaks  $\{c_a(i)\}_i^{N_p}$  are statistically independent, the sum in Equation (3.117) statistically converges to the normal distribution based on the CLT. In this case, the false-alarm probability can be evaluated according to equation (3.31).

### Detection of Chirp Spread Spectrum Signals by The APB-ACD Technique

In digital communications, Chirp Spread Spectrum (C-SS) is a spread spectrum technique that uses wideband linear frequency modulated chirp pulses to encode information [114]. A chirp is a sinusoidal signal of frequency that increases or decreases over time. This frequency variation is performed with a polynomial expression for the relationship between time and frequency. The rate at which the frequency changes is called the chirp rate. As with other spread spectrum methods, chirp spread spectrum uses its entire allocated bandwidth to broadcast a signal, making it robust to channel

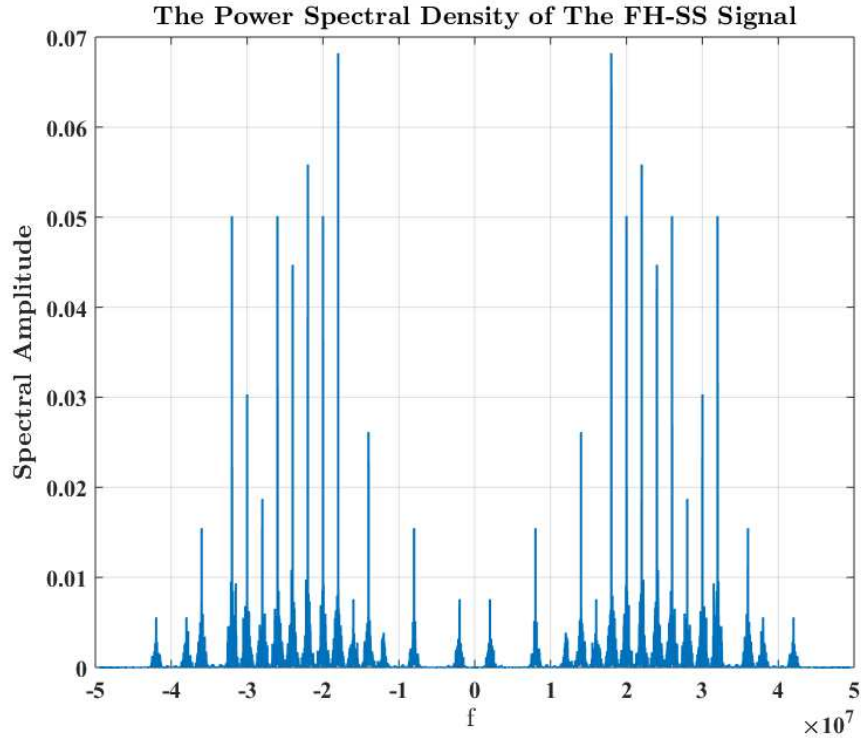


Figure 3.15 – The power spectral density of the SFH-SS/FSK signal

noise. Further, because the chirps utilize a broad band of the spectrum, chirp spread spectrum is also resistant to multipath fading even when operating at very low power.

The chirp spread spectrum technique was originally designed to compete with ultra-wideband for precision ranging and low-rate wireless networks in the 2.45 GHz band. However, since the release of IEEE 802.15.4a (also known as IEEE 802.15.4a-2007), it is no longer actively being considered by the IEEE for standardization in the area of precision ranging [115]. Chirp spread spectrum is ideal for applications requiring low power usage and needing relatively low data rates (1 Mbps or less). Since C-SS uses broadband chirp pulses, it offers resistance against narrowband pulses and also it reduces the required power that is needed for transmission over a given distance. A chirp waveform can be given by [114]:

$$s_{c-ss}(t) = a_E(t)g_E(t) \quad (3.118)$$

where  $a_E(t)$  is the envelope of the chirp signal,  $g_E(t) = \cos(\theta(t))$ . The instantaneous frequency  $f_{c-ss}(t) = \frac{1}{2\pi} \frac{d}{dt} \phi_{c-ss}(t)$ , and  $\phi_{c-ss}(t)$  is the chirp angle. Then the chirp rate

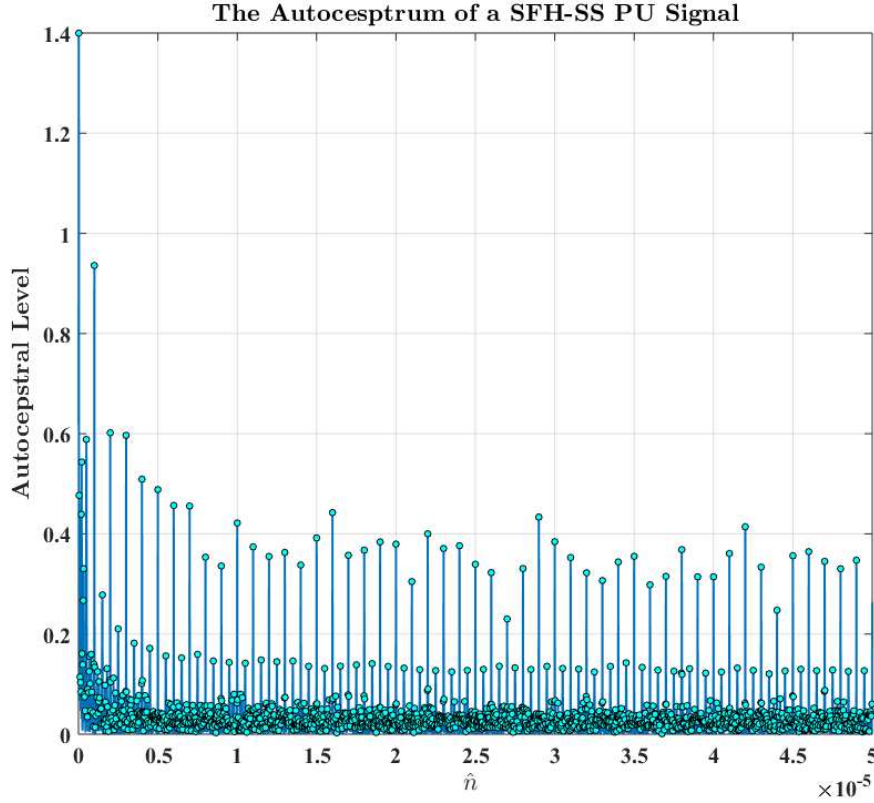


Figure 3.16 – The autocepstral peaks of the SFH-SS/FSK signal

is defined by  $\mu_{c-ss}(t) = \frac{d}{dt}f_{c-ss}(t)$  where  $\mu_{c-ss}(t) > 0$  denotes the up chirp and the down chirp is represented by  $\mu_{c-ss}(t) < 0$ . In case of a linear chirp signal,  $\mu_{c-ss}(t)$  is constant and  $f_{c-ss}(t)$  is a linear function of  $t$ . The bandwidth of the chirp signal is the frequency range of the instantaneous frequency. As up and down chirp signals are almost orthogonal, they can be used for Binary Orthogonal Keying (BOK) modulation scheme. Moreover, Pseudo Noise (PN) Chirp signal, referred to as PN-Chirp, is a signal in which the center frequency of it is varied according to a PN-sequence.

To calculate the autocepstrum of the PN-Chirp signal, first, we have to derive an expression for the PSD of the chirp signal. Let us assume that the signal envelope is given by:

$$a_E(t) = \Pi\left(\frac{t}{T_p}\right), -\frac{T_p}{2} < t < \frac{T_p}{2} \quad (3.119)$$

where  $\Pi(t)$  denotes a rectangular pulse shape,  $\theta_{c-ss}(t) = 2\pi f_c t + \pi\mu_{c-ss}t^2 + \Phi_{c-ss0}$ ,  $T_p$  is the pulse duration, and  $f_c$  the carrier frequency,  $\mu$  is the chirp rate and we set

$\theta_{c-ss_0} = 0$  for simplicity. Based on equation (3.118), the PSD of  $s_{c-ss_0}(t)$  is given by:

$$S_{s_{c-ss}}(f) = S_{a_E}(f) * S_{g_{c-ss}}(f) \quad (3.120)$$

where  $S_{g_{c-ss}}(f) = |\mathcal{F}\{g_{c-ss}(t)\}|^2 = |G(f)|^2$  and  $S_{a_E}(f) = |\mathcal{F}\{a_E(t)\}|^2 = |A_E(f)|^2$  where  $*$  denotes the convolution operator and  $A_E(f)$  denotes the Fourier transform of the pulse shaping function which is given by:

$$S_{a_E}(f) = T_p^2 \text{sinc}^2(T_p f) \quad (3.121)$$

To obtain the PSD of  $g(t)$ :

$$g_{c-ss}(t) = \frac{1}{2} \left[ \exp(j2\pi f_c t) \exp(j\mu_{c-ss} t^2) + \exp(-j2\pi f_c t) \exp(-j\mu_{c-ss} t^2) \right] \quad (3.122)$$

let us assume that:

$$g_{c-ss_1}(t) = \frac{1}{2} \left[ \exp(-j2\pi f_c t) \exp(-j\mu_{c-ss} t^2) \right] \quad (3.123)$$

The spectrum of a complex Gaussian function of the form  $h_g(t) = \exp(-j\sigma_g t^2)$  is given by [116]:

$$H_g(f) = \sqrt{\frac{\pi}{\sigma_g}} \exp \left[ j \left( \frac{\pi^2}{\sigma_g} f^2 - \frac{\pi}{4} \right) \right], \sigma_g > 0 \quad (3.124)$$

and for  $\sigma_g < 0$  we have:

$$H_g(f) = \sqrt{\frac{\pi}{|\sigma_g|}} \exp \left[ -j \left( \frac{\pi^2}{|\sigma_g|} f^2 - \frac{\pi}{4} \right) \right] \quad (3.125)$$

then based on equations (3.123) and (3.124), we obtain:

$$G_{c-ss_1}(f) = \frac{1}{2\sqrt{\mu_{c-ss}}} \exp \left( j \left[ \frac{\pi}{\mu_{c-ss}} (f + f_c)^2 - \frac{\pi}{4} \right] \right) \quad (3.126)$$

similarly, if  $g_{c-ss_2}(t) = \frac{1}{2} [\exp(j2\pi f_c t) \exp(j\mu_{c-ss} t^2)]$ , we get:

$$G_1(f) = \frac{1}{2\sqrt{\mu_{c-ss}}} \exp \left( -j \left[ \frac{\pi}{\mu_{c-ss}} (f - f_c)^2 - \frac{\pi}{4} \right] \right) \quad (3.127)$$

if  $\Phi_{c-ss}(f) = \frac{\pi}{\mu_{c-ss}}(f^2 + f_c^2) - \frac{\pi}{4}$  and by further mathematical simplification, we obtain:

$$G_{c-ss}(f) = \frac{1}{\sqrt{\mu}} \cos(\Phi_{c-ss}(f)) \exp\left(j \frac{w_c f}{\mu_{c-ss}}\right) \quad (3.128)$$

consequently, the PSD is given by:

$$S_{g_{c-ss}}(f) = \frac{1}{\mu_{c-ss}} \cos^2(\Phi(f)) \quad (3.129)$$

accordingly,  $S_s(f)$  of the chirp signal can be expressed as:

$$S_s(f) = \frac{T_p^2}{2\mu_{c-ss}} \text{sinc}^2(T_p f) + \left[ \frac{T_p^2}{2\mu_{c-ss}} \text{sinc}^2(T_p f) * \cos(2\Phi_{c-ss}(f)) \right] \quad (3.130)$$

If we assumed that  $S_{s_1}(f) = \frac{T_p^2}{2\mu_{c-ss}} \text{sinc}^2(T_p f)$  and  $S_{s_2}(f) = \frac{T_p^2}{2\mu_{c-ss}} \text{sinc}^2(T_p f) * \cos(2\Phi_{c-s}(f))$  and  $T_p$  is the envelope duration in msec, we note that term  $\text{sinc}^2(T_p f)$  varies slower than  $\cos(2\Phi_{c-ss}(f))$ . Thus, we can approximate the convolution of  $\cos(2\Phi_{c-ss}(f))$  with  $\text{sinc}(T_p f)$  as if convolving  $\cos(2\Phi_{c-ss}(f))$  with a constant within the main lobe of  $\text{sinc}^2(T_p f)$ ,  $-\frac{1}{T_p} < f < \frac{1}{T_p}$ . Accordingly, an approximated expression for the linear C-SS signal can be obtained as:

$$S_s(f) \approx \frac{T_p^2}{2\mu_{c-ss}} \text{sinc}^2(T_p f) + \frac{T_p^2}{2\mu_{c-ss}} \cos(2\Phi_{c-ss}(f)) \quad (3.131)$$

A Pseudo Noise (PN) chirp signal, referred to as PN-Chirp, is a signal in which the center frequency of it is varied according to a PN-sequence. This signal is given by:

$$s_{PN-C}(t) = c(t)s_{c-ss}(t) \quad (3.132)$$

where  $c(t)$  is the waveform of the PN-sequence and  $s_{c-ss}(t)$  is the chirp signal. We assume that both  $c(t)$  and  $s_{c-cc}(t)$  are independent. The PSD of the  $s_{c-ss}(t)$  is given by:

$$S_{PN-C}(f) = S_c(f) * S_{c-ss}(f) \quad (3.133)$$

From the literature, a generated pseudo random sequence by a maximal length shift

register has the following PSD [113]:

$$S_c(f) = \frac{N_s + 1}{N_s^2} \sum_{i=-\infty, i \neq 0}^{\infty} \text{sinc}^2\left(\frac{i}{N_s}\right) \delta\left(f - \frac{i}{N_s T_c}\right) + \frac{1}{N_s^2} \delta(f) \quad (3.134)$$

where  $N_s = 2^{m_s} - 1$  denotes the PN sequence length,  $m_s$  is the degree of the employed primitive polynomial, and  $T_c$  is the chirp duration. If we apply the representation  $S_{PN-C}(f) = S_{PN-C_1}(f) + S_{PN-C_2}(f)$ , where  $S_{PN-C_1}(f)$  and  $S_{PN-C_2}(f)$  are defined by:

$$S_{PN-C_1}(f) = \frac{N_s + 1}{N_s^2} \frac{T_c^2}{2\mu} \left[ \sum_{i=-\infty, i \neq 0}^{\infty} \text{sinc}^2\left(\frac{i}{N_s}\right) \left( \text{sinc}^2\left(T_c\left(f - \frac{i}{N_s T_c}\right)\right) + \cos\left(2\Phi\left(f - \frac{i}{N_s T_c}\right)\right) \right) \right] \quad (3.135)$$

$$S_{PN-C_2}(f) = \frac{T_c^2}{2\mu N_s^2} \left[ \text{sinc}^2(T_c f) + \frac{T_c^2}{2\mu_{c-ss}} \cos(2\Phi_{c-ss}(f)) \right]$$

and if we assume that  $\mathfrak{A} = \frac{N_s + 1}{N_s^2} \frac{T_c^2}{2\mu_{c-ss}}$  and  $\mathfrak{B}(i) = \text{sinc}^2\left(\frac{i}{N_s}\right)$ , we can rewrite  $S_{PN-C_1}(f)$  as:

$$S_{PN-C_1}(f) = \mathfrak{A} \left[ \sum_{i=-\infty, i \neq 0}^{\infty} \mathfrak{B}(i) \left( \text{sinc}^2\left(T\left(f - \frac{i}{N_s T_c}\right)\right) + \cos\left(2\Phi\left(f - \frac{i}{N_s T_c}\right)\right) \right) \right] \quad (3.136)$$

where for  $i = m \frac{N_s}{2}$ ,  $\mathfrak{B}(i) = 0$  where  $m$  is an integer number. As explained previously, the natural logarithm of  $\text{sinc}(\cdot)$  function gives rise to spectral lines and its inverse Fourier transform reveals a cepstral peak for  $i = 1$ , thus, the same concept applies for  $\text{sinc}^2(\cdot)$  as well as the chirp signal term in equation (3.135) for different values of  $i$ . Therefore, we the APB-ACD as applied in the case of the FH-SS signal.

To demonstrate the concept, we give an example of a linear chirp/FSK spread spectrum signal in Figure 3.17. The time duration to sweep from the starting frequency to the final frequency using up-chirp is 100 msec. The swept bandwidth of the chirp signal is 10 MHz. The binary FSK signaling modulates 10000 binary samples by switching between  $f_1 = 1$  kHz and  $f_2 = 10$  kHz for a sampling frequency of 1 MHz. The evaluation of the autocepstrum of the given signal with the illustration of the autocepstrogram is shown in Figure. 3.18. The autocepstrum of the chirp signal shows a group of

significant peaks reflecting the variations of the signal’s frequency.

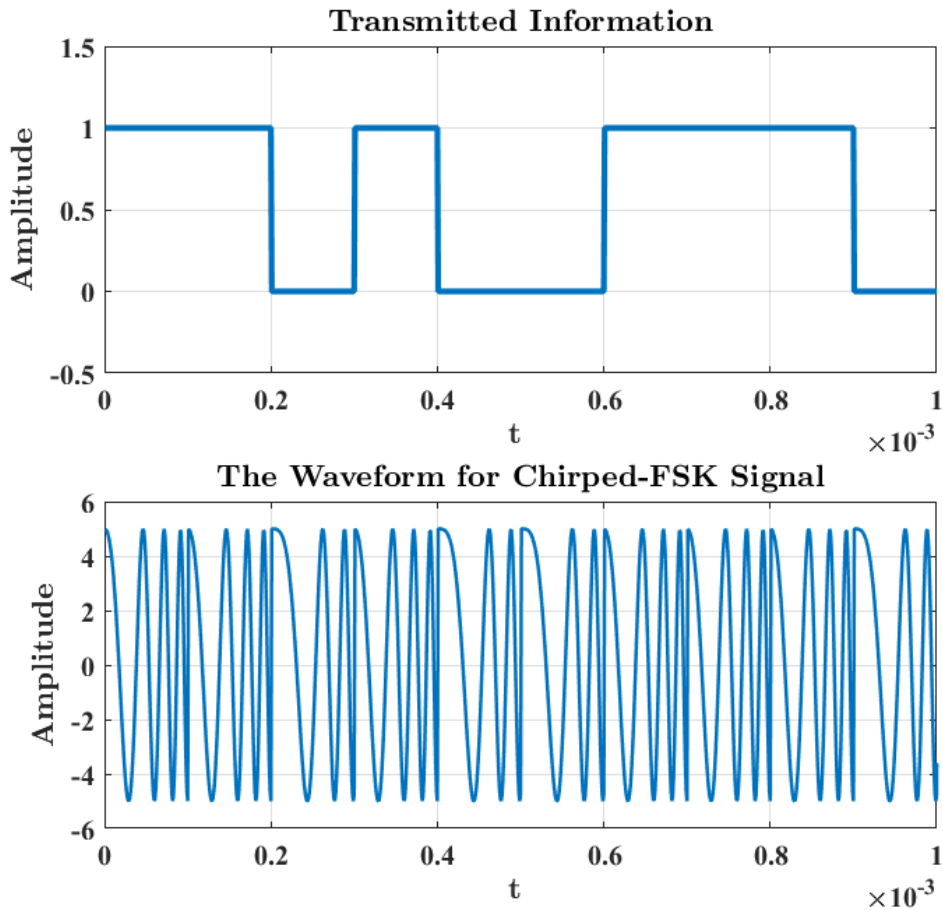


Figure 3.17 – An example of the chirp/FSK signal that sweeps within 1 msec

For example, the autocepstral peaks that occur in the range of [2.1,3] msec are insignificant which correspondingly show light color in the autocepstrogram. The chirp rate is 1 GHz/sec. Also, the relation between the time and quefrequency is illustrated in the autocepstrogram. Similar to the spectrogram and the cepstrogram, the autocepstrogram computes and plots an array of autocepstra that is computed on partitions of data. The autocepstrogram finds the relation between the time at which significant frequencies in the signal occurs and the quefrequency unit. The employed window type is the hamming window with a size of 512 samples. In an autocepstral slice, a prominent autocepstral peak is shown as a dark slice. Also, the peaks with low amplitudes in the higher quefrequency values give no significant information along the autocepstral slices. Accordingly, we can design the APB-ACD detector by averaging the autocep-

stral peaks and neglecting the peak at the zeroth quefrequency value, thus we can detect possible chirp PU signals without knowledge of the chirp rate.

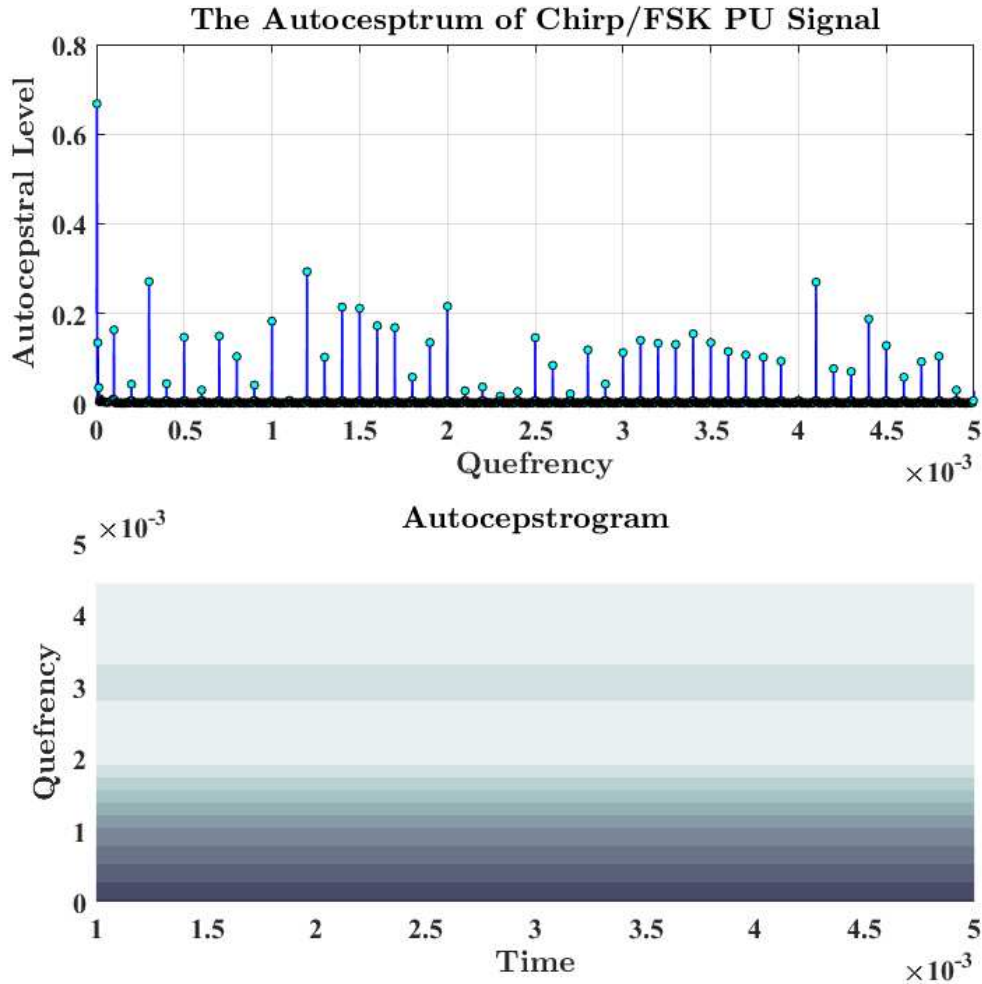


Figure 3.18 – A demonstration of the autocepstrum and the autocepstrogram of a chirp/FSK signal

### 3.5 Spectrum Sensing by The Smoothed PB-ACD Technique

In the PB-ACD technique, we estimate the autocorrelation of the received wideband signal, and then evaluate the cepstrum. To enhance the detector performance, we aim to reduce the fluctuations experienced in the ACEs before evaluating the PSD of the

received signal. The functional block diagram of the smoothing process is shown in Figure 3.19. In the literature, there are many methods employed for signals denoising which include linear, Wiener, and wavelet-based filtering. In these approaches, the noisy received signal is being processed provided that prior knowledge of the noise statistics and the transmitted signal shape is not available. However, in a non-cooperative semi-blind CR context, this information is not available so the conventional techniques would fail especially in the case of noise-like signals.

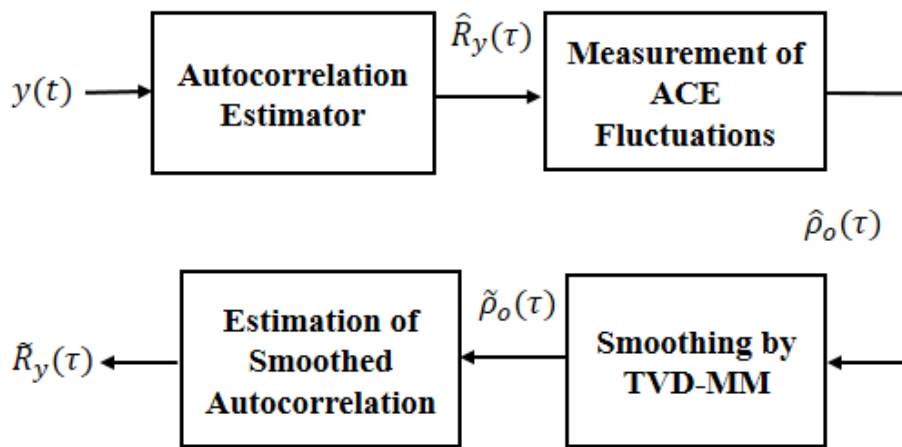


Figure 3.19 – The proposed smoothing process;  $\hat{R}_y(\tau)$  is the autocorrelation estimate of the received signal;  $\hat{\rho}_o(\tau)$  is the ACE fluctuations;  $\tilde{\rho}_o(\tau)$  is the smoothed ACE fluctuations;  $\tilde{R}_y(\tau)$  represents the smoothed autocorrelation estimate

Recently, variational calculus has been employed in modern communication systems and statistical signal processing for different purposes such as choosing an optimal signaling function, and deciding on certain statistical distributions that minimizes Fisher’s information [117]. Moreover, variational methods have drawn a great interest in solving image processing problems that including image denoising and deblurring [118]. Our choice to process the fluctuations of the ACEs rather than the autocorrelation itself or the noisy observed time domain signal is motivated by the following:

- Denoising a SS signal in time domain without having a prior information about the coding pattern is a difficult task and could fail due to its similarity with noise.
- Analysis of an underlying signal using its autocorrelation provides means to enhance significant patterns that identify the signal.

- It has been shown in the work of Burel in [94] that the fluctuations of ACEs of noise differs from that of a spread spectrum signal. This distinguishing feature can be applied to eliminate the noisy variation in the autocorrelation of the received SS signal.

In order to compute the autocorrelation estimator, we can divide the received time domain signal into  $M$  segments over a time rectangular window of a duration  $T_p$ . Then, we can evaluate the ACE for the  $m^{\text{th}}$  segment by [94]:

$$\hat{R}_y^m(\tau) = \frac{1}{T_p} \int_0^{T_p} y(t) y^*(t - \tau) dt \quad (3.137)$$

where  $y^*(t)$  denotes the complex conjugate of the received signal, and  $\tau$  is the time lag. In the statistical description of random processes, the second order moment describes the random fluctuations of a signal. Since the variance may characterize the random fluctuations around the mean value, the fluctuations of the ACEs are identified by their mean and variance as mentioned in [94]. The measure of the fluctuations in terms of the second order moment of the ACE is given by:

$$\hat{\rho}_{R_y}(\tau) = \langle |\hat{R}_y(\tau)|^2 \rangle \quad (3.138)$$

or approximately,

$$\hat{\rho}_{R_y}(\tau) = \frac{1}{M} \sum_{m=0}^{M-1} |\hat{R}_y^m(\tau)|^2 \quad (3.139)$$

where  $\langle . \rangle$  in Equation (3.139) represents the averaging operator. If the signal and noise are considered uncorrelated then we get:

$$\hat{R}_y(\tau) \approx \hat{R}_s(\tau) + \hat{R}_w(\tau) \quad (3.140)$$

where  $R_s(\tau)$  and  $R_w(\tau)$  are the autocorrelation of the noise-free signal and the noise at the CR receiver, respectively. In this case, we can define the underlying fluctuations of the ACEs of the received signal according to equation (3.140) by:

$$\hat{\rho}_{R_y}(\tau) = \hat{\rho}_s(\tau) + \hat{\rho}_w(\tau) \quad (3.141)$$

### 3.5.1 Fluctuations Smoothing by The Total Variation Denoising Based on The Majorization-Minimization Algorithm:

In general, the variational calculus is employed to find local extrema in a functional by solving differential equations. Signal denoising is one of its essential applications. An important aspect of signal denoising is to preserve signal features, and also identify signal trends. An approach for the signal denoising by variational calculus is the Total Variation Denoising (TVD), through which the output is obtained by minimizing a particular cost function [119]. Unlike conventional filtering, the TVD is defined in terms of an optimization problem. To formulate our smoothing problem, we should illustrate first the following notations:

- The  $L$ -point signal  $\hat{\rho}_s$  is represented by the vector:

$$\hat{\rho}_s = [\hat{\rho}_s(0), \dots, \hat{\rho}_s(L-1)]^T \quad (3.142)$$

- The  $\ell_1$  norm of the vector  $\mathbf{d}$ , which represents the discrete notations of the continuous variable  $t$ , is given by:

$$\|\mathbf{d}\|_1 = \sum_{\ell} |d(\ell)| \quad (3.143)$$

- The  $\ell_2$  norm of the vector  $\mathbf{d}$  is given by:

$$\|\mathbf{d}\|_2 = \sqrt{\left[ \sum_{\ell} |d(\ell)|^2 \right]} \quad (3.144)$$

- The diagonal matrix  $\mathbf{D}$  is given by:

$$\mathbf{D} = \begin{bmatrix} 1 & 0 & 0 & 0 \\ -1 & 1 & 0 & 0 \\ 0 & \ddots & 1 & 0 \\ 0 & 0 & -1 & 1 \end{bmatrix}$$

by which the first-order difference of a  $L$ -point signal  $\hat{\rho}_s$  is denoted by:  $\mathbf{D}\hat{\rho}_s$

— The measurement of the total variation of a  $L$ -point signal  $\hat{\rho}_s$  is given by [120]:

$$TV(\hat{\rho}_s) = \sum_{l=1}^{L-1} |\hat{\rho}_s(l) - \hat{\rho}_s(l-1)| = \|\mathbf{D}\hat{\rho}_s\|_1 \quad (3.145)$$

— The optimization problem, defining the smoothing of the ACEs fluctuations, is given by:

$$\hat{\rho}_s(l) = \arg \min_{\hat{\rho}_s(l)} \{F(\hat{\rho}_s(l))\} \quad (3.146)$$

where  $F(\cdot)$  is the functional to be minimized in order to find the desired estimate. This functional can be defined in terms of mean squared error, such as [120]:

$$F(\hat{\rho}_s(l)) = \frac{1}{2} \sum_{l=0}^{L-1} |\hat{\rho}_o(l) - \hat{\rho}_s(l)|^2 + \alpha_r TV(\hat{\rho}_s) \quad (3.147)$$

where  $L$  is the maximum time lag at which the ACEs fluctuations function is evaluated,  $\hat{\rho}_o(l)$  denotes the observed fluctuations, for the case of uncorrelated signal and noise, that is given by:

$$\hat{\rho}_o(\tau) = \hat{\rho}_s(\tau) + \hat{\rho}_w(\tau) \quad (3.148)$$

and  $\alpha_r > 0$  represents the regularization parameter that controls the smoothing degree. An appropriate value of  $\alpha_r$  can be found heuristically.

In order to solve the minimization problem defined in equation (3.146), various algorithms can be employed, such as the TVD clipping algorithm [121]. However, the appropriate choice of an algorithm depends on the desired accuracy level and the convergence rate. For example, the Majorization-Minimization (MM) algorithm is applied to solve the TVD problem, which provides a significant accuracy on the expenses of the convergence time. The MM algorithm solves the minimization problem using a sequence of functions, called majorizer functions, that are easier to solve than the original cost function. To use the MM algorithm and reduce the computation burden, one must choose carefully an optimization function denoted by  $G(\hat{\rho}_s)$  to approximate  $F(\hat{\rho}_s)$ . To choose  $G(\cdot)$ , the MM approach requires that:

1.  $G(\hat{\rho}_s)$  is a majorizer of  $F(\hat{\rho}_s)$ :  
 $G(\hat{\rho}_s) \geq F(\hat{\rho}_s), \forall \hat{\rho}_s(l).$
2. The majorizer coincides with the  $F(\cdot)$  at each iteration,  $i$ :  $G_i(\hat{\rho}_s(l)) = F(\hat{\rho}_s(l)).$

3.  $G(\hat{\rho}_s)$  must be a convex function, so that the MM algorithm obtains the solution at each  $i^{th}$  iteration by minimizing the majorizer function.

### 3.5.2 Application of the Proposed Smoothing Process to the Case of Detecting a DS-SS Signal:

To anticipate a constructive example for showing the applicability of the proposed smoothing process to our detection problem, consider the case of a passband DS-SS signal,  $s(t)$ , occupying a wideband of interest with the autocorrelation function given by [105]:

$$R_s(\tau) = \frac{A^2}{2} R_d(\tau) R_p(\tau) \cos(2\pi f_c \tau) \quad (3.149)$$

where  $R_d(\tau)$  and  $R_p(\tau)$  are the autocorrelation of the data and spreading waveform, respectively, and they are given by [105]:

$$\begin{aligned} R_d(\tau) &= \Lambda\left(\frac{\tau}{T_d}\right) = \frac{1 - |\tau|}{T_d} \\ R_p(\tau) &= -\frac{1}{N_s} + \frac{N_s + 1}{N_s} \sum_{i=-\infty}^{\infty} \Lambda\left(\frac{\tau - iN_s T_c}{T_c}\right) \end{aligned} \quad (3.150)$$

where  $T_d$  is the symbol duration,  $T_c$  is the chip duration and  $\Lambda(\cdot)$  is the triangular function;  $N_s = 2^{m_s} - 1$  is the length of the m-sequence pseudo random spreading code;  $m_s$  is the degree of a chosen primitive polynomial. Based on the baseband version of equation (3.149), we can express the ACEs fluctuation function of  $s(t)$  by:

$$\hat{\rho}_s(\tau) \approx \rho_p \sum_{i=-\infty}^{\infty} \Lambda\left(\frac{\tau - iN_s T_c}{T_c}\right) \quad (3.151)$$

in which  $\hat{\rho}_s(\tau)$  viewed as a periodic triangular wave form with peak values  $\rho_p$ . According to equation (3.151), a convenient majorizer function,  $G_i(\hat{\rho}_s(\tau)) = g_{MM}(t)$ , at the  $i^{th}$  iteration for one period of  $\hat{\rho}(\tau)$  is given by:

$$g_{MM}(t) = c_{MM} - b_{MM} t^2 \quad (3.152)$$

From the MM algorithm,  $g_{MM}(t)$  must satisfy:

$$g(t)_{MM} \geq f_{MM}(t), \forall t \quad (3.153)$$

where  $f_{MM}(t)$  is the original cost function. Equivalently, if we set  $\rho_p = 1$ , then we should have:

$$c_{MM} - b_{MM}t^2 \geq \frac{1-t}{T_c}, \forall t > 0 \quad (3.154)$$

In this case, we need to evaluate the constants  $c_{MM}$  and  $b_{MM}$  to validate that the chosen function in equation (3.152) is a majorizer. The mathematical analysis to find  $c_{MM}$  and  $b_{MM}$  yields the following:

$$b_{MM} = \frac{1}{2T_c|t_i|}, \quad c_{MM} = \frac{1-2|t_i|}{2T_c} \quad (3.155)$$

(See Appendix B for the proof). Clearly, an upper bound of one period of  $f_{MM}(t)$  is given by  $g_{MM}(t)$ , then by substituting  $c_{MM}$  and  $b_{MM}$  in equation (3.154), we get:

$$\frac{1-2t_i}{2T_c} - \frac{t^2}{2T_c t_i} \geq \frac{1-|t|}{T_c}, \forall t \in \mathbb{R} \quad (3.156)$$

To obtain the required cost function, we use  $d(l)$  for the discrete notation instead of  $t$ , and then by summing over  $l$ , we obtain:

$$\sum_{l=1}^L \left( \frac{1-2|d_i(l)|}{2T_c} - \frac{d^2(l)}{2T_c|d_i(l)|} \right) \geq \sum_{l=1}^L \frac{1-|d(l)|}{T_c} \quad (3.157)$$

By using vector notations, we can rewrite equation (3.157) in a compact form as:

$$\left( -\frac{N_s}{2} - \|\mathbf{d}_i(l)\|_1 - \frac{1}{2}\mathbf{d}^T \mathbf{\Delta}_i^{-1} \mathbf{d} \right) \geq -\|\mathbf{d}\|_1 \quad (3.158)$$

where  $\mathbf{\Delta}_i = \text{diag}(|d_i(l)|)$  denotes a diagonal matrix. Recalling the definition of the TVD in equation (3.145), then by replacing  $\mathbf{d}$  with  $\mathbf{D}\hat{\boldsymbol{\rho}}_s$  in equation (3.158), multiplying it by the regularity parameter  $\alpha_r$ , and adding the error data term  $e_r(l) = \frac{1}{2}\|\hat{\boldsymbol{\rho}}_o(l) - \hat{\boldsymbol{\rho}}(l)\|_2^2$  to its both sides, then we get:

$$e_r(l) - \frac{\alpha_r N_s}{2} - \alpha_r \|\mathbf{D}\hat{\boldsymbol{\rho}}_{s_i}(l)\|_1 - \frac{\alpha_r}{2} \hat{\boldsymbol{\rho}}_s^T \mathbf{D}^T \mathbf{\Delta}_i^{-1} \mathbf{D}\hat{\boldsymbol{\rho}}_s \geq e_r(l) - \alpha_r \|\mathbf{D}\hat{\boldsymbol{\rho}}_s\|_1 \quad (3.159)$$

Clearly, the majorizer of the cost function is given by:

$$G_i(\hat{\boldsymbol{\rho}}_s) = e_r(l) - \frac{\alpha_r N_s}{2} - \alpha_r \|\mathbf{D}\hat{\boldsymbol{\rho}}_{s_i}(l)\|_1 - \frac{\alpha_r}{2} \hat{\boldsymbol{\rho}}_s^T \mathbf{D}^T \mathbf{\Delta}_i^{-1} \mathbf{D}\hat{\boldsymbol{\rho}}_s \quad (3.160)$$

Using equation (3.160), we seek to obtain the update equation  $(\hat{\rho}_s)_{i+1}$  as follows:

- Set the iteration index  $i$  to 0 and initialize  $(\hat{\rho}_s)_0$ .
- Set  $(\hat{\rho}_s)_{i+1}$  as a minimizer of  $G_i(\hat{\rho}_s)$  such that:

$$(\tilde{\rho}_s)_{i+1} = \arg \min_{\hat{\rho}_s} G_i(\hat{\rho}_s) \quad (3.161)$$

- Set  $i = i + 1$  and go to step 2.

Accordingly, by differentiating equation (3.160) and equating the results to zero, it yields:

$$(\tilde{\rho}_s)_{i+1} = (\mathbf{I} + \mathbf{U})^{-1} \hat{\rho}(\mathbf{l}) \quad (3.162)$$

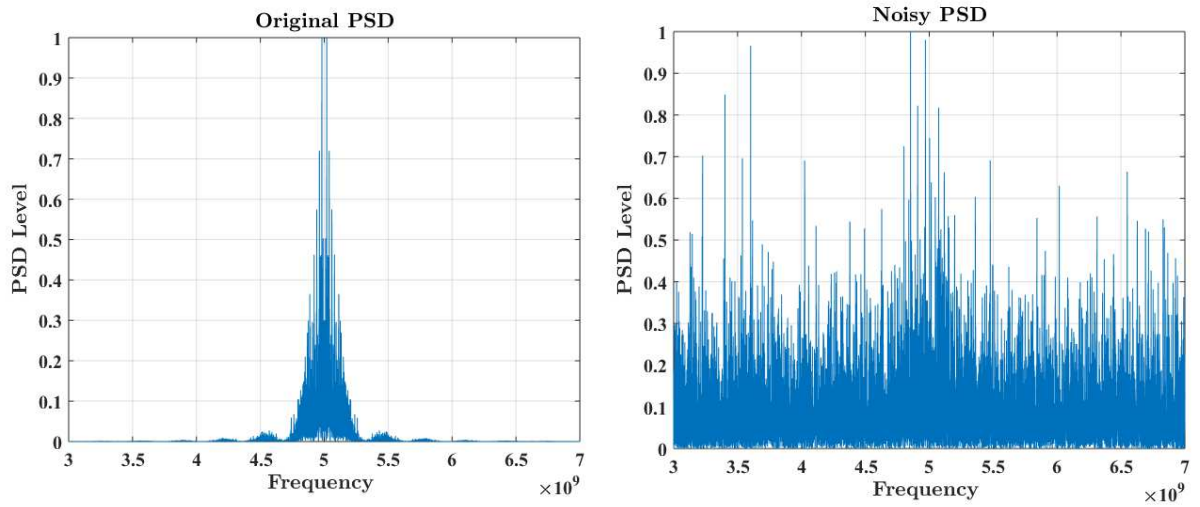
where  $\mathbf{I}$  is the identity matrix, and  $\mathbf{U}$  is defined by:

$$\mathbf{U} = \alpha_r \mathbf{D}^T \Delta_i^{-1} \mathbf{D} \quad (3.163)$$

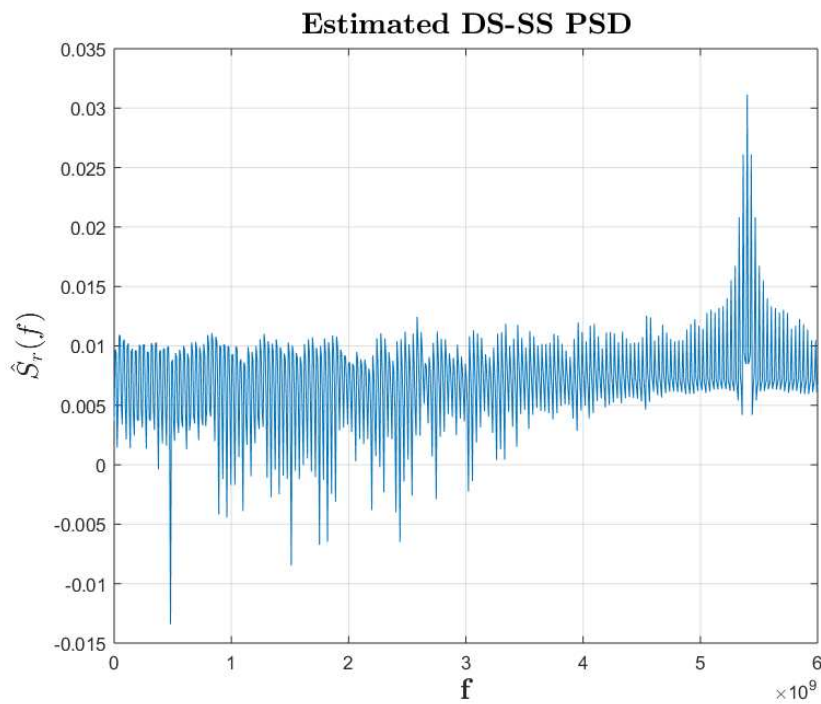
In Figure 3.20, we illustrate the effect of applying the smoothing process for the case of a DS-SS signal at SNR of -10 dB.

The operating specifications are based on the IEEE802.11a standards that uses DS-SS signal with 5 GHz as the operating frequency and 54 Mbps for the data rate [105]. It is important to clarify that despite the effective results provided by the proposed smoothing process on the estimated PSDs, there is an 8% estimation error in the operating frequency. For this reason, it is essential that the PU detector operates independently on the operating frequency value. Taking into account that random ACEs fluctuations of the DS-SS signal and that of the AWGN are distinguishable, the smoothed PB-ACD exploits the advantage of denoising the fluctuations of the ACEs by the TVD-MM algorithm. The calculation of the ACEs fluctuations involves dividing the time domain signal into  $M$  segments. By respecting Nyquist's rate  $f_{s_N}$ , the estimated PSD maintains the exact frequency information as shown in Figure 3.21. However, in case of oversampling the signal, the estimated PSD experiences a minor loss of frequency localization [122].

As the number of samples increases within each signal segment, in case of oversampling, the summation of the segmented autocorrelation will smooth out the signals details. Therefore, the maxima presented in the sum will be more smoothed resulting in minor frequency shift in the estimated PSD. Also, as the oversampling increases above double the Nyquist's rate, a substantial loss of frequency localization occurs.



(a) The original PSD of a DS-SS signal      (b) The received signal PSD at SNR of -10 dB



(c) The estimated PSD  $\hat{S}_r(f)$  in decibels after applying the TVD-MM algorithm to the fluctuations of the ACEs of the received signal in case of oversampling

Figure 3.20 – The effect of applying the smoothing process on the estimated PSD

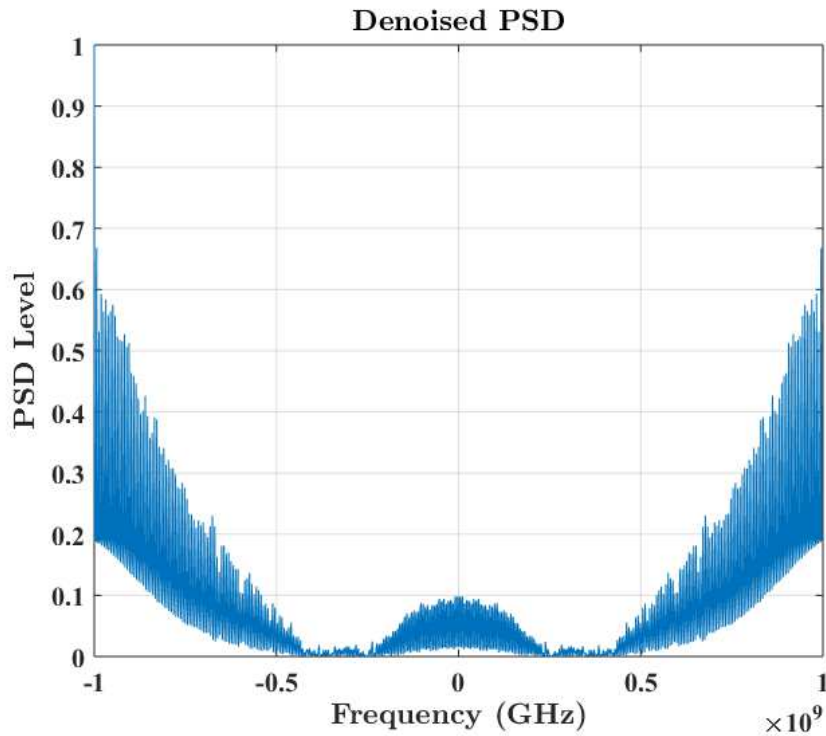


Figure 3.21 – The estimated PSD after applying the TVD-MM algorithm to the fluctuations of the ACEs of the received signal; the signal is sampled at Nyquist's rate

Despite the fact that oversampling a time domain signal is supposed to improve the process of estimating the autocorrelation, it is shown in [122] that oversampling short data sequences at Nyquist's rate increases the variance of the autocorrelation estimate such that the mean-squared error of the estimate increases.

On the other hand, it is sufficient to sample at the Nyquist's rate for long data sequences (i.e., as in our presented case) such that the variance of the autocorrelation estimate attains its minimum value. To demonstrate the effect of varying the sampling rate in calculating the ACEs, Figures 3.20-a, 3.20-b, and 3.20-c show the original, the noisy PSD of the PU signal and the estimated PSD after applying the smoothing process, respectively.

When the signal is sampled at the Nyquist's rate, no loss of frequency localization is encountered as shown in Figure 3.21. The TVD employs the regularity parameter,  $\alpha_r$ , to control the degree of smoothing. Increasing  $\alpha_r$  gives more weight to the term that measures the fluctuations of the signal. In this case, choosing small values for the regularity parameter translates into reduced spectral fluctuations but may affect

the level of the exact spectral boundaries. Therefore, before choosing the regularity parameter, we have to be aware of the required detection accuracy level to avoid over-smoothing the analyzed signal and hence increasing the misdetection probability.

### 3.6 Numerical Results and Discussions

In order to prove the efficacy of the autocepstrum detector, we evaluate the detection performance as compared to different state-of-the-art techniques. The simulations are averaged over 3000 realizations with an observation interval of 0.7 sec and the chip duration is  $1.54 \mu\text{sec}$ . In the simulations, we employed a Boolean parameter  $\Theta$ , which is uniformly distributed and takes randomly a value of 0 or 1 in order to include the presence or absence of a DS-SS PU signal. The used spreading code is based on a primitive polynomial defining the m-sequence code in the form of  $x^6 + x + 1$  [113]. The length of the spreading code is 63 sample to generate a long PN sequence, and the PN sequence length of the analyzed signal is 4410 sample. The modulation type is the passband BPSK modulation scheme with a carrier frequency of 5 GHz, and a sampling frequency  $f_s$  of 30 GHz.

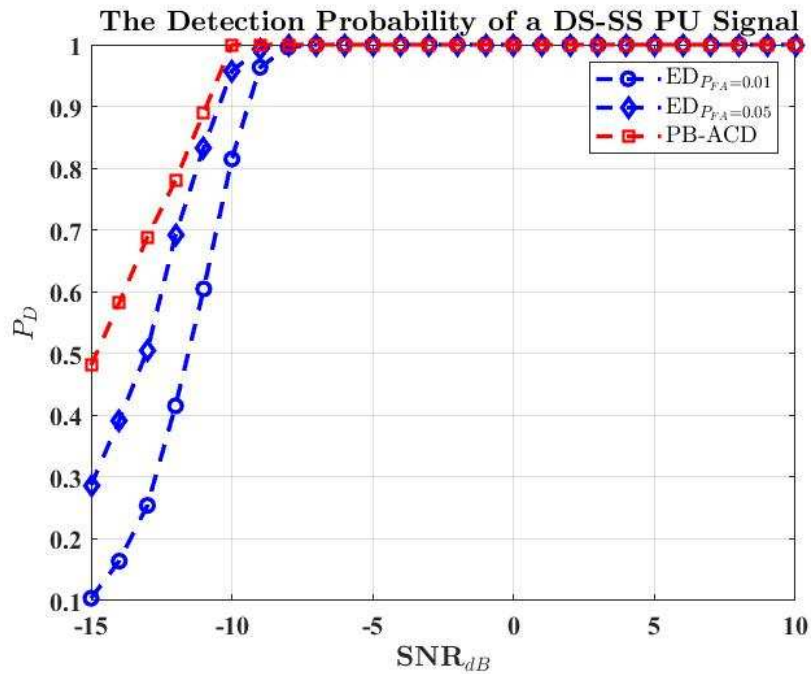


Figure 3.22 – Performance evaluation of the PB-ACD as compared to ED for fixed  $P_{FA}$

The performance of the proposed autocepstrum detector is measured in terms of the detection probability which is evaluated from -15 dB to 10 dB. The required noise statistics are evaluated through histogram estimation. All simulations are carried on under the CLT assumption. It can be seen from Figure 3.22 that the proposed detector outperforms energy detection at low SNR although there is no noise uncertainty that is assumed. It means that the PB-ACD can detect a signal hidden in noise by -15 dB with probability of approximately 0.1 for  $P_{FA} = 0.01$ . Further, at the same SNR and for  $P_{FA} = 0.05$ , PB-ACD gives 0.5 detection probability which is approximately double the ED's detection performance.

Also, to elaborate more on higher-order and advanced modulations, Figure 3.23 shows a comparison of the detection performance of the PB-ACD technique with ED for detecting 16-QAM and 64-QAM PU signals. In wireless communication, the 64-QAM modulation scheme is used in 4G systems in the uplink and provides the most benefit in small cell environments under good uplink conditions. Moreover, we simulated the PB-ACD technique, as shown in Figure 3.24, to test its detection performance for detecting OFDM PU signals and compare them with ED and the EVD. The simulations are conducted for 2000 Monte Carlo iterations. In simulating OFDM modulated signals, we considered the parameters defined in the IEEE802.11 specifications [85]. The number of total subcarriers (i.e., FFT size) is 64, for 48 data subcarriers and 4 pilot subcarriers. The FFT duration is 3.2  $\mu$ sec, the number of symbols is  $10^4$ , and the OFDM bandwidth is 20 MHz. In Figure 3.24, the OFDM PU signal can be detected by the PB-ACD technique by over about 40% than ED and EVD at -15 dB. In section 3.5, we proposed a solution for improving the detection performance of the PB-ACD technique for detecting noise-like signals through a smoothing process. Indeed, the detection of low-power signals in CR is a spectrum sensing challenge, especially when the CR receiver has no knowledge of the specifications of the noise-like signal. Further, we have discussed the capability of the PB-ACD technique for detecting a DS-SS signal under the AWGN channel in case of the SBSA. Hereinafter, we aim to evaluate the performance of the smoothed PB-ACD in terms of the detection probability for DS-SS and an IR-UWB signals.

To provide more improvement over the ED technique, we applied the proposed smoothed PB-ACD technique and compare it with different state-of-the-art spectrum sensing techniques, such as the EVD, and the MFD. The detection probability is evaluated as shown in Figure 3.25.

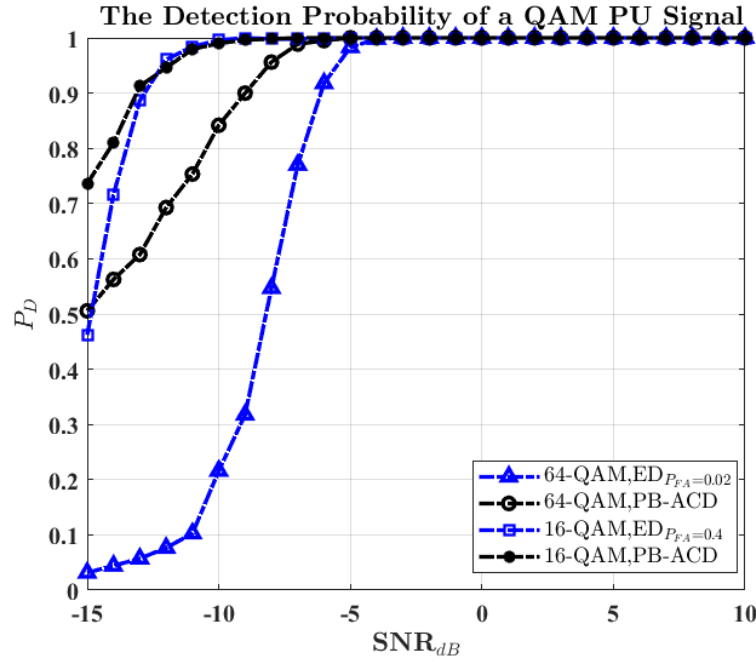


Figure 3.23 – Detection probability of the PB-ACD as compared to ED for 64-QAM PU signal

Also, from Figure 3.25, the detection performance of the PB-ACD technique outperformed the ED and EVD techniques in the SNR range  $[-15, -6]$  dB. For the EVD technique, the detection performance is based on evaluating the eigenvalues of the covariance matrix of the received signal.

The inherited correlation between signal samples can be reflected on the eigenvalues of the covariance matrix which can be used to formulate the detection test statistic. Deciding on the presence or absence of the PU signal depends on a specific choice of the EVD techniques which comprise the EME, the ME, and the MME techniques. For comparison, we employed the EME detection technique. If the noise variance is exactly known, such that the noise uncertainty is zero, the Energy Detection technique is optimal and outperforms the EME technique. On the other hand, the MME technique becomes superior to the ED for longer collected signal samples [62]. Despite the fact that the EVD technique does not require any knowledge on the transmitted signal characteristics neither on the noise variance, its high computational complexity due to the high data processing is the main drawback.

For the MFD, its drawbacks are related to the perfect knowledge of the PU signal

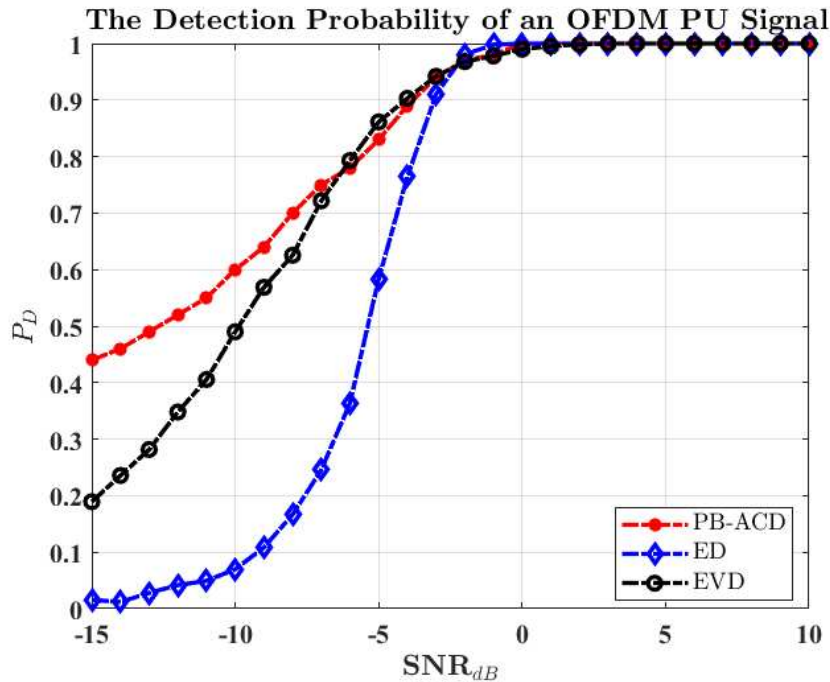


Figure 3.24 – Detection probability of the PB-ACD as compared to ED for an OFDM PU signal in AWGN channel

and the noise variance. In [123], the detection threshold of the suggested MFD is given as a function of SNR so at low SNR, the value of the detection threshold becomes higher such that the detection performance deteriorates. In Figure 3.25, the matched filter detector has the highest detection probability among the energy Detector and the eigenvalue-based detector at SNR of -15 dB, whereas the PB-ACD technique is higher in detection probability by 30% than the matched filter detector. However, as the SNR slightly increases to -12 dB, the PB-ACD and the MFD techniques performs similarly. By applying the smoothing process to the PB-ACD, the detection results increased by 40%.

The detection results illustrate the efficacy of the PB-ACD technique to be the less likely to miss-detect the presence of a DS-SS PU signal among the considered state-of-the-art techniques. For the IR-UWB signal, we used a Gaussian monocycle waveform to generate the transmitted pulses along with the passband BPSK modulation scheme. The impulse duration is 0.5 nsec, and the carrier frequency is 6 GHz. Our choice of the IR-UWB signal is due to its very low power level.

The number of segments used to calculate the autocorrelation estimates in 630 seg-

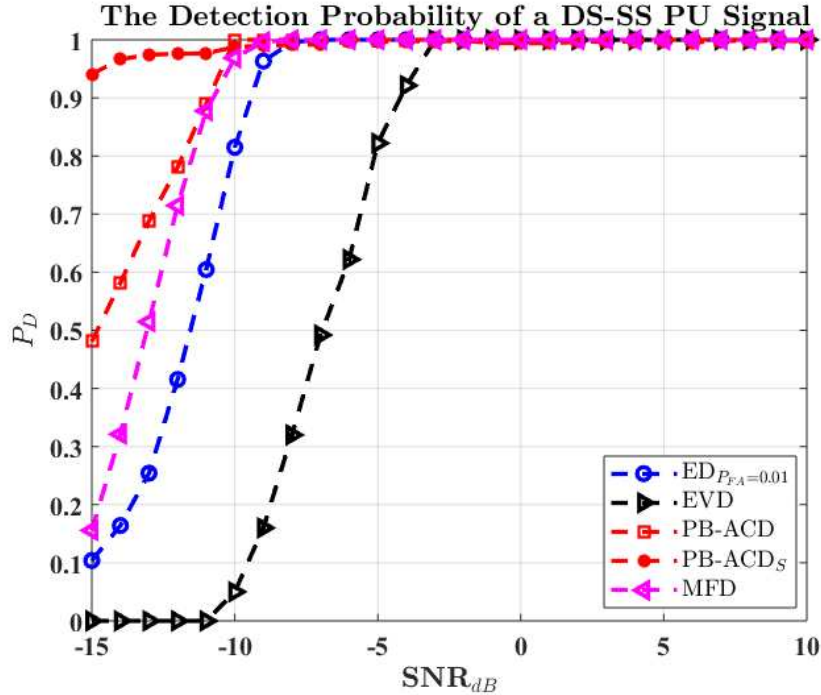


Figure 3.25 – The detection probability of the PB-ACD as compared to the smoothed PB-ACD and different state-of-the-art techniques for detection a DS-SS signal; PB-ACD<sub>s</sub> denotes the smoothed PB-ACD technique

ments, the regularity parameter  $\alpha_r$  for the TVD-MM algorithm is set to 0.01 and the number of iterations is 10. In Figure 3.26, the PB-ACD outperforms the three considered state-of-the-art techniques over the SNR [-15,-9] dB. At -8 dB, the PB-ACD and the Matched filter techniques have the same detection probability. Over about -8 dB, the Matched Filter Detector gives the highest detection performance than the PB-ACD and the considered state-of-the-art techniques. To provide more improvement, we applied the smoothed PB-ACD. As shown in Figure 3.26, the smoothed PB-ACD technique is able to detect the presence of the IR-UWB signal by approximately 40% detection probability as opposed to the PB-ACD technique. In other words, it gives the lowest mis-detection probability at low SNR values as opposed to the other considered detection techniques. Moreover, we extend our evaluation to test the detection capability of the APB-ACD technique to detect FH-SS and chirp/FSK signals as shown in Figures 3.27 and 3.28, respectively. The SFH-SS signal demonstrated in Figure 3.13 is employed for detection using the APB-ACD technique. The average of the autocepstral peaks performs as a significant indicator for the presence of the SFH-SS signal in the AWGN. For

$P_{FA} = 0.02$ , the probability of detection of the APB-ACD technique is evaluated and compared to that of the MME, ME, and ED techniques for the sample size of 1000 samples, a 2000 Monte Carlo realizations, and a smoothing factor of the sample covariance matrix of 8 samples, as employed in [62], to reduce the calculation complexity.

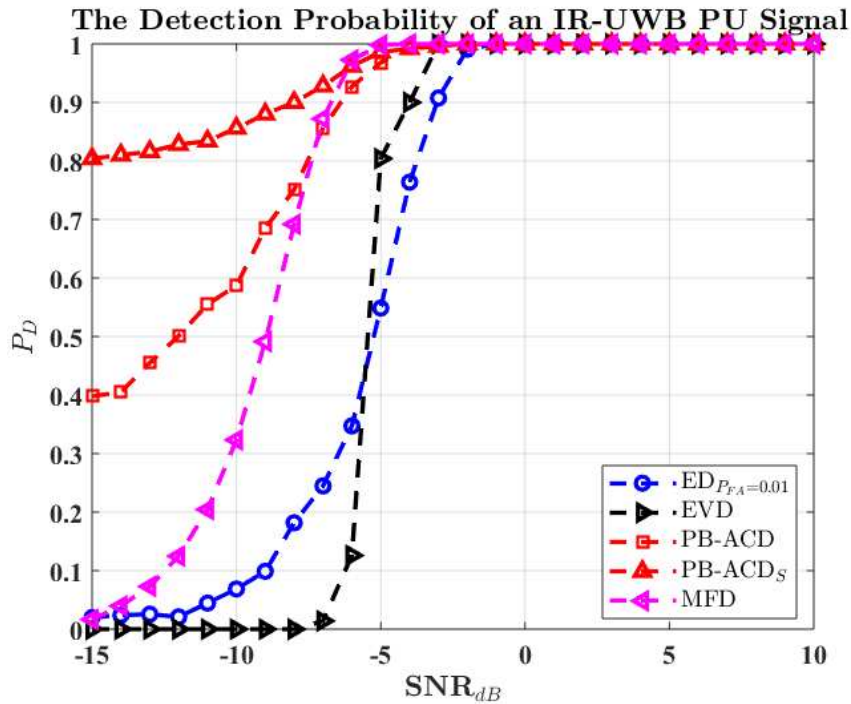


Figure 3.26 – The detection probability of the PB-ACD as compared to the smoothed PB-ACD and different state-of-the-art techniques for detection an IR-UWB signal; PB-ACD<sub>s</sub> denotes the smoothed PB-ACD technique

Since the concept of the autocepstrum lies in measuring the cepstral correlation of the received signal, we find that at a low SNR value, the autocepstral peak that is only present at the zeroth quefrequency value is not sufficiently strong to diminish the strength of the autocepstral peaks of the SFH-SS signal. This property occurs as a superior detection performance of the APB-ACD technique at -20 dB than the MME, ME, and the ED techniques. However, as the SNR increases, the detection behavior of the APB-ACD technique increases slower than that of the MME, ME, and the ED techniques. This is due to the influence of the autocepstral peak of the AWGN that is accounted in evaluating the average of the autocespstrum peaks. Despite the superior performance of the APB-ACD technique at -20 dB, its slow detection behavior makes its performance approaches as the EVD technique. The rationale of this result is that the low level au-

tocepstral peaks of the FH-SS signal are not being sufficiently enhanced as the SNR increases.

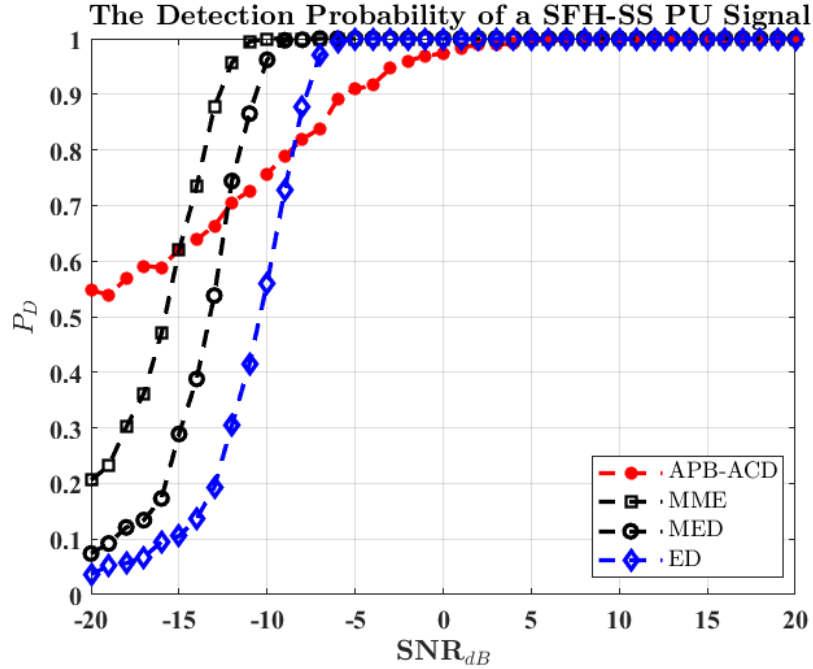


Figure 3.27 – The detection probability of the APB-ACD as compared to ED and EVD techniques to detect SFH-SS PU signal

In Figure 3.28, we evaluate the APB-ACD technique for detecting the chirp/FSK signal that is employed in the example given in Figure 3.17. The detection results are averaged over 2000 Monte Carlo realizations for a signal size of 1000 samples. For comparison, we simulate the ED technique with or without noise uncertainty. At noise uncertainty case, the threshold is always set based on the assumed/estimated noise power, while the real noise power is varying in each Monte Carlo realization.

In Figure 3.28 As the SNR increases, the APB-ACD technique outperforms the ME technique. We notice that in the chirp/FSK signal, the frequency variation reflects a correlation in the autocepstrum that is more strong than the correlation inhibited in evaluating the EVD techniques. One possible solution for enhancing the cepstral peaks for PU signals to improve the detection results of the APB-ACD technique is proposed in chapter 5 by introducing the Cepstral Covariance Detection (CCD) technique. The algorithms to compute the MME, and the EME techniques are given in Appendix B.

To address the trade-off problem between the computational complexity of the detection algorithms and the detection accuracy, we find that the computational complex-

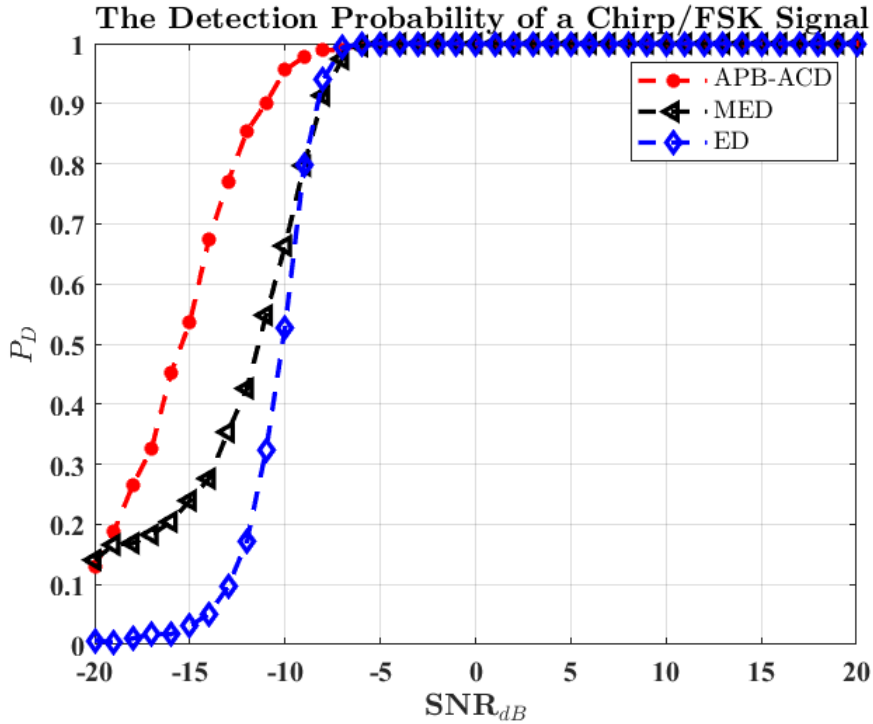


Figure 3.28 – The detection probability of the APB-ACD as compared to ED and EVD techniques to detect a chirp/FSK PU signal

ity of the EVD techniques comes from the computation of the covariance matrix and the eigenvalue decomposition of the covariance matrix. To evaluate the covariance matrix,  $L_s N$  multiplications and  $L_s(N - 1)$  additions are needed, where  $N$  is the length of the received signal and  $L_s$  denotes the smoothing factor to calculate the sample eigenvalues. To evaluate the eigenvalues, generally,  $O(L_s^3)$  multiplications and additions are needed. On the other hand, the energy detection technique requires  $N$  multiplications and  $N - 1$  additions. In calculating the proposed PB-ACD technique, the autocorrelation process requires  $O(N^2)$  operations, the FFT and IFFT requires  $O(N_r \log N)$  operations, and the natural logarithm using the arithmetic geometric mean method requires over about  $O(N \log N)$ . We find that the energy detection technique has the lowest computational complexity whereas the EVD and the PB-ACD techniques have approximate computational complexity.

## 3.7 Summary

In this chapter, we show that cepstral signal processing can be significant in CR for detecting DS-SS PU signal by employing the autocepstrum concept for the SBSA model. We offer a solution for the hidden spread spectrum PU problem that causes misdetection due to the nature of the PU signal. We formulate a spectrum sensing algorithm that is based on an autocepstral peak appearing at a quefrequency value equals to the carrier signal duration. On the other hand, the fact that zero autocepstral peaks appearing at the same quefrequency value for the AWGN case enables a CR receiver to differentiate between noise-like PU signal and thermal noise. Further, we derive expression for the probability distribution of the autocepstrum of the received signal under the null hypothesis. Also, we present an analytical framework for evaluating the mean and variance of the detection test statistic, and we formulate an expression for the detection threshold in case of having cepstral coefficients that follow  $\log -\chi_v^2$  distribution. For performance evaluation, the proposed detector is compared to different state-of-the-art techniques and shows better performance than ED in low SNR environment. A mathematical analysis for the autocepstrum approach for the FH-SS and C-SS signals is carried out. The sensing-throughput-threshold trade-off of the PB-ACD technique is analytically discussed.

Through the PB-ACD technique, the detection process merely depends on identifying a significant peak in the cepstral domain at the reciprocal of center frequency of the target spectral band. However, in a low SNR environment (e.g., -15 dB) in which high noisy fluctuations are experienced, identifying this major peak will be a difficult task. For this purpose, we introduce an improved version of the PB-ACD technique by providing a smoothing process. We formulate a novel signal smoothing technique that involves the use of the TVD approach through the MM algorithm. We start by evaluating the fluctuations of the ACEs of the received noise-like signal (i.e., spread spectrum signal) to which we apply the TVD-MM algorithm, and then estimating the smoothed spectrum before applying the PB-ACD approach. Since we assume working in a non-cooperative detection environment, and knowing that most of the denoising techniques depend on some knowledge provided of the received signal, noise statistics, and channel information, we apply the TVD-MM algorithm in semi-blind theme without a prior knowledge of the nature of the noise-like signal. Precisely, we utilize the fact that the fluctuations of the autocorrelation estimators of the received SS signal

and that of the AWGN are distinguishable [94], the TVD-MM algorithm is applied on the ACEs of the received CR signal utilizing this discriminating feature. The purpose of applying the smoothing process is to reduce possible false alarms. For the case of multiband spectrum access model, we introduce in chapter 4 a wideband spectrum sensing technique by employing CR approaches.

# WIDEBAND SPECTRUM SENSING TECHNIQUE BY CEPSTRAL ANALYSIS APPROACHES

---

## 4.1 Introduction

The process of sensing a wide radio spectrum is performed through two phases, namely: the edge detection phase, and the PU detection phase. Through the edge detection phase, the wideband of interest is analyzed to identify the subbands spectral boundaries, which are characterized by irregularities appearing in the spectrum. For instance, The Wavelet-Based Detection (WBD) approaches employ Wavelet Transform (WT) as a powerful mathematical tool for singularities detection [124]. These singularities, which represent irregular signal structures, define the subband edges (i.e., boundaries). As for the PU detection phase, one of the conventional NarrowBand Spectrum Sensing (NBSS) techniques can be utilized, such as Energy Detection (ED), Matched-Filter Detection (MFD), Cyclostationary feature detection (CFD), and Compressive Spectrum Sensing (CSS) [9]. In general, there are two main methods to apply NBSS: sequentially, or through parallel sensing. In the sequential sensing method, a narrowband detector senses multiple bands in a serial manner. The major disadvantage of employing sequential sensing is the slow processing time, and also the requirement of retuning the used filters and oscillators. While the theme of the parallel sensing method assures a better processing time, the increased complexity of the CR receiver architecture becomes a drawback. This increased complexity is due to the integrated multiple narrowband detectors at the CR receiver.

Since possible errors in the edge detection results consequently affect the performance of the PU detection phase, the crucial challenge in applying the WideBand Spectrum Sensing (WBSS) techniques is the devised edge detection algorithm. In other

words, false alarms can be generated due to the presence of spurious edges caused by noisy spectral variations. Moreover, errors in estimating the location of an exact spectral boundary may lead to the misdetection problem. Thus, the promising accuracy of the chosen edge detection approach is vital to assure the overall efficiency of the WBSS process. Clearly, further advancements in wideband sensing are required to provide a high detection robustness against noisy spectral variations with offered low complexity. Therefore, we should highlight the trade-off between the detection accuracy, and the computational burden or the offered hardware complexity. For example, despite the fact that the wavelet-based detector provides a reliable detection accuracy in an Additive White Gaussian Noise (AWGN) channel on the one hand, but on the other hand its hardware and computational complexities are significant. This is because a wavelet-based detector is basically implemented as a bank of multiresolution filters; So for better detection results, the signal analysis is carried out through all dyadic scales which increases the computational cost.

Moreover, the CS exploits the signal sparsity in the frequency domain knowing that a scarce or underutilized spectrum is sparse. This sparsity invokes a few number of measurements to be used, hence a performance degradation is expected due to the reduced Signal-to-Noise Ratio (SNR) despite the hardware simplicity of the CS detector. Motivated by these insights, in this chapter, we present a novel WBSS technique that is based on the Cepstral Analysis (CA) in the context of CR. We introduce an edge detection algorithm based on calculating the Differential Log-Spectral Density (DLSD) of the received wideband signal. This is to identify the spectral boundaries and characterize the number of occupied subbands. In order not to confuse the readers, evaluating the DLSD is slightly different than the conventional differential cepstrum. For a given signal, the DLSD evaluates the derivative of the natural logarithm of the signal's Power Spectral Density (PSD), whereas the differential cepstrum calculates the derivative of a signal's Fourier Transform (FT). A mathematical framework of the proposed edge detection algorithm is analytically illustrated to show the effect of the noisy spectral fluctuations on the resultant spectral boundaries. The proposed algorithm is compared to different wavelet-based edge detection algorithms at different noise power levels to validate its efficacy.

In the literature, the CA has a strong impact on several applications comprising audio and speech processing, as well as mechanical systems. It is also employed in the fields of signal classification or feature detection. Thus, the CA approach is used to

identify certain features hidden in a signal that can be revealed in the cepstral domain. According to the variants of the CA approach, a certain CA variant is chosen in order to fit a specific application. That is why a researcher must be aware of the problem under analysis, and whether employing the CA approach will unleash significant details about the signal in the logarithmic domain.

By completing the edge detection phase, we eventually obtain the required information about the spectral boundaries of the sensed wide spectrum. Afterwards, we proceed to identify the presence of possible PUs in the sensed frequency bands. The ED technique is a versatile NBSS technique that does not require a prior information about the PU signal. However, its susceptibility to noise variations results in a poor performance in low SNR environments [31]. Employing the ED technique for detecting a PU signal assumes that the frequency band of interest is exactly defined and recognized by its spectral boundaries. However, in WBSS, the performance of ED deteriorates. Since the PSD level within a certain subband is evaluated by the integration of the PSD over certain frequency bands, it should take into account the PSD level within the estimated frequency boundaries which are subjected to possible errors. Also, in the case of practical blunt spectrum shapes, the PSD leakage related to the PU signal outside the spectral boundaries will not be considered in the energy calculation [125]. Thus, this may cause the misdetection of a PU. To overcome these drawbacks, the Broadened Energy Detection (BED) and the Weighted Energy Detection (WED) are suggested in [125]. However, the increased resulting complexity is pushing ED to lose its simplicity property amongst different semi-blind NBSS techniques.

Although the PB-ACD technique has shown its efficacy in detecting a DS-SS PU signal in [126], with an exact knowledge of the subbands center frequencies, its performance deteriorates when applied in the MBSA scenario due to the potential errors in estimating the subbands center frequencies. These errors may result in the misdetection and false-alarm problems. As a solution, we introduce the BaseBand AutoCepstrum Detector (BB-ACD) that exploits the periodicity feature that can be revealed of the baseband digital signals in the cepstral domain. Accordingly, we propose a non-coherent detection of the received signal via a circular topological filter, which consists of Hilbert Filtering (HF) and a Square-Law Device (SLD). This is to extract the baseband version of a signal before evaluating the power cepstrum of the received signal, so that the detection process does not depend on the exact knowledge of the center frequency of a specific subband. In this chapter, A novel edge detection algorithm is

introduced by the DLSD approach to identify the spectral boundaries of the subbands comprising the target wideband spectrum. A mathematical framework of the DLSD approach is illustrated in low, medium, and high SNR environments. An analytical expression of the detection threshold characterizing the proposed DLSD detector is derived under AWGN channels. The BB-ACD technique is formulated for detecting noise-like signals under the subband center frequency uncertainty problem. A mathematical analysis of the detection threshold is presented according to the statistical distribution of the devised detection test statistic. Through simulations, we provided comparisons of the BB-ACD technique with the PB-ACD technique to show the efficacy of the proposed technique when the problem of center frequency errors is encountered.

This chapter is organized as follows: section 4.2 gives a brief state-of-the-art on edge detection, and also summarizes the advantages and critics of the wavelet-based edge detection techniques. Section 4.3 states the mathematical foundation of the problem under investigation and describes the overall proposed system architecture. The proposed edge detection and the CA-based PU detection techniques are introduced in section 4.4, with the mathematical analysis of both techniques. In section 4.5, the numerical results are illustrated, and the chapter summary is given in section 4.6.

## 4.2 Related Work

As it was previously mentioned, CA has been utilized differently in the field of signal detection. For example, it has been applied for echoes detection in seismic waves [18]. Further, it has been used to estimate the multipath time delay as introduced in [93], or for detecting audio watermarks [15]. In the contexts of spectrum sensing and signal detection in CR, CA approaches have been rarely utilized. For instance, the authors in [19] have employed CA techniques in waveform classification and for detecting OFDM signals and also for estimating their parameters. Moreover, the authors of [104] have introduced a WideBand Temporal Sensing (WBTS) approach based on a cepstral envelope detector. Precisely, the involvement of the cepstrum-based spectrum envelope detector is to adapt to dynamic changes that may occur in the configuration of a PU channel. The rationale of this approach is to use a cepstral feature vector to detect the changes in the spectrum envelope of a PU signal within a given frequency band. Based on the recursive temporal spectrum sensing algorithm proposed in [127], [128], the authors in [104] have proposed the use of cepstral analysis to monitor the

change of the PU's configuration instead of the conventional ED front end.

In the WBTS approach, a given frequency band is divided into narrowband channels of equal bandwidths. Every narrowband channel is then sensed individually using a Hidden Markov Model (HMM)-based approach [129]. The employed HMM model is trained by an observation sequence that consists of average received signal powers. The parameters of the trained HMM model is estimated by the Baum algorithm<sup>1</sup> [130]. According to a modified correlation metric, the adjacent channels are aggregated to form larger channels. After being conducted in a recursive manner, this process eventually results in the identification of a set of PU channels with their HMM estimated parameters. At the same time, a cepstrum-based envelope detector is applied to monitor the transition of the PU channel to a different configuration. The spectrum envelope detector is designed based on the HMM model in which the employed observation vector corresponds to the signal's cepstrum. Our proposed cepstrum-based WBSS approach differs from the WBTS approach such that it introduces the following:

- Identification of the number of occupied subbands in a target wide spectrum. This is formulated as an edge detection problem and accomplished by developing the DLSD algorithm.
- Detection of noise-like PU signals such as spread spectrum signals. For this purpose, we reviewed our proposed PB-ACD technique in chapter 3 which detects the presence of a DS-SS signal by monitoring a major autocepstral peak. The improved PB-ACD technique is proposed for improving the detection process by providing a smoothing to the fluctuation so the ACEs.
- Detection of noise-like signals under the uncertainty problem of the subbands center frequencies is accomplished by introducing the BB-ACD technique.
- To the best of our knowledge, the proposed WBSS approach is the first to consider the use of the DLSD algorithm for edge detection in CR and also improved PB-ACD technique for detecting noise-like PU signals. Also, exploiting the cepstral features of the baseband signals for PU detection when the uncertainty problem of the subbands center frequencies is relatively novel.

In some approaches, the process of wideband spectrum sensing starts with detecting the edges of the spectral boundaries. Many researches have presented the process of edge detection as a peak detection problem. The notion of a peak depends on the

---

1. The Baum algorithm is a special case of the Expectation-Maximization (EM) algorithm that is used to find the unknown parameters of an HMM.

function representing the required set of peaks in a signal. A peak function is one that characterizes a peak detector. It captures the spikiness of a significant feature in a signal, or generally, in a given time-series. Generally, there are some standard approaches to detect peaks, such as:

- i Fitting a smoothed time series to a known function (e.g., wavelet analysis).
- ii Matching a known peak shape to a given time series.
- iii Detection of zero-crossings in the differences between a specific points and its neighbors (e.g., Hilbert Filtering) [131].

Amongst many peak detection approaches, the wavelet analysis approach is significant in determining sharp variations appeared in a signal. So, in this section, we present a brief overview of the wavelet-based detection techniques. Further, we illustrate the applications of CA in CR and the importance of applying CA in the WBSS problem as compared to the wavelet-based detection techniques.

Wavelet analysis is considered as an efficient mathematical tool to describe the irregular structure in a signal by defining its singularities. Based on this concept, it has been adopted to identify the boundaries of non-overlapping subbands in a wide spectrum so as to classify them into white, gray, or black spectral holes. In [132], Tian and Giannakis introduced the use of Wavelet Transform Modulus Maxima (WTMM) approach to allocate wideband edges, and hence simultaneously identify all piece-wise flat frequency bands. One major limitation of this approach is its sensitivity to noisy fluctuations. Even by thresholding, all spurious components cannot be eliminated. Further, the authors suggested the use of Wavelet Transform Multiscale Product (WTMP) [133], to enhance the multiscale modulus coefficients while suppressing noise. However, this results in misdetecting an exact edge that is heavily corrupted with noise. On the other hand, WTMP exploits the correlation provided to improve the detection performance. The disadvantages of this approach are the loss of signals details, and losing the property of the multiresolutional analysis to distinguish between narrowband and wideband signals. To reduce this effect, the authors of [134] suggested the analysis of small and large scales separately. As an alternative approach, Wavelet Transform Multiscale Sum (WTMS) was discussed in [134] for an information preservation as well as avoiding attenuation that possibly occurs because of multiplication operations.

Despite the offered advantage of the WTMS over the WTMP, the dramatic increase of the scales throughout the analysis causes edges localization loss. A solution of this problem has been addressed in [135] by employing a non-orthogonal class of wavelet

functions such as the Gaussian wavelet function. Moreover, Sahil *et al.* in [136] has tested the work of Tian and Giannakis in a multipath fading channel, and they found that a good performance is achievable in moderate fading, but it is dropped significantly in deep fading channels. In [136], the authors suggested applying a logarithmic scaling preceded by thresholding in order to enhance the small modulus maxima values at the exact edges. However, the computation burden becomes a consequence of applying their proposed technique. Also, this enhancement affects negatively the spurious edges by magnifying them. This increases false alarms at high noise variance. In this sense, discrete wavelet transform based algorithm is suggested in [137] to alleviate this problem. The discrete wavelet transform algorithm can perform edge detection and denoising simultaneously providing reliable performance in high SNR scenarios. In the case of low SNR scenarios, a moving averaging filtering strategy is adopted. As a result, a better performance is achieved at lower scales, thus the computation time is reduced on the expenses of the increased hardware complexity.

At the best of our knowledge, a WBSS approach based on CA been introduced rarely in the literature. Since our goal is to identify the frequency locations of non-overlapping spectrum bands and detect the presence of spectral holes, the adaptation of CA for WBSS as opposed to the wavelet based approach is motivated by the following insights:

- Using wavelet analysis to the intended spectrum depends on the applied wavelet function, so the accuracy and the performance will also depend on the appropriate choice of the mother wavelet.
- The complexity of the wavelet approach offered, due to the consecutive scaling and shifting operations, affects the sensing time.
- CA has the property of revealing hidden harmonics and periodic features of analyzed signals.
- CA is lower in the implementation complexity as opposed to wavelet analysis.

### 4.3 Problem Formulation of Wideband Spectrum Sensing

The main target of employing wideband sensing is to provide more spectral opportunities. It means that the SU must recognize precisely the number of subbands in the

wide sensed spectrum before testing the occupancy of each one of them. To design the wideband detector, we should take into account the problem of edge detection and the identification of spectral holes. Further, there are some challenges, facing the design of the wideband detector, that must be clarified. They are summarized as follows:

- The inspected subband may be licensed to certain wireless devices, such that they consume small portion of the reserved bandwidth, yet the total bandwidth might be considered occupied. In this case, the SU must be aware of the percentage of the spectral occupancy accurately to avoid interfering with the licensed user, and to be able to configure properly its transmission to exploit the non-utilized portion. This is illustrated in Figure 4.1.
- Subbands are assumed to be non-overlapping and have identical bandwidths; and the occupied channels are uncorrelated, in contrast to systems such as WiLAN and Broadcast TV in which subchannels are correlated.
- The detection of a PU, transmitting a wideband signal in a deep fading channel is challenging because without providing the CR systems with subchannels correlation information, the SU may interfere with the PU when resuming its transmission.

### 4.3.1 Phase I: Identification of Spectral Boundaries

In a cognitive communication network in which heterogeneous wireless devices are supported, a CR user must be able to sense the wireless environment at a specific time and place within a wide spectrum. In particular, the SU must acquire the knowledge of the subchannel edges characterizing the spectral boundaries. Once the boundaries are estimated, we can define their center frequencies, and eventually the PU occupancy can be examined. In this context, we can formulate the problem statement for the edge detection in WBSS as follows:

*In order to detect a specific spectral hole in a predefined wide frequency band by a cognitive radio receiver, we need to identify the parameters characterizing the wideband spectral environment which are: the number of subbands  $N_{sub}$ , their corresponding center frequencies  $\{f_{c_{n_s}}\}_{n_s=1}^{N_{sub}-1}$ , and the spectral boundaries  $\{f_{n_s}\}_{n_s=1}^{N_{sub}-1}$ .*

Before representing our proposed solution to this problem, some basic assumptions are drawn:

- The entire wide band under scrutiny is modeled as a train of consecutive fre-

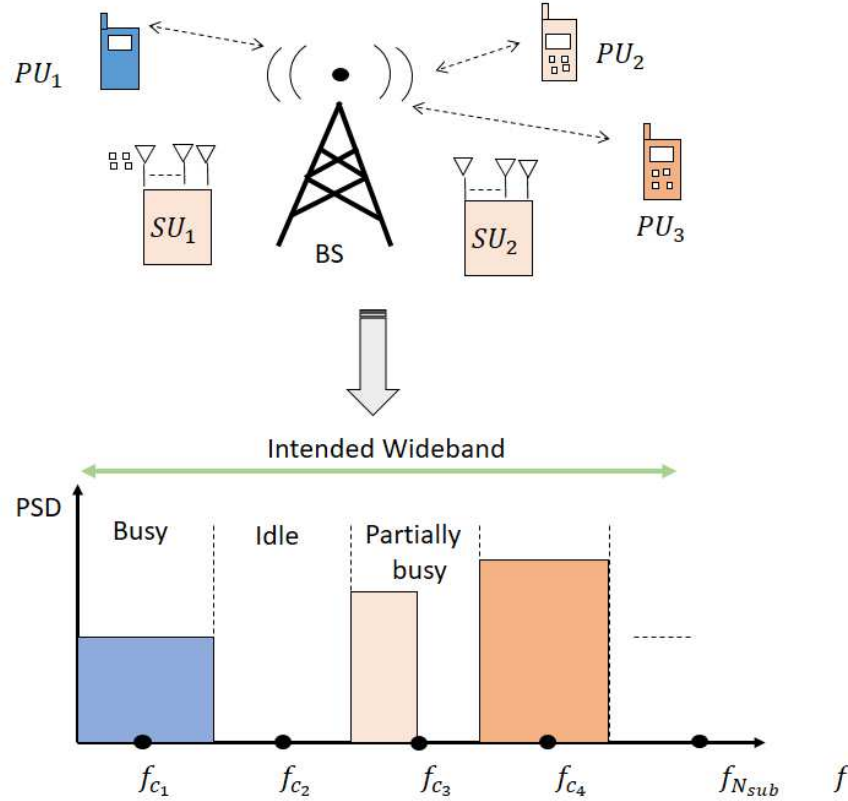


Figure 4.1 – A general description of the wideband spectrum sensing problem

quency subbands, where the power spectral characteristic is analyzed under two conditions:

- i Piece-wise flat spectrum that exhibits a discontinuous change between adjacent subbands.
- ii Blunt-shaped spectrum generated by a raised-cosine pulse shaping filter as a practical example.

These changes are irregularities in the PSD. They carry key information on sub-band locations.

- The wide spectrum of interest denoted by  $\mathcal{B}$  is defined in the frequency range  $[f_0, f_{N_{sub}}]$  provided that the spectral boundaries  $f_0$  and  $f_{N_{sub}}$  are known by the CR system.
- The  $n_s^{th}$  subband within  $\mathcal{B}$  is defined by  $\mathcal{B}_{n_s}$  such that:  $f \in \mathcal{B}_{n_s} : f_{n_s-1} \leq f < f_{n_s}$ , and the frequency boundaries of the consecutive bands are denoted by  $f_0 \cdots f_{N_{sub}}$ , where  $N_{sub}$  is the number of frequency bands within  $\mathcal{B}$ .

- The number of frequency bands is unknown to the CR as well as the frequency boundaries.
- The ambient noise is assumed to be an additive white Gaussian noise, with zero mean and two-sided PSD:

$$S_w(f) = \frac{N_0}{2}, \forall f \quad (4.1)$$

- We consider the case of a slotted medium access in the interweave CR system, by which the SU performs a periodic sensing on segmented time frames.
- The effect of adjacent channel interference is neglected by assuming the  $n^{\text{th}}$  sub-band PSD  $S_{n_s}(f) = 0, \forall f \notin [f_{n_s-1}, f_{n_s}]$ .

### Signal and Channel Models

Let us define the received wideband signal by the CR receiver by:

$$\begin{aligned} r(t) &= s(t) + w(t) \\ &= \sum_{n_s=1}^{N_{sub}} s_{n_s}(t) + w(t) \end{aligned} \quad (4.2)$$

where  $s(t)$  is the transmitted PU signal,  $w(t)$  is the AWGN signal, and  $s_{n_s}(t)$  is the  $n_s^{\text{th}}$  signal occupying the  $n_s^{\text{th}}$  subband,  $\mathcal{B}_{n_s}$ , which is given by:

$$s_{n_s}(t) = x_{n_s}(t) * h_{n_s}(t) \quad (4.3)$$

where  $x_n(t)$  is the transmitted signal that is represented by a sequence of a digitally modulated pulses in the  $n^{\text{th}}$  band. The channel impulse response between the PU and the SU at the  $n^{\text{th}}$  subband is denoted by  $h_n$ , whereas the symbol  $*$  denotes the convolution product. In the case of a narrowband channel, we can rewrite equation (4.3) as:

$$s_{n_s}(t) = a_{n_s} \sum_{k=-\infty}^{\infty} b_k p(t - kT_s) \exp(j2\pi f_{c_{n_s}} t) \quad (4.4)$$

where  $a_n$  represents the attenuation suffered by the transmitted signal in the  $n^{\text{th}}$  subband. Also,  $\{b_k\}$  are the set of digital symbols,  $p(t)$  is the pulse shaping function,  $f_{c_{n_s}} = \frac{f_{n_s} + f_{n_s-1}}{2}$  is the subband center frequency, and  $f_{n_s}$  is the  $n_s^{\text{th}}$  frequency bound-

ary. The PSD of the observed signal  $r(t)$  at the CR front-end can be written as:

$$S_r(f) = \sum_{n_s=1}^{N_{sub}} a_{n_s}^2 S_x(f) + S_w(f), f \in [f_0, f_{N_{sub}}] \quad (4.5)$$

where  $a_{n_s}^2$  is the PSD level in the  $n_s^{th}$  band due to the channel attenuation,  $S_x(f)$  is the PSD of transmitted digital signal, and  $S_w(f)$  is the noise PSD.

### 4.3.2 Phase II: Primary User Detection

Following the edge detection phase, the WBSS problem requires the CR receiver to solve  $N_{sub}$  binary hypothesis testing problems. For an independent subchannel occupancy, the WBSS problem definition can be defined as:

$$\mathbf{r} = \begin{cases} \mathbf{w} & : \text{Under } H_0^{n_s} \\ \mathbf{x} + \mathbf{w} & : \text{Under } H_1^{n_s} \end{cases} \quad (4.6)$$

where  $\mathbf{r} = [\mathbf{r}_1, \mathbf{r}_2, \mathbf{r}_3, \dots, \mathbf{r}_{N_{sub}}]$  denotes the received signal matrix,  $\mathbf{w}$  is the noise vector at each subband, and  $H_0^{n_s}, H_1^{n_s}$  represents the  $n_s^{th}$  null and alternative hypothesis, respectively. As seen from equation (4.6), the complexity of the detection problem increases as the number of subchannels increases. The decision rule, represented by the test statistic  $\mathcal{T}[r_{n_s}]$  and the detection threshold  $\zeta_{n_s}$ , can be given by:

$$\mathcal{T}[r_{n_s}] \underset{H_0^{n_s}}{\overset{H_1^{n_s}}{\gtrless}} \zeta_{n_s} \quad (4.7)$$

It is important to indicate that the definition of the test statistic depends on the type of the applied narrowband detector. Also, The formulation of the detection threshold depends on the statistical distribution of the noise in the detector test statistic. In the following sections, we illustrate the proposed approach in both phases.

## 4.4 The Proposed Wideband Spectrum Sensing Approach

In this work, we develop a complete framework of the WBSS approach based on the CA of the received signal. In our investigation, we seek a reduced system complexity

and a reliable detection accuracy in the edge detection and the PU detection phases. The channel estimate at each subband can be provided by the pilot-insertion method after being identified [13].

#### 4.4.1 Identification of Spectral Boundaries By Cepstral Analysis

First, we introduce the Differential Log Spectral Density (DLSD) technique and mathematically analyze the detection process in the case of high, medium, and low SNR scenarios. The three SNR cases are considered for an example of a wideband spectrum that consists of consecutive subbands, each one has a specific spectral density level. So, based on the average spectral density level, we vary the AWGN power level, denoted by  $\sigma_w^2$ , to consider the three SNR cases. Precisely, for the case of having the SNR  $< 0$  dB (i.e., equivalently the noise power  $\sigma_w^2 > 20$  dB), the considered wideband spectrum is analyzed in a low SNR environment. The sequence of operations of the proposed CA-based WBSS approach is shown in Figure 4.2.

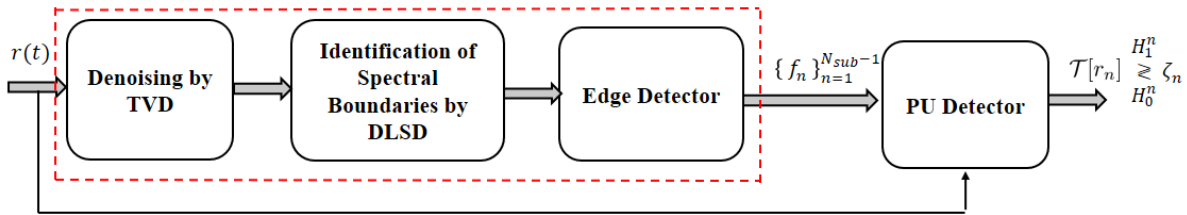


Figure 4.2 – The sequence of operations of the proposed WBSS approach

#### Edge-Detection by The Differential Log-Spectral Density Algorithm

For a compact representation, the PSD of the received signal under  $H_0$ , defined in equation (4.6), can be given by:

$$S_r(f) = S(f) + S_w(f) \quad (4.8)$$

where  $S(f) = \sum_{n_s=1}^{N_{sub}} S_{n_s}(f)$  denotes the sum of PSDs of the signals occupying the sensed wide spectrum. To apply the DLSD algorithm, we perform the following:

1. Evaluate the autocorrelation estimate of the received signal and then, its PSD.

2. Evaluate the first derivative of the autocepstrum of the received signal in the frequency domain.

For convenience, by applying the natural logarithm to equation (4.8), we obtain:

$$\begin{aligned} Z_r(f) &= \log S_r(f) \\ &= \log[S_w(f)] + \log[\gamma_0(f) + 1] \end{aligned} \quad (4.9)$$

where  $\gamma_0(f) = \frac{S(f)}{S_w(f)}$  defines the relative PSD variations of the transmitted wideband signal to the noise. The  $n_s^{th}$  spectral peak identifying the  $n_s^{th}$  subband boundary is located at:

$$f_{n_s} = \arg \{ |D(f)| \}, f_{n_s} \in [f_1, f_{N_{sub}-1}] \quad (4.10)$$

where  $\arg(\cdot)$  defines the argument of a function within the round parenthesis, and  $D(f) = \frac{d}{df} Z_r(f)$  represents the DLSD function. Accordingly, we need to analyze  $Z_r(f)$  in case of a medium-to-high SNR environment as well as a low SNR environment. Since the PSD level of the noise is assumed to be constant, getting its natural logarithm decreases the PSD value. Therefore, the value  $Z_w(f) = \log[S_w(f)]$  is much lower than  $\log[\gamma_0(f) + 1]$ . By taking the derivative of  $Z_r(f)$ , we can consider that  $D_w(f) = \frac{d}{df} \log[S_w(f)] \approx 0$ , then we obtain:

$$D(f) = \frac{d}{df} \log[\gamma_0(f) + 1] = \frac{1}{1 + \gamma_0(f)} \frac{d}{df} \gamma_0(f) \quad (4.11)$$

substituting equation (4.8) in equation (4.11), we get:

$$D(f) = \frac{1}{S(f) + S_w(f)} \sum_{n=1}^{N_{sub}} \frac{d}{df} S_n(f) \quad (4.12)$$

According to equation (4.12), and for the case of a medium-to-high SNR, the relative PSD variations is assumed  $\gamma_0(f) \gg 1$ , then equation (4.12) can be reduced to:

$$D(f) \approx \frac{1}{S(f)} \frac{d}{df} S(f) \quad (4.13)$$

whereas for the low SNR case,  $\gamma_0(f) \ll 1$ , then we obtain:

$$D(f) \approx \frac{2}{N_0} \frac{d}{df} S(f) \quad (4.14)$$

To clarify the concept, Figure 4.3 shows the low PSD level of the AWGN after applying the DLSD technique and justifies the approximation applied in equation (4.11). Figure 4.4 gives another example of the wideband spectrum scenario that consists a group of consecutive flat piece-wise subchannels. In that example, the wideband spectrum is ranging from 50 to 250 GHz, such that each subband has a specific spectral density level within its corresponding bandwidth. Also, in Table 4.1 indicates the SNR values for each subband with respect to the noise variance.

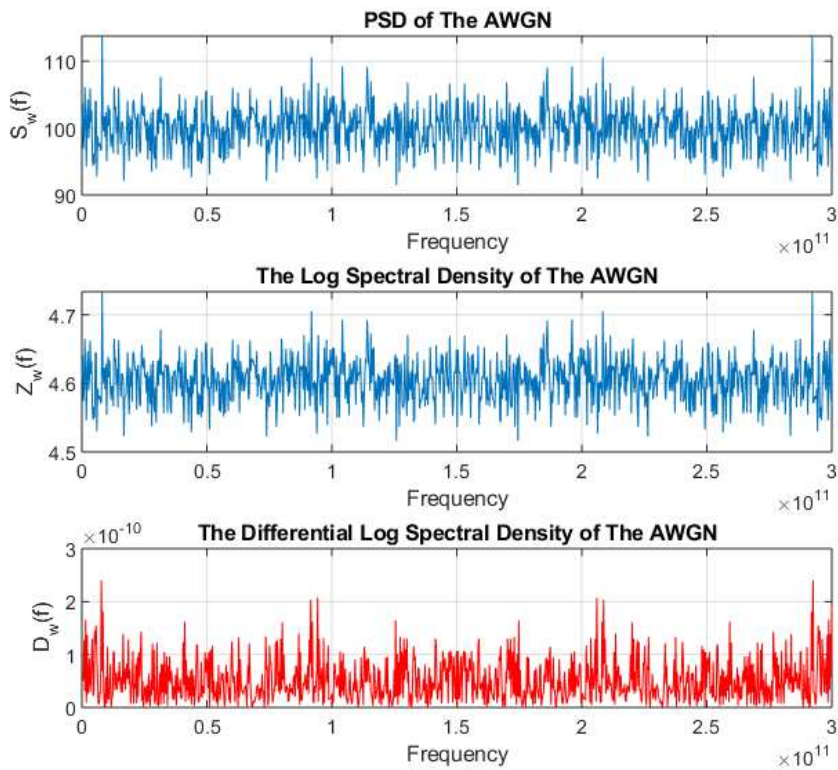


Figure 4.3 – Illustration of the effect of applying the DLSD to the AWGN spectrum

The effect of applying the proposed DLSD technique for the case of low, medium or high noise power with respect to the average PSD level of the consecutive subbands is illustrated in Figure 4.5, 4.6, and 4.7. For the case of low and medium noise variances (precisely,  $\sigma_w^2 = 14.7$  dB and  $\sigma_w^2 = 20$  dB), the spectral boundaries are clearly distinguishable from the noisy edges. When the noisy spectral variations are high, as shown in Figure 4.7, the actual spectral boundaries are hardly being differentiated from the spurious edges and may result in detection errors.

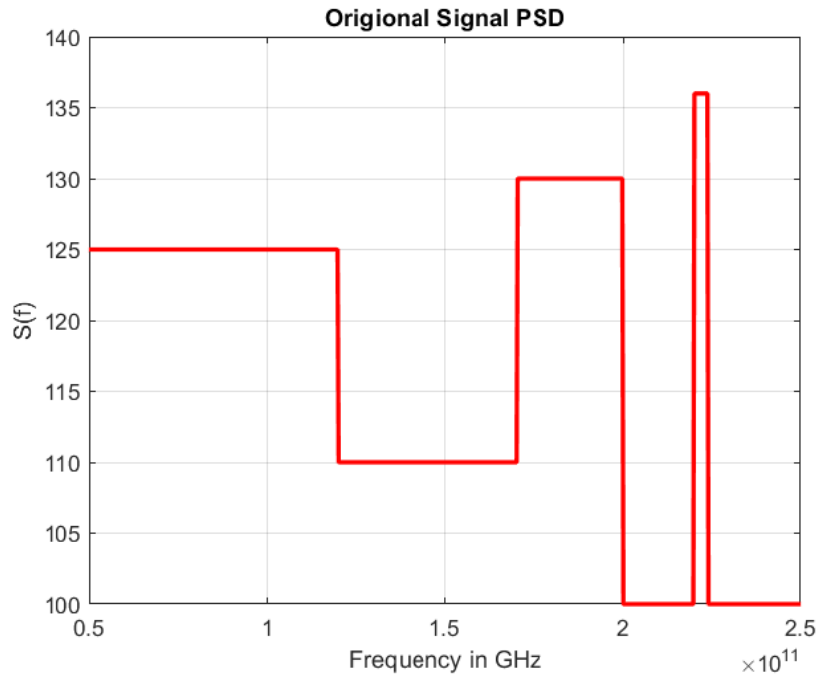


Figure 4.4 – An example of a wideband spectrum that consists of consecutive subbands

Table 4.1 – The SNR specifications per subband of an example of a wideband spectrum

Band Order	Band Range (GHz)	PSD Level (dB/Hz)	High SNR $\sigma_w^2 = 14.7$ (dB)	Medium SNR $\sigma_w^2 = 20$ (dB)	Low SNR $\sigma_w^2 = 24$ (dB)
1	50-120	21	6.3	1	-3
2	120-170	20.4	5.7	0.4	-3.6
3	170-200	21.1	6.4	1.1	-2.9
4	200-220	20	5.3	0	-4
5	220-225	21.3	6.6	1.3	-2.7
6	225-250	20	5.3	0	-4

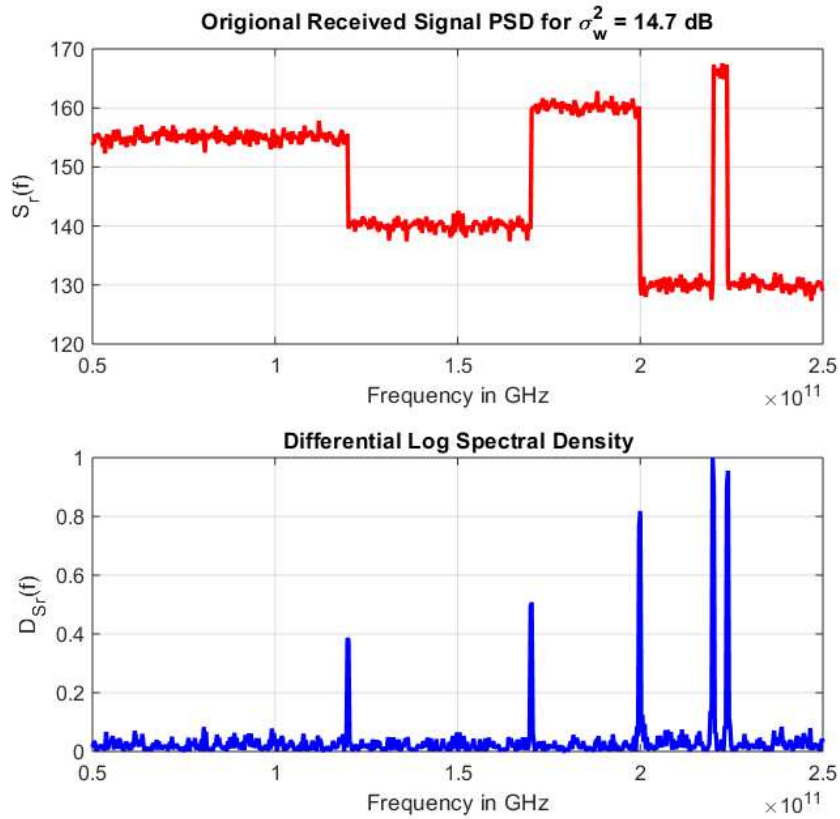


Figure 4.5 – The spectral edges when applying the proposed DLSD algorithm for the high SNR case (the average SNR is 5.9 dB for  $\sigma_w^2 = 14.7$  dB)

To solve the high noisy spectral peaks, we employed the TVD-MM algorithm to reduce the noisy spectral fluctuation before applying the DLSD algorithm. Indeed, we notice that if the average SNR  $< 0$  dB ( $\sigma_w^2 > 20$  dB), the spectral edges of the subbands can be well identified when the DLSD technique is applied in conjunction to denoising as shown in Figure 4.8.

In fact, the performance of the TVD-MM algorithm is affected by the choice of the regularity parameter as well as the number of iterations taken by the MM algorithm to converge. According to our assumptions on the wideband spectrum scenario, it becomes adequate to apply the TVD-MM algorithm over about 10 iterations to reduce the spurious edges and to significantly identify the spectral boundaries if  $\sigma_w^2 > 20$  dB (i.e., the average SNR  $< 0$  dB). In this case, the elapsed time measured for 10 iterations was 0.357 sec on a Intel(R) Core(TM) i7-8550U processor (1.8 GHz), with a R2018a MATLAB program. However, the elapsed time measured for employing the WTMM edge detection algorithm under the same simulation conditions was 7 sec.

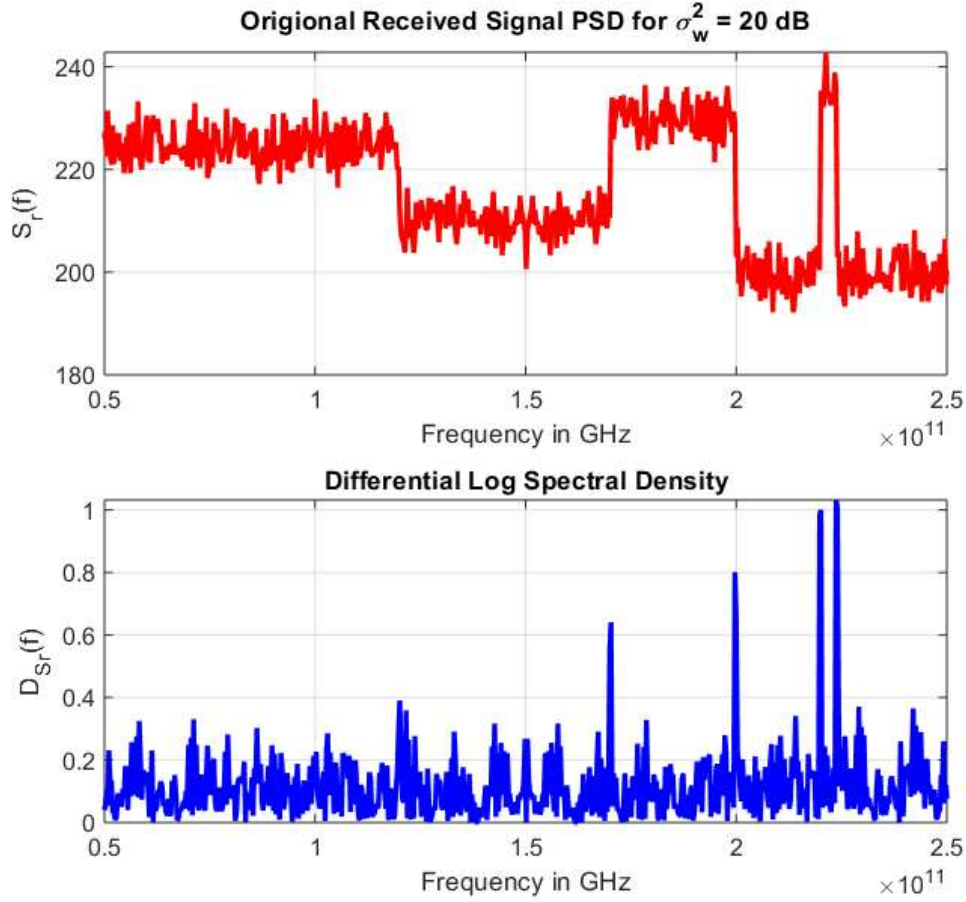


Figure 4.6 – The spectral edges when applying the proposed DLSD algorithm for the medium SNR case (the average SNR is 0.6 dB for  $\sigma_w^2 = 20$  dB)

Thus, in accordance to our application and the stated wideband criterion, the processing time of the DLSD after applying the denoising technique is much lower than that of the WTMM algorithm. The results of 1000 Monte Carlo simulations for the proposed DLSD algorithm are shown in section 4.5 to justify our argument.

### Noise Characteristic in The DLSD Technique

In our cepstrum-based edge detection approach, differential cepstral peaks may arise not only due to the exact spectral edges but also due spurious edges generated from AWGN, impulsive noise, or very-narrowband interference. Therefore, it is important to identify the degrading effect of these sources on the target wide spectrum as follows:

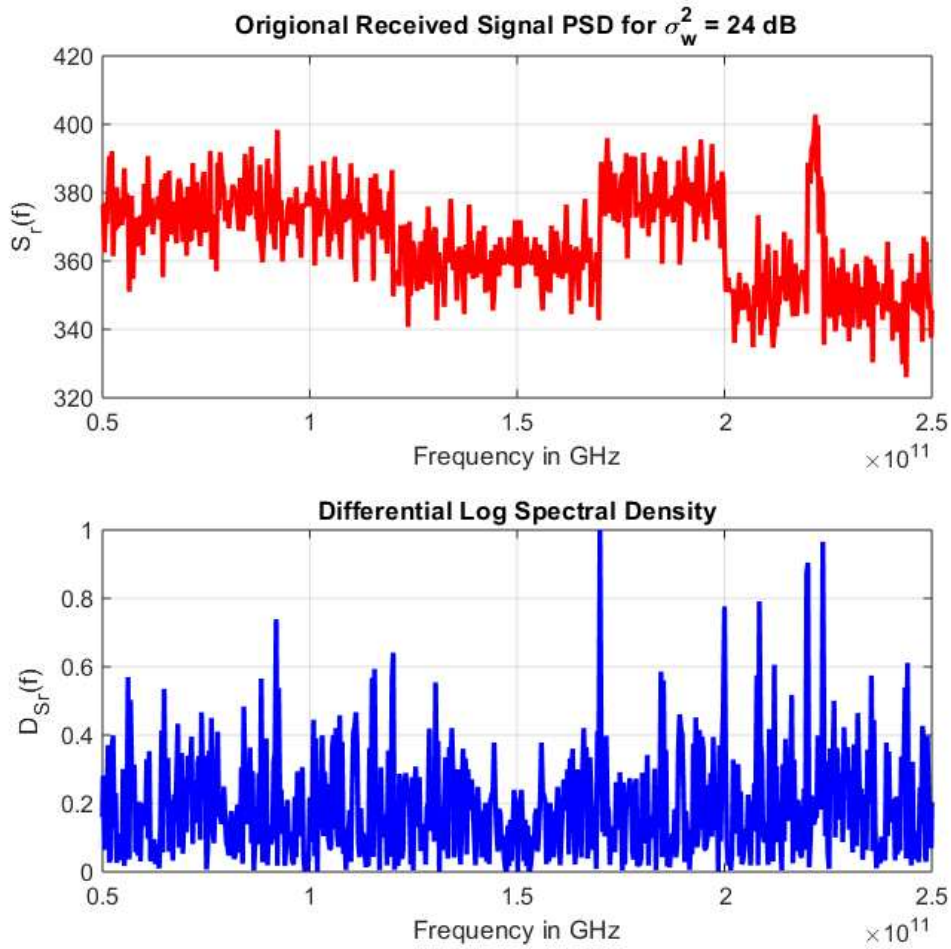


Figure 4.7 – The spectral edges when applying the proposed DLSD algorithm for the low SNR case (the average SNR is -3.4 dB for  $\sigma_w^2 = 24$  dB)

- Concerning the ambient noise, we find that the effect of the AWGN in our DLSD technique is not harmful when it is applied in a high-to-medium SNR environment. Also, when denoising is employed before the DLSD technique, the spectral edges became more recognizable in a low SNR environment.
- In wideband CR receivers, the impulsive noise and very-narrowband interference occur as narrow peaks in a spectral hole. Thus, it is desired not to identify these peaks during spectrum sensing. In Figure 4.9, we illustrate the effect of applying the DLSD technique to the target wide spectrum for an average SNR of 5.7 dB and we find that the spectral peaks can be easily identified. Further, we applied the DLSD technique after denoising the spectral fluctuations and we find that the spectrum is smoothed out while the spectral boundaries are well

recognized as shown in Figure 4.10. Practically, some wideband receivers have a built-in capability to handle very-narrowband [132].

### Design Characteristics of DLSD Edge Detector

In our devised edge detection algorithm, the peak function evaluates its value at each sample point. In this case, all positive sample points are candidate peaks. In order to reduce the effect of false peaks, we need to rule out these peaks based on their statistical distribution. Therein, we analyze the statistical characteristics of the peak function defining the DLSD approach. For the case of a baseband Binary Phase Shift Keying (BPSK) signal occupying the wideband of interest, the PSD of the BPSK signal is given by [36]:

$$S_x(f) = T_d^2 \text{sinc}^2(T_d f) \quad (4.15)$$

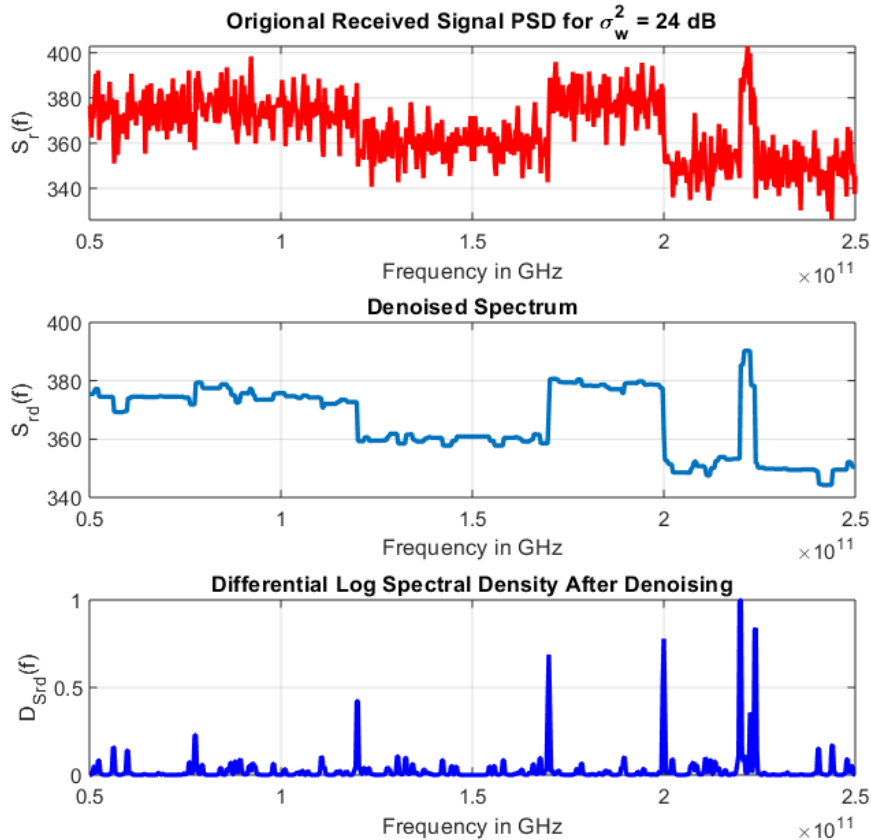


Figure 4.8 – The spectral edges when applying the proposed DLSD algorithm with denoising for the low SNR case (the average SNR is -3.4 dB for  $\sigma_w^2 = 24$  dB)

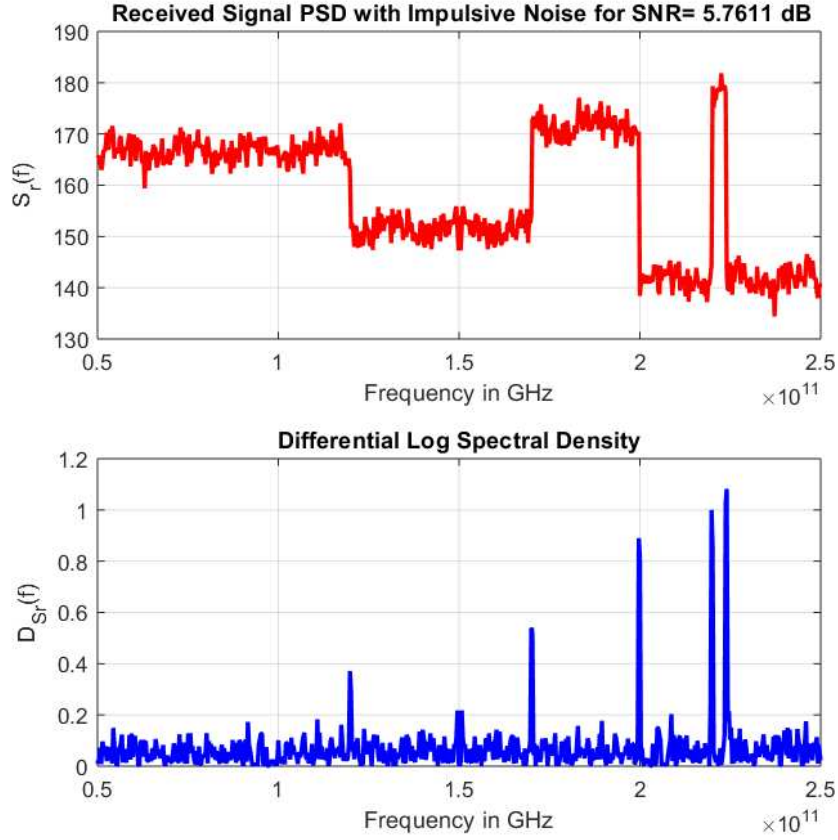


Figure 4.9 – The spectral edges when applying the proposed DLSD algorithm if impulsive noise is imposed at average SNR of 5.7 dB

where  $T_d$  denotes the symbol duration. The peak function, based on the DLSD approach described in Equation (4.12), is given by:

$$\mathbb{P}(f) = |D(f)| = \left| \frac{\frac{d}{df} S_r(f)}{S(f) + S_w(f)} \right| \quad (4.16)$$

in this case, if the noise at the CR receiver is assumed to be real Gaussian and based on equation (4.1), the estimate of  $S_w(f)$  follows a Chi-squared distribution,  $\chi_1^2$ , with one degree of freedom. Accordingly, the edge detection problem can be formulated as a binary hypothesis test by:

$$\mathbb{P}(f) = \begin{cases} \mathbb{P}_0(f) = \left| \frac{\frac{d}{df} S_r(f)}{S_w(f)} \right| & : \text{Under } H_0 \\ \mathbb{P}_1(f) = \left| \frac{\frac{d}{df} S_r(f)}{S(f) + S_w(f)} \right| & : \text{Under } H_1 \end{cases} \quad (4.17)$$

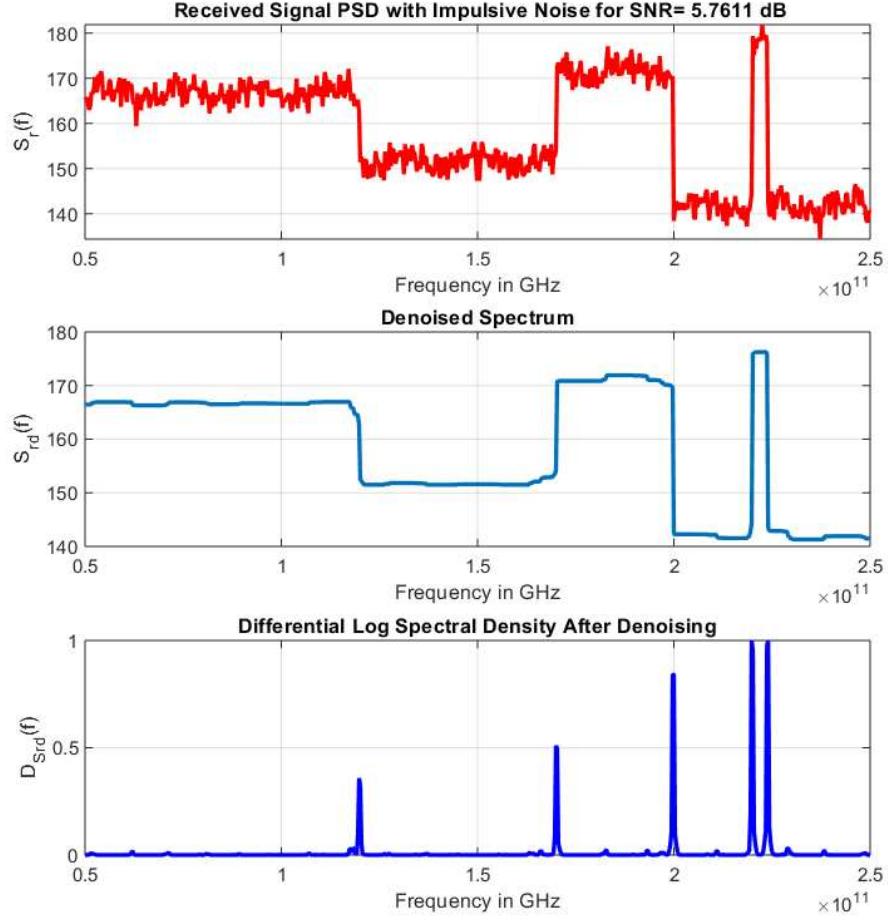


Figure 4.10 – The spectral edges when applying the proposed DLSD algorithm with denoising if impulsive noise is imposed at average SNR of 5.7 dB

$\mathbb{P}_0(f)$  is the set of spurious edges due to noisy spectral fluctuations, and  $\mathbb{P}_1(f)$  is the set of noisy spectral boundaries. In order to design the detector, we need to find the detection threshold based on the distribution of equation (4.17) under the null hypothesis. In this case, we must obtain the right-tail probability of the proposed test statistic under  $H_0$  for a fixed value  $\alpha_{FA}$  of the false alarm probability denoted by  $P_{FA}$  [54]:

$$P_{FA} = \int_{\{\mathbb{P}: \mathcal{T} > \eta_p\}} f_{\mathbb{P}}(\mathbb{P}; H_0) d\mathbb{P} = \alpha_{FA} \quad (4.18)$$

where  $\mathcal{T}$  is the detector test statistic,  $\eta_p$  is the detection threshold,  $\alpha_{FA}$  is the  $P_{FA}$  value, and  $f_{\mathbb{P}}(\mathbb{P}; H_0)$  is the probability density function of every peak value defined based on

the peak function  $\mathbb{P}(f)$ . In other words, the detector test statistic is defined by:

$$\mathcal{T}[\mathcal{A}] = \{\mathcal{A}[i], \text{ if } \underset{H_0}{\overset{H_1}{\mathcal{A}[i] \geq \eta_p}}\}; 1 < i < L \quad (4.19)$$

where  $\mathcal{A}[i]$  represents each peak value within the set of peaks of length  $L_p$  points defined in the quefrequency domain. For positive peak values, we find that the statistical distribution of each point in  $\mathbb{P}(f) = |D(f)|$  follows also  $\chi_1^2$ , which is defined by:

$$f_{\mathcal{A}}(a) = \frac{\exp(-\frac{a}{2})}{\sqrt{2a\pi}}, a > 0 \quad (4.20)$$

then by solving for equation (4.18), we obtain:

$$P_{FA} = \frac{2}{\sqrt{\pi}}Q(\sqrt{\eta_p}) \quad (4.21)$$

Thus, the threshold of the DLSD edge detector for a given false-alarm probability is given by:

$$\eta_p = \left[ Q^{-1} \left( P_{FA} \frac{\sqrt{\pi}}{2} \right) \right]^2 \quad (4.22)$$

To sum up, the DLSD edge detection algorithm is illustrated as follows:

---

**Algorithm 1** DLSD Edge Detection algorithm

---

- 1: **Input:**  $\mathbb{P}(f, L_p, i, |D(f)|_i), L_p, \alpha_{FA}, \eta_p$
  - 2: **Output:**  $O$  // set of detected edges
  - 3: **Begin**  $O = \emptyset$  // initially empty set
  - 4: **for**  $(i = 1; i < L_p; i++)$  **do**
  - 5:  $A[i] = \mathbb{P}(f, L_p, i, |D(f)|_i)$
  - 6: **if**  $A[i] > \eta_p$  **then**
  - 7:      $O = O \cup A[i]$
  - 8: **end if**
  - 9: **end for**
-

## 4.5 PU Detection Under Frequency Uncertainty by The BB-ACD Technique:

The proposed BaseBand-AutoCepstrum Detection (BB-ACD) Technique consists of a circular topological filter followed by the PB-ACD. The circular topological filter utilizes the circular topology of a typical sinusoidal signal to separate the baseband signal or its squared version. The detection of a noise-like PU signal, or a conventional digitally modulated signal, by the PB-ACD technique depends on the presence of a strong peak appearing at a quefrequency value equivalent to the reciprocal of the center frequency of a certain subband. Due to the possible frequency estimation errors from the edge detection phase, the PB-ACD gives a poor performance. Thus, our objective is to utilize the baseband features of the target signal appearing in the power cepstrum of the received signal. Specifically, we exploit the peaks reflecting the periodicity appears in the power cepstrum of the  $n_s^{th}$  baseband signal. These peaks interpret the presence of digitally modulated symbols of a possible PU signal. By using the combination of the Hilbert Filtering (HF) and the Square Law Device (SLD), we can obtain the required term representing the baseband signal. A functional block diagram of the proposed BB-ACD is shown in Figure 4.11. To illustrate the concept, we notice in Figure 4.12 that the autocepstrum of a passband DS-SS signal reveals a major peak that appears at the reciprocal of the carrier frequency after getting the inverse Fourier Transform of the autocepstrum, whereas a periodicity is revealed in the baseband version of the frequency domain version of the autocepstrum in Figure 4.13. This is shown at multiples of the reciprocal of the bit duration of the DS-SS signal.

To illustrate the calculus, consider a digitally modulated carrier signal,  $B_d(t)$ , which is defined by:

$$B_d(t) = B(t) \cos(2\pi f_{c_n} t) \quad (4.23)$$

where  $B(t)$  is the baseband signal, and  $f_{c_n}$  is the carrier frequency (i.e., the center frequency of the  $n_s^{th}$  subband). Assuming that  $B(t)$  is narrow band as compared to  $f_{c_n}$ , the output  $O(t)$  of the CLT after applying Hilbert filtering to equation (4.23), is given by:

$$O(t) = B_d^2(t) + [B_d^H(t)]^2 = B^2(t) \quad (4.24)$$

where  $(.)^H$  denotes the Hilbert version. Practically, the carrier frequency will be replaced with  $f_e = f_{c_n} \pm \delta f$ , where  $f_e$  indicates the estimated center frequency.

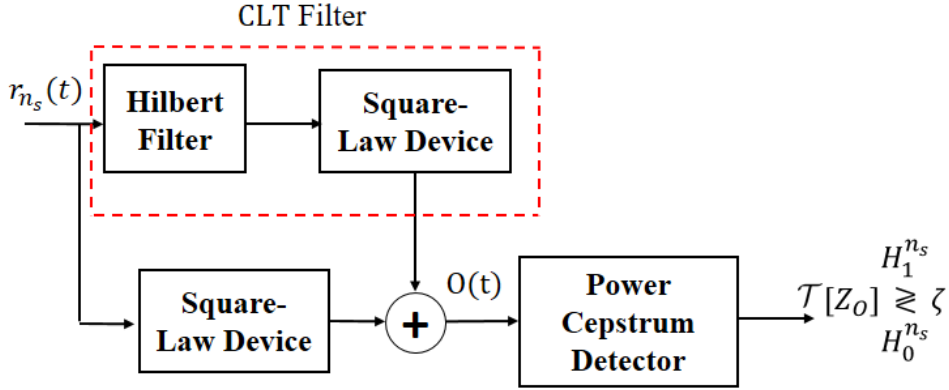


Figure 4.11 – The system architecture of the proposed baseband autocepstrum technique; CLT denotes the circular topological filter

Also,  $\delta f$  is the frequency deviation from the actual carrier frequency that causes the estimation error. The noise effect at the CR receiver is considered for the AWGN noise  $w(t)$ , hence, the output  $O(t)$  becomes:

$$\begin{aligned} O(t) &= [B_d(t) + w(t)]^2 + [B_d^H(t) + w^H(t)]^2 \\ &= B_s(t) + \mathcal{E}_s(t) + 2B(t) [w(t)\cos(2\pi f_{c_n}t) + w^H(t)\sin(2\pi f_{c_n}t)] \end{aligned} \quad (4.25)$$

In equation (4.25), the squared baseband version of the signal,  $B^2(t)$ , is denoted by  $B_s(t)$ , and  $\mathcal{E}_s(t) = w^2(t) + (w^H(t))^2$  denotes the squared envelope of the noise signal. However, it is required to eliminate the high frequency terms before defining the detector test statistic. A possible solution is to apply the autocepstrum approach. To do this, first, we determine the autocorrelation of  $O(t)$  such that:

$$R_O(\tau) \approx R_{B_s}(\tau) + R_{\mathcal{E}_s}(\tau) \quad (4.26)$$

then, by getting the Fourier Transform of  $R_O(\tau)$ , we obtain the corresponding PSD terms by:

$$S_O(f) \approx S_{B_s}(f) + S_{\mathcal{E}_s}(f) \quad (4.27)$$

By taking the natural logarithm of  $S_O(f)$ , we get the autocepstrum by:

$$Z_O(f) = \log[S_{B_s}(f) + S_{\mathcal{E}_s}(f)] \quad (4.28)$$

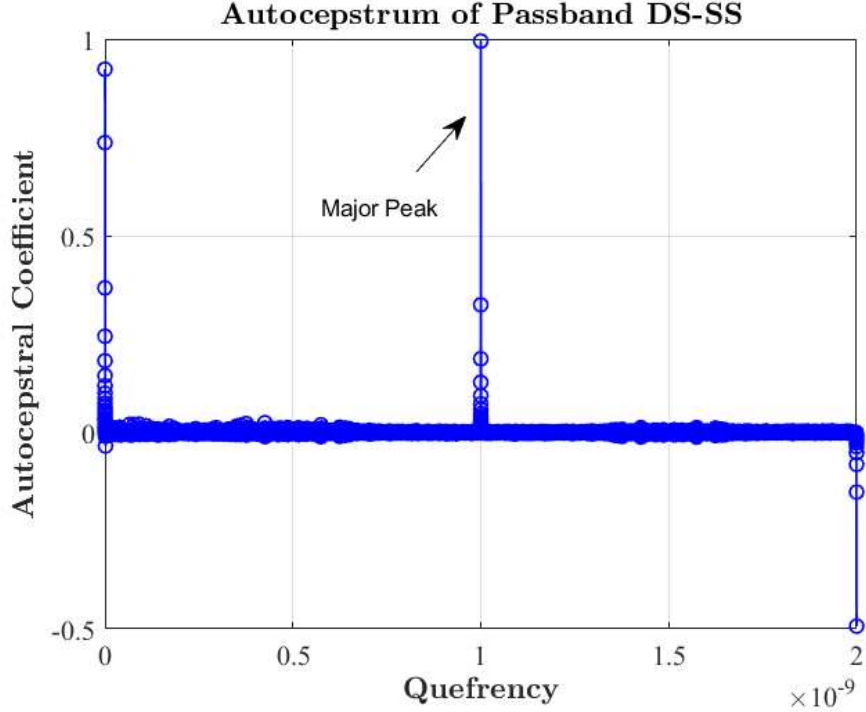


Figure 4.12 – The autocepstrum of the passband DS-SS signal; a large peak is located at a quefrequency value that is equivalent to the reciprocal of the signal’s operating frequency of 1 GHz

Since the BB-ACD utilizes the periodicity that may occur in the log-PSD of the received signal, we need to show at the beginning that the  $S_{B_s}(f)$  is periodic in the cepstral domain, and then consider the noisy periodicities in  $Z_O(f)$  due to the spectral fluctuations from  $S_{\mathcal{E}_s}(f)$ . Consequently, this periodic feature can be utilized to formulate the detector test statistic. In order to generalize the BB-ACD approach to digitally modulated signals, consider the following baseband version of equation (4.4) which is defined by:

$$B(t) = \sum_{k=-\infty}^{\infty} b_k p(t - kT_s) \quad (4.29)$$

Conventionally,  $B(t)$  is a polar signal and the pulse shape is the rectangular function  $p(t) = \Pi(t)$ . Let us define the spectrum of  $B_s(t)$  by  $B_s(f) = |B(f)| * |B(f)|$ , since we consider the magnitude of the spectrum, and the symbol  $*$  denotes the convolution product. For a truncated binary sequence of size  $N_T$ , and with  $T_d$  being the symbol duration,  $|B(f)| \approx N_T b_k P(f)$ , where  $P(f) = \text{sinc}(T_d f)$ .

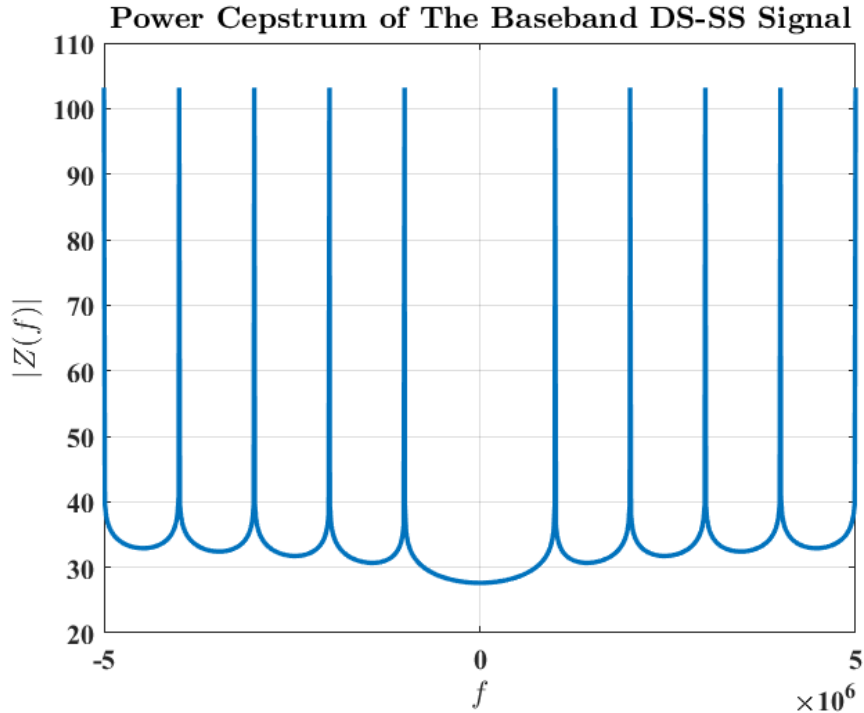


Figure 4.13 – The frequency domain version of the autocepstrum of the baseband DS-SS signal which reveals periodicity at multiples of 1 MHz

We can obtain the required  $B_s(f)$  from the time domain and then evaluating the Fourier transform to get:

$$B_s(f) \approx N_T^2 b_k^2 \text{sinc}^2(T_d f) \quad (4.30)$$

The natural logarithm of  $B_s(f)$  results in a negative periodic function thus, in order to have a reliable detector test statistic, we choose to combine all periodic peaks appeared in  $Z_O(f)$  by defining:

$$\mathcal{T}_s[Z_O] = \frac{1}{L_p} \sum_{i=1}^{L_p} |Z_O(i)| \quad (4.31)$$

where  $L_p$  is the number of peaks presented in the autocepstral signal. To devise a suitable detection threshold, we should find the statistical distribution of  $\mathcal{T}_s$ . If the AWGN  $w(t)$  is distributed as a Circularly Symmetric Complex Gaussian (CSCG) process, the squared-envelope of  $w(t)$  is distributed as a  $\chi_2^2$  process with two degrees of freedom, whose PDF is given by [107]:

$$f_W(w) = \frac{1}{2} \exp\left(-\frac{w}{2}\right), w > 0 \quad (4.32)$$

Thus, the statistical distribution of  $\mathcal{T}$  follows a Modulus Log Chi-Squared (MLCS) (i.e., Modulus-log  $-\chi_{(2)}^2$ ) distribution. By using the PDF approach of the transformation of random variables, the MLCS distribution is given by:

$$f_{\mathcal{T}_s}(t_s) = \frac{1}{2} \exp\left(t_s - \frac{1}{2} \exp(t_s)\right) + \frac{1}{2} \exp\left(-t_s - \frac{1}{2} \exp(-t_s)\right) \quad (4.33)$$

as demonstrated in Appendix C.

In order to get an expression for the detector threshold  $\zeta$ , we follow the same concept indicated in equation (4.18) for a fixed false-alarm probability  $P_{FA}$ . By employing the method of substitution, we obtain:

$$P_{FA} = \exp\left(-\frac{\exp(\zeta)}{2}\right) - \exp\left(-\frac{\exp(-\zeta)}{2}\right) + 1 \quad (4.34)$$

also, we can simplify equation (4.34) by decomposing the exponential terms and substitute for  $\sinh(\zeta) = 0.5[\exp(\zeta) + \exp(-\zeta)]$ , then we obtain:

$$P_{FA} = \exp\left(-\frac{\exp(\zeta)}{2}\right) + 2 \exp\left(-\frac{\exp(-\zeta)}{4}\right) \sinh\left(\frac{\exp(-\zeta)}{4}\right) \quad (4.35)$$

The approximation of the hyperbolic function can be given by Taylor expansion. However, the Taylor series diverges to infinity, so a closed form expression for  $\zeta$  cannot be found analytically, and equation (4.35) can be solved numerically by different methods such as the Newton Raphson Method [138].

## 4.6 Numerical Results and Discussions

In order to validate the efficacy of the proposed wideband spectrum sensing approach, we begin with evaluating the performance of the proposed DLSD technique as opposed to different wavelet-based edge detection techniques. This evaluation includes calculating the average detection error probability  $P_e$  as mentioned in [135], which is given in terms of the probability of misdetecting an actual spectral boundary,  $P_{MD}$ , and the probability of falsely detecting a spurious edge  $P_{FD}$ . Then, we show the applicability of the proposed BB-ACD technique to different digitally modulated signals. We also address the problem of detecting noise-like signals by the PB-ACD

technique under the carrier frequency uncertainty, and we show the advantage of applying the proposed BB-ACD instead.

#### 4.6.1 Performance Evaluation of The Proposed Edge Detection Approach:

The frequency of the wideband spectrum under consideration extends from 30 GHz to 300 GHz. The proposed algorithm is simulated through randomly generated spectrum models for generalization. The average PSD level within each occupied subband is maintained to 6 W/Hz assuming 60% of spectrum occupancy rate. Although the assumed average PSD level is large as opposed to normal radiation levels in practical settings, it is chosen to match the chosen specifications in [132] for the sake of comparison. The characteristics of each spectrum model are generated randomly. They include the number of subchannels within the wideband of interest, the exact spectral boundaries, and the signal power specified in each subband. These subbands are assumed to have different bandwidths to match up with the diversity of the transmission technologies.

Further, depending on the distance between the CR receiver and the transmission station in the occupied subband, as well as the status of the spectrum occupancy, the SNR level is assumed to differ from one subband to another. The performance of the proposed technique is tested by adding white Gaussian noise with the same power to the received RF stimuli corresponding to the whole sensed spectrum while maintaining the same average PSD level in all spectrum models. A summary of the simulation parameters are listed in Table 4.2. For clarification, Table 4.3 shows the detailed information of an example of a randomly generated PSD model shown in Figure 4.14. The Simulations are done with R2018a MATLAB, and the obtained results are based on 1000 Monte Carlo trials.

First, we discuss the effects of applying the DLSD algorithm on spurious edges generated by the noisy spectral variations in  $P_{FD}$ . In Figure 4.15, at considerably low-to-medium noise power (i.e., over the range [10,22] dB), we notice that the proposed DLSD algorithm outperforms the WTMM, the WTMS, or the improved WTMM algorithms. Thanks to the ability of the cepstral analysis approach to reduce the noisy spectral variations. In fact, the white Gaussian noise's cepstrum becomes a Dirac impulse at the zeroth quefrequency value. Clearly, this characterization of the AWGN in the

cepstral domain helps in rejecting potential spurious edges. These results match the concluding insights from Figures 4.5, 4.6, and 4.7. This means that the DLSD algorithm can characterize and reject the false edges.

Table 4.2 – Simulation parameters of the edge-detection phase

Parameter/Tool	Description
Frequency Band	30-300 GHz
Spectral Estimation Method	Periodogram
Sample Size	1024
Number of PSD Models per Simulation	20
Spectrum Occupancy	60%
Average PSD Level in Occupied Channels	6 W/Hz
Noise Power	10 to 30 dB
Number of Monte Carlo Iterations	1000

Table 4.3 – Spectral Specifications of one randomly generated spectral model; the noise variance  $\sigma_w^2 = 20$  dB

Channel (N <15)	Boundaries (GHz)	Bandwidth (GHz)	PSD Level (W/Hz)	Signal Power (dB)	SNR
1	[30,36]	6	0	NA	NA
2	[36,142]	106	14.677	31.919	10.919
3	[142,190]	48	6.099	24.665	4.665
4	[190,224]	34	0	NA	NA
5	[224,240]	16	12.689	23.075	3.075
6	[240,300]	60	2.532	21.816	1.816

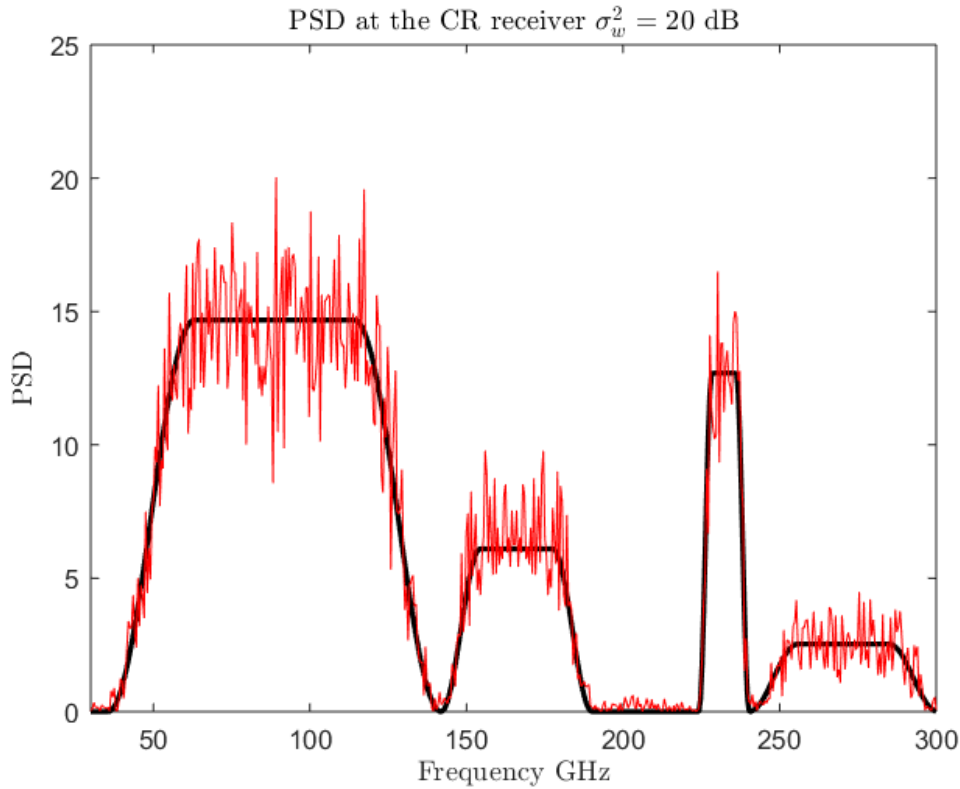


Figure 4.14 – An example of a noisy spectral model

From literature, the major drawback of the WTMM algorithm is the increased number of spurious edges which cannot be eliminated even with a threshold-based detection [11]. The superior performance of the WTMS technique over the WTMM technique is due to the averaging effect of the WTMS algorithm over the noisy spectral edges. However, as shown in Figure 4.7, if the noise power increases (i.e., above 22 dB), the performance of the DLSD algorithm decreases due to the increased number of spurious edges. To improve the DLSD performance, we employed the TVD-MM algorithm in order to reduce the noisy fluctuations before applying the DLSD technique. We employed the TVD-MM algorithm on about 10 iterations with two different regularity parameters:  $\alpha = 0.9$  and 1.2 respectively. As seen in Figures 4.8 and 4.15, the employment of denoising before applying the DLSD algorithm helped in reducing the spurious edges and hence reducing the  $P_{FD}$ .

Precisely, for a noise power value over the range [10,22] dB, the DLSD algorithm with denoising outperforms the four considered algorithm, and performs similar to the improved WTMM algorithm for  $\sigma_w^2 > 22$  dB. Considering the probability of misde-

tecting and actual spectral boundary, the  $P_{MD}$  is plotted for the five considered algorithms in Figure 4.16. We notice that the DLSD algorithm and the WTMS perform similarly over the noise power range [10,18] dB. Since the WTMS algorithm enhances the wavelet modulus maxima that represent the spectral edges, it outperforms the WTMM and the improved WTMM techniques in this performance criterion. As the noise power increases above 18 dB, the DLSD algorithm falls behind the WTMS algorithm due to the lack of edge enhancement.

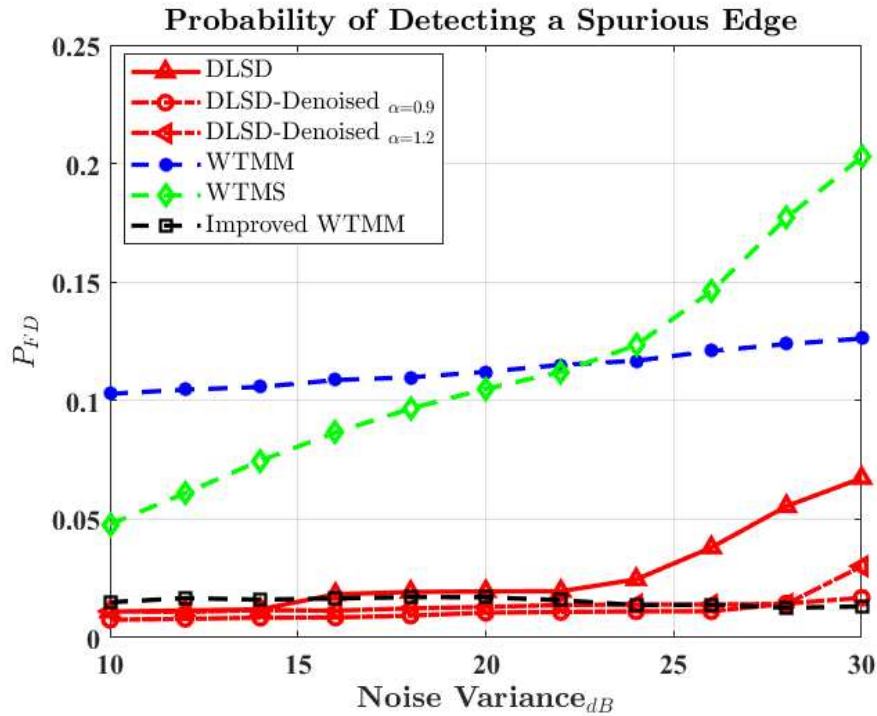


Figure 4.15 – A comparison of the probability of false detection of an original edge by the DLSD technique evaluated as opposed to wavelet-based techniques

While the denoising effect of the DLSD technique reduces the false detection probability, it affects the misdetecting probability as well. In other words, the suppression of noisy spectral fluctuations may result in suppressing a correct spectral boundary. This is due to the fact that the noisy spectral fluctuations tends to deform the actual spectral boundaries, so as the noise power increases, this deformation increases as well which causes the DLSD detector to reject some of the original subbands edges falsely. Remarkably, by using the DLSD algorithm in conjunction with the TVD-MM, the misdetection probability decreases and becomes the lowest among the probabilities of the other four considered algorithms for  $\sigma_w^2$  up to 28 dB.

Above the threshold of 28 dB, the WTMS algorithm has the lowest  $P_{MD}$ . The average detection error probability is plotted for the five considered algorithms in Figure 4.17. The proposed DLSD algorithm has the superior performance over the noise variance range of [10,22] dB. The improved WTMM algorithm has the superior performance over the range [22,28] dB. The proposed DLSD algorithm with denoising gives the best performance over the other considered algorithms when the noise power is above 28 dB. It is worth mentioning that the level of denoising offered by the TVD-MM algorithm is affected by the regularity parameter. Thus, this parameter must be chosen suitably according to the application to provide the required level of denoising and to avoid over smoothing which may diminish the characterization of the spectral boundaries. Table 4.4 provides a comparison between the proposed approach as opposed to the chosen wavelet-based techniques.

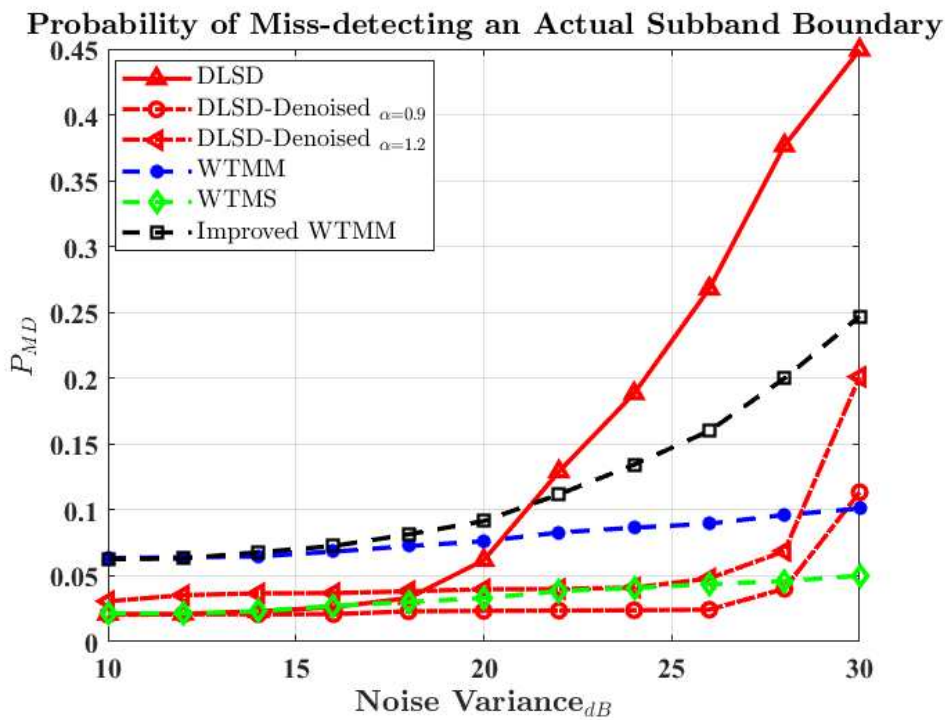


Figure 4.16 – A comparison of the probability of misdetecting an original spectral boundary by the DLSD technique evaluated as opposed to wavelet-based techniques

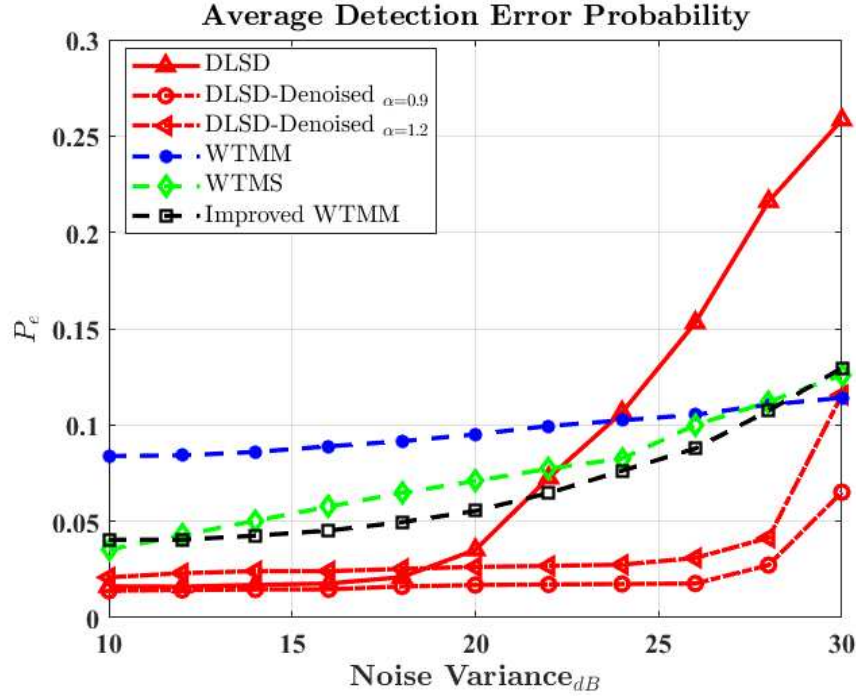


Figure 4.17 – A comparison of the average detection error probability of the DLSD technique evaluated as opposed to wavelet-based techniques

#### 4.6.2 Detection of Noise-Like Signals Under Carrier Frequency Uncertainty By The BB-ACD Technique:

In the single-band signal detection scenario, the operating frequency is usually known to the SU receiver. However, under multiband spectrum sensing scenario, and due to the edge-detection phase, the center frequencies of the subbands are unknown and may be subjected to frequency estimation errors. Thus, the BB-ACD technique is proposed to detect noise-like signals under carrier frequency uncertainty and its performance is compared with that of the PB-ACD technique. The simulations are averaged over 3000 Monte-Carlo realizations with the following parameters: the carrier frequency  $f_c = 5$  GHz, and the employed sampling frequency  $f_s$  is 20 GHz. The performance of the proposed narrowband detector is measured in terms of the detection probability versus the SNR evaluated from -15 to 10 dB. To include the effect of carrier frequency uncertainty, we employed the example illustrated in Figure 3.13 which results in a frequency shift of 0.4 GHz.

The applicability of the proposed BB-ACD technique for detecting different digital

modulation schemes is tested for the case of the BPSK, QPSK, and 16-QAM modulation schemes as well as BPSK/OFDM PU signal as shown in Figure 4.18. Further, we compare the BB-ACD technique with the PB-ACD when the operating carrier frequency is known to the CR receiver in Figure 4.19. When the PB-ACD technique is applied under exact knowledge of the subband center frequency, the achieved detection probability becomes approximately 50% higher than the same technique applied when there are errors in the center frequency values of the subbands of interest at SNR of -15 dB due to the detection dependency on the carrier frequency value. On the other hand, the proposed BB-ACD technique results in 50% detection probability at -15 dB and slowly increases to 100% at SNR of -6 dB. Precisely, the detection test statistic of the BB-ACD technique depends on averaging the periodic peaks that appeared in the power cepstrum of the baseband signal. At low SNR, these peaks have relatively low values as compared to the major peak that characterizes the test statistic of the PB-ACD technique. Thus, as the SNR increases, we notice a gradual increase in the detection performance of the BB-ACD technique.

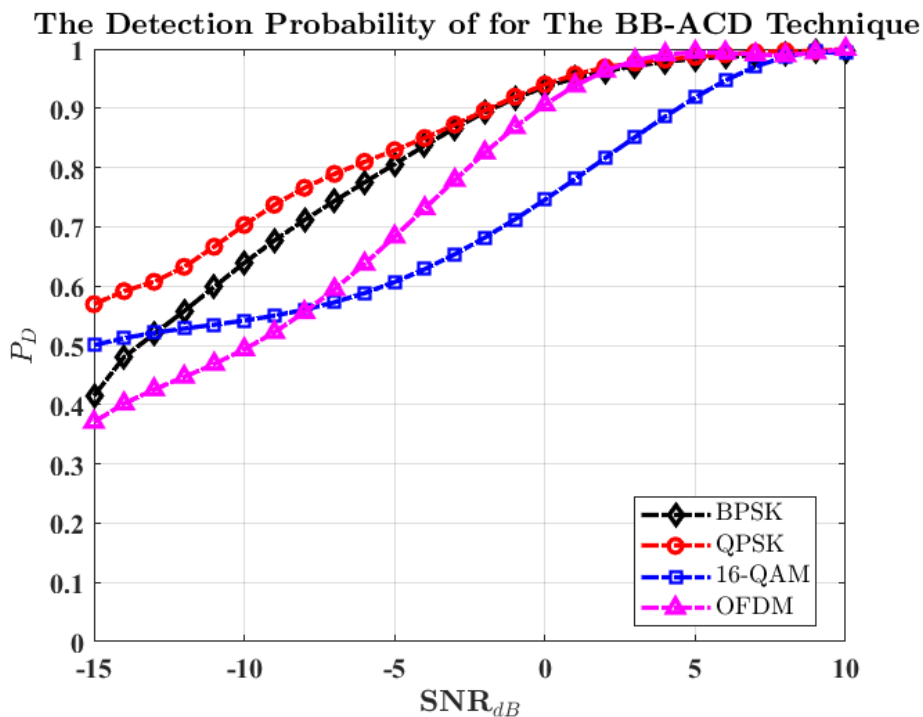


Figure 4.18 – The detection probability of the BB-ACD technique for different modulation schemes

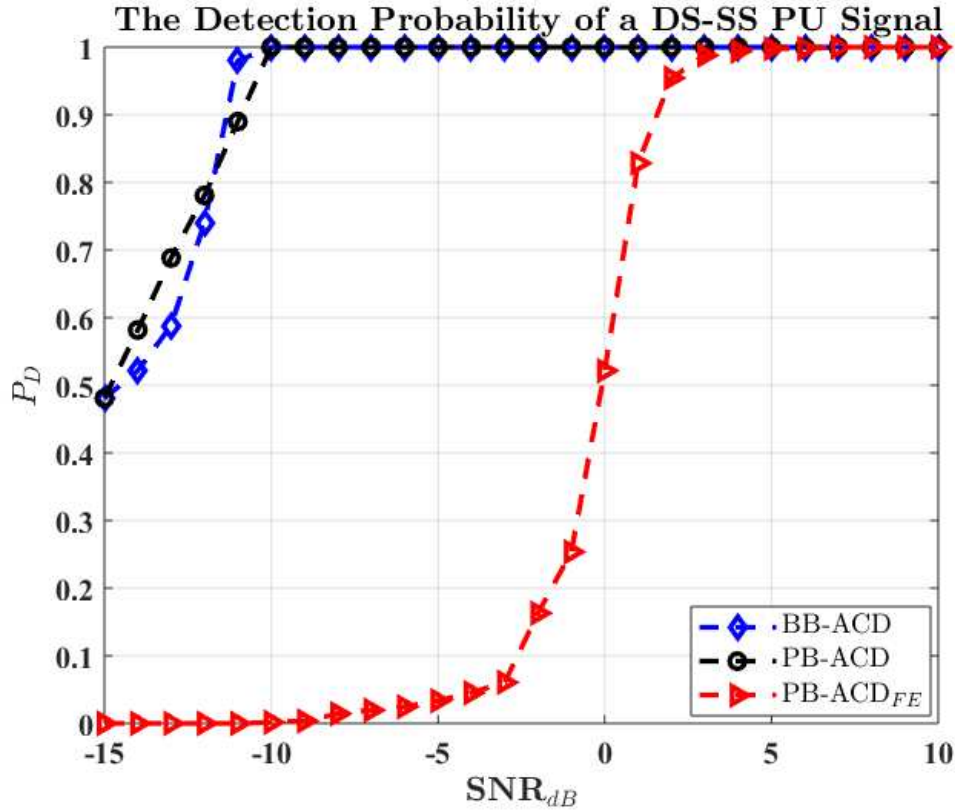


Figure 4.19 – The detection probability of the BB-ACD as compared to the PB-ACD under carrier frequency uncertainty for detecting a DS-SS signal; PB-ACD<sub>FE</sub> refers to the applying the PB-ACD in case of frequency errors

Moreover, to test the robustness of the proposed BB-ACD technique in fading channels, we evaluate its detection performance as compared to the PB-ACD technique for detecting PU signals in a Rayleigh fading channel. Figure 4.20 shows that the detection performance of the BB-ACD technique is superior to the PB-ACD for detecting a BPSK PU signal. Also, we notice a performance deterioration of the PB-ACD technique by around %40 when the PU signal experiences fading such that the detection probability drops to 0 at -15 dB. On the other hand, the detection probability of the BB-ACD technique drops to %20 at -15 dB when Rayleigh fading is encountered. We also tested the performance of the proposed BB-ACD technique to detect an OFDM PU signal in frequency selective channel and compared the obtained results with the PB-ACD technique. The simulation of OFDM signals in AWGN or a frequency selective channel follows the IEEE 802.11 specifications [29]. The frequency selective channel is implemented as a 4-taps Finite Impulse Response (FIR) filter.

Table 4.4 – Comparing wavelet analysis to cepstral analysis for edge detection in wide-band spectrum sensing

Approach	Wavelet Analysis	Cepstral Analysis
<b>Post Processing</b>	Local maxima are found through differentiating the filtered PSD.	Local maxima are found through differentiating the natural logarithm of a signal's PSD.
<b>White Noise Characteristics</b>	<p><b>WTMM:</b> calculates the wavelet modulus maxima in the frequency domain. However, the noise impact affects detection of spectral boundaries.</p> <p><b>Improved WTMM:</b> exploits the singularity characteristics of the wavelet multiscale to identify spurious edges and reject them. Its performance is degraded in low SNR environment.</p> <p><b>WTMP:</b> The product of the first derivative of WT is developed for noise suppression and edge sharpening, but it results in attenuating the edges due to the multiplication operation.</p> <p><b>WTMS:</b> It preserves the edges information and avoids edges attenuation. Increasing the scales leads to a better detection performance but at higher complexity.</p>	<p><b>Cesptrum:</b> AWGN fluctuations are suppressed at all the quefrecencies values except for a major peak at the zero<sup>th</sup> quefrecency.</p> <p><b>DLSD:</b> It reduces the noisy spectral variations.</p>
<b>Application Versatility</b>	The detection performance depends on the analyzed signal and the used mother wavelet function.	The CA approach depends on the type of the cepstral algorithm used that is suitable for the problem under analysis
<b>Implementation Complexity</b>	WT is implemented as a bank of filters. Reducing spurious edges can be accomplished by processing the signal of interest through all scales which substantially increases the computational burden.	Relatively lower than the WBD

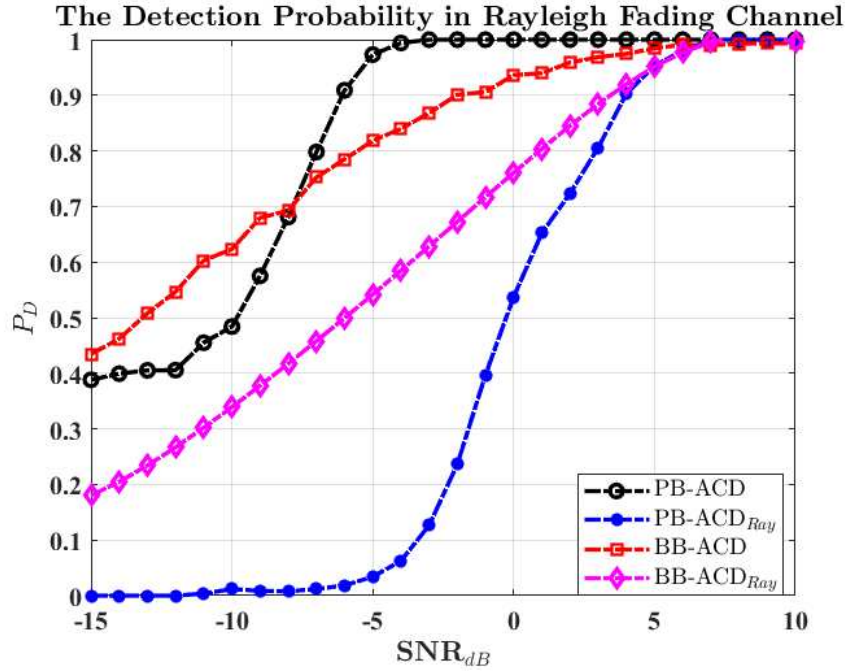


Figure 4.20 – The detection performance of the BB-ACD technique as compared to the PB-ACD technique in Rayleigh fading channel; PB-ACD<sub>Ray</sub> refers to employing the PB-ACD technique in Rayleigh fading channel

The path delays vector is given as  $\tau_p = [0, 100, 35, 120] \mu\text{sec}$ , and the average path gains vector is given by  $P_G = [0, -1, -1, -3] \text{ dB}$ . For a sample period  $T_s = 1 \mu\text{sec}$ , the maximum Doppler frequency equals 100 kHz. The detection performance of the BB-ACD as compared to the PB-ACD under the Doppler frequency shift due to the frequency selective fading channel is shown in Figure 4.21.

According to our simulations, we find that the proposed BB-ACD technique gives better detection results than the PB-ACD technique at -15 dB, whereas the PB-ACD starts to significantly detect the PU presence above -4 dB. This means that the effect of the Doppler frequency shift deteriorates the PB-ACD performance, especially at low SNR values, while the BB-ACD technique can detect the OFDM PU signal successfully.

Another important performance metric to evaluate the efficacy of the proposed techniques is computational complexity. In this regard, we analyze the computational complexity of the DLSD edge detection algorithm followed by the BB-ACD technique and compare it with the WTMP edge detection technique followed by ED. For a 1D signal of size  $N$ , the edge detection algorithm given by the WTMP technique involves evaluating the autocorrelation of the received signal followed by the FFT operation to

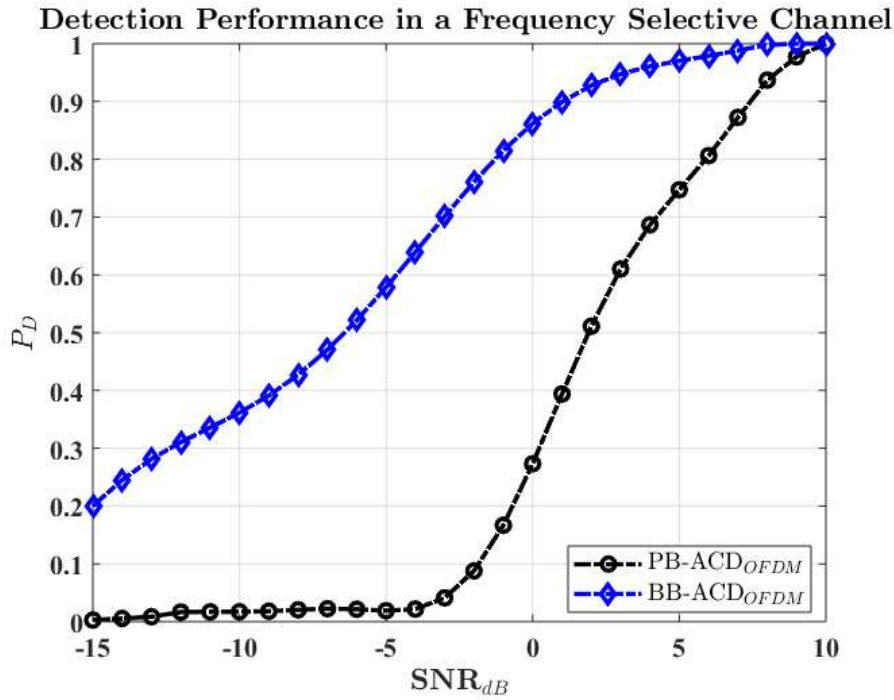


Figure 4.21 – The detection performance of the BB-ACD technique as compared to the PB-ACD technique in a frequency selective fading channel

obtain the PSD. To identify the spectral boundaries, the received signal's PSD is filtered by the Fourier Transform of the smoothing wavelet function through a convolution operation. On the other hand, the proposed DLSD algorithm involves getting the autocorrelation, the PSD of the received signal followed by the gradient of the natural logarithm of the signal's PSD. Table 4.5 summarizes the complexity of the arithmetic operations involved in evaluating both algorithms.

To perform energy detection, the computational complexity requires  $O(N)$  multiplications and  $O(N - 1)$  for the averaging. For the BB-ACD technique, it requires  $O(NK)$  for convolving the received signal with the Hilbert filter of size  $K$ ,  $O(N)$  for the square-law device, and for the power cepstrum the complexity is similar to the DLSD algorithm except for that of the differentiation step. Based on Table 4.5, we find that the complexity of the WTMP is higher than the DLSD algorithm since the complexity of evaluating linear convolution is greater than that of the natural logarithm [139]. However, under the problem of frequency uncertainty, the BB-ACD has a higher complexity than ED or the BED despite its high detection accuracy. A trade-off analysis between the computational complexity and the maximum detection accuracy can be

further investigated to highlight the competence of the proposed approach.

Table 4.5 – Summary of the computational complexity of the DLSD algorithm as compared to the WTMP algorithm

WTMP		DLSD	
Arithmetic Operations	Complexity	Arithmetic Operations	Complexity
Autocorrelation	$O(N^2)$	Autocorrelation	$O(N^2)$
FFT	$O(N \log N)$	FFT	$O(N \log N)$
Linear Convolution by a kernel of size $K$	$O(NK)$	Natural Logarithm using Arithmetic-Geometric Mean	$O(N \log N)$
Product of Modulus Maxima	$O(N)$	Automatic or numerical Differentiation	$O(N)$

## 4.7 Summary

In this chapter, we proposed a wideband spectrum sensing approach based on the cepstral analysis of the received signal. It is shown that the spectral boundaries of the subbands comprising the target wide band can be well identified, in medium-to-high SNR environment, by employing the proposed DLSD algorithm. Although the detection of the spectral edges becomes difficult in low SNR environment, the performance of the proposed DLSD algorithm provides good detection results as compared to different wavelet-based approaches when further denoising is applied. For the PU detection phase, we tackled the problem of detecting noise-like signals in the SBSA and the MBSA scenarios. Further, we addressed the problem of the carrier frequency uncertainty in the MBSA and presented the BB-ACD technique to provide better detection of possible noise-like signals in a low SNR environment. The applicability of the proposed BB-ACD algorithm to different digitally modulated signals is evaluated, and also its reliability is validated as opposed to the PB-ACD technique for detecting PU signals in frequency selective fading channels. The periodicity of the baseband digitally modulated signals that is revealed in the cepstral domain can be effectively utilized for signal detection. Based on this observation, the Cepstral Covariance Detection (CCD) is introduced in chapter 5.

# SPECTRUM SENSING BY CEPSTRAL COVARIANCE DETECTION IN COGNITIVE RADIO

---

## 5.1 Introduction

Hereinafter, we aim to enhance the Power Cepstrum (PC) of digitally modulated signals to formulate a generalized spectrum sensing approach. We propose the Cepstral Covariance Detection (CCD) technique is to exploit the inherited periodicity of the digitally modulated baseband signals that is presented in their Power Cepstrum (PC). In this Chapter, our objective is to utilize the CCD technique to detect the presence of a possible PU signal in the background noise. Despite being simple and reliable in high SNR communication environment, the conventional ED has a poor detection performance when the spectral noisy variations exceed the Power Spectral Density (PSD) level of a PU signal. This is due to the fact that the calculation of the test statistic of the Energy Detection (ED) technique includes the noise effect. So in a low SNR scenario, the detector may give false decision about the PU presence which causes false-alarms. In this case, the CR receiver will initiate the transmission of the SU signal which will cause harmful interference to the PU signals.

In fact, the concept of the pseudo-autocovariance technique was first applied to estimate the time delay between a signal arrival and the arrival of an echo [20]. Precisely, the presence of digitally modulated signals (i.e., phase or amplitude modulation schemes) in noise manifests itself as periodic peaks in the PC. In order to take advantage of this property, we introduce the CCD technique for spectrum sensing in CR systems to improve the process of signal detection in a noisy environment. By correlating the signals' PC to a sinusoidal signal having a fundamental frequency equals to the PC's periodic frequency, the signal component will be enhanced and the detector will

simultaneously reject the noisy spectral variations that lead to possible false-alarms.

The rest of the chapter is organized as follows: section 5.2 describes the proposed system and the signal model. Section 5.3 represents the analytical framework of the proposed detection technique based on NPL. In section 5.4, the expression of the distribution of the detection test statistic under the null hypothesis is derived, and the detection threshold is evaluated. The numerical results are discussed in section 5.5 and the summary is given in section 5.6.

## 5.2 Signal Model and System Description

In the following, we apply the signal model we employed in chapter 2. Recall the formulation of the detection problem, which is given by;

$$y(t) = \begin{cases} w_S(t) & : \text{Under } H_0 \\ s(t) * h_{sens}(t; \tau) + w(t) & : \text{Under } H_1 \end{cases} \quad (5.1)$$

where  $s(t)$  is the transmitted PU signal,  $h_{sens}(t; \tau)$  is the sensing channel which is generally described as a time varying fading channel with delay defined by  $\tau$ , the convolution product is denoted by  $*$ , and  $w(t)$  is the thermal noise presented at the SU receiver which is modeled as an Additive White Gaussian Noise (AWGN). We assume the channel information is provided at the CR system, so that we only focus on the spectrum sensing problem. Accordingly, we consider the sum of faded PU signal  $x_P(t)$ , which is given by:

$$x_P(t) = s(t) * h_{sens}(t; \tau) \quad (5.2)$$

## 5.3 Detection By The Cepstral Covariance Technique

In chapter 3 and chapter 4, we have discussed the employment of the autocepstral technique for detecting noise-like signals. Based on the proposed BaseBand AutoCepstrum Detection (BB-ACD) technique, which is introduced in chapter 4, our aim is to enhance the periodic peaks reflecting the data rate of a given digital signal by employing the CCD technique. For example, in case of medium-to-high SNR, we can easily identify the peaks in the BB-ACD technique of the signal reflecting the repetition of the pseudo random code at the reciprocal of the chip duration  $T_c$  for a Direct Sequence-

Spread Spectrum (DS-SS) PU signal. A functional block diagram of the proposed detector in Figure 5.1.

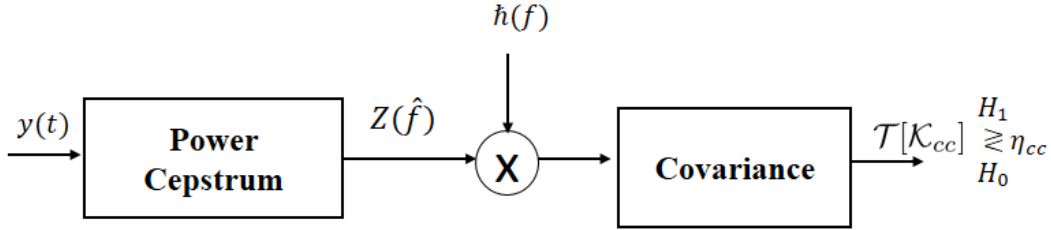


Figure 5.1 – A functional block diagram of the proposed System;  $\mathcal{T}[\mathcal{K}_{cc}]$  denotes the test statistic of the proposed detector

In our proposed detection technique, we utilize the inherited periodicity of typical digitally modulated signals that occur in their PC for spectrum sensing. In particular, we enhance the periodic peaks in the PC by employing a sinusoidal shaping function characterized by a fundamental frequency that is equivalent to the bit rate,  $T_b$ , of the baseband PU signal. For example, the baseband Power Spectral Density (PSD) of a Phase Shift Keying (PSK) signal is given by:

$$S_{sl} = T_b^2 \text{sinc}^2(T_b f) \quad (5.3)$$

The natural logarithm of equation (5.3) is given by:

$$Z_{sl}(\hat{f}) = 2 \log[T_b] + 2 \log[\sin(\pi T_b f)] - 2 \log[\pi T_b f] \quad (5.4)$$

where  $\hat{f}$  denotes the corresponding frequency parameter in the cepstral domain. As analyzed in chapter 3, the signal defined in equation (5.4) experiences a negative periodicity, so by knowing the value of  $T_b$ , this peak values of this periodicity can be captured by a sinusoidal shaping function,  $\hat{h}(f)$ , which is defined by:

$$\hat{h}(f) = \cos(2\pi\tau_e f) \quad (5.5)$$

where  $\tau_e$  denotes the time between two consecutive peaks in the PC and also the reciprocal of the duration  $\tau_e$  represents the fundamental frequency of the shaping function

$\hat{h}(f)$ . Consequently, the cepstral covariance of enhanced PC can be evaluated by:

$$\mathcal{K}_{cc}(\tau_e) = \int_{f_1}^{f_2} Z_{sl}(f) \hat{h}(f) df \quad (5.6)$$

where the frequency range  $f_2 - f_1$  is the bandwidth of the received signal within the observation interval  $T$ . Therefore, we can define the detection test statistic by:

$$\mathcal{T}[\mathcal{K}_{cc}] = |\mathcal{K}_{cc}(\tau_e)| \underset{H_0}{\overset{H_1}{\gtrless}} \eta_{cc} \quad (5.7)$$

where  $\eta_{cc}$  denotes the detection threshold of the proposed detector.

## 5.4 Design Characteristics of The Cepstral Covariance Detector

To evaluate the detection threshold of the proposed detector, we need to find the statistical distribution of the detection test statistic, which is given in equation (5.7). First, we can apply further simplifications to the cepstral covariance function,  $\mathcal{K}_{cc}$ , by representing the integral in equation (5.6) using *Riemann sums* [140]. For example, Let  $\mathbb{F}(x)$  represents a function of which we wish to find a particular definite integral. The *Riemann sums* equivalent to an arbitrary integral can be given by [140]:

$$\int_a^b \mathbb{F}(x) dx = \lim_{N \rightarrow \infty} \sum_{i=1}^N \Delta x \mathbb{F}(x_i) \quad (5.8)$$

where  $a$  and  $b$  are arbitrary constants defining the integral limits, the small segments of the function  $\mathbb{F}(x)$  are denoted by  $\Delta x = \frac{b-a}{N}$ ,  $x_i = a + i \Delta x$ , and  $N$  is the size of the target function. Similarly, if we define:

$$\mathbb{F}(f) = Z(\hat{f}) \hat{h}(f) \quad (5.9)$$

thus, the *Riemann sums* equivalent to the integral, defined in equation (5.6), can be rewritten as:

$$\mathcal{K}_{cc}(\tau_e) = \int_{f_1}^{f_2} \mathbb{F}(f) df = \lim_{N \rightarrow \infty} \sum_{i=1}^N \Delta f \mathbb{F}(f_i) \quad (5.10)$$

where the frequency segments are given by  $\Delta f = \frac{f_2 - f_1}{N}$ , and  $f_i = f_1 + i\Delta f$ .

Assume that the received PSD of the PU signal at the CR receiver is given by:

$$S_y = S_s(f) + S_w(f) \quad (5.11)$$

where  $S_s(f)$  and  $S_w(f)$  denote the PSDs of the PU signal and the background noise, respectively. Therefore, the enhanced PC can be evaluated by:

$$\begin{aligned} \mathbb{F}(f) &= \log[S_s(f) + S_w(f)](\cos(2\pi f\tau_e)) \\ &= \log[S_s(f)](\cos(2\pi f\tau_e)) + \log[1 + \mathcal{L}(f)](\cos(2\pi f\tau_e)) \end{aligned} \quad (5.12)$$

where  $\mathcal{L}(f) = \frac{S_w(f)}{S_s(f)}$ . Clearly, the statistical characterization of the enhanced PC,  $\mathbb{F}(f)$ , depends on the statistical distribution of  $\mathcal{L}(f)$ . If we consider the case of having a good PSD estimate of the transmitted PU signal, such that  $\mathcal{L}(f) \ll 1$ , thus we can approximate  $\log[1 + \mathcal{L}(f)] \approx \mathcal{L}(f)$  [20]. In this case, if  $w(t)$  is a real-valued Gaussian noise, then  $S_w(f)$  follows Chi-squared distribution,  $\chi^2$ . Also, if we only consider a group of peaks,  $N_p$ , among the noisy PC, we can redefine the cepstral covariance by:

$$\mathcal{K}_{avg}(\tau_e) \approx \frac{1}{N_p} \sum_{i=1}^{N_p} |\mathbb{F}(f_i)| \quad (5.13)$$

where  $f_i$  denotes the location of the  $i^{th}$  peak within  $N_p$ . If  $N_p$  is sufficiently large and the enhanced power cepstral peaks are IID, then  $\mathcal{K}_{avg}(\tau_e)$  follows a Gaussian distribution denoted by  $\mathcal{N}(\mu_{\mathbb{F}}, \frac{\sigma_{\mathbb{F}}^2}{N_p})$ , where  $\mu_{\mathbb{F}}$  and  $\sigma_{\mathbb{F}}^2$  are the mean and the variance of the enhanced PC. Consequently, the false-alarm probability can be given by:

$$P_{FA} = Q\left(\frac{\eta_{cc} - \mu_{\mathbb{F}}}{\sqrt{\frac{\sigma_{\mathbb{F}}^2}{N_p}}}\right) \quad (5.14)$$

and the detection threshold of the CCD technique is given by:

$$\eta_{cc} = Q^{-1}(P_{FA}) \frac{\sigma_{\mathbb{F}}}{\sqrt{N_p}} + \mu_{\mathbb{F}} \quad (5.15)$$

Further, if  $\mathcal{L}(f) \gg 1$ , we find that equation (5.12) holds and the statistical distribution

of  $\mathbb{F}(f_i)$  follows  $\log -\chi_v^2$  distribution as demonstrated in equation (3.22) in chapter 3.

## 5.5 Numerical Results and Discussions

### 5.5.1 Detection Performance of The CCD Algorithm

In this section, we show the efficacy of the proposed CCD technique through simulations. We evaluate the detection performance of the proposed detector as compared to the conventional Energy Detection (ED) and EigenValue-based Detection (EVD) techniques. The performance of the proposed CCD technique is measured in terms of the detection probability against the Signal-to-Noise-Ratio (SNR) ranging from -15 dB to 10 dB. The simulations are averaged over 2000 realizations under the CLT assumption. We set the target false-alarm probability,  $P_{FA} = 0.02$  and the sample size equals to 1000 samples. For the EVD technique, we employ the ME Detection proposed in [62].

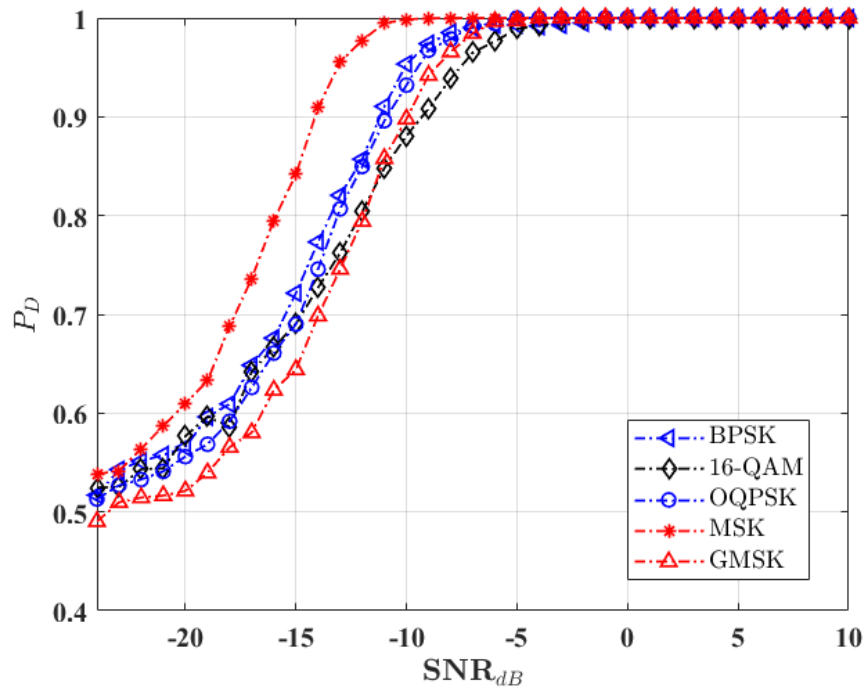


Figure 5.2 – The detection probability of the CCD technique for different modulation schemes

In Figure 5.2 we show the employment of the proposed technique to detect different

digitally modulated signals such as BPSK, OFDM, Minimum Shift Keying (MSK) and QAM signals. The simulation parameters for the OFDM signal follows the IEEE802.11 specifications for a sample period of  $1\mu\text{sec}$ . Due to its simplicity of generation and its typical distribution in the signal space, the detection probability for detecting the BPSK signal is higher than that for the MSK, OFDM, and 16-QAM signals, whereas the 16-QAM signal gives the lowest detection probability.

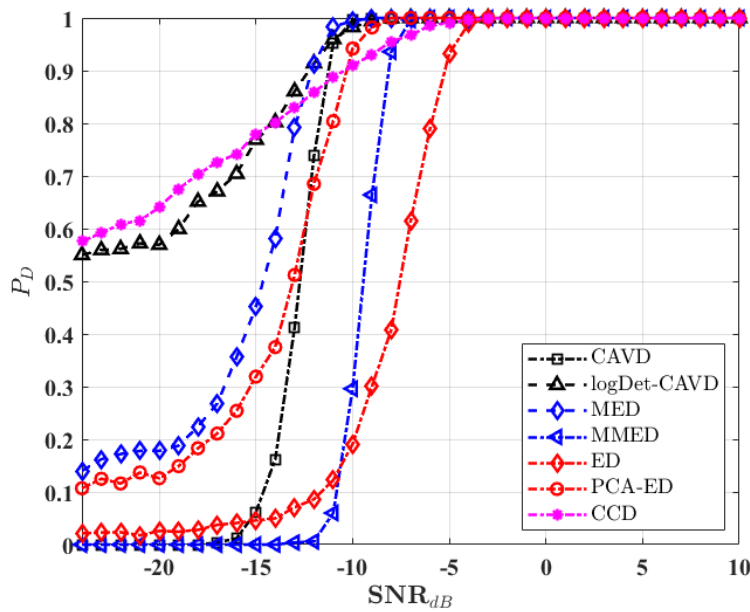


Figure 5.3 – The detection probability of the CCD technique in case of a wireless microphone signal

In the following, we consider two types of signals. First, we consider the case of the wireless microphones operating in TV bands as shown in Figure 5.3. They transmit FM modulated signals with a power of about 50 mW and a bandwidth of 200 kHz. The sampling rate at the receiver is 6 MHz (i.e., the same as the TV bandwidth in USA). If the Secondary Users (SU) are several hundred meters away from the microphone devices, the received SNR may be below -20 dB which causes miss-detection of the PU signal.

From the literature, Covariance Absolute Value Detection (CAVD), logDet-CAVD and EVD techniques are considered as statistical covariance based detection techniques [62]. The CAVD technique evaluates the absolute value of the statistical covariance of the received signal where the computation burden is affected by the smoothing factor

when calculating the sample covariance matrix. Particularly, it evaluates the ratio between the off-diagonal to the diagonal elements of the sample covariance matrix and compare it to a detection threshold. A major limitation of the CAVD algorithm is that its performance is highly affected by the correlation of the received signals. Therefore, its performance deteriorates for detecting uncorrelated signals. To test the detectability of the proposed CCD algorithm to FM-WM signals, we consider a soft peaker audio signal operating in an indoor environment for a frequency deviation of 32.6 kHz and a carrier frequency of 3.26 MHz, which is chosen from a 6 MHz band from 2.38 MHz to 8.38 MHz. In Figure 5.3, the CCD algorithm achieves high detection probability, thanks to strength of the cepstral covariance that reflects the presence of the power cepstral peaks of the FM-WM signal with respect to the power cepstrum of the background noise. The logDet-CAVD technique shows a similar behavior but on the expenses of increased complexity which will be discussed next. Also, the EVD-based techniques shows a superior performance to the ED techniques due to their ability to utilize the correlation of the WM signal.

However, we notice in Figure 5.3 the slow increase of the detection probability of the CCD technique as compared to the ED and the EVD techniques as the SNR increases gradually. This is because the average of the cepstral peaks may include some spurious peaks occur at the fundamental frequency of the sinusoidal shaping function. The next type of signals to consider for detection is the IID signals. These types of signals model a sum of received signals from different antennas. From the literature, it is well-known that energy detection is optimal for detecting white IID noise. Based on NPL, the likelihood ratio test is maximized for IID received PU signals under  $H_1$  [13].

In Figure 5.4, the detection probability is evaluated for the proposed CCD algorithm as opposed to different state-of-the-art techniques. We find that the detection performance of the CCD algorithm is superior to ED, PCA-based ED, EVD and CAVD techniques. Precisely, based on the calculations of the PC of the received PU signal under  $H_1$ , provided that the PU signal and the background noise are uncorrelated, we obtain:

$$\begin{aligned} Z(f) &= \log[S_s(f) + S_w(f)] \\ &= \log\left[\frac{S_s(f)}{S_w(f)} + 1\right] + \log[S_w(f)] \end{aligned} \quad (5.16)$$

If the average signal's PSD is higher than the average noise PSD, the power cepstrum of

the IID signal dominates over the power cepstrum of the noise, so that the evaluated cepstral covariance represents the signal presence over the noise. Nevertheless, the CAVD technique fails to detect the presence of the IID PU signal since it requires the existence of correlated samples of the received PU signal to be able to differentiate between a PU signal and the noise. Although the detection probability of the logDet-CAVD technique is higher than the proposed CCD technique by about 10% at -24 dB, its high computation complexity makes its implementation difficult.

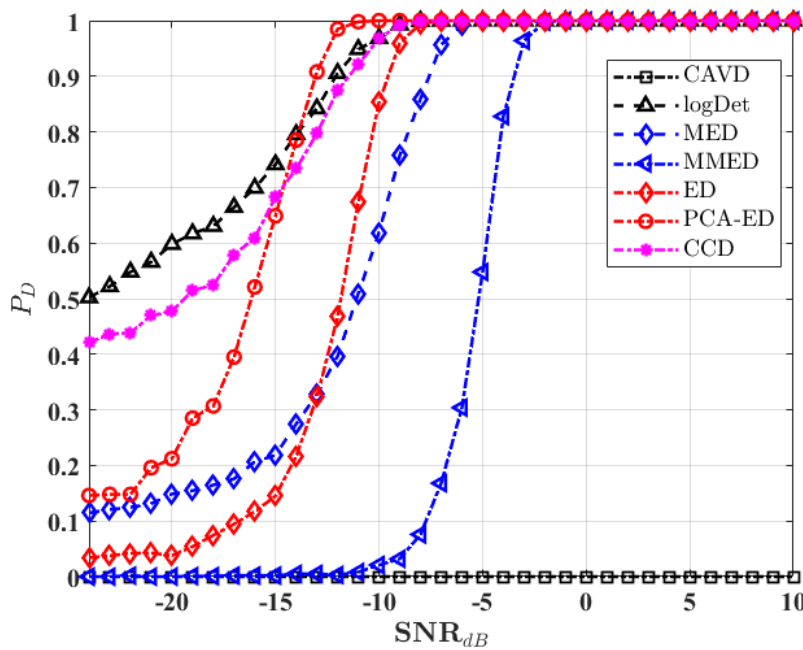


Figure 5.4 – The detection probability of the CCD technique for detecting IID Gaussian signals

## 5.5.2 Complexity Analysis

The computation complexity of an algorithm is related to the number of arithmetic operations that are needed to execute it. For example, the energy detection technique needs about  $N$  multiplications and additions. For the CAVD algorithm, the computation of the autocorrelation of the received signal requires about  $L_s N$  multiplications and additions, where  $L_s$  denotes the size of the sample covariance matrix and  $N$  is the number of samples in the received signal. Also, the ratio of the average of the off-

diagonal elements to the diagonal elements of the sample covariance matrix requires  $L_s^2$  additions. Thus, the total number of multiplications and additions is about  $L_s N + L_s^2$ .

For the EVD techniques, the computation of the sample autocorrelation requires  $L_s N$  multiplications and additions, whereas the computation of the extreme eigenvalues needs about  $O(L_s^3)$  operations. Therefore, the overall computation complexity is about  $L_s N + O(L_s^3)$ . Since the  $N > L_s$ , hence the first term in the computation complexity is dominant.

The complexity of the proposed CCD algorithm includes the evaluation of the autocorrelation of the received signal, the calculation of the FFT to get the PSD, obtaining the natural logarithm of the PSD to get the power cepstrum, and finally getting the cepstral covariance. Thus, the total computation complexity of the CCD algorithm is about  $L_s N + N \log N$ .

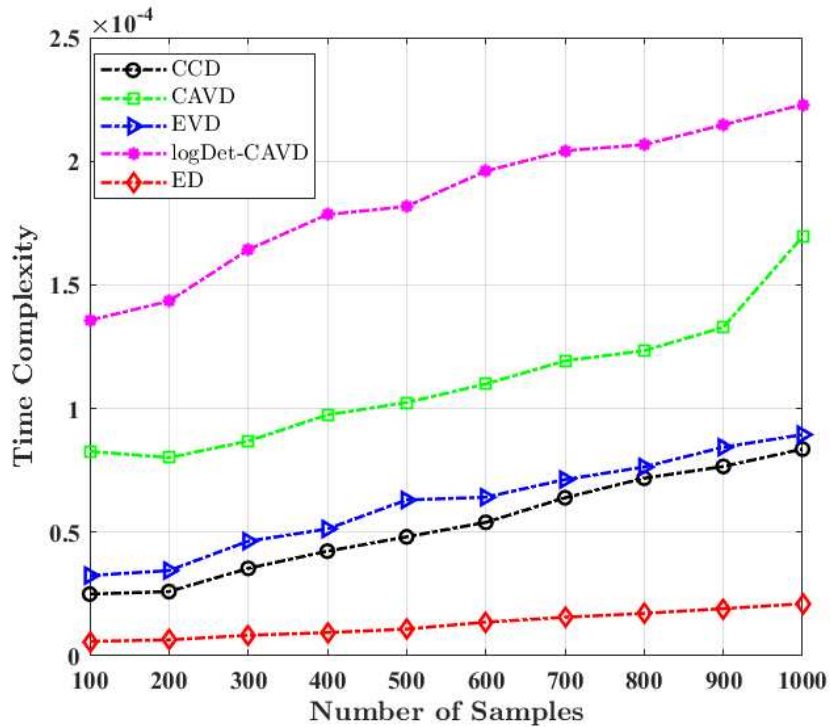


Figure 5.5 – The time complexity analysis of the proposed CCD algorithm as compared to ED, EVD, CAVD, and logDet-CAVD algorithms

To show the time complexity for executing the aforementioned algorithms, we measure the time complexity of each algorithm as compared to the number of samples of the received signal. In Figure 5.5, the ED algorithm has the fastest convergence time

due to its low computation complexity. Following the ED algorithm, the CCD technique and the EVD based techniques have similar behavior as the number of samples increases. Despite the reliable detection performance of the logDet-CAVD algorithm, it has the longest convergence time amongst the considered algorithms.

## 5.6 Summary

In this chapter, the CCD algorithm is proposed for spectrum sensing in CR systems. The purpose of the proposed technique is to formulate a versatile approach that is able to sense the activity of digitally modulated PU signals at low SNR levels. The CCD algorithm is based on exploiting the inherited periodicity in the power cepstrum of digitally modulated signals for the spectrum sensing and it aims to mitigate the false-alarm problem that may be caused by the spectral fluctuation of the background noise. To reduce the false-alarms, the power cepstrum of the PU signal is enhanced through evaluating the cepstral covariance of its power cepstrum with a sinusoidal shaping function. By knowing the data rate of the PU signal, the shaping function is able to capture the cepstral peaks and reject the spurious peaks caused by the background noise. The CCD technique is tested with different digital modulation schemes and it has shown its applicability and reliability at low SNR values over EVD, ED, PCA-based ED, and CAVD techniques. Although the logDet-CAVD technique is slightly superior to the CCD technique, its computation complexity limits its application. For future perspectives, further analysis of the CCD algorithm can be studied with the involvement of multipath fading communication channels.

# CONCLUSION AND FUTURE WORK

---

## 6.1 Conclusions

Over the last several years, the data transmission of wireless technologies has tremendously grown [141]. This growth is driven largely by people employing different applications such as video streaming and scrolling through social media. To meet this demand, an efficient spectrum allocation must be managed, such that different wireless technologies cannot have exclusive frequencies, but must share their available spectral resources. The concept of Cognitive Radio (CR) has provided conceptual possibilities for improving the utilization of the heavily congested radio spectrum.

As the name implies, a CR system is a communication system that is aware of its surrounding and it is able to adapt its parameter according to the collected information. Monitoring the spectrum resource is referred to as spectrum sensing. The obtained sensing results are used to optimize spectrum sharing amongst different networks, thus integrating the CR concept with wireless communication systems adds cognitive intelligence. This motivates the importance of providing reliable spectrum sensing techniques.

In the literature, there are different spectrum sensing techniques to allow for a secondary user (SU), which is a lower-priority user than a primary user (PU), to occupy a licensed frequency band. These techniques are classified into non-cooperative and cooperative methods. The non-cooperative methods include semi-blind techniques which imply no prior information about PU signal is provided at the SU receiver. These approaches encompass energy detection (ED), and the Eigenvalue-based Detection (EVD). In the cooperative techniques, some information about PU must be provided for detection. These techniques include waveform based detection (WBD), and matched filter detection (MFD). The ED technique is very simple to apply and implement but it is sensitive to noise. Although the EVD does not require prior information about the noise power, the increased processing burden is a drawback. Moreover, the MFD

---

requires knowledge of the pulse shape of the transmitted signal which impractical to provide.

The spectrum sensing process in a CR system confronts many challenges that affect its performance. Some of these challenges include hardware complexity, the hidden PU problem, achieving the optimum sensing duration, and signal detection in a low SNR communication environment. Beside these challenges, there two factors mainly affect the detection performance of a spectrum sensing technique, namely: false-alarm and misdetection. The former occurs due to noise uncertainty presents at CR receiver which may lead to false detection of a spectral occupancy and this lost spectral opportunity affects SU transmission. On the other hand, the misdetection problem occurs when a weak signal occupies a desired frequency band but it is undetectable by the CR receiver. This problem is either due to the transmission channel effects, such as multipath fading, or the nature of the signal itself.

Although the field of Cepstral Analysis (CA) is not novel, it has proven its efficacy in the field of signal detection and classification. The advantage of the CA-based techniques lies in their ability to reveal some features characterizing the signal of interest. In our thesis, we formulated different spectrum sensing techniques by taking advantage of the strength of the Cepstral Analysis approaches. We introduced reliable cepstrum-based detectors that are suitable for narrowband and wideband spectrum sensing processes in Cognitive Radio (CR) systems. We aimed to combat the misdetection problem of detecting possible Spread Spectrum (SS) Primary Users (PUs) without knowledge of the spreading pseudo random code. A non-cooperative detection process is considered a challenge for detecting SS signals. For this reason, we presented the PassBand AutoCepstrum Detection (PB-ACD) technique that employs an autocepstral peak detector for spectrum sensing. The proposed detectors was sufficiently able to distinguish between noise and noise-like signals, such as SS and Ultra-WideBand (UWB) signals.

To improve the performance of the PB-ACD technique, we employed a smoothing process as a preceding stage before the PB-ACD process. The role of the improved PB-ACD technique is to smooth out the fluctuations of the autocorrelation estimators. The proposed smoothing process is performed by using the Total Variation Denoising (TVD) algorithm to improve the detection of a potential PU signal by the PB-ACD technique when the transmission medium experiences high noisy spectral fluctuations. Also, we analyzed the autocepstral behavior of the Frequency Hopping-Spread Spec-

---

trum (SS) and Chirp-Spread Spectrum (C-SS) schemes and we utilized the periodic autocepstral peaks to formulate the Averaged PassBand-AutoCepstral Detection (APB-ACD) technique.

Moreover, we broadened our study to wideband spectrum sensing. We developed a cepstrum-based WideBand Spectrum Sensing (WBSS) approach that includes two processes: edge detection and PU signal detection. At the best of our knowledge, our proposed WBSS approach is the first to formulate the Differential Log Spectral Density (DLSD) algorithm to identify the spectral boundaries of the target wideband spectrum. The proposed DLSD technique showed a high detection accuracy and a low processing time required to identify the wideband spectral edges as compared to different wavelet-based edge detection techniques.

Furthermore, we addressed the problem of erroneous spectral boundaries that may be encountered in WBSS. For this purpose, introduced the BaseBand AutoCepstrum Detection (BB-ACD) technique to process the received signal in its baseband version, to reduce the dependency factor of the PU detection process on the carrier frequency value. The proposed technique showed high detection efficacy in detecting PU signals in frequency fading channels that experiences Doppler frequency shifts. Based on our investigations of the periodicity of the power cepstrum, inherited in basic digitally modulated signals, we introduced the Cepstral Covariance Detection (CCD) technique. The job of the CCD technique is to capture the periodic peaks of the digital signals and evaluate the cepstral covariance of its enhanced power cepstrum. Through simulations, the presented detector showed a high detection accuracy for different digital modulation schemes.

## 6.2 Recommendations for Future Work

The results of this dissertation point to several intriguing paths, which can be pursued in future work. For example:

- A tradeoff study between the complexity and detection accuracy of the proposed techniques with that of the wideband sensing technique of similar kind can be considered to provide a broader competence view.
- The involvement of a reliable channel estimation process is essential to include its effect on the spectrum sensing results. In this regards, A dual spectrum sens-

---

ing and channel estimation by the autocepstrum approach can be investigated. Originally, the purpose of the Power Cepstrum (PC) was to determine the echo arrival times in a composite signal as discussed in [18], since delayed echoes appear as ripples in the logarithmic spectrum of the input data sequence  $x(n)$  [100]. Conventionally, the PC of a signal can be defined as the sequence of the inverse  $\mathcal{Z}$ -transform of the logarithm of the magnitude squared of the  $\mathcal{Z}$ -transform of the data sequence. This is can be written by:

$$x_{PC}(n) = \mathcal{Z}^{-1}\{\log |X(\mathcal{Z})|^2\}^2 \quad (6.1)$$

where  $X(z)$  represents the  $\mathcal{Z}$  transform of the data sequence  $x(n)$ . If the data sequence consists of two convolved sequences, such as a modulated signal  $y(n)$  and the impulse response of the communication channel  $h(n)$ , we obtain:

$$x(n) = y(n) * h(n) \quad (6.2)$$

this equation can be rewritten as the multiplication of the Fourier transform of the two sequences:

$$|X(z)|^2 = |Y(z)|^2 \cdot |V(z)|^2 \quad (6.3)$$

by taking the logarithm of both sides of the equation (6.3), we obtain:

$$\log |X(z)|^2 = \log |Y(z)| + \log |V(z)|^2 \quad (6.4)$$

To further elaborate on the power spectrum analysis, let us assume that the time-invariant multipath channel impulse response is given as:

$$h(n) = \delta(n) + \gamma_f \delta(n - n_o) \quad (6.5)$$

where  $\delta(n)$  denotes the unit impulse response function and  $\gamma_f$  denotes the fading coefficient. On the basis of this equation, we can further write:

$$|X(z)|^2 = |Y(z)|^2 |1 + \gamma_f Z^{-n_o}|^2 \quad (6.6)$$

by taking the logarithm of both sides and substituting by  $Z = \exp(j\omega)$ , we ex-

---

pand equation (6.6) as:

$$\begin{aligned} \log |X(\exp(j\omega))|^2 &= \log |Y(\exp(j\omega))| + \log (1 + \gamma_f^2) \\ &+ \log \left( 1 + \frac{2\gamma_f}{1 + \gamma_f^2} \cos(\omega n_o) \right) \end{aligned} \quad (6.7)$$

In equation (6.7), we can observe that the PC of the data sequence contains sinusoidal components (ripples). The amplitude and frequencies of these ripples correspond to the amplitude of every impulsive component and the time delay corresponds to the delayed multipath component. By taking the inverse  $\mathcal{Z}$ -transform of (6.7), we obtain:

$$x_{PC}(n) = y_{PC}(n) + h_{PC}(n) \quad (6.8)$$

In the literature, the CA of a multipath signal is carried out for the purpose of estimating the communication channel coefficients provided that prior information about the transmitted signal are available at the receiver. However, in a non-cooperative transmission reception scenario, such as in CR system, knowledge of the PU signal characteristics is not provided. This makes a dual channel estimation and spectrum sensing an important argument to be addressed in further studies.

- Cooperative sensing could be the target of our next area of research for the performance enhancement of CR systems when combined with artificial intelligence. In this regard, the employment of artificial intelligence algorithms can be considered to dynamically sense the target spectrum and consequently make a decision to share the spectrum based on reasoning [141]. In particular, some research advances in artificial intelligence-based 5G studies discussed the application of artificial intelligence algorithms in the radio networks [142]. These networks would be permitted to utilize a specific frequency band after an optimized decision of an artificial intelligence algorithm.

# APPENDIX A

---

## A.1 Derivation of The Generalized Expression of The $\log - \chi^2_\nu$ for $\nu$ Degrees of Freedom

Recall the computation of the autocepstrum of an underlying signal  $X(n)$ , which is given by:

$$c_a(\hat{n}) = \frac{1}{\sqrt{N_r}} \sum_{\hat{k}=0}^{N_r-1} Z(\hat{k}) \exp\left(\frac{j2\pi\hat{k}\hat{n}}{N_r}\right) \quad (\text{A.1})$$

where  $Z(\hat{k})$  is the natural logarithm of the signal's PSD which can be given by:

$$Z(\hat{k}) = \begin{cases} \log[\sigma_w^2 S_w(\hat{k})] & : H_0 \\ \log[\sigma_s^2 S_s(\hat{k}) + \sigma_w^2 S_w(\hat{k})] & : H_1 \end{cases} \quad (\text{A.2})$$

where the variances,  $\sigma_w^2$  and  $\sigma_s^2$ , represents also the PSD levels of the spectra of the noise and the PU signal. Precisely, we can re-define equation (A.1) under  $H_0$  by:

$$\begin{aligned} \sqrt{N_r} c_a(\hat{n}) &= \sum_{\hat{k}=0}^{N_r-1} \left( \log[\sigma_w^2] + \log[S_w(\hat{k})] \right) \exp\left(\frac{j2\pi\hat{k}\hat{n}}{N_r}\right) \\ &= (\log[\sigma_w^2]) \delta(\hat{n}) + c_{a_w}(\hat{n}) \end{aligned} \quad (\text{A.3})$$

where  $\delta(\hat{n})$  denote the delta Dirac function and  $c_{a_w}(\hat{n})$  represents the autocepstrum of the noise signal. By dividing both sides of equation (A.3) by  $\sigma_{w_{\log}}^2 = \log[\sigma_w^2]$ , we obtain:

$$\frac{\sqrt{N_r} c_a(\hat{n})}{\sigma_{w_{\log}}^2} = \delta(\hat{n}) + \hat{c}_{a_w}(\hat{n}) \quad (\text{A.4})$$

where  $\hat{c}_{a_w}(\hat{n})$  denotes the normalized noise autocepstrum. Likewise, the autocepstrum of the received signal under  $H_1$  is given by:

$$\sqrt{N_r}c_a(\hat{n}) = \sum_{\hat{k}=0}^{N_r-1} \left[ \log[\sigma_w^2 S_w(\hat{k})] [\gamma \gamma_0(\hat{k}) + 1] \right] \exp\left(\frac{j2\pi\hat{k}\hat{n}}{N_r}\right) \quad (\text{A.5})$$

where  $\gamma$  denotes the SNR level and  $\gamma_0(\hat{k}) = \frac{S_s(\hat{k})}{S_w(\hat{k})}$  denotes the spectral variation between the signal and the noise. To simplify equation (A.5), we approximate the term  $\log[\gamma \gamma_0(\hat{k}) + 1] \approx \log[\gamma \gamma_0(\hat{k})]$  for  $\gamma \gamma_0(\hat{k}) \gg 1$ , thus we obtain:

$$\sqrt{N_r}c_a(\hat{n}) = (\log[\sigma_w^2])\delta(\hat{n}) + c_{a_w}(\hat{n}) + \log[\gamma]\delta(\hat{n}) + \sum_{\hat{k}=0}^{N_r-1} \log\left[\gamma_0(\hat{k}) \exp\left(\frac{j2\pi\hat{k}\hat{n}}{N_r}\right)\right] \quad (\text{A.6})$$

thus, equation (A.6) can be reduced to:

$$\sqrt{N_r}c_a(\hat{n}) = \log[\sigma_s^2]\delta(\hat{n}) + \sum_{\hat{k}=0}^{N_r-1} \log[S_s(\hat{k})] \exp\left(\frac{j2\pi\hat{k}\hat{n}}{N_r}\right) \quad (\text{A.7})$$

equivalently, it can be expressed by:

$$\frac{\sqrt{N_r}c_a(\hat{n})}{\sigma_{s_{\log}}^2} = \delta(\hat{n}) + \hat{c}_{a_s}(\hat{n}) \quad (\text{A.8})$$

where  $\sigma_{s_{\log}}^2 = \log[\sigma_s^2]$  and  $\hat{c}_{a_s}(\hat{n}) = \frac{c_{a_s}(\hat{n})}{\sigma_{s_{\log}}^2}$  denotes the normalized cepstrum of the target signal. Thus, we can describe the statistical distribution of  $c_a(\hat{n})$  under the null and the alternative hypotheses by:

$$f_{C_a}(c_a) = \begin{cases} \frac{\sigma_{w_{\log}}^2}{\sqrt{N_r}} f_{\log-\chi^2}\left(\frac{\sigma_{w_{\log}}^2}{\nu} c_a, \nu\right) & : H_0 \\ \frac{\sigma_{s_{\log}}^2}{\sqrt{N_r}} f_{\log-\chi^2}\left(\frac{\sigma_{s_{\log}}^2}{\nu} c_a, \nu\right) & : H_1 \end{cases} \quad (\text{A.9})$$

where  $f_{\log-\chi^2}$  denotes the probability density function of the  $\log-\chi^2$  with  $\nu$  degrees of freedom. By using the method of transformation of random variables,  $f_{\log-\chi^2}$  under

---

$H_0$  is given by:

$$f_{C_a}(c_a; H_0) = \frac{\sigma_{w_{\log}}^2 \exp(c_a)}{\nu \Gamma(\frac{\nu}{2}) 2^{\frac{M}{2}}} \left( \frac{\exp(c_a) \sigma_{w_{\log}}^2}{\nu} \right)^{\frac{\nu}{2}-1} \exp\left(-\frac{\exp(c_a) \sigma_{w_{\log}}^2}{\nu}\right) \quad (\text{A.10})$$

## A.2 Expression for The False-alarm Probability

To find expression for the false-alarm probability, we evaluate the following integral:

$$\begin{aligned} P_{FA} &= \int_{\eta_1}^{\infty} f_{C_a}(c_a; H_0) dc_a \\ &= \left( \frac{\sigma_{w_{\log}}^2}{\nu} \right)^{\frac{\nu}{2}} \frac{1}{\Gamma(\frac{\nu}{2}) 2^{\frac{\nu}{2}}} \int_{\eta_1}^{\infty} \exp(c_a)^{\frac{\nu}{2}} \exp\left(-\frac{\exp(c_a) \sigma_{w_{\log}}^2}{\nu}\right) \end{aligned} \quad (\text{A.11})$$

where  $\eta_1$  denotes the detection threshold of an autocepstrum detector. Using the methods of substitution by assuming  $x_0 = \exp(c_a)$ , we obtain:

$$P_{FA} = \mathbb{A} \int_{\exp(\eta)}^{\infty} (x_0)^{\frac{\nu}{2}} \exp\left(-\frac{x_0 \sigma_{w_{\log}}^2}{\nu}\right) dx_0 \quad (\text{A.12})$$

where  $\mathbb{A} = \left( \frac{\sigma_{w_{\log}}^2}{\nu} \right)^{\frac{\nu}{2}} \frac{1}{\Gamma(\frac{\nu}{2}) 2^{\frac{\nu}{2}}}$ . If we assume that  $s = \frac{\nu}{2}$  and  $t = \frac{x_0 \sigma_{w_{\log}}^2}{\nu}$ , then we can rewrite equation (A.12) as:

$$P_{FA} = \left[ \frac{\nu}{\sigma_{w_{\log}}^2} \right]^2 \mathbb{A} \int_{\frac{\sigma_{w_{\log}}^2}{\nu} \exp(\eta_1)}^{\infty} t^{s-1} \exp(-t) dt \quad (\text{A.13})$$

where the integral resembles that defined by the *upper incomplete gamma* function, which is given by:

$$\Gamma(s, x) = \int_x^{\infty} t^{s-1} \exp(-t) dt \quad (\text{A.14})$$

By applying equation (A.14), the false-alarm probability becomes:

$$P_{FA} = \left( \frac{\sigma_{w_{\log}}^2}{\nu} \right)^{\frac{\nu}{2}-2} \mathbb{Q}(s, x) \quad (\text{A.15})$$

---

where  $Q(s, x)$  represents the *regularized gamma* function, which is expressed by:

$$Q(s, x) = \frac{\Gamma\left(\frac{\nu}{2}, \frac{\sigma_w^2 \log x}{\nu} \exp(\eta_1)\right)}{\Gamma\left(\frac{\nu}{2}\right) 2^{\frac{\nu}{2}}} \quad (\text{A.16})$$

# APPENDIX B

---

## B.1 Maximum-to-Minimum Eigenvalue Detection Algorithm

1. Compute the sample covariance matrix of the received signal of size  $N$ .
2. Obtain the maximum and the minimum eigenvalues of the covariance matrix for a smoothing factor of size  $L_s$ .
3. The detection decision is obtained by comparing the ratio of the maximum-to-minimum eigenvalues to the detection threshold, which is given by [62]:

$$\eta_{MME} = \frac{(\sqrt{N} + \sqrt{L_s})^2}{(\sqrt{N} - \sqrt{L_s})^2} \left( 1 + \frac{(\sqrt{N} + \sqrt{L_s})^{-2/3}}{(NL_s)^{1/6}} F_1^{-1}(1 - P_{FA}) \right) \quad (\text{B.1})$$

where  $F_1$  denotes the cumulative distribution function of the Tracy-Widom distribution of order 1 [62].

## B.2 Energy with Minimum Eigenvalue Detection Algorithm

1. Compute the sample covariance matrix of the received signal.
2. Compute the average power of the received signal and obtain the minimum eigenvalue of the covariance matrix.
3. The detection decision is obtained by comparing the ratio of the average power of the received signal-to-minimum eigenvalue to the detection threshold, which is given by [62]:

$$\eta_{EME} = \left( \sqrt{\frac{2}{N}} Q^{-1}(P_{FA} + 1) \right) \frac{N}{(\sqrt{N} - \sqrt{L_s})^2} \quad (\text{B.2})$$

# APPENDIX C

---

## C.1 Validation of a Chosen Majorizer Equation

We need to get the constants  $c_{MM}$  and  $b_{MM}$  in order to verify that the chosen function  $g_{MM}(t)$  is a valid majorizer for  $f_{MM}(t)$ , so based on the second condition of MM algorithm, we have:

$$g_{MM}(t = t_k) = f_{MM}(t = t_k) \quad (\text{C.1})$$

accordingly, we get:

$$c_{MM} = \frac{1}{T_c} - t_k \left( \frac{1}{T_c} - b_{MM} t_k \right) \quad (\text{C.2})$$

referring to the inequality in equation (3.153), we have:

$$b_{MM} t^2 - \frac{t}{T_c} + \left( \frac{1}{T_c} - c_{MM} \right) < 0 \quad (\text{C.3})$$

then for  $b_{MM} > 0$ :

$$4b \left( \frac{1}{T_c} - c_{MM} \right) = \frac{1}{T_c^2} \quad (\text{C.4})$$

substitute equation (C.2) in equation (C.4), for  $u_{MM} = b_{MM} T_c t_k$  we have:

$$u_{MM}^2 - u_{MM} + \frac{1}{4} \geq 0 \quad (\text{C.5})$$

thus, for a general expression:

$$b_{MM} = \frac{1}{2T_c |t_k|}, \quad c_{MM} = \frac{1 - 2|t_k|}{2T_c} \quad (\text{C.6})$$

# APPENDIX D

---

## D.1 The Statistical Distribution of A Random Variable follows Modulus Log Chi-Squared Distribution

Consider a random process  $J = |\log[V]|$ , and we seek the distribution of  $J$  if  $V$  follows  $\chi_{(2)}^2$ . Thus,  $J$  follows MLCS distribution. Based on the probability density function approach, we find the required distribution by:

$$f_J(j) = \frac{f_V(v)}{|dJ/dV|} \Big|_{V=\pm J} \quad (\text{D.1})$$

then, by substituting for  $\frac{dJ}{dV} = \frac{V}{|V|}$ , we get:

$$f_J(j) = \frac{1}{2} \left[ \exp\left(j - \frac{1}{2}\exp(j)\right) + \exp\left(-j - \frac{1}{2}\exp(-j)\right) \right] \quad (\text{D.2})$$

# APPENDIX E

---

## E.1 Review on General Expressions of The PSD of Basic Digitally Modulated Signals

The signal's PSD can be evaluated by using either a deterministic or a stochastic approach. To evaluate the PSD by the deterministic approach, a particular data sequence is assumed to be known, whereas the data sequence is assumed to be randomly generated in the stochastic approach. The general expression for a digitally modulated signal is given by:

$$S_s(f) = \frac{|P(f)|^2}{T_s} \sum_{k=-\infty}^{\infty} R(k) \exp(j2\pi f T_s) \quad (\text{E.1})$$

where  $P(f)$  is the FT of the pulse shaping function  $p(t)$  and  $R(k)$  is the autocorrelation of the random data sequence which is given by:

$$R(k) = \sum_{i=1}^I (a_n a_{n+k}) P_i \quad (\text{E.2})$$

where  $a_n$  and  $a_{n+k}$  are the voltage levels of the data pulses at the  $n^{\text{th}}$  and  $(n+k)^{\text{th}}$  symbol positions, respectively, and  $P_i$  is the probability of having the  $i^{\text{th}}$   $a_n a_{n+k}$  product. From equation (E.1), we note that the signal's PSD depends on the pulse shaping function and the statistical properties of the data. By few mathematical manipulation, the PSD of some basic digital signals with data modulation of rectangular bit shape are given as follows [36]:

— The PSD of the baseband Amplitude Shift Keying (ASK) signals:

$$S_s(f) = \frac{A_c^2 T_b}{4} \text{sinc}^2(f T_b) \left[ 1 + \frac{1}{T_b} \delta(f) \right] \quad (\text{E.3})$$

where  $A_c$  is the carrier amplitude

- 
- The PSD for the complex envelope of MPSK or QAM signals:

$$S_s(f) = C_\sigma l T_b \text{sinc}^2(f l T_b) \quad (\text{E.4})$$

where  $l$  denotes the number of bits per symbol and  $C_\sigma$  is a positive number denoting the variance of the complex valued random variable representing the multilevel value during the  $n^{\text{th}}$  symbol pulse.

- The PSD for the complex envelope of Minimum Shift Keying (MSK) signals:

$$S_s(f) = \frac{16A_c^2 T_b^2}{\pi^2} \left[ \frac{\cos^2(2\pi T_b f)}{(1 - (4T_b f)^2)^2} \right] \quad (\text{E.5})$$

where the normalized power of the MSK signal is  $A_c^2/2$ .

- The PSD of OFDM signals: The PSD of an OFDM signal can be obtained relatively easily, since an OFDM signal consists of orthogonal carriers modulated by data with rectangular pulses of duration of  $T_s$ . Consequently, the PSD of each carrier is of the form  $\text{sinc}^2(T_s(f - f_n))$  hence, the overall PSD of the complex envelope of the OFDM signal is given by:

$$S_s(f) = A_c^2 P_{w_n} \sum_{n=0}^{N-1} |\text{sinc}(T_s(f - f_n))|^2 \quad (\text{E.6})$$

where  $P_{w_n}$  is the normalized power of the  $n^{\text{th}}$  element of the  $N$ -element parallel data vector in the OFDM signal.



# LIST OF PUBLICATIONS

---

## International Journals

- 1- **A. Moawad**, K. Yao, A. Mansour, R. Gautier, "A Wideband Spectrum Sensing Approach in Cognitive Radio Based on Cepstral Analysis", IEEE open journal of the communications society, vol. 1, no. 20, pp. 863–888, 2020.
- 2- **A. Moawad**, K. Yao, A. Mansour, R. Gautier, "Spectrum Sensing By Cepstral Covariance Detection in Cognitive Radio", submitted to the journal of IEEE Communication Letters.

## Conferences

- 1- S E. El Khamy, Amr M. El Helw, and **A. Moawad**, "Classification of Multi-rate CDMA Signals Using Compressed Cyclostationary Features," Proceedings of the Progress In Electromagnetics Research Symposium (PIERS), pp. 1361-1365, Kuala Lumpur, Malaysia, Mar 2012.
- 2- S. E. El Khamy, A. M. El Helw, and **A. Moawad**, "Digital Signal Classification by Compressed Cyclostationary Features," The 29th National Radio Science Conference (NRSC), Cairo, Egypt, Apr 2012
- 3- S. E. El Khamy, A. M. El Helw, and **A. Moawad**, "Spectral Separation of Compressed Cyclostationary Signals Using Adaptive FRESH Filtering," Proceedings of the Progress In Electromagnetics Research Symposium (PIERS), Stockholm, Sweden, Aug 2013
- 4- **A. Moawad**, K. Yao, A. Mansour, R. Gautier, "Spectrum Sensing by Scattering Operators in Cognitive Radio," in Proceedings of the 2nd International Conference on Advanced Technology and Applied Science, pp. 388-395, Alex, Egypt, Sept 2017.

- 
- 5- **A. Moawad**, K. Yao, A. Mansour, R. Gautier, "Enhancement of Primary User Detection in Cognitive Radio by Scattering Transform," in Proceedings of the 19th International Conference on Electronics and Wireless Communications, pp. 2384-2390, Istanbul, Turkey, Oct 2017.
  - 6- **A. Moawad**, K. Yao, A. Mansour, R. Gautier, "Autocepstrum Approach for Spectrum Sensing in Cognitive Radio," in Proceedings of the 15th International Symposium on Wireless Communication Systems (ISWCS), Lisbon, Portugal, Aug 2018.



# BIBLIOGRAPHY

---

- [1] J. Mitola and G. Q. Maguire, "Cognitive radio: making software radios more personal," *IEEE Personal Communications*, vol. 6, no. 4, pp. 13–18, 1999.
- [2] S. Haykin, "Cognitive radio: brain-empowered wireless communications," *IEEE Journal on Selected Areas in Communications*, vol. 23, no. 2, pp. 201–220, 2005.
- [3] S. Sasipriya and R. Vigneshram, "An overview of cognitive radio in 5g wireless communications," in *IEEE International Conference on Computational Intelligence and Computing Research (ICCRIC)*, pp. 1–5, New Tehri, India, Dec 2016.
- [4] F. W. Vook, A. Ghosh, E. Diarte, and M. Murphy, "5g new radio: Overview and performance," in *52nd IEEE Asilomar Conference on Signals, Systems, and Computers*, pp. 1247–1251, CA, USA, Oct 2018.
- [5] E. Yaacoub and M.-S. Alouini, "A key 6g challenge and opportunity—connecting the remaining 4 billions: A survey on rural connectivity," *arXiv preprint arXiv:1906.11541*, 2019.
- [6] I. Abdo, T. Fujimura, T. Miura, A. Shirane, and K. Okada, "A 300ghz dielectric lens antenna," in *12th IEEE Global Symposium on Millimeter Waves (GSMM)*, pp. 17–19, Sendai, Japan, May 2019.
- [7] A. Garhwal and P. P. Bhattacharya, "Dynamic spectrum access in cognitive radio: a brief review," *International Journal of Computer Application in Engineering Sciences, Special Issue on Computer Networks & Security*, vol. 1, pp. 149–153, 2011.
- [8] Y.-C. Liang, Y. Zeng, E. C. Peh, and A. T. Hoang, "Sensing-throughput trade-off for cognitive radio networks," *IEEE Transactions on Wireless Communications*, vol. 7, no. 4, pp. 1326–1337, 2008.
- [9] Y. Arjoune and N. Kaabouch, "A comprehensive survey on spectrum sensing in cognitive radio networks: Recent advances, new challenges, and future research directions," *Sensors*, vol. 19, no. 1, p. 126, 2019.
- [10] T. Yucek and H. Arslan, "A survey of spectrum sensing algorithms for cognitive radio applications," *IEEE Communications Surveys & Tutorials*, vol. 11, no. 1, pp. 116–130, 2009.

- 
- [11] M. K. Tsatsanis and Z. Xu, "Pilot symbol assisted modulation in frequency selective fading wireless channels," *IEEE Transactions on Signal Processing*, vol. 48, no. 8, pp. 2353–2365, 2000.
- [12] Z. Fan, Z. Lu, and Y. Hu, "Reliable channel estimation based on bayesian compressive sensing for tds-ofdm systems," in *IEEE International Conference on Communication Systems*, pp. 620–624, IEEE, Macau, China, Nov 2014.
- [13] M. C. Gursoy and S. Gezici, "On the interplay between channel sensing and estimation in cognitive radio systems," in *IEEE Global Telecommunications Conference-GLOBECOM 2011*, pp. 1–5, IEEE, Texas, USA, Dec 2011.
- [14] Y. Yilmaz, Z. Guo, and X. Wang, "Sequential joint spectrum sensing and channel estimation for dynamic spectrum access," *IEEE Journal on Selected Areas in Communications*, vol. 32, no. 11, pp. 2000–2012, 2014.
- [15] G. Hua, J. Goh, and V. L. Thing, "Cepstral analysis for the application of echo-based audio watermark detection," *IEEE Transactions on Information Forensics and Security*, vol. 10, no. 9, pp. 1850–1861, 2015.
- [16] J. K. Lee, M. Kabrisky, M. E. Oxley, S. K. Rogers, and D. W. Ruck, "The complex cepstrum applied to two-dimensional images," *Pattern Recognition*, vol. 26, no. 10, pp. 1579–1592, 1993.
- [17] P. Borghesani, P. Pennacchi, R. Randall, N. Sawalhi, and R. Ricci, "Application of cepstrum pre-whitening for the diagnosis of bearing faults under variable speed conditions," *Mechanical Systems and Signal Processing*, vol. 36, no. 2, pp. 370–384, 2013.
- [18] E. Flinn, T. Cohen, and D. McCowan, "Detection and analysis of multiple seismic events," *Bulletin of the Seismological Society of America*, vol. 63, no. 6-1, pp. 1921–1935, 1973.
- [19] J. Jäntti, S. Chaudhari, and V. Koivunen, "Detection and classification of ofdm waveforms using cepstral analysis," *IEEE Transactions on Signal Processing*, vol. 63, no. 16, pp. 4284–4299, 2015.
- [20] B. P. Bogert, M. J. R. Healy, and J. W. Tukey, "The quefrency alanalysis of time series for echoes; cepstrum, pseudo-autocovariance, cross-cepstrum and saphe cracking," in *Proceedings of Time series analysis*, pp. 209–243, M. Rosenblatt, Ed., New York, Wiley ,1963, ch. 15.

- 
- [21] T. S. Rappaport, Y. Xing, O. Kanhere, S. Ju, A. Madanayake, S. Mandal, A. Alkhatteeb, and G. C. Trichopoulos, "Wireless communications and applications above 100 ghz: Opportunities and challenges for 6g and beyond," *IEEE Access*, vol. 7, pp. 78729–78757, 2019.
- [22] S. Dang, O. Amin, B. Shihada, and M.-S. Alouini, "What should 6g be?," *Nature Electronics*, vol. 3, no. 1, pp. 20–29, 2020.
- [23] F. Tariq, M. Khandaker, K.-K. Wong, M. Imran, M. Bennis, and M. Debbah, "A speculative study on 6g," *arXiv preprint arXiv:1902.06700*, 2019.
- [24] I. Union, "Imt traffic estimates for the years 2020 to 2030," *Report ITU*, pp. 1–51, 2015.
- [25] J. Mitola, *Cognitive radio*. PhD thesis, Institutionen för teleinformatik, 2000.
- [26] E. Hossain, D. Niyato, and Z. Han, *Dynamic spectrum access and management in cognitive radio networks*. Cambridge university press, 1st Ed., New York, USA, 2009.
- [27] E. Biglieri, A. J. Goldsmith, L. J. Greenstein, N. B. Mandayam, and H. V. Poor, *Principles of cognitive radio*. Cambridge University Press, 1st Ed., New York, USA, 2013.
- [28] A. Khattab and M. A. Bayoumi, "Standardization of cognitive radio networking: a comprehensive survey," *Annals of Telecommunications-Annales des téléCommunications*, vol. 70, no. 11-12, pp. 465–477, 2015.
- [29] K. Kim, Y. Xin, and S. Rangarajan, "Energy detection based spectrum sensing for cognitive radio: An experimental study," in *IEEE Global Telecommunications Conference GLOBECOM*, pp. 1–5, Florida, USA, Dec 2010.
- [30] D. Bao, L. De Vito, and S. Rapuano, "A histogram-based segmentation method for wideband spectrum sensing in cognitive radios," *IEEE Transactions on Instrumentation and Measurement*, vol. 62, no. 7, pp. 1900–1908, 2013.
- [31] B. Shent, L. Huang, C. Zhao, Z. Zhou, and K. Kwak, "Energy detection based spectrum sensing for cognitive radios in noise of uncertain power," in *International Symposium on Communications and Information Technologies*, pp. 628–633, IEEE, 2008.
- [32] R. Tandra and A. Sahai, "Snr walls for signal detection," *IEEE Journal of Selected Topics in Signal Processing*, vol. 2, no. 1, pp. 4–17, 2008.

- 
- [33] R. Tandra and A. Sahai, "Noise calibration, delay coherence and snr walls for signal detection," in *3rd IEEE Symposium on New Frontiers in Dynamic Spectrum Access Networks*, pp. 1–11, IEEE, 2008.
- [34] I. E. Atawi, O. S. Badarneh, M. S. Aloqlah, and R. Mesleh, "Energy-detection based spectrum-sensing in cognitive radio networks over multipath/shadowed fading channels," in *Wireless Telecommunications Symposium (WTS)*, pp. 1–6, IEEE, New York, USA, Apr 2015.
- [35] D. M. M. Plata and Á. G. A. Reátiga, "Evaluation of energy detection for spectrum sensing based on the dynamic selection of detection-threshold," *Procedia Engineering*, vol. 35, pp. 135–143, 2012.
- [36] L. W. Couch, *Digital & Analog Communication Systems*. Prentice Hall, 6th Ed., New Jersey, USA, 2011.
- [37] S. Upadhyay and S. Deshmukh, "Blind parameter estimation based matched filter detection for cognitive radio networks," in *International Conference on Communications and Signal Processing (ICCSP)*, pp. 0904–0908, IEEE, Chengdu, China, Oct 2015.
- [38] F. Salahdine, H. El Ghazi, N. Kaabouch, and W. F. Fihri, "Matched filter detection with dynamic threshold for cognitive radio networks," in *International Conference On Wireless Networks and Mobile communications (WINCOM)*, pp. 1–6, IEEE, Marrakech, Morocco, Oct 2015.
- [39] Y. Zeng and Y.-C. Liang, "Eigenvalue-based spectrum sensing algorithms for cognitive radio," *IEEE Transactions on Communications*, vol. 57, no. 6, pp. 1784–1793, 2009.
- [40] P. Aparna and M. Jayasheela, "Cyclostationary feature detection in cognitive radio using different modulation schemes," *International Journal of Computer Applications*, vol. 47, no. 21, 2012.
- [41] A. Al-Dulaimi, N. Radhi, and H. Al-Raweshidy, "Cyclostationary detection of undefined secondary users," in *Third International Conference on Next Generation Mobile Applications, Services and Technologies*, pp. 230–233, IEEE, Wales, United Kingdom, Sept 2009.
- [42] A. H. Ansari and S. Gulhane, "Cyclostationary method based spectrum sensing and analysis using different windowing method," in *International Conference on Energy Systems and Applications*, pp. 684–688, IEEE, Pune, India, Nov 2015.

- 
- [43] O. P. Awe, *Machine learning algorithms for cognitive radio wireless networks*. PhD thesis, Loughborough University, 2015.
- [44] Y. Yao, Y. Liu, Y. Yu, H. Xu, W. Lv, Z. Li, and X. Chen, "K-svm: An effective svm algorithm based on k-means clustering.," *Journal of Computers*, vol. 8, no. 10, pp. 2632–2639, 2013.
- [45] B. Khalfi, A. Zaid, and B. Hamdaoui, "When machine learning meets compressive sampling for wideband spectrum sensing," in *13th International Wireless Communications and Mobile Computing Conference (IWCMC)*, pp. 1120–1125, IEEE, Valencia, Spain, Jun 2017.
- [46] Z. Li, W. Wu, X. Liu, and P. Qi, "Improved cooperative spectrum sensing model based on machine learning for cognitive radio networks," *IET Communications*, vol. 12, no. 19, pp. 2485–2492, 2018.
- [47] D. L. Donoho, "Compressed sensing," *IEEE Transactions on information theory*, vol. 52, no. 4, pp. 1289–1306, 2006.
- [48] Y. L. Polo, Y. Wang, A. Pandharipande, and G. Leus, "Compressive wide-band spectrum sensing," in *IEEE International Conference on Acoustics, Speech and Signal Processing*, pp. 2337–2340, IEEE, Taipei, Taiwan, Apr 2009.
- [49] Y. Arjoun and N. Kaabouch, "Wideband spectrum sensing: A bayesian compressive sensing approach," *Sensors*, vol. 18, no. 6, p. 1839, 2018.
- [50] M. Lopes, "Estimating unknown sparsity in compressed sensing," in *International Conference on Machine Learning*, pp. 217–225, Atlanta, USA, Jun 2013.
- [51] S. Kyperountas, N. Correal, Q. Shi, and Z. Ye, "Performance analysis of cooperative spectrum sensing in suzuki fading channels," in *2nd International Conference on Cognitive Radio Oriented Wireless Networks and Communications*, pp. 428–432, IEEE, Florida, USA, Aug 2007.
- [52] S. Nallagonda, S. D. Roy, and S. Kumdu, "Performance of cooperative spectrum sensing in fading channels," in *1st International Conference on Recent Advances in Information Technology (RAIT)*, pp. 202–207, IEEE, Dhanbad, India, Mar 2012.
- [53] R. Wan, L. Ding, N. Xiong, W. Shu, and L. Yang, "Dynamic dual threshold cooperative spectrum sensing for cognitive radio under noise power uncertainty," *Human-centric Computing and Information Sciences*, vol. 9, no. 1, p. 22, 2019.
- [54] S. M. Kay, *Fundamentals of statistical signal processing, Vol. II: Detection Theory*. Prentice Hall, 1st Ed., New Jersey, USA, 1993.

- 
- [55] L. Korolov and Y. G. Sinai, *Theory of probability and random processes*. Springer Science & Business Media, 2nd Ed., Heidelberg, Germany, 2010.
- [56] D. M. M. Plata and Á. G. A. Reátiga, "Evaluation of energy detection for spectrum sensing based on the dynamic selection of detection-threshold," *Procedia Engineering*, vol. 35, pp. 135–143, 2012.
- [57] D. R. Joshi, D. C. Popescu, and O. A. Dobre, "Adaptive spectrum sensing with noise variance estimation for dynamic cognitive radio systems," in *44th Annual Conference on Information Sciences and Systems (CISS)*, pp. 1–5, IEEE, New Jersey, USA, Mar 2010.
- [58] A. Bagwari and G. S. Tomar, "Adaptive double-threshold based energy detector for spectrum sensing in cognitive radio networks," *International Journal of Electronics Letters*, vol. 1, no. 1, pp. 24–32, 2013.
- [59] B. A. Odhavjibhai and S. Rana, "Analysis of matched filter based spectrum sensing in cognitive radio," *International Research Journal of Engineering and Technology*, vol. 4, no. 4, pp. 578–581, 2017.
- [60] P. Alvarez, N. Pratas, A. Rodrigues, N. R. Prasad, and R. Prasad, "Energy detection and eigenvalue based detection: An experimental study using gnu radio," in *14th International Symposium on Wireless Personal Multimedia Communications (WPMC)*, pp. 1–5, IEEE, Brest, France, Oct 2011.
- [61] L. Du, M. Laghate, C. Liu, D. Cabric, and Y. Chen, "Improved eigenvalue-based spectrum sensing via sensor signal overlapping," in *8th IEEE International Conference on Communication Software and Networks (ICCSN)*, pp. 122–126, IEEE, Beijing, China, Jun 2016.
- [62] Y. Zeng, C. L. Koh, and Y.-C. Liang, "Maximum eigenvalue detection: Theory and application," in *IEEE International Conference on Communications*, pp. 4160–4164, IEEE, Beijing, China, May 2008.
- [63] S. K. Sharma, S. Chatzinotas, and B. Ottersten, "Maximum eigenvalue detection for spectrum sensing under correlated noise," in *IEEE International Conference on Acoustics, Speech and Signal Processing (ICASSP)*, pp. 7268–7272, IEEE, Florence, Italy, May 2014.
- [64] W. A. Gardner, "Introduction to random processes with applications to signals and systems((book))," *2nd Ed.*, New York, MacMillan, 1986.

- 
- [65] D. C. Simic and J. Simic, "The strip spectral correlation algorithm for spectral correlation estimation of digitally modulated signals," in *4th International Conference on Telecommunications in Modern Satellite, Cable and Broadcasting Services. TELSIKS'99 (Cat. No. 99EX365)*, vol. 1, pp. 277–280, IEEE, 1999.
- [66] J.-M. Kadjo, K. C. Yao, and A. Mansour, "Blind detection of cyclostationary features in the context of cognitive radio," in *IEEE International Symposium on Signal Processing and Information Technology (ISSPIT)*, pp. 150–155, Limassol, Cyprus, Dec 2016.
- [67] S. Rajendran, W. Meert, D. Giustiniano, V. Lenders, and S. Pollin, "Deep learning models for wireless signal classification with distributed low-cost spectrum sensors," *IEEE Transactions on Cognitive Communications and Networking*, vol. 4, no. 3, pp. 433–445, 2018.
- [68] U. Côté-Allard, C. L. Fall, A. Drouin, A. Campeau-Lecours, C. Gosselin, K. Glette, F. Laviolette, and B. Gosselin, "Deep learning for electromyographic hand gesture signal classification using transfer learning," *IEEE Transactions on Neural Systems and Rehabilitation Engineering*, vol. 27, no. 4, pp. 760–771, 2019.
- [69] P. Hossain, A. Komisarczuk, G. Pawetczak, S. Van Dijk, and I. Axelsen, "Machine learning techniques in cognitive radio networks," *arXiv preprint arXiv:1410.3145*, 2014.
- [70] H. Anandakumar and K. Umamaheswari, "Supervised machine learning techniques in cognitive radio networks during cooperative spectrum handovers," *Cluster Computing*, vol. 20, no. 2, pp. 1505–1515, 2017.
- [71] A. Nasser, A. Mansour, K. C. Yao, H. Charara, and M. Chaitou, "Efficient spectrum sensing approaches based on waveform detection," in *3rd International Conference on e-Technologies and Networks for Development (ICeND2014)*, pp. 13–17, IEEE, Beirut, Lebanon, May 2014.
- [72] A. Nasser, A. Mansour, K.-C. Yao, H. Abdallah, M. Chaitou, and H. Charara, "Spectrum sensing enhancement using principal component analysis," in *IEEE International Symposium on Signal Processing and Information Technology (ISSPIT)*, pp. 263–267, IEEE, Limassol, Cyprus, Dec 2016.
- [73] A. Nasser, A. Mansour, K. C. Yao, H. Abdallah, and H. Charara, "Spectrum sensing based on cumulative power spectral density," *EURASIP Journal on Advances in Signal Processing*, vol. 2017, no. 1, p. 38, 2017.

- 
- [74] A. Nasser, A. Mansour, K.-C. Yao, H. Charara, and M. Chaitou, "Spectrum sensing for full-duplex cognitive radio systems," in *International Conference on Cognitive Radio Oriented Wireless Networks*, pp. 363–374, Springer, May 2016, Grenoble, France.
- [75] J.-M. Kadjo, K. C. Yao, and A. Mansour, "Blind spectrum sensing based on recurrence quantification analysis in the context of cognitive radio," in *26th European Signal Processing Conference (EUSIPCO)*, pp. 1835–1839, IEEE, Rome, Italy, Sept 2018.
- [76] G. Hattab and M. Ibnkahla, "Multiband spectrum access: Great promises for future cognitive radio networks," *Proceedings of the IEEE*, vol. 102, no. 3, pp. 282–306, 2014.
- [77] X. Yanwei, Z. Jianhua, and Z. Ping, "Compressed sensing based multi-rate sub-nyquist sampling system," *The Journal of China Universities of Posts and Telecommunications*, vol. 22, no. 2, pp. 89–95, 2015.
- [78] Z. Dai, Y. Chen, W. Wen, and Y. Zheng, "Compressed sensing based sub-nyquist sampling of multiple sinusoids with dual rate channels," *Review of Scientific Instruments*, vol. 89, no. 12, p. 125113, 2018.
- [79] Z. Tian and G. B. Giannakis, "Compressed sensing for wideband cognitive radios," in *IEEE International Conference on Acoustics, Speech and Signal Processing (ICASSP)*, vol. 4, pp. IV–1357, IEEE, Hawaii, USA, Apr 2007.
- [80] H. Sun, A. Nallanathan, C.-X. Wang, and Y. Chen, "Wideband spectrum sensing for cognitive radio networks: a survey," *IEEE Wireless Communications*, vol. 20, no. 2, pp. 74–81, 2013.
- [81] Y. LeCun, K. Kavukcuoglu, and C. Farabet, "Convolutional networks and applications in vision," in *IEEE International Symposium on Circuits and Systems*, pp. 253–256, IEEE, Paris, France, May 2010.
- [82] J. Bruna and S. Mallat, "Invariant scattering convolution networks," *IEEE Transactions on Pattern Analysis and Machine Intelligence*, vol. 35, no. 8, pp. 1872–1886, 2013.
- [83] J. Andén and S. Mallat, "Deep scattering spectrum," *IEEE Transactions on Signal Processing*, vol. 62, no. 16, pp. 4114–4128, 2014.

- 
- [84] A. Moawad, K.-C. Yao, A. Mansour, and R. Gautier, "Spectrum sensing by scattering operators in cognitive radio," in *2nd International Conference on Advanced Technology and Applied Science (ICATAS)*, pp. 1–6, Alex, Egypt, Sept 2017.
- [85] A. Goldsmith, *Wireless communications*. Cambridge university press, 2nd Ed., USA, 2005.
- [86] G. Matz and F. Hlawatsch, "Fundamentals of time-varying communication channels," in *Wireless Communications Over Rapidly Time-Varying Channels*, pp. 1–63, Academic Press, Amsterdam, 2011.
- [87] M. Stephane, "A wavelet tour of signal processing," *The Sparse Way*, 1st Ed., Massachusetts, 1999.
- [88] D. T. Lee and A. Yamamoto, "Wavelet analysis: theory and applications," *Hewlett Packard journal*, vol. 45, pp. 44–44, 1994.
- [89] R. X. Gao and R. Yan, "From fourier transform to wavelet transform: A historical perspective," in *Wavelets*, pp. 17–32, Springer Science+Business Media, Heidelberg, 2011.
- [90] I. S. Gradshteyn and I. M. Ryzhik, *Table of integrals, series, and products*. Academic press, 6th Ed., Massachusetts, 2014.
- [91] A. R. Bahai, B. R. Saltzberg, and M. Ergen, "Channel estimation and equalization," *Multi-Carrier Digital Communications: Theory and Applications of OFDM*, pp. 117–165, Boston, 2004.
- [92] A. Moawad, K.-C. Yao, A. Mansour, and R. Gautier, "Enhancement of primary user detection in cognitive radio by scattering transform," in *19th International Conference on Electronics and Wireless Communication (ICEWC)*, pp. 1–6, Istanbul, Turkey, Sept 2017.
- [93] E. L. Ferguson, S. B. Williams, and C. T. Jin, "Improved multipath time delay estimation using cepstrum subtraction," in *IEEE International Conference on Acoustics, Speech and Signal Processing (ICASSP)*, pp. 551–555, Brighton, UK, May 2019.
- [94] G. Burel, "Detection of spread spectrum transmissions using fluctuations of correlation estimators," in *IEEE International Symposium on Intelligent Signal Processing and Communication Systems (ISPACS)*, vol. 11, p. B8, Hawaii, USA, Nov 2000.
- [95] Z. Deng, L. Shen, N. Bao, B. Su, J. Lin, and D. Wang, "Autocorrelation based detection of dsss signal for cognitive radio system," in *International Conference*

---

on *Wireless Communications and Signal Processing (WCSP)*, pp. 1–5, IEEE, Kerala, India, Feb 2011.

- [96] S. Rostami, K. Arshad, and K. Moessner, “Order-statistic based spectrum sensing for cognitive radio,” *IEEE Communications Letters*, vol. 16, no. 5, pp. 592–595, 2012.
- [97] R. B. Randall, “A history of cepstrum analysis and its application to mechanical problems,” *Mechanical Systems and Signal Processing*, vol. 97, pp. 3–19, 2017.
- [98] D. G. Childers, D. P. Skinner, and R. C. Kemerait, “The cepstrum: A guide to processing,” *Proceedings of the IEEE*, vol. 65, no. 10, pp. 1428–1443, 1977.
- [99] Z. N. Karam and A. V. Oppenheim, “Computation of the one-dimensional unwrapped phase,” in *15th International Conference on Digital Signal Processing*, pp. 304–307, IEEE, Wales, UK, Jul 2007.
- [100] A. V. Oppenheim and R. W. Schaffer, “From frequency to quefrency: A history of the cepstrum,” *IEEE signal processing Magazine*, vol. 21, no. 5, pp. 95–106, Oct 2004.
- [101] C. Peeters, P. Guillaume, and J. Helsen, “Vibration-based bearing fault detection on experimental wind turbine gearbox data,” in *3rd European Conference of the Prognostics and Health Management Society*, pp. 1–10, Bilbao, Spain, Jul 2016.
- [102] W.-J. Zeng, X. Jiang, X.-L. Li, and X.-D. Zhang, “Deconvolution of sparse underwater acoustic multipath channel with a large time-delay spread,” *The Journal of the Acoustical Society of America*, vol. 127, no. 2, pp. 909–919, 2010.
- [103] A. Stéphane and B. Champagne, “Cepstral prefiltering for time delay estimation in reverberant environments,” in *International Conference on Acoustics, Speech, and Signal Processing*, vol. 5, pp. 3055–3058, IEEE, 1995.
- [104] H. Cheng, B. L. Mark, and Y. Ephraim, “Wideband temporal spectrum sensing using cepstral features,” in *IEEE 20th International Symposium on “A World of Wireless, Mobile and Multimedia Networks” (WoWMoM)*, pp. 1–6, IEEE, Washington DC, USA, June 2019.
- [105] T. S. Rappaport *et al.*, *Wireless communications: principles and practice*, vol. 2. Prentice Hall, 2nd Ed., New Jersey, 1996.
- [106] S. E. Pav, “Moments of the log non-central chi-square distribution,” *arXiv preprint arXiv:1503.06266*, 2015.

- 
- [107] K. Krishnamoorthy, *Handbook of statistical distributions with applications*. Chapman and Hall/CRC, 1st Ed., 2006, Florida.
- [108] N. Batir, "On some properties of digamma and polygamma functions," *Journal of Mathematical Analysis and Applications*, vol. 328, no. 1, pp. 452–465, 2007.
- [109] G. Navas-Palencia, "Extending error function and related functions to complex arguments," 2016.
- [110] S. Abrarov and B. Quine, "Accurate approximations for the complex error function with small imaginary argument," *arXiv preprint arXiv:1411.1024*, 2014.
- [111] G. Di Blasio and A. Neri, "Modified q-functions and their use in detection analysis," *IEEE transactions on information theory*, vol. 37, no. 4, pp. 1123–1142, 1991.
- [112] G. K. Karagiannidis and A. S. Lioumpas, "An improved approximation for the gaussian q-function," *IEEE Communications Letters*, vol. 11, no. 8, pp. 644–646, 2007.
- [113] R. L. Peterson, R. E. Ziemer, and D. E. Borth, *Introduction to spread-spectrum communications*, vol. 995. Prentice hall, 1st Ed., 1995, New Jersey.
- [114] M. Kowatsch and J. Lafferl, "A spread-spectrum concept combining chirp modulation and pseudonoise coding," *IEEE Transactions on Communications*, vol. 31, no. 10, pp. 1133–1142, 1983.
- [115] E. Karapistoli, F.-N. Pavlidou, I. Gragopoulos, and I. Tsetsinas, "An overview of the iee 802.15. 4a standard," *IEEE Communications Magazine*, vol. 48, no. 1, pp. 47–53, 2010.
- [116] T. Rebane and P. Vitushinskii, "Complex gaussian functions for four-particle systems," *Optics and Spectroscopy*, vol. 92, no. 1, pp. 17–19, 2002.
- [117] J.-F. Bercher and C. Vignat, "On minimum fisher information distributions with restricted support and fixed variance," *Information Sciences*, vol. 179, no. 22, pp. 3832–3842, 2009.
- [118] M. N. Kohan and H. Behnam, "Denoising medical images using calculus of variations," *Journal of medical signals and sensors*, vol. 1, no. 3, p. 184, 2011.
- [119] L. Chato, S. Latifi, and P. Kachroo, "Total variation denoising method to improve the detection process in ir images," in *IEEE 8th Annual Ubiquitous Computing, Electronics and Mobile Communication Conference (UEMCON)*, pp. 441–447, IEEE, New York City, NY, USA, Oct. 2017.

- 
- [120] I. Selesnick, "Total variation denoising (an mm algorithm)," *NYU Polytechnic School of Engineering Lecture Notes*, 2012.
- [121] A. Chopra and H. Lian, "Total variation, adaptive total variation and nonconvex smoothly clipped absolute deviation penalty for denoising blocky images," *Pattern Recognition*, vol. 43, no. 8, pp. 2609–2619, 2010.
- [122] S. Kay, "The effect of sampling rate on autocorrelation estimation," *IEEE Transactions on Acoustics, Speech, and Signal Processing*, vol. 29, no. 4, pp. 859–867, Aug 1981.
- [123] F. Salahdine, H. El Ghazi, N. Kaabouch, and W. F. Fihri, "Matched filter detection with dynamic threshold for cognitive radio networks," in *the International Conference on Wireless Networks and Mobile Communications (WINCOM)*, pp. 1–6, Marrakech, Morocco, Oct 2015.
- [124] S. Mallat and W. L. Hwang, "Singularity detection and processing with wavelets," *IEEE Transactions on Information Theory*, vol. 38, no. 2, pp. 617–643, 1992.
- [125] E.-N. S. E.-D. Youssef, "Advanced wavelet-based approach to spectrum sensing for cognitive radio networks," Master's thesis, Arab Academy for Science and Technology and Maritime Transport, Cairo, Egypt, 2013.
- [126] A. Moawad, K.-C. Yao, A. Mansour, and R. Gautier, "Autocepstrum approach for spectrum sensing in cognitive radio," in *15th International Symposium on Wireless Communication Systems (ISWCS)*, pp. 1–6, Lisbon, Portugal, Aug 2018.
- [127] Y. Sun, B. L. Mark, and Y. Ephraim, "Online parameter estimation for temporal spectrum sensing," *IEEE Transactions on Wireless Communications*, vol. 14, no. 8, pp. 4105–4114, 2015.
- [128] J. M. Bruno and B. L. Mark, "A recursive algorithm for wideband temporal spectrum sensing," *IEEE Transactions on Communications*, vol. 66, no. 1, pp. 26–38, 2017.
- [129] T. Nguyen, B. L. Mark, and Y. Ephraim, "Spectrum sensing using a hidden bivariate markov model," *IEEE Transactions on Wireless Communications*, vol. 12, no. 9, pp. 4582–4591, 2013.
- [130] P. Gopalakrishnan, D. Kanevsky, A. Nadas, and D. Nahamoo, "A generalization of the baum algorithm to rational objective functions," in *International Conference on Acoustics, Speech, and Signal Processing*, pp. 631–634, IEEE, 1989.

- 
- [131] S. Rezk, C. Join, and S. El Asmi, "An algebraic derivative-based method for r wave detection," in *19th European Signal Processing Conference*, pp. 1578–1582, Barcelona, Spain, Aug 2011.
- [132] Z. Tian and G. B. Giannakis, "A wavelet approach to wideband spectrum sensing for cognitive radios," in *1st international conference on cognitive radio oriented wireless networks and communications*, pp. 1–5, Mykonos Island, Greece, Jun 2006.
- [133] Z. Xiaoli, "Edge detection algorithm based on multiscale product with gaussian function," *Procedia Engineering*, vol. 15, pp. 2650–2654, 2011.
- [134] K. Divakaran, N. Manikandan, S. Hari, *et al.*, "Wavelet based spectrum sensing techniques for cognitive radio—a survey," *International Journal of Computer Science and Information Technology*, vol. 3, no. 2, pp. 123–137, 2011.
- [135] S. E. El-Khamy, M. S. El-Mahallawy, and E.-N. S. Youssef, "Improved wideband spectrum sensing techniques using wavelet-based edge detection for cognitive radio," in *International Conference on Computing, Networking and Communications (ICNC)*, pp. 418–423, San Diego, USA, Jan 2013.
- [136] S. Jindal, D. Dass, and R. Gangopadhyay, "Wavelet based spectrum sensing in a multipath rayleigh fading channel," in *20th National Conference on Communications (NCC)*, pp. 1–6, Kanpur, India, Feb 2014.
- [137] A. Kumar, S. Saha, and R. Bhattacharya, "Wavelet transform based novel edge detection algorithms for wideband spectrum sensing in crns," *AEU-International Journal of Electronics and Communications*, vol. 84, pp. 100–110, 2018.
- [138] S. C. Chapra, R. P. Canale, *et al.*, *Numerical methods for engineers*. Boston: McGraw-Hill Higher Education,, 2010.
- [139] R. E. Blahut, *Fast algorithms for signal processing*. Cambridge University Press, 1st Ed., 2010, Cambridge.
- [140] V. Sealey, "Definite integrals, riemann sums, and area under a curve: What is necessary and sufficient," in *Proceedings of the 28th annual meeting of the North American Chapter of the International Group for the Psychology of Mathematics Education*, vol. 2, pp. 46–53, Yucatan, Mexico, 2006.
- [141] P. Tilghman, "Ai will rule the airwaves: A darpa grand challenge seeks autonomous radios to manage the wireless spectrum," *IEEE Spectrum*, vol. 56, no. 6, pp. 28–33, 2019.

- 
- [142] D. Wang, B. Song, D. Chen, and X. Du, "Intelligent cognitive radio in 5g: Ai-based hierarchical cognitive cellular networks," *IEEE Wireless Communications*, vol. 26, no. 3, pp. 54–61, 2019.

---

**Titre :** Amélioration de la détection du spectre dans la radio cognitive : offrir des opportunités spectrales fiables

**Mot clés :** Radio Cognitive, des signaux à spectre étalé, l'analyse cepstrale

**Résumé :** L'objectif principal de la thèse est de concevoir un système de détection fiable, capable de détecter un signal assimilable au bruit, dans un contexte non-coopératif. Nous avons proposé l'approche autocepstrum pour détecter les signaux de type bruit. Les techniques proposées ont montré une grande fiabilité pour la détection des signaux à spectre étalé et des signaux ultra large bande (UWB). Pour améliorer le processus de détection, nous lissons les fluctuations des estimateurs d'autocorrélation en utilisant l'algorithme TVD (Total Variation Denoising). Nous avons étendu nos travaux au cas du spectre à très large bande composé de

plusieurs sous-bandes de fréquences. À cet effet, nous avons introduit l'algorithme DLSD (Differential Log Spectral Density) pour identifier les limites spectrales du spectre large bande cible. Ensuite, pour la détection du signal du PU, nous avons développé le détecteur BaseBand-AutoCepstrum (BB-ACD) qui extrait les informations du signal en bande de base pour tenir compte des erreurs possibles dans les limites spectrales. Enfin, la méthode du cepstre de puissance améliorée est introduite par le détecteur de covariance Cepstrale (CCD) pour détecter les signaux modulés numériquement.

---

**Title:** Enhancement of Spectrum Sensing in Cognitive Radio: Providing Reliable Spectral Opportunities

**Keywords:** Cognitive radio, spread spectrum, cepstrum analysis

**Abstract:** The main objective of the thesis is to devise a reliable non-cooperative spectrum sensing system that is able to detect noise-like signals. We harness the strength of cepstral analysis to develop a system able to detect spread spectrum signals. We have proposed the autocepstrum approach to detect noise-like signals. The proposed techniques showed reliability for detecting spread spectrum and Ultra-Wide Band (UWB) signals. For improved detection process, we smoothen the fluctuations of the autocorrelation estimators by using the Total Variation Denoising (TVD) algorithm. We formulate a wideband spectrum sensing problem which based on detecting the

spectral boundaries followed by the PU detection phase. In this regard, we introduced the Differential Log Spectral Density (DLSD) algorithm to identify the spectral boundaries of the target wideband spectrum. For the PU detection, we introduced the BaseBand-AutoCepstrum Detection (BB-ACD) which extracts the baseband information before applying the auto-cepstrum detection technique to take into account the frequency uncertainty that may result from falsely detected spectral boundaries. Finally, an enhanced power cepstrum is introduced by the Cepstral Covariance Detection (CCD) for detecting digitally modulated signals.